THE UNIVERSITY OF MICHIGAN

INDUSTRY PROGRAM OF THE COLLEGE OF ENGINEERING

Donald G. Anderson

A dissertation submitted in partial fulfillment
of the requirements for the degree of
Doctor of Philosophy
(Civil Engineering)
in The University of Michigan
1974

May 1974

IP-857

ABSTRACT

DYNAMIC MODULUS OF COHESIVE SOILS

by

Donald Gordon Anderson

Co-Chairmen: F. E. Richart, Jr., R. D. Woods

This dissertation describes the results of a laboratory and field study of the dynamic modulus of cohesive soils. Nine undisturbed and two remolded soils were evaluated during the course of the investigation. These materials represented a variety of different soil conditions which might be encountered at typical field sites.

The overall objective of the investigation was to study the influence of the following effects on the dynamic characteristics of cohesive soils: (1) time after pressure application, (2) shearing strain amplitude, (3) number of repetitions of shearing strain, and (4) temperature. In addition, the stress-history effects of high amplitude straining, the rate of time-dependent regain in modulus after high amplitude straining and the relationship between field and laboratory results were analyzed.

Laboratory test results were obtained by performing resonant column dynamic tests. Strain amplitudes during these tests varied from 0.0001 percent to 1.0 percent; the number of repetitions of strain varied from 200 to 100,000.

The cross-hole seismic technique was used in field tests to measure shear wave velocities in situ. These determinations were limited to low strain amplitudes and to in situ pressure conditions.

It was found that the shear wave velocity measured during the laboratory test showed a time-dependent variation throughout the duration of load application. After approximately 1000 minutes of confinement, the velocity increased linearly with the logarithm of time. The rate of increase in velocity per logarithmic cycle of time varied with the confining pressure, the mean particle diameter of the soil, the initial void ratio of the material and the undrained shearing strength of the specimen.

The amplitude of shearing strain affected dynamic response once the magnitude of oscillation exceeded 0.01 percent. When strains were greater than this threshold limit, a nonlinear decrease in shear modulus occurred as the amplitude of straining increased. Either a modified hyperbolic or a Ramberg-Osgood relationship could be used to approximate the nonlinear behavior. Sustained repetitions of strain beyond the threshold limit caused additional reduction in shear modulus.

Repetitions of high amplitude strain (cycling) caused a reduction in the low amplitude shear modulus measured immediately after the end of high amplitude cycling. The magnitude of reduction depended on the amplitude and the number of repetitions of strain. However, the reduction in low amplitude modulus was temporary. The modulus increased with time until it reached the level noted prior to high amplitude cycling.

Temperature was observed to have only a slight influence on the dynamic behavior of cohesive soils. During long-term tests the magnitude of shear wave velocity, measured after 1000 minutes of confinement,

increased when the temperature was lowered from 22° to 4°C. The change varied from 0 percent to 12.5 percent. As temperature decreased the rate of increase in velocity per logarithmic cycle of time decreased. Short-term temperature changes caused an immediate change in shear wave velocity. This variation essentially disappeared when pore pressures equalized.

Finally, it was found that laboratory values of shear wave velocity corresponding to 1000-minute test duration were appreciably lower than the field values of velocity. The difference was attributed to the logarithmic increase in velocity with time measured during the laboratory test. When the laboratory velocity was modified by adding a 20-year extrapolation of the velocity increase, the modified velocity corresponded, in most cases, with the velocity measured in the field.

ACKNOWLEDGMENTS

The writer wishes to extend his sincere appreciation to the following persons:

— his co-chairmen, Professors F. E. Richart, Jr., and R. D. Woods, for their continued guidance and encouragement throughout the writer's research,

— his committee members, Professors D. H. Gray, H. N. Pollack, A. S. Winemen and E. B. Wylie, for providing technical advice during the investigation,

his colleagues in soil dynamics at The University of Michigan, N. F. Allen, C-S. Chon, K. Karel and F. Somogyi, for assisting in the performance of laboratory and field tests and the preparation of the dissertation, and

— his other friends, S.E.A. Afifi, W. A. Haupt, L. F. Kahn, D.L.N. Lee, Y. K. Lin and R. Sagesser, for their stimulating interest.

Furthermore, the writer would like to thank the following groups of people:

— the National Science Foundation for supporting the research described herein (Grant N. GK-21455) and for providing the writer with a National Science Foundation Traineeship for the first three years of his program,

— the Industry Program of the College of Engineering at The

University of Michigan for contributing to the cost of reproducing this dissertation, and

— the technical personnel at G. G. Brown Laboratory, in particular B. E. Bourland, H. G. Chalmers and L. E. North, for assisting with electrical and mechanical modifications to test equipment.

Finally, the writer wishes to especially thank the following individuals:

— Professor K. H. Stokoe, II, for assisting in the initial planning and testing phases of this investigation,

— Professor J. R. Bell for introducing the writer to soil mechanics and for providing the writer with sufficient background to enter a doctoral program, and

— Janna, his wife, for her patience and sacrifice during the past three and one-half years.

TABLE OF CONTENTS

TABLE OF CONTENTS (Continued)

TABLE OF CONTENTS (Continued)

TABLE OF CONTENTS (Continued)

TABLE OF CONTENTS (Concluded)

LIST OF APPENDIXES

LIST OF TABLES

LIST OF FIGURES

LIST OF FIGURES (Continued)

LIST OF FIGURES (Continued)

LIST OF FIGURES (Concluded)

NOTATION

A	- Constant for rheological model—depends on soil structure and temperature (Eq. (2.13))
a	- Hardin and Drnevich's cycle adjustment factor—$a = 1.0 + 0.25 \log N$ (Eq. (2.9))
B	- Constant for rheological model—depends on soil structure and temperature (Eq. (2.13))
b	- Soil constant—equals 1.3 for cohesive soils (Eq. (2.8))
C_c	- Compression index
CU	- Consolidated-undrain triaxial test
c'	- Cohesion intercept in terms of effective stress (kg/cm^2)
D	- Damping ratio—ratio of viscous damping to critical damping
D_{50}	- Mean particle diameter (mm)
d	- Distance between soil particles (Å)
E	- Young's modulus (psi)
E_1, E_2	- Elastic moduli from rheological model (Eq. (2.13))
e	- Void ratio
e_o	- Initial void ratio
exp	- Exponential
f_n	- Frequency at resonance (Hz)
G	- Shear modulus (psi)
G_{after}	- Shear modulus measured at low strain amplitudes 1 min after the end of high amplitude cycling (psi)
G_{before}	- Shear modulus measured at low strain amplitudes just before high amplitude cycling (psi)
G_{max}	- Shear modulus at low amplitude shearing strains (psi)
G_N	- Shear modulus at Nth cycle of high amplitude strain (psi)
G_r	- Shear modulus at time of interest divided by modulus at 100 percent consolidation
G_s	- Specific gravity of soil
G_t	- Shear modulus measured at low strain amplitude t min after high amplitude cycling (psi)

G_{500} - Shear modulus at 500th cycle of high amplitude strain (psi)

$(G/G_{max})_N$ - Ratio of G/G_{max} at Nth cycle of high amplitude strain (%)

$(G/G_{max})_{1000}$ - Ratio of G/G_{max} at 1000th cycle of high amplitude strain (%)

h - Height of soil specimen (ft)

I - Mass moment of inertia of the soil specimen (gm cm sec^2)

IF - Interparticle force (Newtons)

I_o - Mass moment of inertia of the drive system and top cap (gm cm sec^2)

I_p - Plasticity index of the soil (%)

K_o - Coefficient of earth pressure at rest—ratio of horizontal to vertical effective stresses

K - Overconsolidation adjustment factor (Figure 2.2)

L - Distance between impulse and pickup hole in cross-hole test (ft)

m_v - Compressibility coefficient for soil structure

m_w - Compressibility coefficient for water

N - Number of cycles of high amplitude straining

n - Soil porosity (%)

OCR - Overconsolidation ratio—ratio of maximum past consolidation stress to present overburden stress conditions

P_c - Preconsolidation pressure (kg/cm^2)

$(PR)_t$ - Percent regain in low amplitude modulus after high amplitude cycling as given by Eq. (7.19) (%)

R - Correlation number for Ramberg-Osgood curve

$\bar{r}$ - Average radius of soil specimen (cm)

S - Specific surface of soil particle (m^2/gm)

S_r - Degree of saturation of soil (%)

S_u - Undrained shearing strength of soil (kg/cm^2)

T_r - Time of interest divided by time to 100 percent primary consolidation

t_a - Time after high amplitude cycling (min)

t_{100} - Time to 100 percent regain in low amplitude modulus after high amplitude cycling (min)

UC - Unconfined compression test

V_m - Total volume of soil specimen

V_p - Velocity of dilation or primary wave (fps)

V_s - Velocity of shear wave (fps)

V_{sEQ} - Velocity of shear wave by empirical equation (fps)

V_{s4} - Velocity of shear wave at 4°C (fps)

V_{s22} - Velocity of shear wave at 22°C (fps)

V_{s1000} - Velocity of shear wave after 1000 min of confinement (fps)

V_{ss} - Volume of mineral solids

V_w - Volume of pore water

VS - Vane shear test

α - Shape factor for Ramberg-Osgood curve

α_s - Thermal coefficient of cubical expansion of mineral solids

α_w - Thermal coefficient of expansion of soil water

α_{st} - Change in volume of soil structure due to temperature induced changes in interparticle force

β - Ratio of $\omega_n h/V_s$

γ - Shearing strain (% or rads)

γ_h - Hyperbolic strain (rads)

γ_r - Reference strain—ratio of τ_{max} to G_{max} (rads)

γ_t - Total unit weight of soil (pcf)

$\gamma_{\theta z}$ - Average shearing strain developed in torsion (% or rads)

Δe - Change in void ratio

$\Delta G/G_{1000}$ - Normalized secondary increase in modulus—change in G_{max} per logarithmic cycle of time divided by G_{max} at 1000 min (%)

$\Delta(G_{after}/G_{before})$ - Decrease in G_{after}/G_{before} per logarithmic cycle of repetitions (%)

$\Delta(G_N/G_{500})$ - Decrease in G_N/G_{500} per logarithmic cycle of repetitions (%)

ΔT - Change in temperature (°C)

Δu - Change in pore pressure (kg/cm^2)

ΔV - Change in velocity (fps)

ΔV_s - Change in shear wave velocity (fps)—implied per logarithmic cycle of time when used in $\Delta V_s/\Delta V_{1000}$

$(\Delta V_{s4})_{\log cycle}$ - Change in shear wave velocity per logarithmic cycle of time at 4°C (fps)

$(\Delta V_{s22})_{\log cycle}$ - Change in shear wave velocity per logarithmic cycle of time at 22°C (fps)

$(\Delta V)_{\Delta T}$ - Change in volume during drain triaxial test due to change in temperature

$(\Delta V_{st})_{\Delta T}$ - Change in volume of soil structure due to temperature induced changes in interparticle forces

δ - Logarithmic decrement

ϵ_a - Axial strain (in./in.)

η - Viscosity term in Murayama's model (Eq. (2.13))

θ_{pp} - Angle of twist about axis of symmetry (rads)

ρ - Mass density—ratio of total unit weight to gravitational acceleration ($lb\text{-}sec^2/ft^4$)

$\bar{\sigma}_o$ - Effective octahedral normal stress (psf or psi)

$\bar{\sigma}_1$ - Effective vertical stress (psi)

$\bar{\sigma}_3$ - Effective horizontal stress (psi)

σ_2 - Stress on dashpot in Murayama's model

σ_{20} - Initial stress on dashpot in Murayama's model

τ - Shearing stress (psi)

τ_{max} - Maximum shearing stress (psi)

τ_o - Octahedral shearing stress (psi)

τ_y - Shearing stress at yield (psi)

ϕ' - Effective angle of internal friction (°)

ω - Circular frequency (rads/sec)

ω_{ll} - Liquid limit (%)

ω_n - Circular frequency at resonance (rads/sec)

ω_o - Initial water content (%)

CHAPTER I

INTRODUCTION

A. Objective

The overall objective of this investigation was to evaluate the influence of the following parameters on the dynamic characteristics of cohesive soils: (1) time after pressure application, (2) shearing strain amplitude, (3) number of repetitions of constant strain amplitude and (4) temperature. During the course of the investigation, several additional effects were also studied. These included the stress-history effects of high amplitude straining on low amplitude soil properties, the rate of thixotropic regain in rigidity after high amplitude cycling, and the difference between low amplitude dynamic characteristics measured in the laboratory and similar characteristics measured in the field.

In addition to determining test values, this investigation compared present test results with existing theoretical and empirical relations. Several new analytical representations were formulated to fit conditions not previously treated.

One fundamental objective was pursued throughout the following presentation. That objective was to report in detail the methods and materials utilized in the research effort, thus enabling the reader to either duplicate tests or to interpret results with respect to different analytical procedures.

B. Background

The field of soil dynamics has received considerable attention in recent years. Much of the interest has been concerned with the performance of soils during earthquake loading. That interest has been intensified since the advent of nuclear power plants.

Various other processes also introduce dynamic loads into soils. Natural phenomena such as winds and water waves load either the soil or a structure supported on the soil. Man also produces dynamic loads by operating reciprocating engines and stamping presses, by blasting, by pile driving and by driving his automobiles and trucks over rough roads.

Each process delivers a time-dependent loading to the soil. The loading may or may not affect the characteristics of the soil. In certain situations a change in dynamic characteristics results in catastrophic consequences; in other situations dynamic effects are negligible. In each case the soils engineer is called upon to evaluate the potential consequences of the dynamic loading and to propose remedial action when necessary.

Before the soils engineer can determine the consequences of the dynamic loading, he must define both the characteristics of the load mechanism and the dynamic response of the soil. A considerable effort has already been devoted to establishing this information.

1. LOAD MECHANISM

As noted in the previous paragraphs, several phenomena can

introduce dynamic loads to a soil mass. Two of the phenomena, earthquakes and water waves, are particularly relevant to this investigation.

Both water waves and earthquakes usually involve large amounts of energy and relatively low frequencies of load repetitions. When this energy is transferred to the soil, large amplitude, time-dependent deformations occur. The magnitude of the deformation is such that the soil behavior changes noticeably. Furthermore, the time-dependent deformation may occur in a random or periodic manner. The properties of the soil must, therefore, be defined not only in terms of deformation but also in terms of the number of cycles of deformation.

a. Earthquakes

Most earthquakes result from rock movement along existing faults. During slip, seismic disturbances are generated. The seismic disturbances propagate outward from the source as a series of random vibrations. If the energy released is sufficiently large, the vibration may be recorded thousands of miles from the source.

The seismic vibration strains the rock or soils as it passes, with the magnitude and duration of straining depending on the amount of energy released during fault movement. Several other factors such as distance from the source, orientation of the fault, attenuation factors and site conditions also play a significant role in determining strain characteristics. For example at certain sites the deformations are amplified as they propagate from bedrock through layers of soft soils.

Actual characteristics of earthquake-induced motion are, therefore,

highly variable. Despite this complexity, several generalizations can be made regarding probable motion. In cases where the soil is located in close proximity to the fault movement, shearing strains within the soil may exceed 1.0 percent. The number of cycles of strong motion generally will be less than 300; however, the same fault movement may induce thousands of cycles of deformation at lesser strain amplitudes. Intense vibrations generally occur for a minute or less; whereas aftershocks or smaller vibrations may persist intermittently for hours.

b. Water Waves

Water waves are caused by many processes: winds, ships, pressure gradients and submarine disturbances. Wind generated, oscillatory surface waves are of particular interest because they occur constantly in oceans and large lakes.

Oscillatory waves introduce hydrostatic pressure variations in the water column with a magnitude which depends on the wave height and the water depth. The oscillatory pressure variation results in pulsating horizontal and vertical forces on a submerged body. If the body is supported on or within the soil, the pulsating forces, in turn, cause oscillating shearing strains in the soil.

The magnitude of shearing strains that occur is subject to considerable conjecture. However, it seems reasonable to assume that in certain conditions strains may exceed 1.0 percent. The number of cycles of strain may vary from several thousand for a 10-hr period to over 100,000 in a two-week period. These numbers are based on a typical wave period of

10 sec. In general, the large amplitude deformations would be associated with short duration storms.

2. SOIL PROPERTIES

The dynamic characteristics of soil have been studied by various individuals (see Chapter II—Literature Review). These individuals have evaluated the influence of stress history, pressure conditions and loading parameters on the dynamic properties of various cohesive and cohesionless materials. Despite the number of previous investigations, much information pertinent to the analysis of cohesive soil behavior during earthquake and water wave loading either fails to exist or requires clarification.

Four areas are of particular concern to the earthquake and water wave problems. The first involves the actual dynamic characteristics of the soil as the strain amplitude and number of cycles of strain are varied. These results can best be determined by performing laboratory tests on specimens of soil.

The other three areas are concerned with the interpretation of laboratory test results with respect to actual field behavior. Laboratory results have been observed to change continuously with time. A problem thus arises in selecting the time at which laboratory results adequately represent field response. The temperature during the laboratory test generally exceeds that of the soil in its natural environment. This variation in temperature was thought to influence dynamic characteristics. Finally soil specimens used in the laboratory tests are assumed

to represent conditions found in the field. This assumption may be satisfied only if field conditions are known. If these three problems can be resolved in some rational manner, then the field behavior can be estimated from laboratory results.

C. Scope and Approach

The objectives of this investigation were satisfied by performing four types of tests. Three of the tests were accomplished in the laboratory, and the fourth was performed in the field. When possible, the tests simulated conditions which might occur during an earthquake or during water wave loading.

1. LOW AMPLITUDE RESONANT COLUMN TESTS

Low Amplitude Resonant Column Tests were performed to evaluate the effect of time of loading on the dynamic characteristics of soil. Time effects were analyzed by determining intermittently over extended intervals of time the shear wave velocity of a soil. A confining air pressure was held constant throughout the test interval. Test duration at a given confining pressure normally varied from five to seven days, and confining pressures typically ranged from 5 to 60 psi. The strain amplitude during each velocity measurement was less than 0.001 percent.

Ten different soils were tested in this manner. The types of soil varied from clays of high plasticity to silty sands. Soil properties were defined and subsequently used when establishing empirical

prediction schemes.

Low Amplitude Resonant Column Tests also provided information about the variation in dynamic characteristics as testing conditions and material properties changed. On the basis of these results, comparisons were made with analytical equations proposed by others.

2. HIGH AMPLITUDE RESONANT COLUMN TESTS

High Amplitude Resonant Column Tests were performed on six soil specimens to evaluate the effects of strain amplitude and cycles of constant strain amplitude on dynamic characteristics of these materials. Specimens were repeatedly strained for a predetermined number of cycles at a constant strain amplitude. The level of straining varied from 0.001 to 1.0 percent, and the number of cycles ranged from 200 to 100,000.

The high amplitude tests (strain amplitude greater than 0.01 percent) were performed in such a manner that it was possible to evaluate two other responses as well. In particular, once high amplitude cycling ended, the low amplitude properties were measured. Any change in behavior from the low amplitude response noted prior to high amplitude cycling was attributed to the effects of high amplitude cycling. It was noted that this change in behavior due to high amplitude cycling was temporary. The response eventually returned to the level measured prior to high amplitude cycling. The rate of return was monitored.

3. TEMPERATURE EFFECTS

A series of temperature controlled, Low Amplitude Resonant Column Tests were performed to determine the effect of temperature on dynamic characteristics of soil. In these tests two specimens of the same material were tested at two temperatures, 4° and 22°C. The temperatures were maintained at these levels throughout the duration of the test. These two temperatures represented typical conditions that might occur in the laboratory (22°C) and extreme conditions which might occur in the field (4°C) except in permafrost zones.

The test procedure conformed in all other respects to that used to study time effects. For example, confining pressures ranged from 5 to 60 psi; test duration at each pressure level varied from five to seven days; strain amplitudes were less than 0.001 percent.

Seven soils were tested in this manner. Soil types varied from sensitive clays to insensitive silty clays. Two of the materials were prepared in the laboratory, and the rest were obtained from field test sites. Samples from the field were assumed to be undisturbed.

4. FIELD TESTS

As noted previously, laboratory results were assumed to define dynamic conditions found in the field. In four cases the assumption was checked by comparing low amplitude dynamic characteristics measured in the field to dynamic behavior defined by laboratory tests. Ideally the results should be the same.

The cross-hole procedure was utilized when defining dynamic characteristics in the field. The test was performed in such a manner that the shear wave velocity versus depth profile was established without disturbing the soil in the test area. Results represented, therefore, average undisturbed dynamic characteristics of the soil.

Laboratory behavior was based on the results of Low Amplitude Resonant Column Tests. The tests were performed in conjunction with the study of time effects. Soil specimens for the laboratory tests were obtained from the test site by utilizing the best available sampling techniques. Therefore, the samples were thought to be a good representation of field conditions. Any difference between laboratory and field results was attributed to sampling, time or temperature effects.

CHAPTER II

REVIEW OF LITERATURE

Laboratory and field studies have been conducted by other investigators in an attempt to evaluate the dynamic behavior of cohesive soils. Synopses of these studies are found in various technical publications. This chapter reviews the current state of knowledge as reported in these publications.

During the review of literature, it became evident that the effect of temperature on the dynamic behavior of soil had not been previously reported. Various publications did, however, document the effect of temperature on certain "static" properties such as strength, compressibility and creep. On the basis of results from "static" tests, several analogies can be made to dynamic behavior. In view of these analogies, a section in the chapter is devoted to the review of temperature effects on "static" soil properties.

A. Laboratory Test Methods

Various laboratory methods are employed when determining the dynamic properties of soil. These methods utilize assorted test apparatus, e.g., resonant column devices, cyclic triaxial devices, simple shear devices and a variety of other forced and free vibrating systems. In general, the more common laboratory methods can be categorized according to

the frequency of the applied load. On the basis of this criterion, two categories of dynamic, laboratory testing methods are considered: low frequency tests and high frequency tests.

1. LOW FREQUENCY DYNAMIC TESTS

The first category is comprised of those tests which impose low frequency, high amplitude cyclic loads to a soil specimen. These tests are generally performed to ascertain soil response during earthquake type loadings. As a consequence, test frequencies range from less than 1.0 Hz to about 15 Hz, strain amplitudes approach or exceed 1.0 percent, and fewer than 300 cycles of load are applied.

The cyclic test is performed by deforming a specimen of soil in a stress or strain controlled test mechanism. During the test, force versus deformation data are recorded from which the dynamic modulus and damping characteristics can be determined. The response of the soil specimen changes as the stress or strain amplitude and the number of cycles of stress or strain change.

Four general types of low frequency, high amplitude tests are reported in the literature. The four types differ according to the shearing mechanism employed during testing.

a. Cyclic Triaxial Test

The cyclic triaxial test is by far the most documented technique for estimating or approximating soil response at high strain amplitudes. The popularity of the test must be attributed to its apparent simplicity.

The test is nearly identical to the "static" triaxial test. It differs only in that an oscillatory axial or lateral load is applied to the specimen. The form of the oscillatory load ranges from sinusoidal to rectangular, depending on the particular equipment used by the investigator. One important feature of the cyclic triaxial test is that the ratio of horizontal to vertical stresses found in the field, K_o, can be included, thereby providing a better approximation of field behavior.

The behavior of cohesive soils during cyclic triaxial tests is reported by various investigators (Murayama and Shibata, 1960; Seed, 1960; Taylor and Hughes, 1965; Seed and Chan, 1966; Lee and Fitton, 1968; Taylor and Bacchus, 1969; Sherif, et al., 1972; Lashine, 1973).

b. Cyclic Simple Shear—Plane Strain

A cyclic plane strain test is used to evaluate soil response during simple shear. The simple shear loading condition closely approximates that which occurs in the field during an earthquake.

Two types of simple shear devices are used to apply cyclic loads to soils: (1) the simple shear box apparatus and (2) the Norwegian Geotechnical Institute (NGI) device. Unfortunately the configuration and complexity of the shear box apparatus presently preclude testing of cohesive soils.

Various investigators documented the use of the NGI simple shear device to test cohesive soils (Seed and Wilson, 1967; Thiers and Seed, 1968 and 1969). The NGI device, as described by these individuals, induced simple shear in a sample by moving the base of the sample while

restraining the top. The sample was cylindrical in shape and confined in a wire reinforced membrane. The reinforcing in the membrane limited bulging of the sample during axial loading.

It should be noted that the current version of the NGI device does not include provisions for pressurizing the soil specimen. Woods (1973) reported that NGI was developing a new simple shear device that would be contained in a triaxial chamber, thus permitting the specimen to be laterally and axially confined during the test.

c. Cyclic Simple Shear—Torsion

Cyclic torsion is also used to test soil specimens in simple shear. The cyclic torsion test is performed by twisting the top of a cylindrical soil sample in torsion while restraining the bottom. The torsion test is generally performed in a confining chamber.

The cyclic torsion test was described in the literature by at least five groups of researchers (Zeevaert, 1967; Hardin and Drnevich, 1972a and 1972b; Ishihara and Li, 1972; Taylor and Parton, 1973; Yoshimi and OH-Oka, 1973). Of these researchers Zeevaert, Hardin and Drnevich, and Taylor and Parton used the torsion test device to evaluate the response of undisturbed cohesive soils. Other investigators restricted their research to the behavior of cohesionless materials.

d. Forced and Free Vibration Tests

Kovacs, et al. (1971a and 1971b), reported a fourth general method for determining the dynamic behavior of cohesive soils. These

researchers evaluated the behavior of blocks of material during either forced or free vibration.

During forced vibration the top of a 12-in. x 12-in. x 6-in. block of soil was deformed in a cyclic manner while the base of the block was restrained. The walls of the block were not constrained, thus eliminating undesirable side friction that often occurs in shear box devices. The block of soil was loaded axially during a test.

The free vibration test was performed in either of two ways. The first method involved deforming the top of a block laterally and then suddenly removing the force causing deformation. The block oscillated in free vibration, from which damping and modulus characteristics were determined. The second method was performed by placing the block on a shaking table. The response at the top of the block was analyzed as the table was vibrated at different frequencies.

2. HIGH FREQUENCY DYNAMIC TESTS

The second category of laboratory test methods is comprised of tests which impose high frequency, transient or steady state loads to a soil specimen. In general, strain amplitudes associated with these loads are significantly less than those cited for low frequency dynamic tests.

a. Ultrasonic Tests

Ultrasonic tests are commonly performed by individuals interested in the acoustic properties of very soft, marine sediments. The

ultrasonic method is used because the acoustic characteristics of these marine soils can be determined while the soil is retained in the core tube. Other dynamic test methods require that the specimen be removed from the core tube and trimmed to a certain configuration. Unfortunately the low strength of many marine sediments precludes any type of handling.

The ultrasonic test method was described in the literature by various investigators (Shumway, 1960; Lawrence, 1963 and 1965; Bamert, et al., 1965; Nacci and Taylor, 1967; Calhoun and Triandafilidas, 1967; Delflanche, et al., 1971; Silver and Moore, 1972). These individuals performed the test by initiating a pressure pulse at one end or side of a soil specimen and detecting its arrival at the other end or side. The time interval required to traverse the known distance was used to calculate the compression, or sound, wave velocity. Young's modulus for the soil was determined on the basis of the wave velocity, other material properties and specimen configuration.

Characteristics of ultrasonic devices were relatively similar. Frequencies of vibration generally exceeded 10,000 Hz, and amplitudes varied from 0.0001 to 0.00001 percent. A barium titanate crystal was often used to generate the pressure pulse.

The ultrasonic method is readily adapted to various test conditions. If the soil exhibits sufficient strength, the ultrasonic test can be performed in a triaxial chamber (Lawrence, 1963 and 1965; Nacci and Taylor, 1967) or in an odeometer (Calhoun and Triandafilidas, 1967;

Delflanche, et al., 1971). Lawrence (1965) described a torsional version of the ultrasonic device which allowed him to define the shear wave velocity and the shear modulus of the soil.

b. Resonant Column Tests

The resonant column test method is used to determine the shear modulus or shear wave velocity of soil as strain amplitude varies from 0.00001 to 1.0 percent. The low amplitude (less than 0.01 percent) results are typically utilized during the design of machine foundations. The low amplitude velocity or modulus is also used to define the initial portion of the high amplitude hysteresis curve (Hardin and Drnevich, 1972b). The high amplitude (greater than 0.01 percent) modulus or velocity is used to approximate dynamic properties which occur during earthquakes, particularly when the earthquakes are small or when the area of interest is a considerable distance from the probable epicenter.

The resonant column test is performed by vibrating a solid or hollow, cylindrical specimen of soil at its lowest, damped natural frequency from which the stiffness of the material can be determined. Strain amplitudes generated by resonant column test devices vary from 0.00001 to 1.0 percent. The specimen may be vibrated torsionally (Hardin and Richart, 1963), longitudinally (Hall and Richart, 1963) or in bending (Haupt, 1973).

Four different types of resonant column systems are currently being used to define the dynamic properties of the soil: the Wilson device, the Hall device, the Hardin device and the High Amplitude Torsional

Device (HATD). These apparatus have different boundary conditions and different strain amplitude capabilities. For example, the specimens in the Hall device and the HATD are fixed at the base and free at the top; the specimen in the Wilson device vibrates at the base but still approximates a fixed-free system; the specimen in the Hardin device is fixed-free but with the driving system operating against an inertia mass. The maximum strain amplitude applied to the specimen by the Hall and Hardin devices is approximately 0.001 percent; whereas the Wilson device and the HATD can impose up to 1.0 percent strain. For additional details about resonant column devices, see Afifi (1970).

B. Comparison of Laboratory Test Methods

The dynamic testing equipment described in the previous section are used by different research groups to determine dynamic properties of soil, e.g., Young's modulus (E), shear modulus (G), damping ratio (D) or logarithmic decrement (δ), compression wave velocity (V_p) and shear wave velocity (V_s). The significance of the test results depends on parameters controlled during the test. Table 2.1 summarizes some of these parameters for the various devices.

Obviously the best test device is the one that comes closest to duplicating field test conditions. Strain amplitude is generally the most important test parameter. Figure 2.1 correlates strain amplitudes found in the field and strain amplitudes obtained by various test devices. In certain situations no single test device satisfies all strain

TABLE 2.1. COMPARISON OF DYNAMIC TEST METHODS

Type of Test	Soil Property Measured	Stress Conditions During Test	Type of Cyclic Load	Initial Stress on Sample	Typical Test Frequency (Hz)	Typical Strain Amplitude (%)	Typical Number of Cycles
Low Frequency Dynamic Tests							
Cyclic Triaxial	E & D	Pulsating Axial or Confining Pressure	Constant Stress	Triaxially Consolidated	1 - 5	10^{-2} - 10.0	1 - 300
Cyclic Bending	G & D	Simple Sheer	Constant Stress or Strain	Axially Loaded	1 - 3	10^{-2} - 0.5	1 - 300
Cyclic Torsion	G & D	Simple Sheer	Constant Stress or Strain Free Vibration	Triaxially Consolidated	0 - 30	10^{-2} - 1.0	1 - 300
Forced & Free Vibration	G & D	Simple Sheer	Constant Stress or Strain Free Vibration	Axially Loaded	1 - 10	10^{-2} - 3.0	1 - 300
High Frequency Dynamic Tests							
Ultrasonic Tests	V_P & E	Dilational Wave	Constant Stress	Triaxially Consolidated	> 10,000	10^{-4}	Single Transient Pulse
Resonant Column							
Wilson Device	V_S,V_P,E,G	Distortional or Dilational Wave	Constant Strain	Isotropically Consolidated	50 - 500	10^{-4} - 10^{-3}	> 1,000
Hall Device	V_S,G,D	Distortional Wave	Constant Strain	Isotropically Consolidated	80 - 500	10^{-4} - 10^{-3}	1,000
Hardin Device	V_S,G,D	Distortional Wave	Constant Strain	Triaxially Consolidated	200 - 500	10^{-4} - 10^{-3}	3,000
HATD	V_S,G,D	Distortional Wave	Constant Strain	Isotropically Consolidated	25 - 100	10^{-3} - 10^{-1}	300 - 100,000

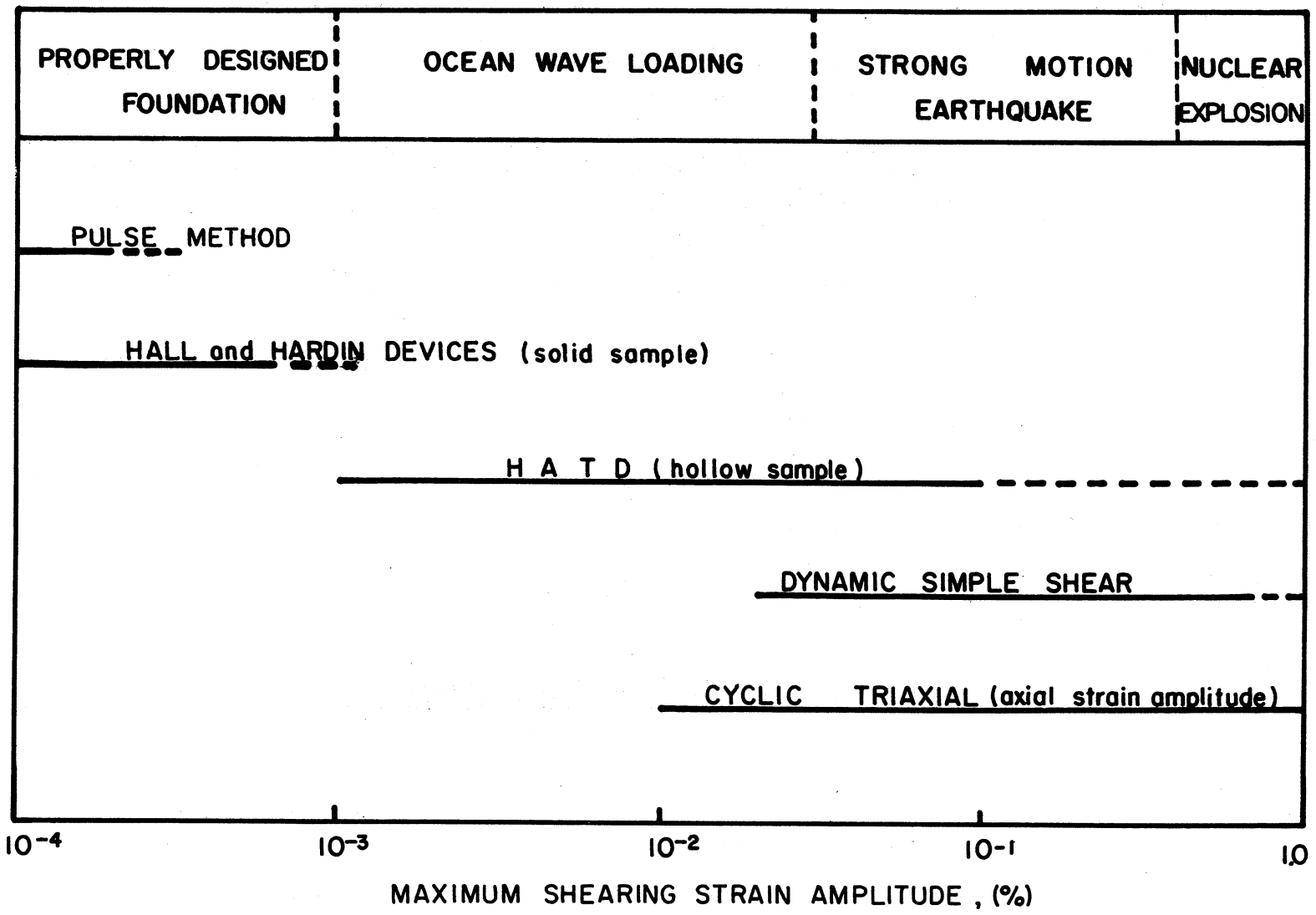

Figure 2.1. Laboratory methods for determining stress-strain properties of soil (after Silver and Moore, 1972).

amplitude requirements. For example when the hysteresis curve is desired for a certain soil, then a high frequency, low amplitude test device is used to define the initial portion of the curve, and a low frequency, high amplitude device is used to define the rest (Hardin and Drnevich, 1972b).

C. Laboratory Test Results

Most cohesive soils exhibit curvilinear stress-strain characteristics. At low amplitudes response is nearly linear, and as strain amplitudes increase, response becomes more nonlinear. Dynamic studies can usually be differentiated on this basis. Certain studies deal exclusively with low amplitude response; others treat high amplitude, nonlinear response. A few studies include both zones.

1. LINEAR DYNAMIC RESPONSE

Soils behave linearly, or nearly elastically, when strain amplitudes during cycling are low, e.g., less than 0.0001 percent. The characteristics of elastic soil behavior are described in the literature by various investigators.

Afifi (1970) reviewed in detail the primary parameters which influence the behavior of cohesive soils at low strain amplitudes. These factors included the effects of void ratio and confining pressure, the effects of the static state of shearing stress, the effects of stress history, the effects of strain amplitude, and time dependent effects.

The following paragraphs summarize the current state of knowledge regarding low amplitude behavior, as described by Afifi and others.

a. Effects of Void Ratio and Confining Pressure

Void ratio and confining pressure effects were evaluated by Hardin and Black (1968) and Humphries and Wahls (1968). On the basis of their results, Hardin and Black suggested that for a first estimate of the low amplitude shear modulus of normally consolidated clays with low surface activity, the following equation could be used

$$G_{max} = \frac{1230\,(2.97 - e)^2}{1 + e}\,\bar{\sigma}_o^{0.5} \qquad (2.1)$$

where G_{max} = shear modulus (psi) at low strain amplitudes

e = void ratio

$\bar{\sigma}_o$ = average effective confining pressure (psi).

In the closure to their article, Hardin and Black (1969) introduced the effects of preconsolidation by modifying the previous equation to the form

$$G_{max} = \frac{1230\,(2.97 - e)^2\,(OCR)^K}{1 + e}\,\bar{\sigma}_o^{0.5} \qquad (2.2)$$

where OCR = overconsolidation ratio

K = function of plasticity index (Figure 2.2).

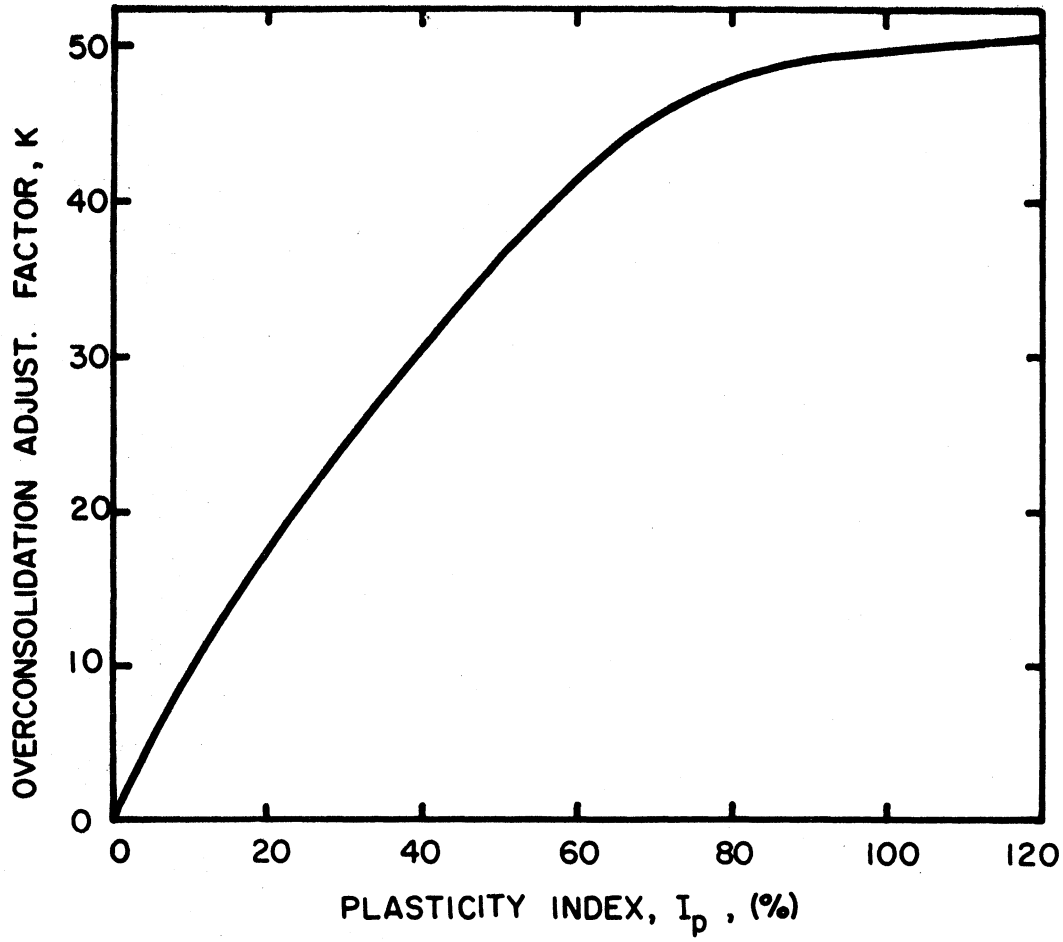

Figure 2.2. Overconsolidation adjustment factor, K, versus plasticity index, I_p (after Hardin and Black, 1969).

Humphries and Wahls (1968) defined the low amplitude modulus, G_{max}, by a complicated series of terms obtained after performing a regression analysis on data from several test cases. The relationship, which resulted from the regression analysis, equated G_{max} to void ratio, confining pressure and overconsolidation terms. This relationship was defined as follows for kaolinite

$$G_{max} = 235.839\bar{\sigma}_o - 2.3267\bar{\sigma}_o^2 + 0.01091\bar{\sigma}_o^3 - 11938.4e + 17655.6 \qquad (2.3)$$

and for bentonite

$$G_{max} = 16.44\bar{\sigma}_o - 0.3681\bar{\sigma}_o^2 + 0.00252\bar{\sigma}_o^3 - 1943e + 24.01 \ln(OCR) + 5060.7 \quad (2.4)$$

Once again G_{max} and $\bar{\sigma}_o$ were defined in psi.

Two things should be noted about Eqs. (2.3 and 2.4). The accuracy of the test method is considerably less than that implied by the equations. In addition during more recent work at North Carolina State University, Marcuson and Wahls (1972) used the Hardin and Black form of the relationship.

b. Effects of Static State of Shearing Stress

Hardin and Black (1966 and 1968) considered the effect of the state of shearing stress as identified by the octahedral shearing stress, τ_o. These investigators reported that for saturated kaolinite clay, G_{max} was essentially independent of the octahedral shearing stress.

c. Effects of Stress History

Humphries and Wahls (1968) and Afifi and Richart (1973) described the effects of stress history on G_{max}. Humphries and Wahls reported that for remolded kaolinite clay the effect of overconsolidation was accounted for by the effects of void ratio and confining pressure. Afifi and Richart noted similar behavior as long as the overconsolidation ratio was less than 3.0. Hardin and Black (1969) introduced the effect of overconsolidation for all soils as shown in Eq. (2.2). The

effect of overconsolidation, as described by Hardin and Black, increased as the plasticity index and the overconsolidation ratio increased.

d. Effects of Strain Amplitude

The effects of high strain amplitudes are considered in detail in Section ? of this chapter. In theory there is a level of strain amplitude below which variations in amplitude have no influence on quantitative results. Hardin and Drnevich (1972b) suggested that G could be considered independent of strain amplitude when strain amplitudes were less than 0.0025 percent. Humphries and Wahls (1968) showed that when the strain amplitude was increased from 0.015 to 0.06 percent, the shear modulus decreased by about 5 percent for kaolinite and only slightly for bentonite.

e. Time Dependent Effects

The stiffness of cohesive soils, as described by G_{max}, was observed to increase with time (Richart, 1961; Lawrence, 1965; Hardin and Black, 1968; Humphries and Wahls, 1968; Gray and Kashmeeri, 1971; Stokoe, 1972; Afifi and Richart, 1973; Stokoe and Richart, 1973a and 1973b). The quantitative rate, extent and characteristics of stiffness buildup were described in detail in three of these publications.

Gray and Kashmeeri (1971) reported the increase in G_{max} with time for unconfined specimens of compacted clay. Tests were performed with a resonant column device on samples of Vicksburg silty clay, Vicksburg fat clay, kaolinite and a bentonite-silica flour mixture. The rate of

increase in G_{max} was shown to vary with clay mineralogy, water content and pore water electrolyte content. Specific details of this study can be found in Kashmeeri (1969).

The effects of time on modulus change for undisturbed cohesive soils were described in detail by Marcuson and Wahls (1972) and Afifi and Richart (1973). Both groups reported that the G_{max} of kaolinite clays increased continuously with time. The rate of increase was found to be linear on a semi-logarithmic plot. Neither group believed that the entire change in G_{max} could be attributed to changes in specimen void ratio.

Marcuson and Wahls introduced the following two equations to account for the time effects. For kaolinite

$$G_r = 1.0 + 0.046 \log T_r \qquad (2.5)$$

and for bentonite

$$G_r = 1.0 + 0.242 \log T_r \qquad (2.6)$$

where T_r = time of interest divided by time to 100 percent primary consolidation

G_r = modulus at time of interest divided by the modulus at 100 percent primary consolidation

For kaolinite G_r typically increased by approximately 5 percent per T_r when the void ratio was held constant and by 10 percent when the void ratio was allowed to change. Constant void ratio conditions were achieved by performing a consolidated, undrained dynamic test; varying

void ratio conditions were obtained by performing a drained, dynamic test. For bentonite the G_r increase was 40 and 25 percent for the drained and undrained case, repectively.

Afifi and Richart showed that the increase in G_{max} varied with the grain size of the material. They normalized the modulus increase by dividing the modulus change per log cycle of time by the modulus at 1000 min, $\Delta G/G_{1000}$, and plotted this ratio against the logarithm of the mean particle size, D_{50} (Figure 2.3). As can be seen in Figure 2.3, the normalized rate of increase varied from 5 to 17 percent for clay size soils. It can be shown that $\Delta G/G_{1000}$ is analogous to the G_r term defined by Marcuson and Wahls.

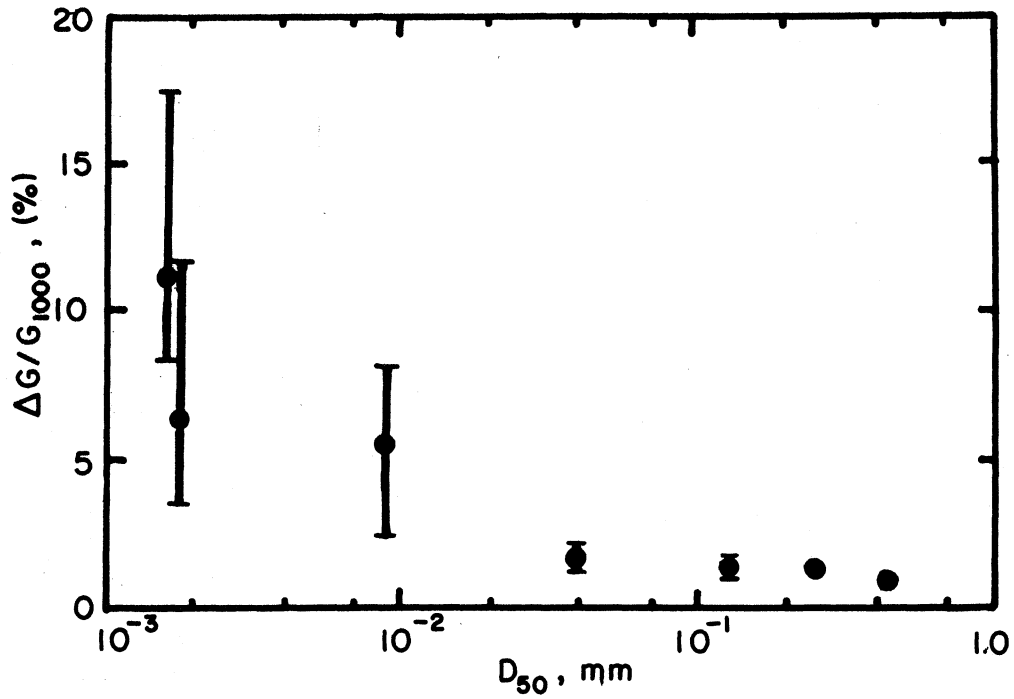

Figure 2.3. Diagram relating average values of time dependent increase in modulus, $\Delta G/G_{1000}$, to mean grain diameter, D_{50} (after Afifi and Richart, 1973).

Afifi (1970) also reported that an increase in the confining pressure of 10 psi typically destroyed 15 to 20 percent of the stiffness developed under a constant effective pressure for 10,000 min. This loss in stiffness was regained during secondary modulus increase at the higher confining pressure.

2. NONLINEAR DYNAMIC RESPONSE

Nonlinear dynamic response was described in the literature by various researchers. The results of these investigations suggested that several parameters, in addition to strain amplitude, influenced soil behavior during high amplitude cycling. These other parameters having a significant influence included cycles of strain, confining pressure, void ratio and degree of saturation. Factors of lesser importance were initial shear stress and test frequency. Test results also suggested that the strength characteristics of soils after high amplitude straining differed from those measured before straining.

The parameters affecting high amplitude results and the consequences of high amplitude straining are considered in the following paragraphs.

a. Strain Amplitude Effects

The shear modulus of cohesive soils was noted to decrease as the strain amplitude increased (Taylor and Hughes, 1965; Krizek and Franklin, 1967 and 1968; Thiers and Seed, 1968; Kovacs, et al., 1971a and 1971b; Hardin and Drnevich, 1972a; Taylor and Parton, 1973). The

magnitude of modulus change was considered in detail by Hardin and Drnevich (1972b) and Seed and Idriss (1970).

Hardin and Drnevich presented a comprehensive study of the non-linear response of cohesive soils. These authors used a modified hyperbolic stress-strain relationship to model curvilinear behavior. On the basis of this idealization a relationship was developed for defining modulus, G, at any strain amplitude, i.e.,

$$G = \frac{G_{max}}{1 + \gamma_h} \tag{2.7}$$

where G_{max} defines the initial tangent modulus of the hyperbolic curve and γ_h is the hyperbolic strain.

Hardin and Drnevich suggested empirical and experimental methods for defining terms in Equation 2.7. The initial tangent modulus, G_{max}, was determined experimentally by performing a low amplitude resonant column test or empirically by Eqs. (2.1) or (2.2). The hyperbolic strain was defined by

$$\gamma_h = \frac{\gamma}{\gamma_r}\left[1 + a \exp\left(\frac{-b\gamma}{\gamma_r}\right)\right] \tag{2.8}$$

where $\gamma_r = \frac{\tau_{max}}{G_{max}}$

γ = shearing strain

τ_{max} = shearing stress at failure

$a = 1.0 + 0.25 (\log N)$ (2.9)

N = number of cycles of strain

b = 1.3 for cohesive soils

The factor in the brackets of Eq. (2.8) distorted the strain scale to make the real stress-strain curve have a hyperbolic shape.

The shearing stress at failure, τ_{max}, was determined experimentally by performing a consolidated undrained triaxial test or empirically by the following equation

$$\tau_{max} = \left\{ \left[\frac{(1 + K_o)}{2} \bar{\sigma}_1 \sin\phi' + c'\cos\phi' \right]^2 - \left[\frac{(1 - K_o)}{2} \bar{\sigma}_1 \right]^2 \right\}^{1/2} \qquad (2.10)$$

where K_o = coefficient of lateral earth pressure at rest

$\bar{\sigma}_1$ = vertical effective stress

c', ϕ' = static strength parameters in terms of effective stress.

For experimental determination, τ_{max} should be defined at the same strain rate as G_{max}.

Seed and Idriss (1970) described an empirical relationship between shear modulus, G, and shearing strain, γ. These authors normalized G with respect to undrained strength, S_u, and expressed the logarithm of the quotient, G/S_u, as a function of the logarithm of γ. The normalization technique accounted for variations in results which are due to clay characteristics. Test data obtained by a number of other investigators and expressed in this form are plotted in Figure 2.4.

b. Cycles Effects

The number of cycles of stress or strain influenced test results during high amplitude loading. For a given value of peak strain, Thiers

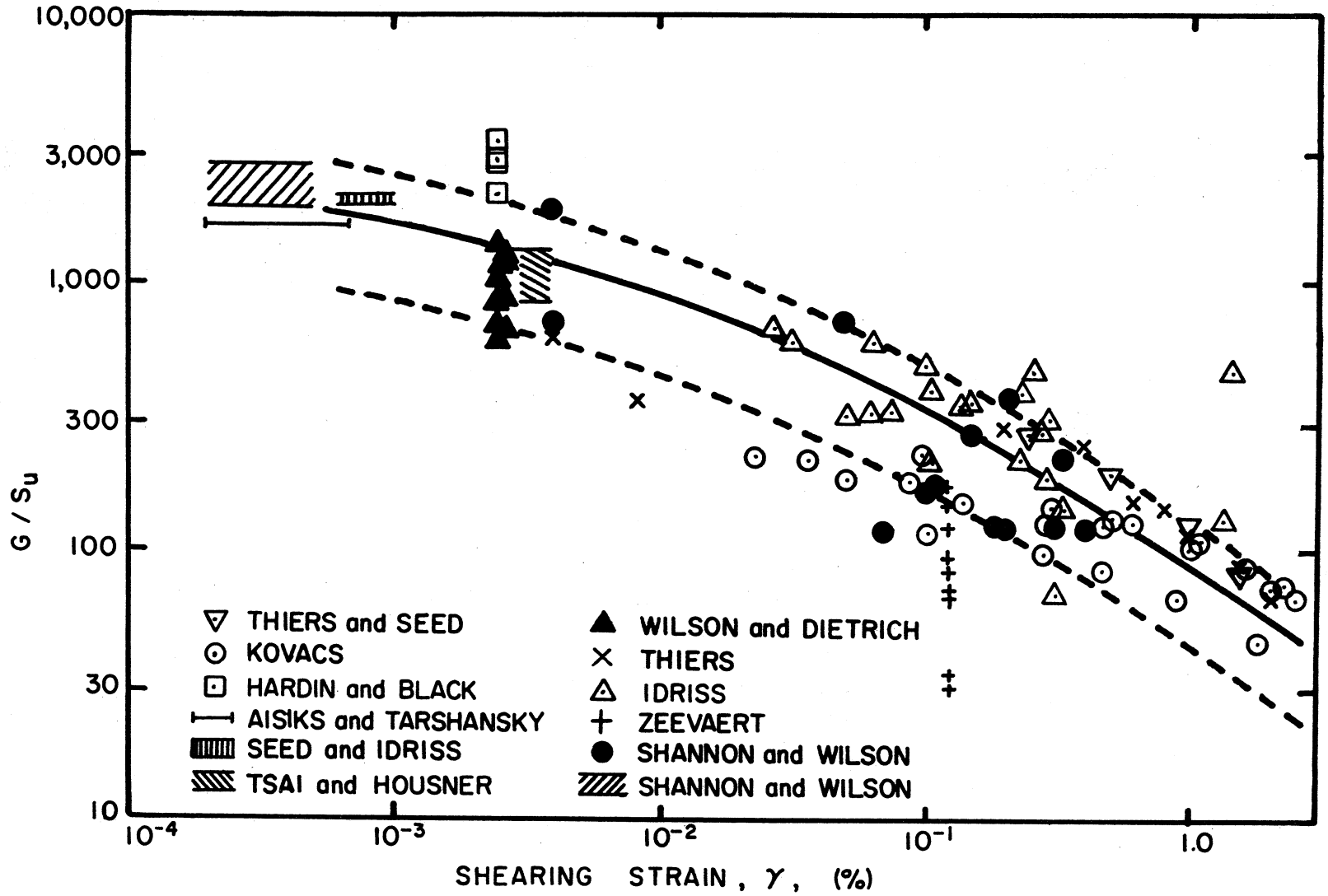

Figure 2.4. Normalized shear modulus, G/S_u, versus shearing strain, γ (after Seed and Idriss), 1970).

and Seed (1968) showed that G decreased about 30 percent during the first 50 cycles of loading; above 50 cycles the moduli were nearly constant. Kovacs, et al. (1971a), described similar behavior. Their results suggested that cycles had a more pronounced effect on G as the strain amplitude increased. Taylor and Hughes (1965) also noted that the effect of cycles was more pronounced during the first 100 cycles.

Hardin and Drnevich (1972a) tended to minimize the significance of the cycle effect. These authors modified their relationships slightly to account for cycles as shown in Eqs. (2.8) and (2.9). They suggested that the large decrease reported by some individuals might have been due to the lack of sample confinement. The next paragraph considers the confinement aspect in greater detail.

c. Confining Pressure Effects

The mean principal stress, or confining pressure, contributed significantly to high amplitude behavior (Hardin and Drnevich, 1972a). At low strain amplitudes G_{max} varied with the 0.5 power of the mean principal stress. As the amplitude increased, the G depended mainly on the strength of the soil, which was more nearly a function of $\bar{\sigma}_o$ to the first power. Consequently, the rate of decrease in G with increasing strain amplitude decreased as the mean principal stress increased. Hardin and Drnevich believed that some of the very low values of G reported in the literature by others may have been due to the lack of confining pressure.

d. Void Ratio and Degree of Saturation Effects

Hardin and Drnevich (1972a) also considered the effect of void ratio and degree of saturation. Their test results showed that changes in void ratio affected G_{max} dramatically. At high strain amplitudes however, they reported that it was difficult to determined the void ratio effect because of the influence of strength and other factors on the shape of the modulus-strain amplitude plot.

A limited number of test results presented by Kovacs, et al. (1971a), showed a decrease in G as the water content increased. Water content was directly related to void ratio because the specimens were prepared at nearly constant degrees of saturation. The influence of water content seemed to be less pronounced as the strain amplitude increased.

The degree of saturation influenced the magnitude of the low amplitude modulus; therefore, Hardin and Drnevich (1972a) believed that it was also an important factor during high amplitude straining. In one example cited by Hardin and Drnevich, the low amplitude modulus decreased from 38 to 17 ksi when the degree of saturation was increased from 70 to 100 percent.

e. Initial Shearing Stress and Frequency Effects

Hardin and Drnevich also discussed the effects of initial shearing stresses on the modulus measured during high amplitude straining. They reported that the effects of initial states of stress involving deviatoric components were small, particularly after 10 cycles of complete

stress reversal.

Several researches evaluated the effects of test frequency on measured dynamic response. Hardin and Drnevich found that an increase in frequency above 0.1 Hz had relatively minor effects on G as long as data were analyzed properly. Taylor and Hughes (1965) reported the opposite effect. For their tests, an increase in frequency from 0.08 to 10 Hz caused a 17 percent decrease in G. Unfortunately Taylor and Hughes did not provide data to substantiate their findings. Hardin and Drnevich (1972a) and Converse (1961) suggested that soil creep becomes more important for lower frequency testing.

f. Effect on Soil Strength After Cycling

Various investigators described the effects of high amplitude cycling on the static strength of the soil (Seed, 1960; Seed and Chan, 1966; Thiers and Seed, 1969; Sherif, et al., 1972). These researchers showed that as the stress or strain amplitude of the dynamic load increased, the static strength after the end of dynamic loading decreased. Also as the number of cycles (at a constant high amplitude stress or strain) increased, the static strength decreased. Sherif, et al., reported that the overconsolidation ratio had an appreciable influence on the static behavior after high amplitude cycling.

Hardin and Drnevich (1972a) described the behavior of soils after high amplitude straining in terms of the low amplitude shear modulus, G_{max}. The low amplitude modulus was used as an indicator of soil strength. The results of their tests showed that high amplitude cycling

caused a decrease in G_{max} measured immediately after high amplitude cycling. Subsequently G_{max} increased with time.

D. Field Test Methods

Two general types of field tests are used to determine the dynamic properties of soils: borehole tests and surface tests. Both tests establish the in situ characteristics of the soil; i.e., the properties are determined without removing the soil from the ground. The borehole test is performed by locating transducers in a borehole and generating waves in another borehole or at the surface. The wave propagation velocity is determined by analyzing the output from the transducers with respect to time and distance. The surface test is performed in a similar manner by recording wave propagation velocities on the soil surface. Murphy (1972) discusses the relative merits of both methods.

1. BOREHOLE TESTS

Borehole tests are described in the literature by various individuals (Miller and Brown, 1972; Murphy, 1972; Schwarz and Musser, 1972; Stokoe and Woods, 1972). These individuals determined the low amplitude, shear wave velocity of the soil by performing cross-hole and down-hole tests.

a. Cross-Hole Tests

Either of two procedures are used to perform cross-hole tests. The first procedure involves recording the time for a transient wave to

traverse a known distance. The known distance is generally the horizontal spacing between two boreholes extended to similar depths. The other procedure involves measuring the phase of a steady-state vibration in two adjacent holes. The steady state vibration is generally introduced in a third hole.

Stokoe and Woods (1972) described in detail the procedure for performing the transient type of cross-hole test and the methods for interpreting test results. These authors also provided a thorough review of literature related to cross-hole work. Miller and Brown (1972) reported current efforts of Shannon and Wilson, Inc., to develop the steady state procedure.

b. Down-Hole Test

The down-hole test is performed by generating a transient vibration at the soil surface and recording the time required for the vibration to reach a certain depth in the borehole, from which the shear wave velocity can be defined as a function of depth. Schwarz and Musser (1972) reviewed the procedures for performing the test, enhancing wave characteristics and interpreting results.

2. SURFACE TESTS

Surface test methods are used to define the low amplitude, compression and shear wave velocities for a soil layer. Richart, et al. (1970), described the three general procedures for performing surface tests, i.e., seismic reflection, seismic refraction and steady state

vibration methods.

Two new surface test methods have evolved since 1970. Schwarz and Musser (1972) described a method for determining the shear wave velocity by performing a refraction test. The test procedure was nearly identical to that reported by Richart, et al., for conducting seismic refraction test; however, the shear wave velocity rather than the compression wave velocity was established. Pang (1972) used an oscillator to vibrate model footings on the soil surface. The response of the oscillator and footing was analyzed as a single degree of freedom system, from which a representative shear modulus at some depth beneath the footing was deduced. The load and size of the footing were varied to investigate the change in dynamic characteristics with depth.

E. Comparison of Laboratory and Field Test Results

Both field and laboratory techniques are of considerable value in the study of dynamic properties of soil. It is necessary, however, to ascertain the validity of the laboratory method with respect to the field method. To satisfy this need, several investigators compared V_s measured in the laboratory to V_s measured in the field.

Stokoe and Woods (1972) and Stokoe and Richart (1973a and 1973b) summarized several field versus laboratory comparisons. In these studies the cross-hole method was used to determine the low amplitude shear wave velocity in the field, and various low amplitude resonant column devices were used to define laboratory results. The laboratory tests

were performed on samples of soil obtained from the borehole used in the cross-hole test.

In nearly every case Stokoe and his co-authors found that the field value of V_s exceeded the laboratory value of V_s. The difference tended to increase as the grain size decreased. These investigators attributed the difference to secondary time effects that occurred during the laboratory test. The laboratory value of V_s increased continuously with time; therefore, the percentage of difference between laboratory and field result depended on the time at which the laboratory result was selected. When these authors selected a velocity which corresponded to the age of the material deposit, the discrepancy between laboratory and field data was small.

Cunny and Fry (1973) presented a more discouraging comparison between field and laboratory results. According to these researchers, the laboratory velocities were above and below the field velocities. They suggested that occurrence was random and could be attributed to the variability in test specimens. It should be noted that the writers used surface seismic methods which tended to average results more than borehole methods. The writers also based their conclusions on data from several different test devices. They also failed to record the secondary increase in V_s as described by many other individuals.

F. Temperature Effects

The effects of temperature on the mechanical properties of soil

has received significantly less attention than other aspects of soil behavior, except in terms of freezing and thawing of soils. A limited number of temperature studies on unfrozen soils are documented in the literature. The results of these studies suggest that temperature influences soil behavior more than has generally been realized.

Mitchell (1969) presented a comprehensive review of the current state of knowledge regarding the effect of temperature on the engineering properties and behavior of soil. The ensuing paragraphs summarize the contents of this paper and other related works.

1. VOLUME CHANGE AND PORE PRESSURE EFFECTS

Saturated cohesive soils undergo volume or pore pressure variations when subjected to fluctuations in temperature. Campanella and Mitchell (1968) expressed the magnitude of change in terms of the thermal expansion of soil components, the compressibility of the soil and physico-chemical effects.

The results of drained triaxial tests performed on cohesive soils by Campanella and Mitchell showed that significant permanent volume decreases occurred during initial temperature increases. The amount of volume change was given by

$$(\Delta V)_{\Delta T} = \alpha_w V_w \Delta T + \alpha_s V_{ss} \Delta T - \alpha_s V_m \Delta T - (\Delta V_{st})_{\Delta T} \qquad (2.11)$$

where α_s = thermal coefficient of cubical expansion of mineral solids

α_w = thermal coefficient of expansion of soil water

V_w = volume of pore water

V_{ss} = volume of mineral solids

V_m = total volume of soil specimen

ΔV_{st} = change in volume of soil structure due to temperature induced changes in interparticle forces

ΔT = change in temperature

It was also noted that the water drained during the first heating cycle was irrecoverable. The effect of heating followed by cooling at a constant confining pressure was thought to have had the same effect as overconsolidation, i.e., pressure increase followed by unloading.

In their study Campanella and Mitchell reported that during undrained conditions, with constant confining pressure, a change in temperature caused a change in pore water pressure. The magnitude of pressure change was given by

$$\Delta u = \frac{n\Delta T\,(\alpha_s - \alpha_w) + \alpha_{st}\,\Delta T}{m_v + n m_w} \qquad (2.12)$$

where n = porosity

α_{st} = physico-chemical temperature coefficient of soil structure volume change

m_v = compressibility of soil structure

m_w = compressibility of water

The most important factors controlling pore pressure change were the thermal expansion of water, the compressibility of the soil structure and the initial effective stress. The results of a limited number of laboratory tests suggested that for each 1°F change in temperature, the

pore pressure changed by about 0.75 to 1.0 percent of the initial effective stress. The magnitude of change increased as the material became more compressible.

Several investigators evaluated the effect of temperature on the consolidation characteristics of clay. Plum and Esrig (1969) reported that at low confining pressures (less than 30 psi) the compressibility of the clay increased as the temperature increased but that at higher confining pressures little difference in compressibility was apparent. They also noted the apparent overconsolidation due to temperature change (Figure 2.5). Campanella and Mitchell also showed that compressibility was independent of temperature when confining pressures exceeded about 30 psi. Finn (1951) and Paaswell (1967) observed an increase in the rate of consolidation as the temperature increased. The increase was attributed to a reduction in pore-water viscosity. Secondary rates of compression were shown to increase as the temperature increased (Gray, 1936; Buisman, 1936; Lo, 1961; Campanella and Mitchell, 1968).

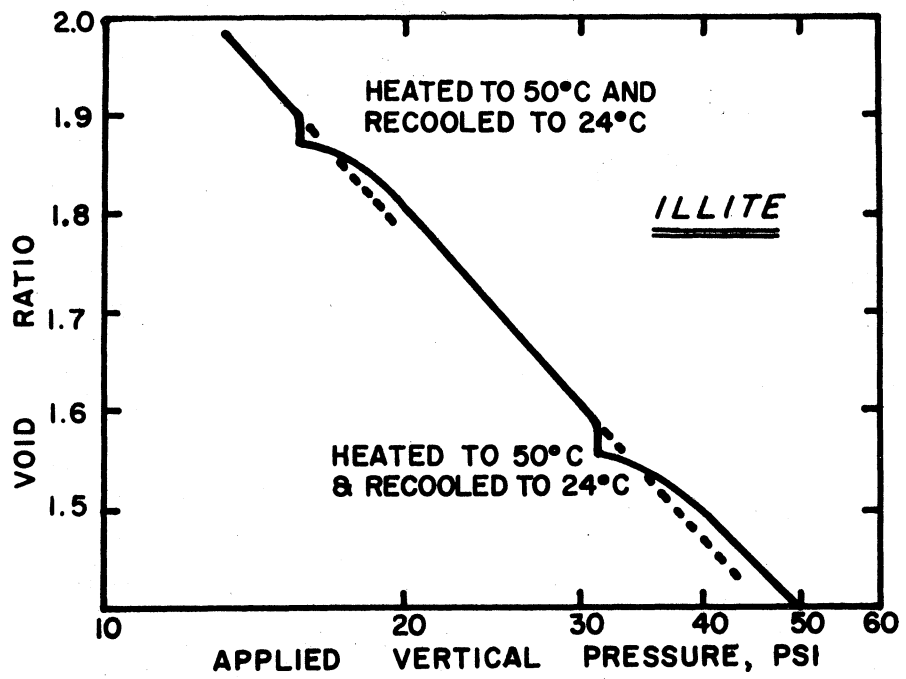

Figure 2.5. Effect of heating and cooling on the results of an odeometer test (after Plum and Esrig, 1969).

2. DOUBLE LAYER REPULSIVE FORCES

Various individuals attempted to explain temperature effects on the basis of changes in interparticle repulsive forces caused by fluctuations in temperatures. Mitchell (1969) showed, however, that when the dielectric constant is assumed to vary with temperature, then repulsive forces are unchanged over the temperature range from 0° to 100°C. He suggested that the interparticle contact structure may be weakened because of the increased thermal energy of constitutent atoms.

Scott and Ko (1969) believed that certain temperature effects may be related to interparticle repulsive forces in the Gouy-Chapman double layer; however, they suggested that the effectiveness of this mechanism would depend on the structure of the soil. An oriented structure of parallel platelets was expected to respond to temperature

changes in a manner more analogous to theory than would a randomly oriented clay structure.

The previously mentioned theoretical predictions were generally based on certain assumptions about the dielectric constant of soil water and its variation with temperature. Unfortunately these assumptions were not fully substantiated by data. Consequently, it was difficult to make quantitative estimates of double layer behavior. The qualitative behavior presented by Mitchell was still considered realistic.

3. ELASTICITY

The elastic properties of engineering materials are temperature dependent. It seems reasonable, therefore, that the elastic characteristics of soil should also be temperature dependent. However, prior to the work presented by Murayama (1969) no data substantiated this assumption.

Murayama employed a rheological model to investigate the effect of temperature on equivalent elastic constants of clay. His model included two Hookean springs, a viscous dashpot and a friction damping element (Figure 2.6). The dashpot coefficient was derived by using rate process theory, i.e.,

$$\eta = \frac{\sigma_2}{2A\ \sigma_{20}\ \sinh\left(\frac{B\sigma_2}{\sigma_{20}}\right)} \qquad (2.13)$$

where σ_2 = stress on dashpot

σ_{20} = initial stress on dashpot

A, B = constants that depend on soil structure and temperature

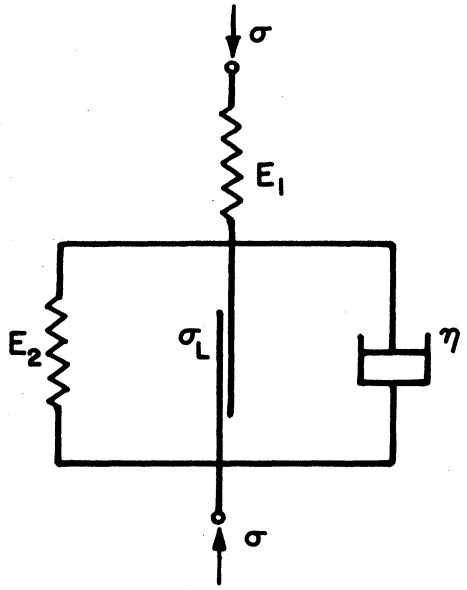

Figure 2.6. Mechanical model of clay skeleton (after Murayama, 1969).

Murayama performed stress relaxation tests to determine the effect of temperature on the two spring constants. Results of these tests showed that as temperature increased the elastic moduli, E_1 and E_2, decreased. The dependence of moduli on temperature is shown in Figure 2.7 for initial strains of less than 2.0 percent.

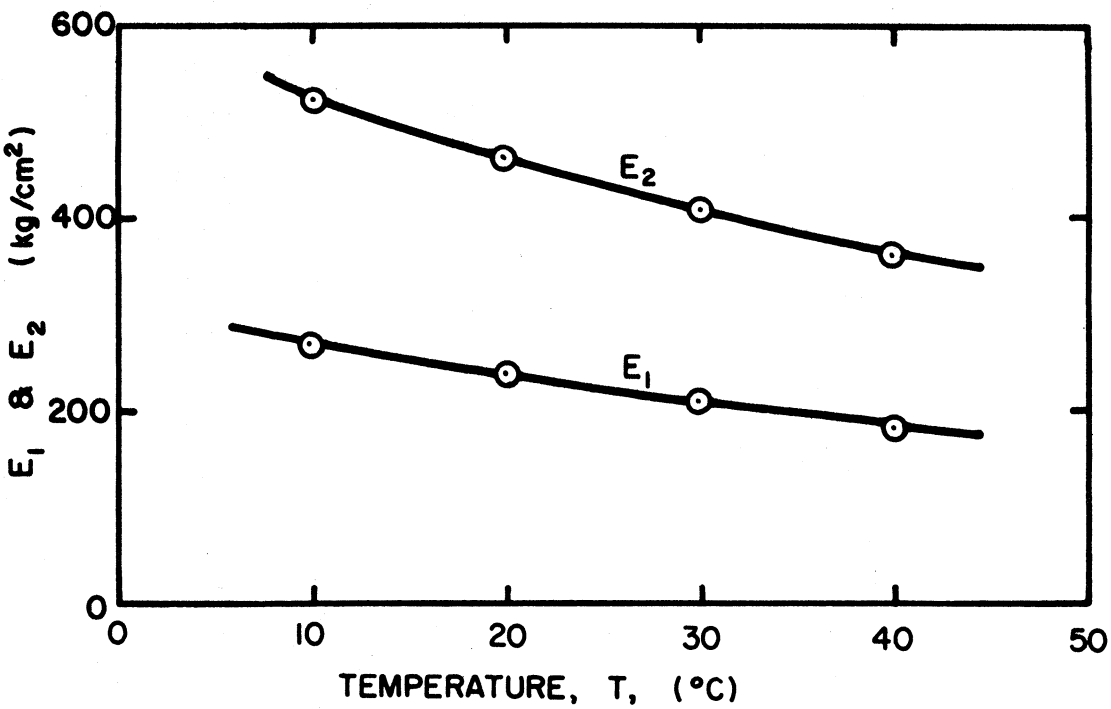

Figure 2.7. Relationship between E_1 and E_2 and temperature (after Murayama, 1969).

Murayama also plotted the initial stress versus the initial strain for the stress relaxation tests (Figure 2.8). If the slopes of the straight line portions of these curves were taken to represent elastic modulus of the material, then it could be deduced that the modulus decreased as temperature increased. Mitchell added that this latter observation did not depend on the validity of the rheologic model.

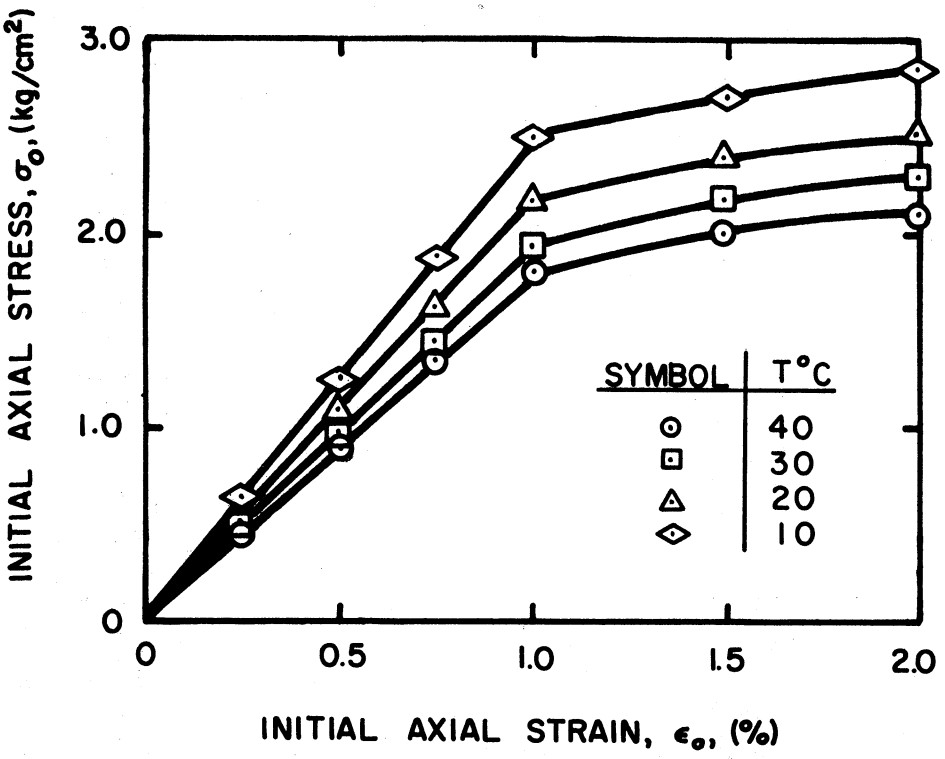

Figure 2.8. Relationship between initial axial stress and initially applied axial strain (after Murayama, 1969).

CHAPTER III

TEST EQUIPMENT

Various test devices and electronic equipment were used to accomplish the laboratory and field tests described herein. The following two sections give a detailed description of the apparatus and equipment. In several cases the apparatus were modified to facilitate control of different parameters. These modifications are also described in detail.

A. Laboratory Equipment

Four different types of laboratory tests were conducted to determine dynamic properties of soils. Each type of test utilized a different apparatus and a different setup. Although the apparatus differed in configuration, each involved a resonant column system with fixed-free boundary conditions. Pertinent calibration data for the laboratory equipment are defined in Appendix B.

Certain other laboratory equipment were used to determine the static properties of soils. These equipment are described in Appendix C.

1. LOW AMPLITUDE RESONANT COLUMN TESTS—HALL DEVICE

The Hall resonant column device was used to measure the shear wave velocity of soil specimens. Velocity measurements were made by torsionally oscillating a specimen and determining frequency of oscillation at resonance. Once resonance was defined, the velocity was determined by

substituting the frequency at resonance (f_n), the specimen height (h) and a function, β, into the following equation

$$V_s = \frac{2\pi h}{\beta} * f_n \tag{3.1}$$

The function β was defined by

$$\beta \tan \beta = \frac{I}{I_o} \tag{3.2}$$

where I = mass moment of inertia of the soil specimen

I_o = mass moment of inertia of the drive system and top cap

Afifi (1970) described in detail the derivation of Eqs. (3.1) and (3.2).

Amplitudes of torsional strain varied from 0.0005 to 0.001 percent. As will be shown in a later chapter, this level of strain was within the "elastic" range of soil response; consequently, V_s did not vary with strain amplitude or number of cycles of strain.

a. Test Device

The Hall test device drove a soil specimen in torsion with a single coil-magnet arrangement (Figure 3.1). A second coil-magnet system located at 90 degrees to the drive system generated an output voltage which varied in proportion to the rotational velocity of the top cap. The resonant frequency of the top cap-soil system was found by varying the frequency of the signal to the drive coil until the pickup coil generated maximum voltage output.

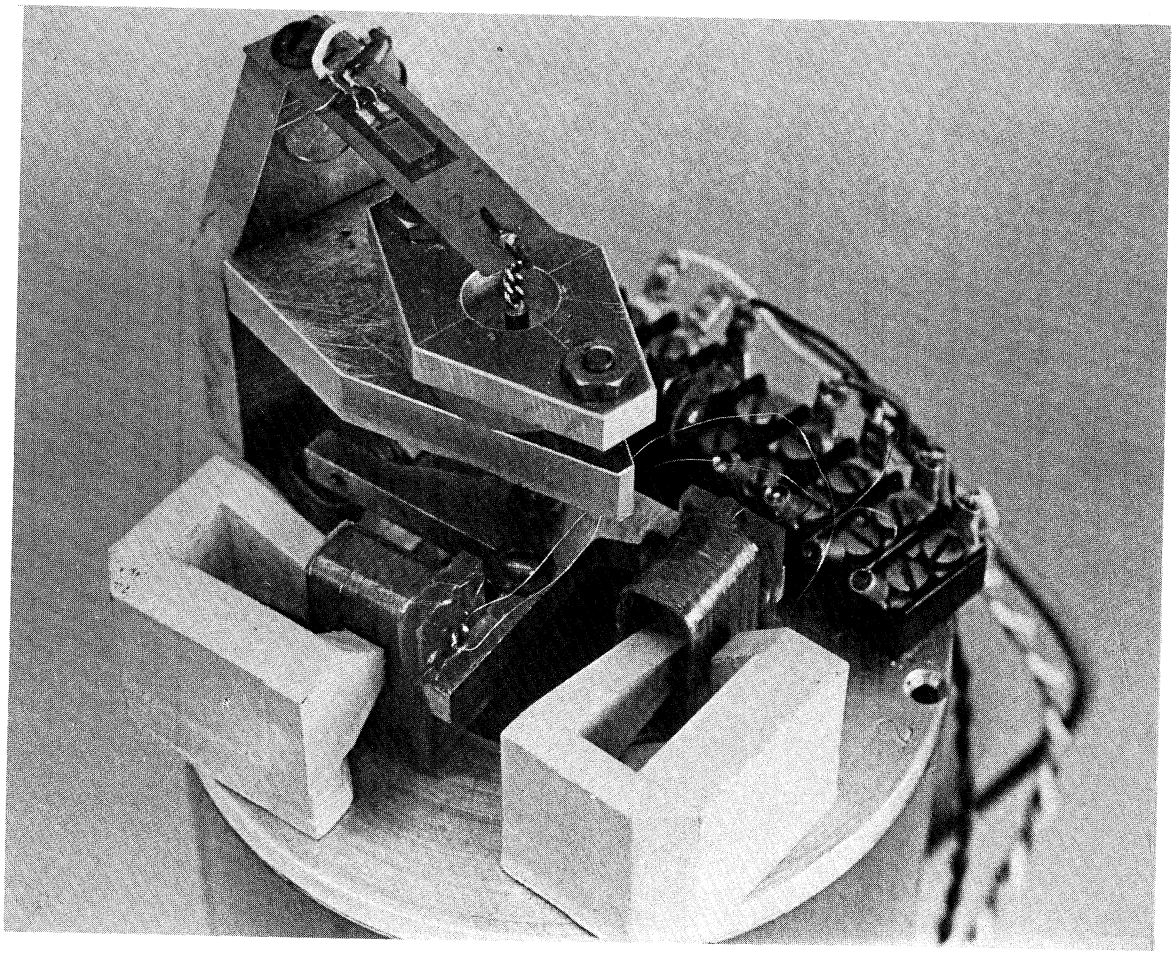

Figure 3.1. Coil-magnet driving system for Hall device.

Other components of the Hall device included the magnet support cylinder and strain-gaged length measuring device, the water bath and base plate, the top cap, and the confining chamber. Figure 3.2 shows these components. The magnet support cylinder is a 4.0 in. diameter (1/4 in. wall thickness) piece of steel pipe which not only supports the drive and pickup magnets at the proper heights but also acts as the reaction body against which the electro-magnetic driving forces are generated. The magnet support cylinder also serves as the fixed reference from which axial deformations are measured.

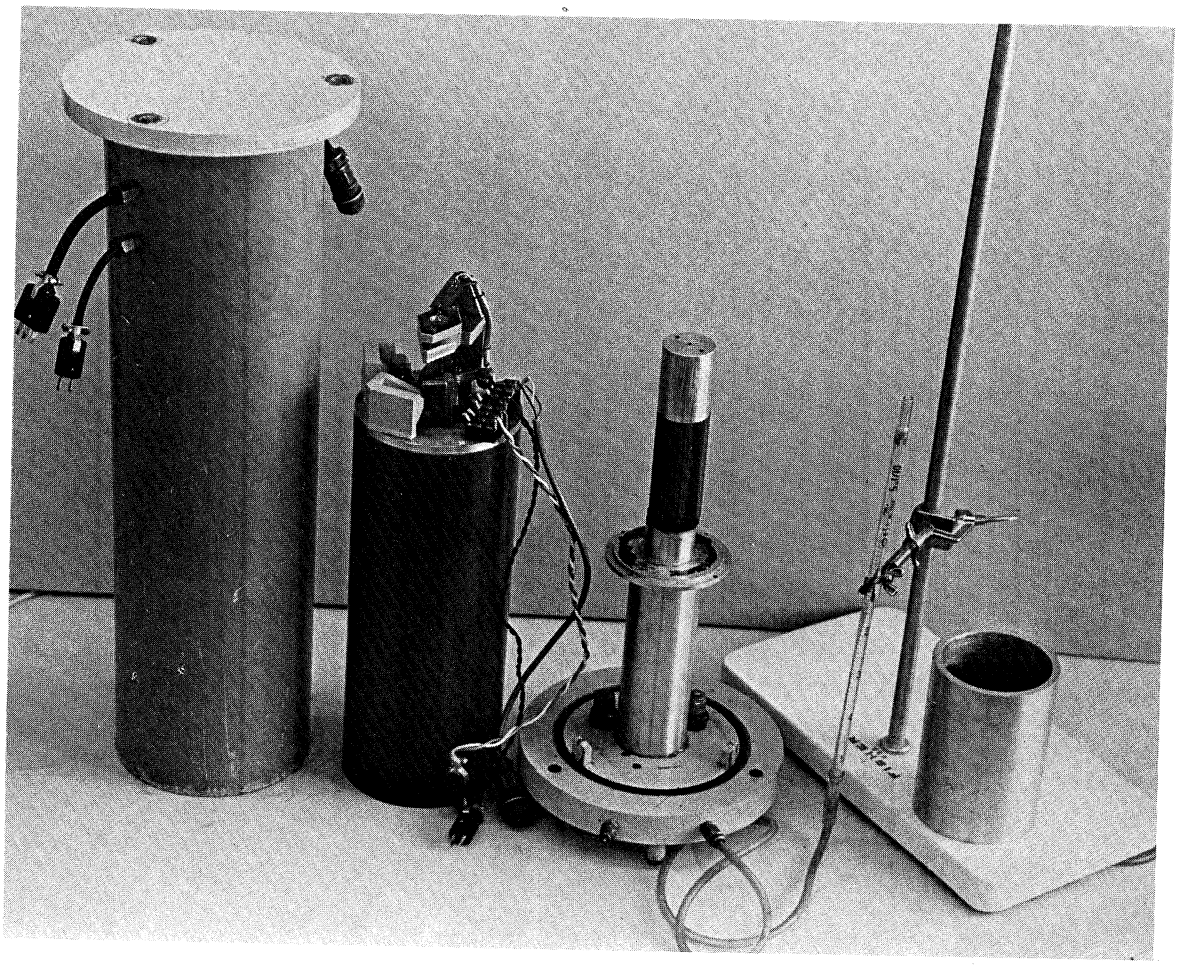

Figure 3.2. Components of Hall device.

The drive and pickup system were attached to the top of a membrane enclosed, cylindrical specimen of soil. Samples were typically 3.6 cm in diameter and 8.0 cm tall. The strain-gaged cantilever was also attached to the top cap. The cantilever was used to measure axial deformations as testing proceeded.

The specimen and drive-pickup system were enclosed in a cylindrical pressure chamber. The chamber permitted the soil specimen to be pressurized to over 100 psi. The confining pressure was hydrostatic, i.e., principal stresses were equal. A drainage line, which passed through

the base of the chamber to the sample, allowed control of sample drainage during the test.

The system was pressurized with air. Air was used because electrical connections within the drive-pickup system precluded the use of water. A water bath was placed around the sample to limit air migration through the sample. Ramifications of air migration are considered in greater detail in Chapter VII (Discussion of Results).

For a more detailed description of the Hall device, see Afifi (1970). Afifi not only provided an excellent written description of the Hall device, but he also included plan drawings and photographs of principal components.

b. Device Modifications

Two modifications were performed on the Hall device during the course of this investigation. The first change involved adding another drive coil-magnet arrangement; the second involved the removal of the long pedestal on the base plate. Figure 3.3 shows the new configuration of the device.

The dual coil-magnet drive system was intended to produce a balanced, torsional driving force on the top of the soil sample. The second coil was located, therefore, diametrically opposite the first drive coil-magnet. The modification was performed when it became evident that certain stiff materials did not behave as expected during testing. It was concluded that the unbalanced driving force introduced a bending

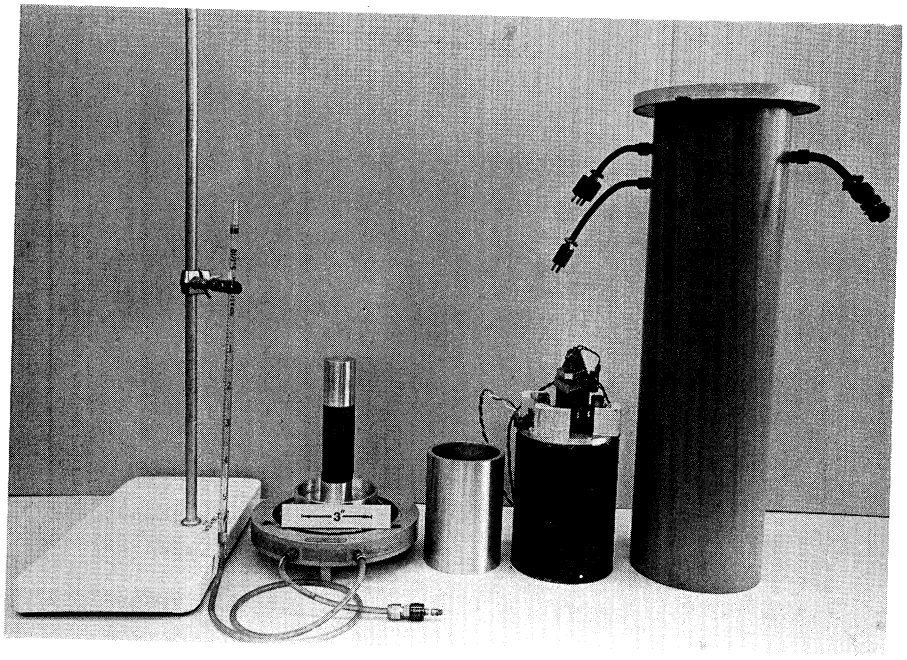

(a)
Overall view of modified Hall device.

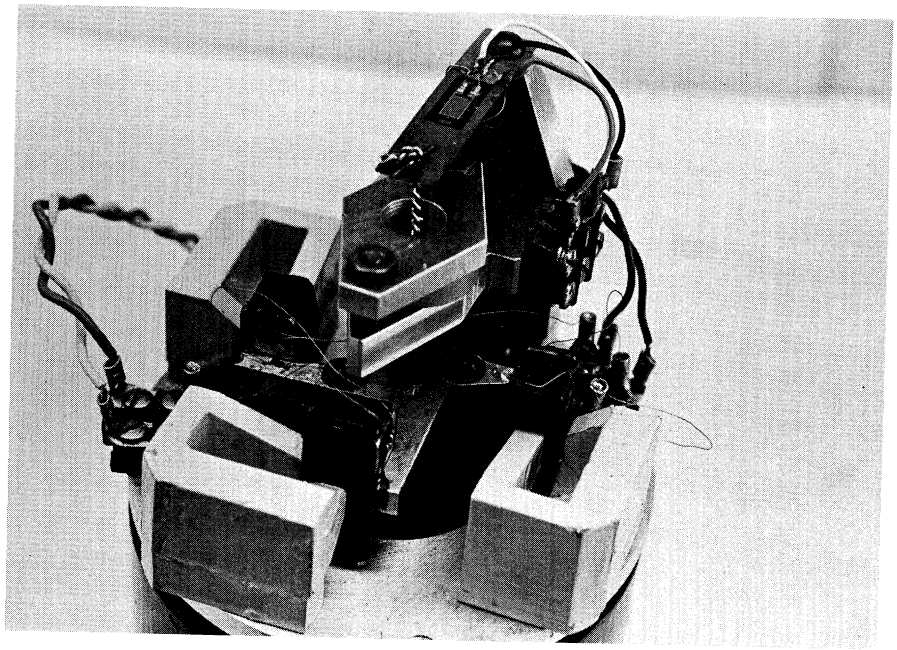

(b)
Close-up of modified drive system.

Figure 3.3. Modified Hall device

motion as well as a twisting motion. The bending motion caused excessively high material damping, which in turn, affected the resolution of the resonant frequency. Once this modification was made, the system behaved as expected.

The second modification was performed to reduce the lengths of the sample support pedestal and the magnet support cylinder. The original Hall device was designed to accommodate specimens between 8 and 28 cm tall. When a short specimen (8.0 cm) was tested, a 20-cm long support pedestal was used. However, it was thought that when the 20-cm pedestal was used the entire soil and support pedestal might participate in torsional motion if the sample were sufficiently rigid. Such behavior was not desired because it would introduce unknown specimen fixity at the base. To avoid this uncertainty, the long pedestal was replaced by a shorter pedestal, and the magnet support stand was shortened to accommodate the new overall length of the pedestal plus sample height.

c. Test Setup

Figures 3.4 and 3.5 show pictorially and schematically the test equipment utilized when performing low amplitude resonant tests with a Hall device. As observed in these figures, the primary components of the setup included a signal generator, a frequency counter, an oscilloscope, a RMS voltmeter and a strain indicator. Table 3.1 gives the manufacturers and model numbers for these devices. The setup also included a switching box that enabled any of five resonant column devices (four Hall and one Hardin) to be operated using the same electronic equipment.

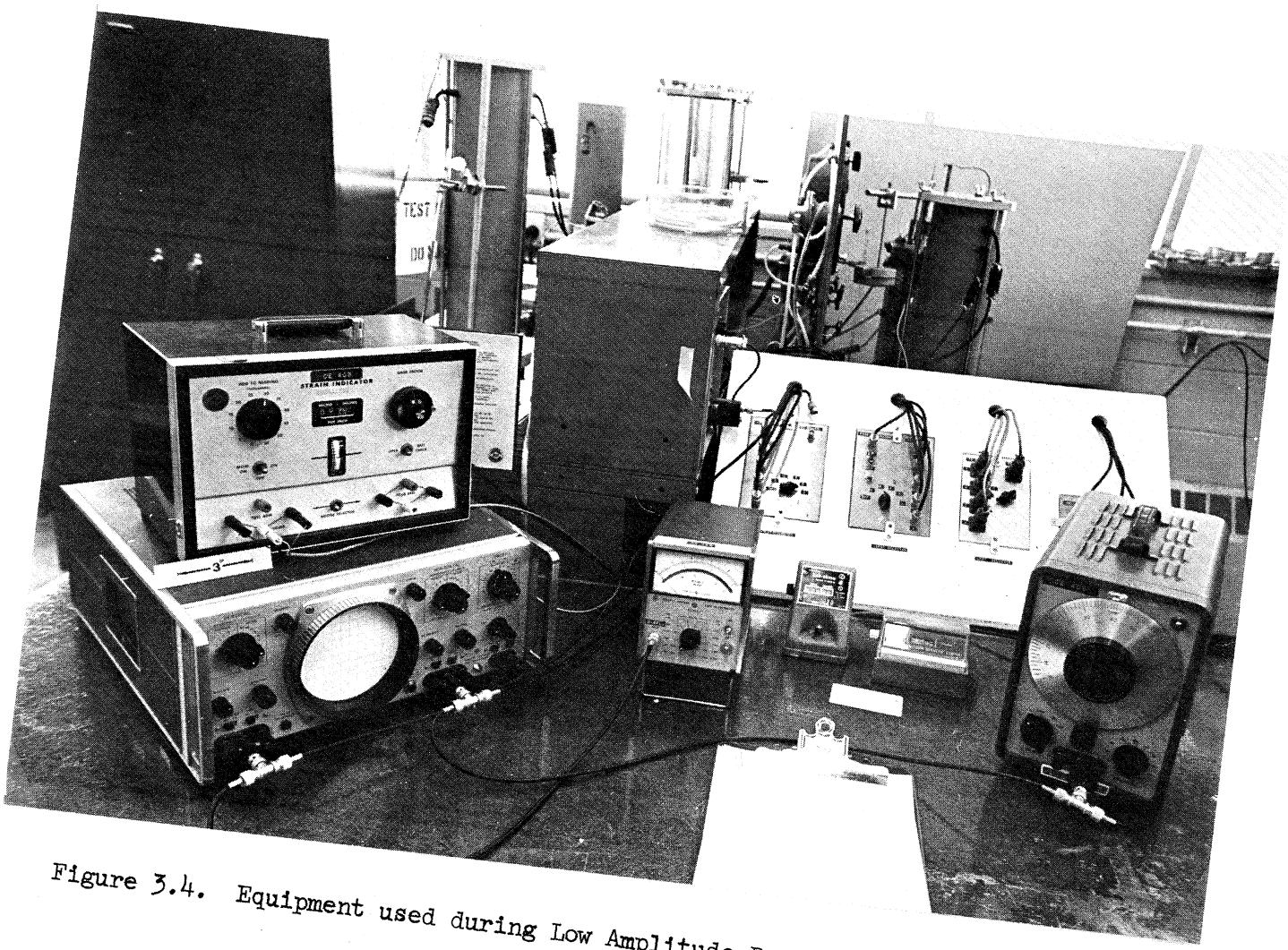

Figure 3.4. Equipment used during Low Amplitude Resonant Column Tests.

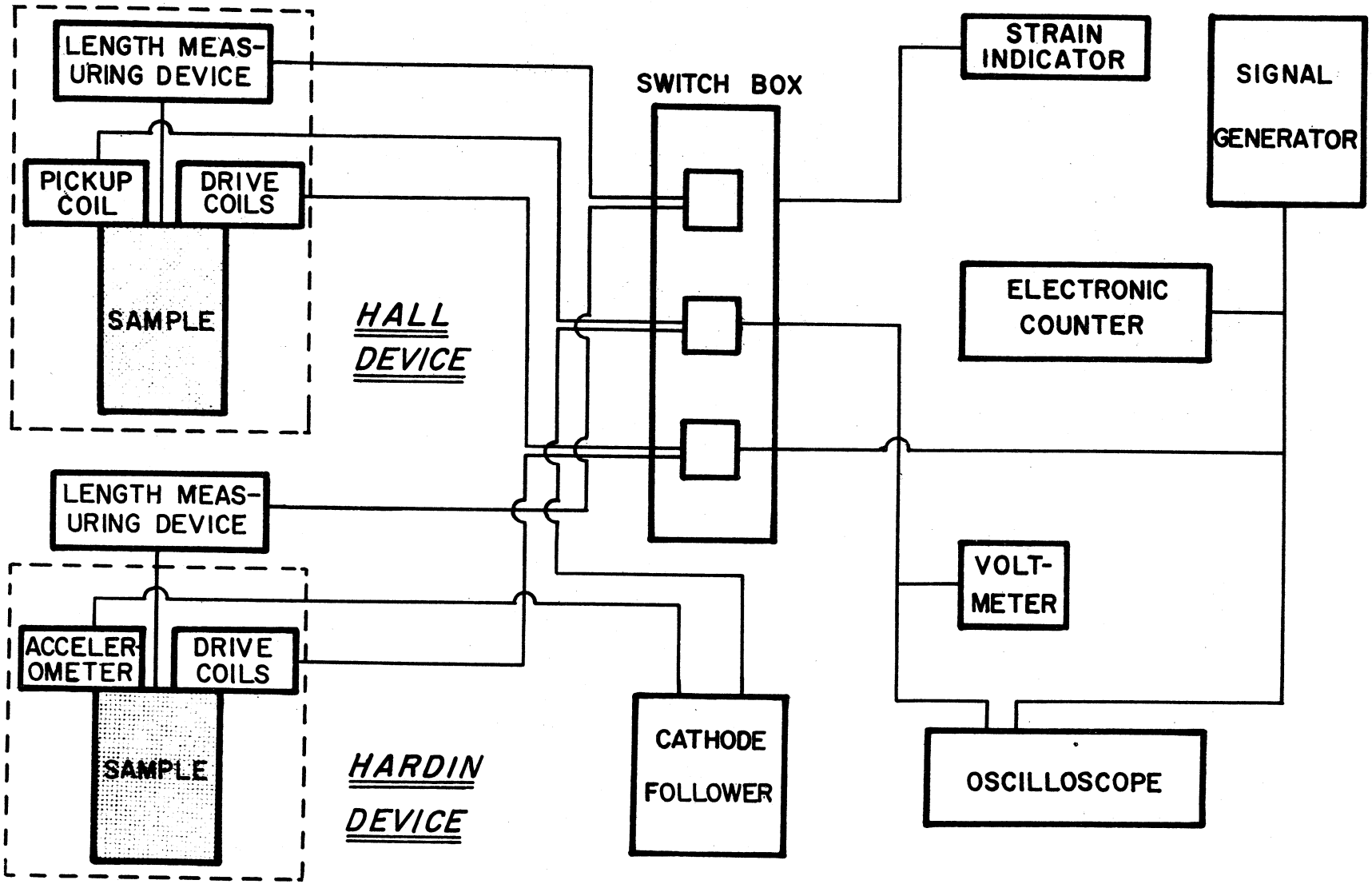

Figure 3.5. Schematic diagram of equipment used during Low Amplitude Resonant Column Test.

TABLE 3.1. EQUIPMENT USED TO PERFORM LOW AMPLITUDE RESONANT COLUMN TESTS

Equipment	Manufacturer	Model No.	Function
Signal Generator (Wide Range Audio Oscillator)	Hewlett-Packard	200D	Supplies sinusoidal input voltage to drive coils. Variable frequency and amplitude.
Frequency Counter (Digital Electronic Counter)	Hewlett-Packard	5223L	Measures and displays period of input signal.
Oscilloscope	Hewlett-Packard	130G	Displays input versus output signal as lissajous figure.
RMS Voltmeter	Hewlett-Packard	400E	Measures and displays level of output voltage from pickup coil (or cathode follower.)*
Strain Indicator	Baldwin-Lima-Hamilton	Type 20	Supplies input voltage to strain-gage bridge circuit on cantilever measuring device. Indicates change in output voltage.
Cathode Follower*	Columbia Research Laboratory	4000	Conditions output signal from accelerometer (converts capacitance to voltage).

*Note: used only with Hardin device.

During the Hall tests, the signal generator supplied a sinusoidal voltage to the driving coils. The frequency counter displayed the period (or frequency) of the input signal. System response was monitored on the oscilloscope. The voltmeter indicated the level of voltage produced by the pickup coil. The strain indicator supplied the input voltage to the strain-gage bridge circuit on the cantilever displacement measuring device and indicated the resulting output voltage for the circuit. A change in indicator reading represented a change in axial length of the specimen.

The oscilloscope actually displayed the vectoral sum of the output voltage from the pickup coil and the input voltage from the signal generator. This X-Y plot was called a lissajous figure. At resonance the X-Y plot theoretically degenerated from an ellipse to a straight line. Prior to the addition of the second drive coil and magnet, lissajous closure did not always occur as theory suggested. A balanced driving system corrected this situation.

Although the oscilloscope displayed the level of voltage produced by the pickup coil, a voltmeter was used to obtain a more accurate indication of voltage magnitude. The magnitude of voltage was related to the amplitude of torsional motion at the top cap. The amplitude of torsion reflected, in turn, the level of shearing strain in the sample. By increasing or decreasing the size of the input signal to the drive coil, the amplitude of output motion changed proportionately. Consequently, a desired strain amplitude was achieved by adjusting the level of the

input signal. In general stiffer materials required a larger input signal to achieve the same strain amplitude.

A second use of the voltmeter arose during determination of resonance. The pickup coil generated maximum output at resonance. Voltage from the pickup coil increased until the resonance and then decreased as resonance was passed. For the Hall tests the point of maximum voltage coincided with the point at which the lissajous figure closed. When the lissajous figure did not close as discussed above, the peak voltage method still served as a precise means of defining the resonance point.

2. LOW AMPLITUDE RESONANT COLUMN TESTS—HARDIN DEVICE

The Hardin device exhibits many of the same characteristics as described for the Hall device. Its principal use was also to measure the shear wave velocity of soil. Measurements were accomplished by torsionally oscillating specimens of soil at different frequencies until resonance was defined. Once the resonant frequency was known, the shear wave velocity was determined by evaluating a series of differential equations in terms of the resonant frequency and the material properties. For additional details about the method for analyzing results, see Hardin and Music (1965). Amplitudes of torsional motion were approximately the same as those noted for the Hall device.

a. Test Device

As mentioned above, the Hardin device had many of the same characteristics as the Hall device (Figure 3.6). Two coil-magnet systems,

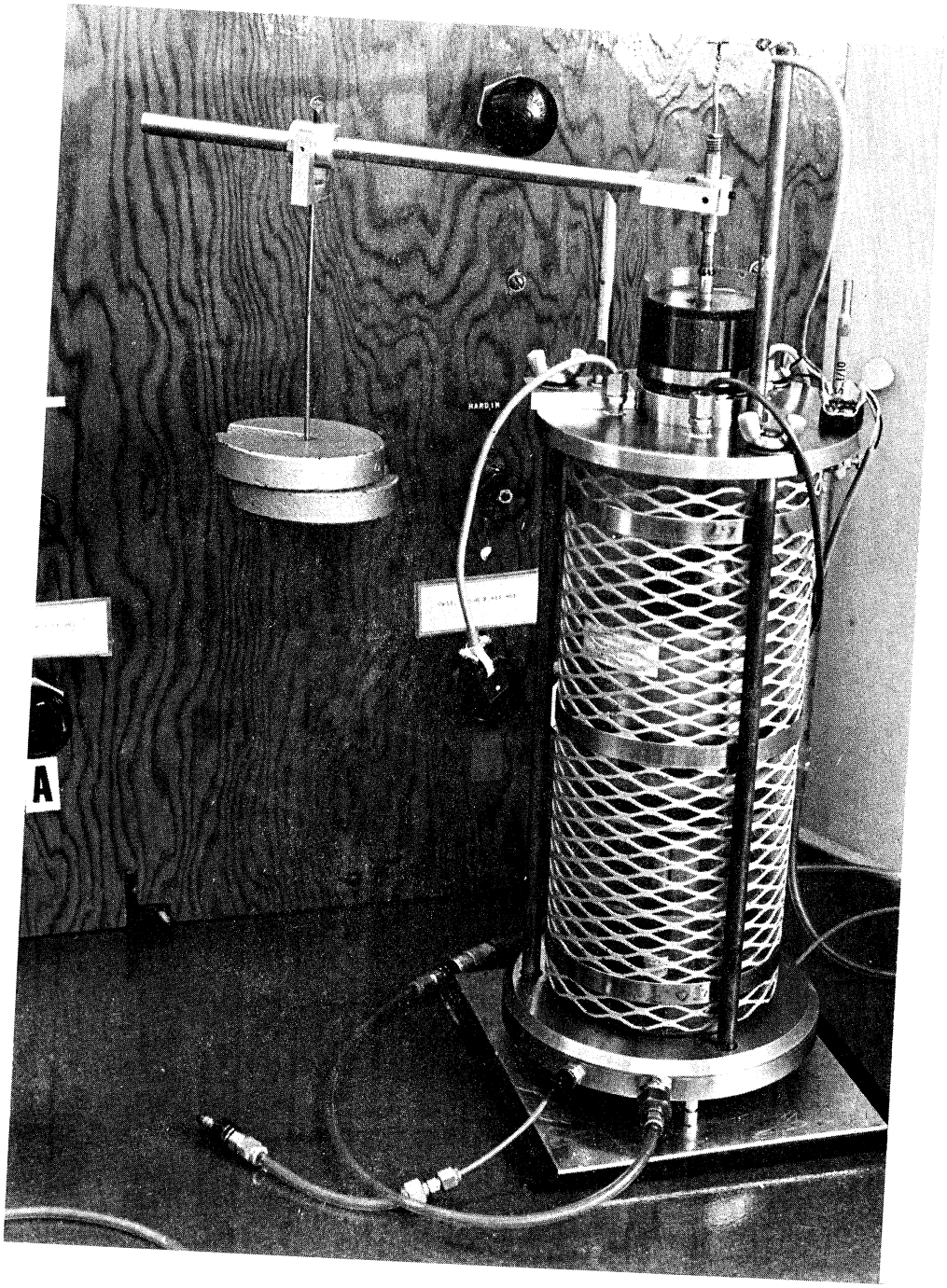

Figure 3.6. Hardin test device.

located diametrically opposite one another, drove the top cap-soil system; a single piezoelectric accelerometer positioned between the two coils produced an output signal which varied in proportion to the acceleration of the top cap-soil system. The driving system was fixed on top of a 3.6-cm diameter by 8.0-cm tall soil specimen. A pressure chamber which enclosed the specimen-drive system allowed the specimen to be pressurized to over 100 psi. Once again air was used to pressurize the specimen; and, consequently, a water bath was placed around the sample to limit air migration. Drainage within the sample was controlled by opening and closing a line connected to the specimen base. A strain-gaged cantilever measuring device was attached to the drive system to monitor axial deformations of the sample.

The Hardin device differed from the Hall device in one significant aspect. The mechanical configuration of the Hardin device was such that soil specimens could be confined anisotropically. By changing the position of a counterbalancing weight, an increase or decrease in axial pressure occurred without a corresponding change in lateral confinement. Such anisotropic loading conditions were thought to represent in situ stress conditions more accurately.

For additional details about the mechanical and electrical configuration of the Hardin device, see Hardin and Music (1965) or Hardin and Mossbarger (1966).

b. Test Setup

The Hardin test utilized virtually the same equipment as did the

Hall setup. The Hardin setup differed only in its use of a cathode follower to condition the output from the accelerometer prior to displaying the signal on the oscilloscope. Figures 3.4 and 3.5 also show the location of the cathode follower. Table 3.1 gives the model number and manufacturer of the cathode follower.

Although a lissajous figure was displayed on the screen of the oscilloscope, the lissajous figure no longer degenerated into a straight line at resonance. The figure behaved differently because the output voltage varied in proportion to system acceleration. Resonance was defined, therefore, by monitoring the voltage output from the accelerometer on the RMS voltmeter. Peak voltage defined the point of resonance.

3. HIGH AMPLITUDE RESONANT COLUMN TESTS—HATD

The High Amplitude Test Device, designated as the HATD by its designer, V. P. Drnevich, was used to determine the behavior of cohesive soils during high amplitude, torsional oscillations. Once again, the material parameter measured was shear wave velocity.

Many characteristics of the HATD were similar to characteristics of the Hall device. A cylindrical sample of soil was oscillated torsionally at different frequencies until resonance was reached. Once the resonant frequency was defined, Eqs. (3.1) and (3.2) were used, in conjunction with material properties, to establish V_s. Drnevich (1967) reviewed the theory of operation in detail.

As its name implies, the HATD was capable of generating low to high

amplitude shearing strains. For tests described herein, amplitudes ranged from 0.005 to 1.0 percent. The actual value at the upper limit of strain differed according to the amount of energy required to achieve system resonance. The amount of energy depended, in turn, on the frequency at resonance and the material stiffness. The average shearing strain in the specimen was defined by

$$\gamma_{\theta z} = \frac{1}{2}\frac{\bar{r}}{h} * \theta_{pp} * 100\% \qquad (3.3)$$

where $\gamma_{\theta z}$ = average shearing strain in torsion (%)—zero to peak

$\bar{r}$ = the average sample radius

h = sample height

θ_{pp} = the angle (peak to peak) through which the top twists (radians)

Two features enhanced the characteristics of the HATD with respect to the objectives of this research effort. The resonant frequencies of most soil specimens when tested in the HATD varied from 20 to 100 Hz. In general lower frequencies occurred at higher strain amplitudes. This feature permitted application of a limited number of strain cycles. For example, at a frequency of 50 Hz, 20 sec of testing elapsed before 1000 cycles of strain were applied to the specimen. It was possible, therefore, to study the effect of cycles on V_s as cycles increased from 200 to 100,000.

The second desirable feature of the HATD involved sample configuration. The HATD accommodated a hollow, cylindrical specimen. The

advantage of the hollow sample arose when strain distribution within the specimen was considered. As a solid, cylindrical sample was twisted torsionally, shearing strains developed. These strains varied from zero at the sample center to a maximum at the periphery. In contrast the hollow specimen exhibited a more uniform distribution of shearing strain across the sample wall during similar twisting. As the wall thickness decreased in the hollow cylinder, the magnitude of variation also decreased. Practical aspects associated with trimming and specimen setup dictated a finite wall thickness in actual application. Strain amplitudes varied by only a factor of two for samples tested in this investigation.

a. Test Device

Figure 3.7 shows the drive system for the HATD. Once again a coil-magnet system was used to twist the sample. The HATD, however, employed four sets of coil-magnets to drive the specimen in torsion. An accelerometer mounted on the drive system generated an output signal which varied according to sample motion.

The drive system was attached to the top of a membrane enclosed, hollow, cylindrical soil specimen. Inner and outer dimensions of the cylinder were 3.0 and 6.0 cm, respectively. The sample height was 12.0 cm. A Linear Variable Differential Transformer (LVDT) was attached to the top of the drive system. The LVDT enabled axial deformations to be monitored during the test.

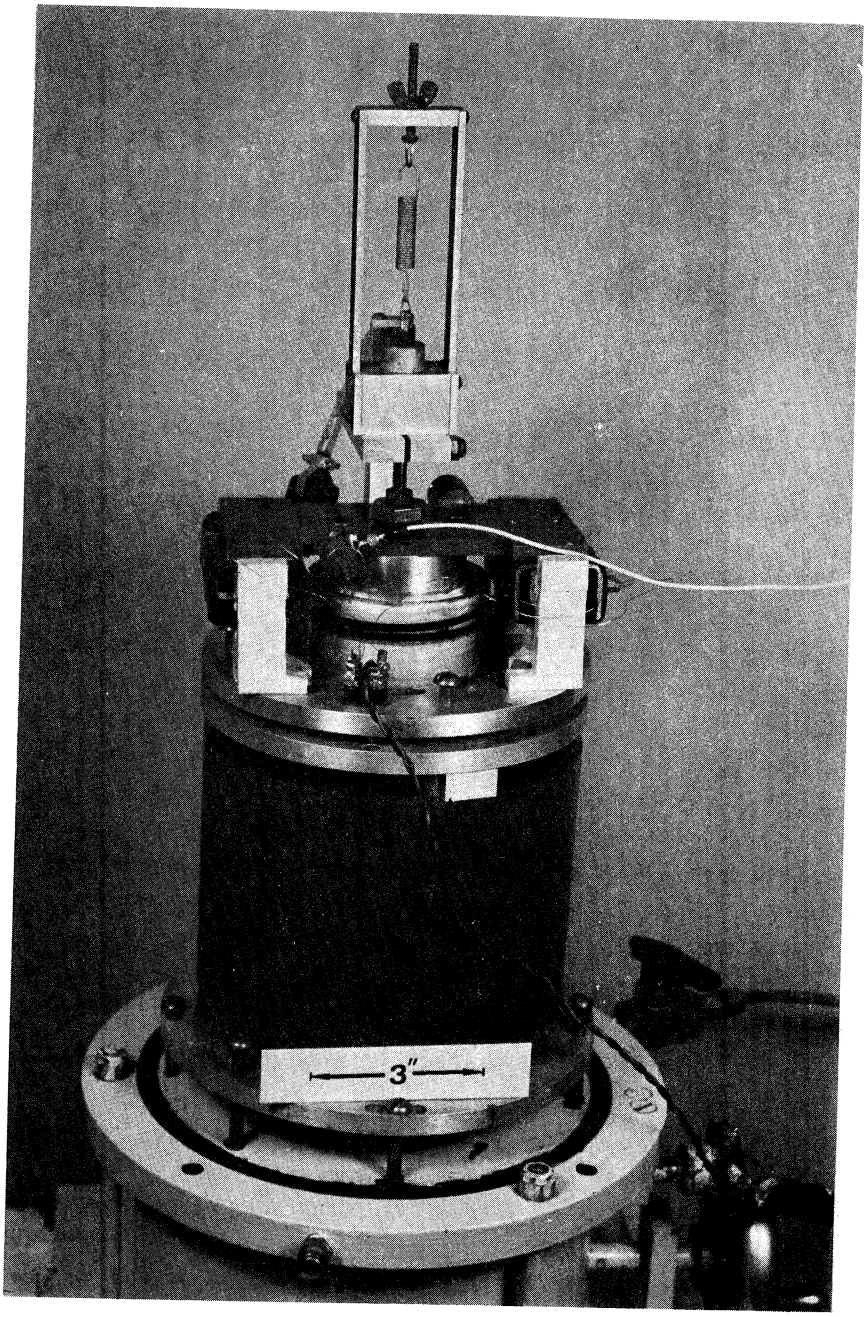

Figure 3.7 Drive system for HATD.

A cylindrical pressure chamber enclosed the specimen and drive system. The chamber could be pressurized to over 200 psi. Mechanics of the drive system were such that only hydrostatic pressure conditions could be imposed on the sample. The HATD also utilized air as a confining medium. A water bath, however, surrounded the sample to limit air migration. Drainage in the specimen was controlled during a test by opening and closing a drainage valve.

Details of the mechanical and electrical configuration of the original HATD can be found in Drnevich (1967), Drnevich, et al. (1967), and Hardin and Drnevich (1972a).

b. Device Modifications

Several modifications were performed during the course of this investigation. In general the changes involved alterations to the base pedestal and to the top cap. The basic magnet-coil drive system and the cylindrical pressure chamber remained unaltered.

Figure 3.8 shows a schematic of the modified base pedestal and top cap. Long term tests made it essential that any potential source of air leakage into the specimen was eliminated. Therefore, the top cap and base pedestal were redesigned to include O-ring seals at strategic points. Drainage lines were also changed to incorporate Swagelok zero volume change connectors.

Two other less significant modifications were also made. An annular porous stone was rigidly mounted on the base pedestal. The porous

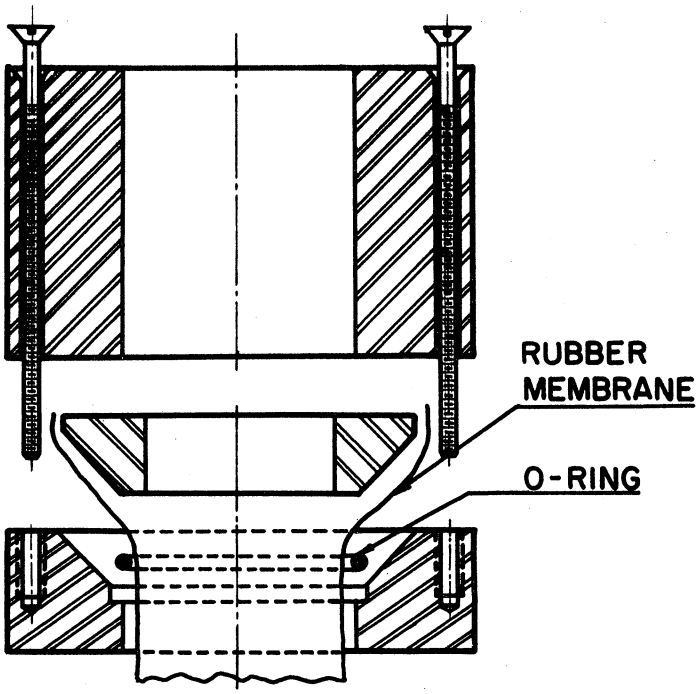

CROSS-SECTION OF MODIFIED TOP CAP

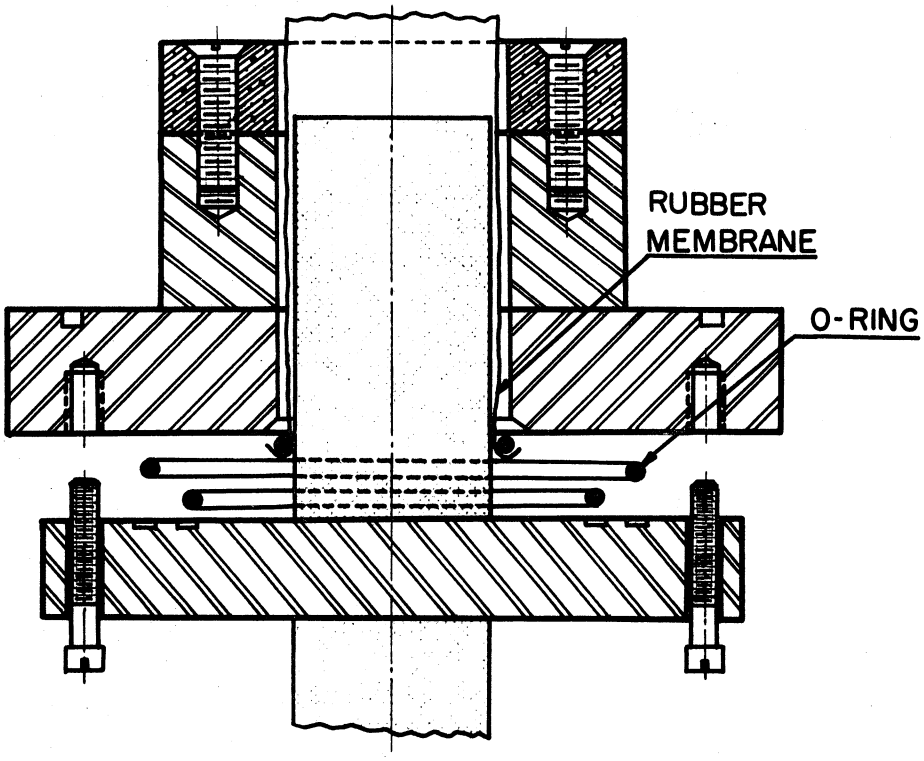

CROSS-SECTION OF MODIFIED BASE PEDESTAL

Figure 3.8. Modified base pedestal and top cap for HATD.

stone created more uniform drainage conditions around the sample base and reduced the chance that the drainage line in the base of the pedestal would be plugged by soil during the test. The other change involved the water bath. The bath was increased in height to cover the top of the rubber membrane. This change minimized the chance of air entering directly into the sample through any space between the membrane and the top cap.

c. Test Setup

The HATD test setup included a signal generator, counter, cathode follower, operational amplifier, oscilloscope, voltmeter and a length monitoring system. Figures 3.9 and 3.10 show pictorially and schematically the arrangement of these equipment. Table 3.2 gives the manufacturers and model numbers for the equipment.

The general function of the HATD test setup was similar in many respects to the function of the Hardin test setup. The signal generator supplied a sinusoidal voltage to the drive coils. The counter indicated the period of the input signal. An accelerometer mounted on the HATD drive system produced a signal which varied in proportion to system acceleration. The signal from the accelerometer was conditioned by the cathode follower and transmitted to an operational amplifier as a voltage. The voltage signal was integrated twice in the operational amplifier. The first integration produced a voltage which varied in proportion to the top cap velocity. The second integration gave a voltage

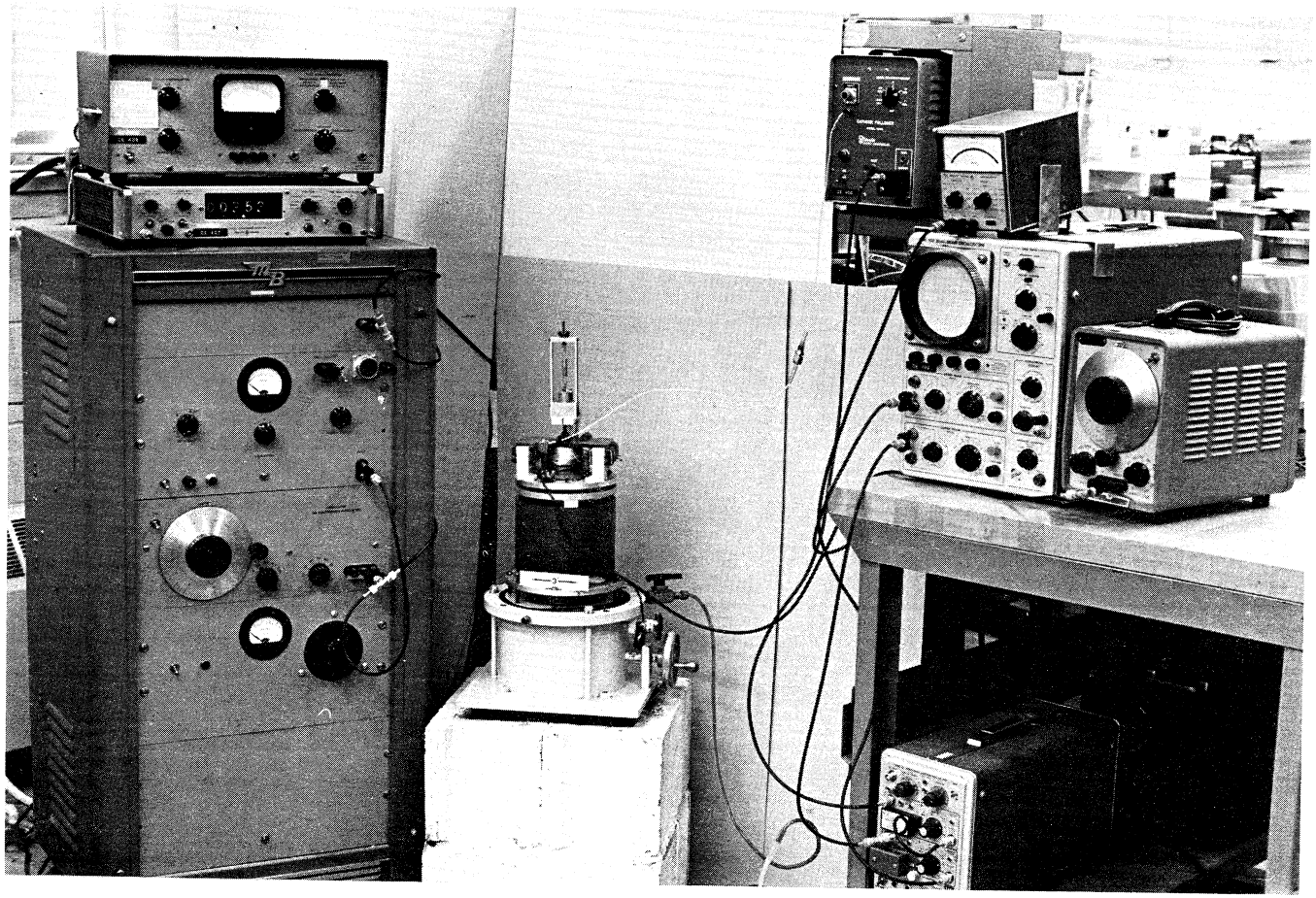

Figure 3.9. Equipment used during High Amplitude Resonant Column Tests.

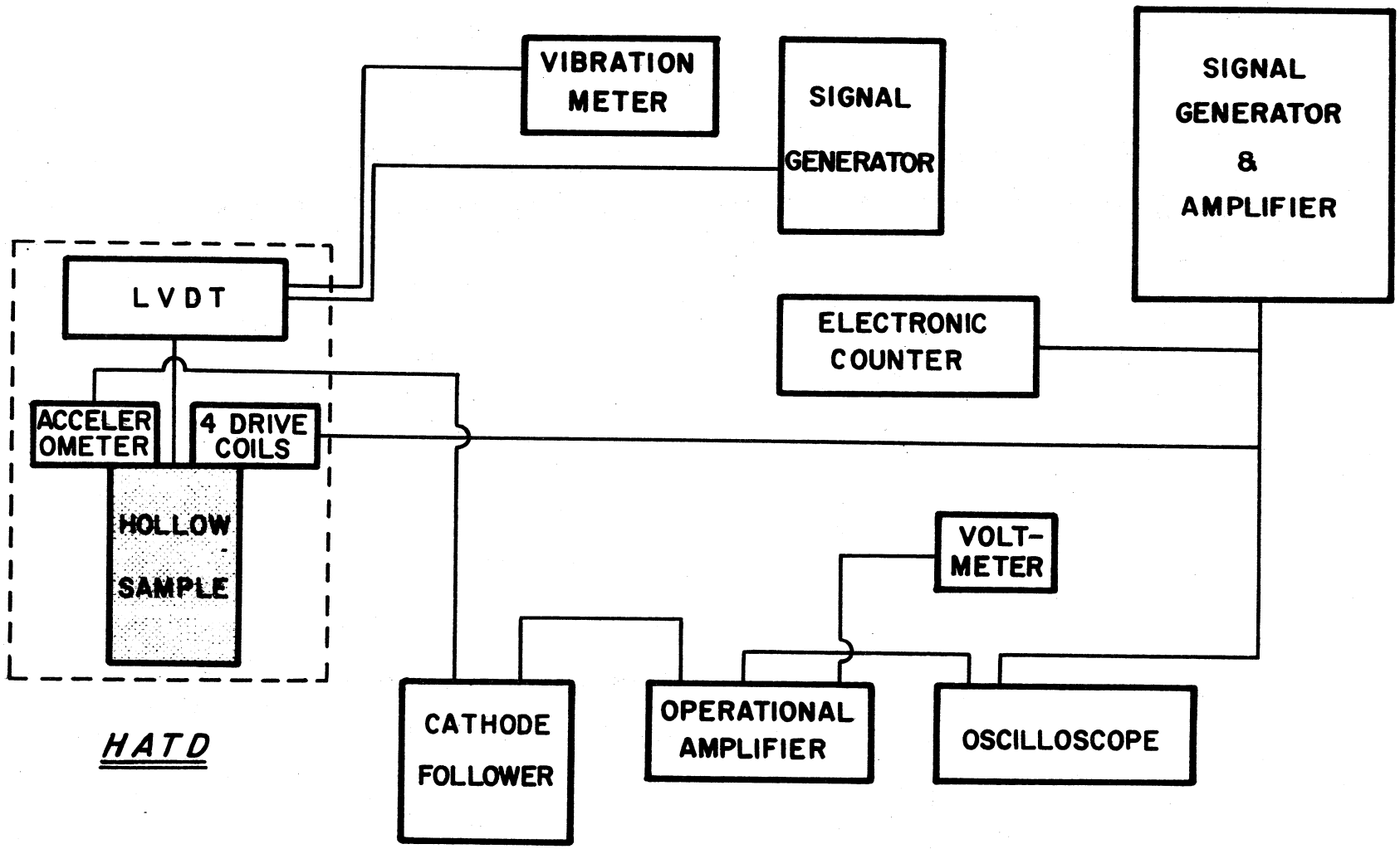

Figure 3.10. Schematic diagram of equipment used during High Amplitude Resonsant Column Tests.

TABLE 3.2. EQUIPMENT USED TO PERFORM HIGH AMPLITUDE RESONANT COLUMN TESTS

Equipment	Trade Name	Manufacturer	Model	Function
Signal Generator	Electronic Power Amplifier	MB Electronics	T132534	Supplies sinusoidal input voltage to drive coils. Variable frequency and amplitude.
	or			
	Differential Amplifier with	U. of Michigan	---	
	Low Frequency Signal Generator	Hewlett-Packard	202A	
Frequency Counter	Digital Electronic Counter	Hewlett-Packard	5223L	Measures and displays period of input signal.
Cathode Follower	---	Columbia Research	4000	Conditions output signal from accelerometer.
Operational Amplifier	---	Tektronix	Type 0	Integrates voltage signal from cathode follower twice.
Oscilloscope	---	Tektronix	502	Display input versus output signal as lissajous figure.
RMS Voltmeter	---	Hewlett-Packard	427A	Measures and displays voltage from 2nd integration.
Length Measuring System	LVDT with	Sanborn	1585DT-100	Audio oscillator supplies 2400 Hz signal to primary coil of LVDT. Vibration meter monitors and displays changes.
	Audio Oscillator &	Hewlett-Packard	200CD	
	Electronic Vibration Meter	MB Electronics	N503	

which was proportional to the displacement of the top cap. The velocity signal was displayed on the oscilloscope; and the displacement signal was monitored with an RMS voltmeter.

The oscilloscope actually displayed the vectoral sum of the input voltage and the once integrated, output voltage. As noted earlier, the X-Y plot produced a lissajous figure. The lissajous figure degenerated into a straight line at resonance because the once integrated output was proportional to the velocity of the top cap.

Although the twice integrated output signal defined a voltage that was proportional to the torsional displacement of the top cap, the relationship between angular displacement and voltage displacement had to be known before the absolute magnitude of displacement could be established. Appendix B, entitled Calibration Data, outlines the method for establishing that relationship. Once this relationship was defined, the strain amplitude could be controlled by varying the amplitude of the input signal until the desired output voltage was measured on the RMS voltmeter.

The primary benefit of integrating the acceleration signal twice involved the form of the relationship between angular displacement and output voltage. When the signal was integrated twice, a constant factor related output voltage to strain amplitude. The factor was constant at all frequencies. If, however, the signal were proportional to the velocity or acceleration, the output voltage would have depended on the frequency of vibration. As the frequency changed the calibration factor

would have changed. Such behavior was not desired.

As noted in Table 3.2, the testing sequence utilized either of two signal generators. The MB Electronics systems supplied power to the drive coils for testing at strain amplitudes of less than approximately 0.1 percent. The characteristics of this amplifier were such that output signal exceeded 180 watts (peak to peak) at frequencies of 70 Hz and above. Power dropped off noticeably at lower frequencies.

A differential amplifier, built at The University of Michigan, was used to achieve higher strain amplitudes. This amplifier delivered approximately 450 watts (peak to peak) at frequencies greater than 100 Hz. Once again power loss occurred at low frequencies; however, output at these frequencies significantly exceeded output from the MB system at the same frequencies. A Hewlett-Packard signal generator supplied the sinusoidal input signal to the differential amplifier.

The length measuring system included an LVDT, a signal generator and an electronic vibration meter. The signal generator supplied a 2400-Hz carrier frequency to the primary coil of the LVDT. The vibration meter demodulated the voltage output from the secondary coil of the LVDT. The meter then indicated any change in output signal.

A calibration factor related the change in meter position to change in axial length of the soil specimen. Appendix B describes the general method utilized when defining the calibration factor. It should be mentioned that the LVDT also assisted in determining the position of the coil in the gap of the permanent magnet. At certain stages during

testing it was necessary to raise the pedestal, specimen and drive coils to re-center the coil in the gap of the permanent magnet.

4. LOW AMPLITUDE RESONANT COLUMN TESTS—TEMPERATURE CONTROLLED

A modified version of the Hall device was used to evaluate the effects of temperature on shear wave velocity. The modification allowed the temperature of a sample to be maintained at some constant level between 4° and 70°C for extended periods of time. Despite this change, principles of operation and methods of analyzing results were the same as described for the Hall device. Strain amplitudes during oscillation also varied from 0.0005 to 0.001 percent.

a. Device Modifications

The original design of the Hall device included no provisions for controlling soil temperature. Consequently, several minor modifications were made to add this capability. The modifications involved a change in the configuration of the water bath and the addition of a temperature coil.

Figure 3.11 shows a schematic diagram of the modified system. As shown in the figure, the temperature coil fit against the inner diameter of the water bath. The inner surface of the coil cleared the outer diameter of the soil specimen by approximately 1/2 in. on each side. The coil was wound from 1/4 in. thin wall copper tubing and soldered on each side to help retain its shape. The inlet and outlet ends of the coil attached to the base of the Hall device at Swagelok connections. Short

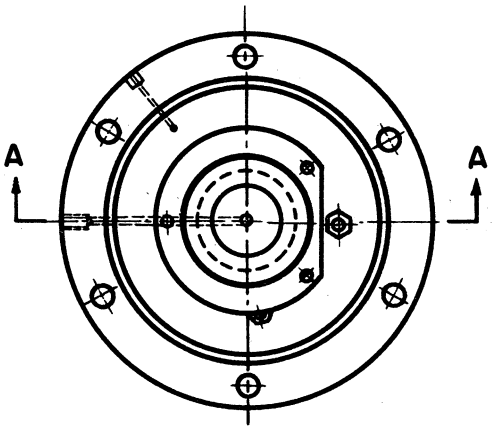

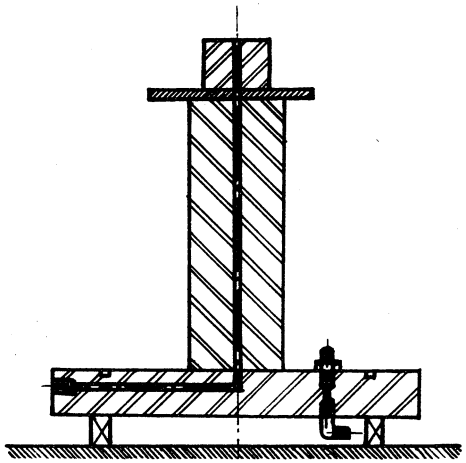

X-SECTION A-A

BASE PLATE and PEDESTAL

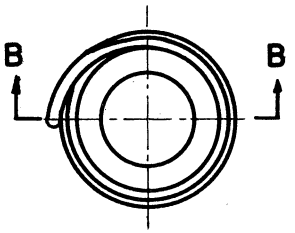

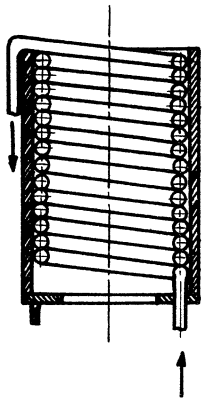

X-SECTION B-B

WATER BATH & TEMPERATURE COIL

Figure 3.11. Schematic diagram of modifications performed on Hall device to add temperature control capability.

sections of flexible nylon tubing between the Hall base and the ends of the coil provided the convenience of flexibility to the system.

An external system, described in the next section, was used to pump hot or cold fluid through the temperature coil. As the water in the water bath was heated or cooled, the temperature of the sample changed proportionately.

The entire device was insulated from room heat with a 1/2-in. layer of fiberglass pipe insulation. Fluid lines to the external circulating system were also wrapped with insulation. Consequently, the temperature within the water bath changed less than 2°C when the room temperature changed 10°C. It should be noted that daily changes in room temperature seldom exceeded 4°C. The temperature control system thus permitted prolonged testing at relatively constant temperatures.

The temperature control device included a thermocouple for monitoring the water bath temperature. A fine pair of copper constantan wires entered the base of the Hall device through a connection sealed with epoxy. The wires were wound around the pedestal and exterior of the water bath to the top of the water bath. The welded tip of the thermocouple was carefully aligned at mid-depth in the water bath. Alignment was such that the thermocouple did not touch the temperature coil or the specimen. If the thermocouple touched the specimen, resonant characteristics of the soil would have changed.

b. Test Setup

Much of the temperature control setup was similar to that described

for the Hall test. The same components drove and monitored response of the system. The setup differed in its use of a cooling and circulating system for controlling the temperature of the water bath. Two pyrometers were also used to monitor temperatures in the water bath and the circulating pump. Table 3.3 lists the manufacturers and model numbers for the temperature control components.

Figure 3.12 shows a schematic diagram of the temperature control system. As seen in the figure, the system included a low temperature cabinet, a constant temperature circulator and a length of copper tubing. The system operated in the following manner. The temperature cabinet lowered the temperature of the fluid (methyl alcohol) in the reservoir of the circulator. The circulator pumped the fluid through plastic tubing to the temperature coils in the Hall device. Heat exchange occurred if the temperature of the circulating fluid differed from the temperature of the water bath. The fluid returned to the temperature cabinet and passed through the length of copper tubing. The fluid cooled as it passed through the tubing. Finally the fluid reentered the circulator.

The circulator included a heating element which controlled fluid temperature within the reservoir as long as the desired temperature was above cabinet temperature. By setting the cabinet temperature 10° to 20°C below the desired temperature and by setting the circulator's heater at the desired temperature, the system maintained a constant supply of fluid cooled to the desired temperature.

TABLE 3.3. EQUIPMENT USED TO PERFORM TEMPERATURE CONTROLLED LOW AMPLITUDE RESONANT COLUMN TEST

Equipment	Trade Name	Manufacturer	Model	Function
Low Temperature Cabinet	---	Cole Palmer	3840	Lowers temperature of circulating fluid.
Constant Temperature Circulator	---	Haake	FJ	Heats circulating fluid to desired test temperature. Pumps fluid to temperature coils in Hall device.
Pyrometer	Gulton Pyrotest	Gulton Industries,	9B	Monitors output of thermocouple in water bath.
Pyrometer	YSI Tele-Thermonmeter	Yellow Springs Instrument Co., Inc.	42SC	Monitors output of temperature probe in reservoir of Constant Temperature Circulator.

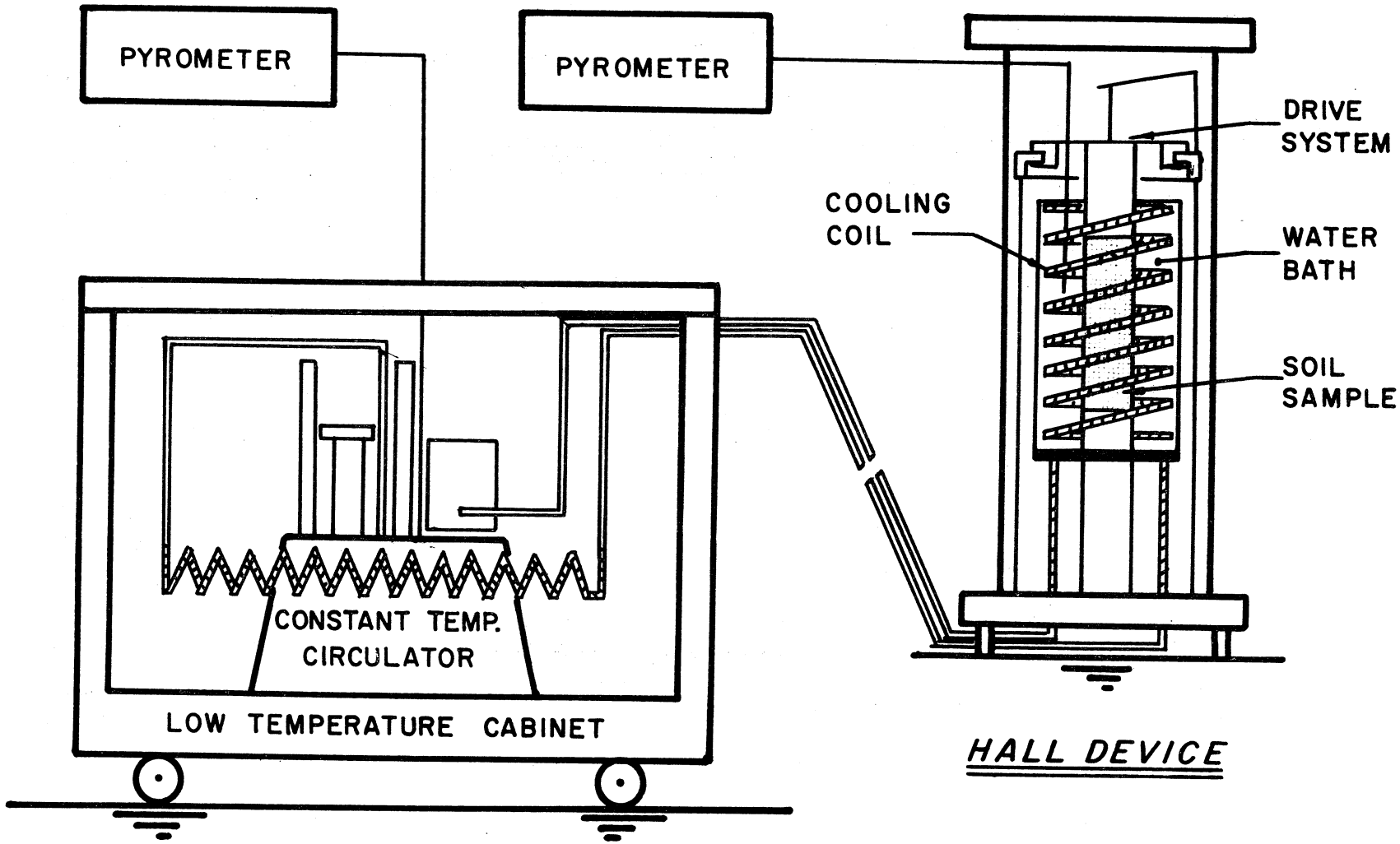

Figure 3.12. Schematic diagram of equipment used during Temperature Controlled Low Amplitude Resonant Column Test.

The pyrometers were used to determine temperature at two points within the cooling system. A Gulton pyrometer monitored the output from the thermocouple in the water bath. The other pyrometer performed a similar function for a probe located in the reservoir of the circulator. The temperature difference between the two pyrometers represented heat loss which occurred between the two points. The magnitude of loss usually did not exceed 1°C.

B. Field Tests

A limited number of field tests were performed during this investigation to determine dynamic characteristics of soils. The cross-hole seismic method was used to define the dynamic characteristics; in this case, the compression and shear wave velocities. Because the method measured dynamic properties in situ, it avoided many of the problems associated with sampling and laboratory testing of soils.

Stokoe and Woods (1972) described the cross-hole method in detail. In general the test was performed by initiating a seismic wave at one point and recording the arrival time of the same wave at another point. The travel distance divided by the arrival time defined the wave velocity.

1. TEST SETUP

Figure 3.13 shows a schematic diagram of equipment utilized during the cross-hole test. As shown in the figure, the primary components of the

test setup were a storage oscilloscope, an oscilloscope camera, and a velocity transducer. The manufacturers and the model numbers of these equipment are tabulated in Table 3.4. Ancillary equipment included a triggering system, a hammer and various lengths of 3/4- and 1-in. galvanized pipe.

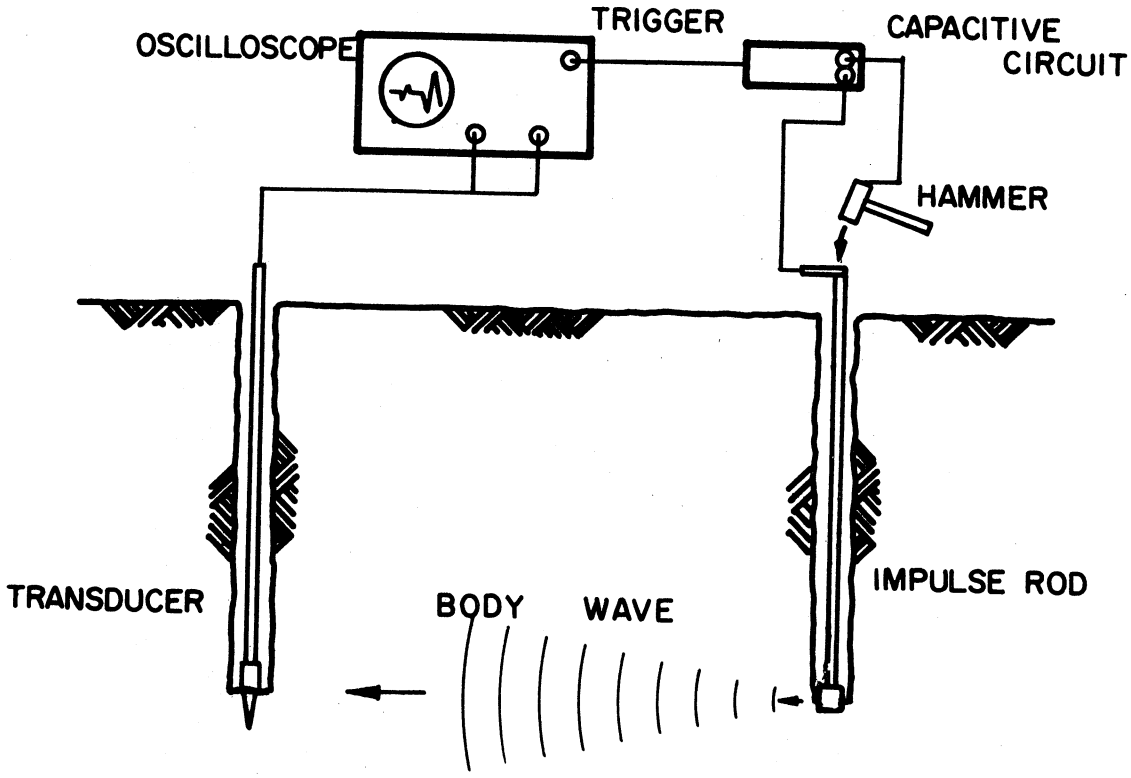

Figure 3.13. Schematic diagram of equipment used during cross-hole tests.

The hammer was used to generate a seismic wave through the pipe to the bottom of the impulse hole. The transducer at the bottom of the pickup hole oscillated as the seismic wave passed. When the transducer oscillated, a voltage was generated that varied in proportion to the velocity of oscillation. The output from the transducer was displayed on the face of the oscilloscope. Once a satisfactory trace was obtained,

TABLE 3.4. EQUIPMENT USED TO PERFORM CROSS-HOLE TEST

Equipment	Trade Name	Manufacturer	Model	Function
Storage Oscilloscope	Oscilloscope w/ Time Base & Dual Trace Amplifier	Hewlett-Packard	141A	Displays output voltage from velocity transducer. Includes storage capability.
Camera	Oscilloscope	Hewlett-Packard	197A	Photographically records trace on oscilloscope screen.
Velocity Transducer	Electro-Tech Geophone	Mandrel Industries	22V	Generates voltage output in response to soil vibration.

the record was preserved by photographing it.

2. TEST MODIFICATIONS

As noted previously, the cross-hole test setup was essentially the same as that described by Stokoe and Woods (1972). Two modifications were, however, made. The first involved the use of a electronic triggering system; the second involved use of an expandable impulse mechanism.

The modified triggering system employed a battery and capacitor connected in series to the impulse hammer and impulse rod (Figure 3.14). This circuit was connected, in turn, to the external input of an oscilloscope. When the hammer struck the rod head, metal to metal contact completed the circuit and initiated current flow. The voltage associated with current flow triggered the trace across the face of the oscilloscope. The triggering voltage exceeded 10 volts; therefore, triggering was nearly instantaneous. The new triggering mechanism no longer depended on the rise time of a triggering transducer, and thus avoided many of the early problems associated with trigger level and travel time calibration.

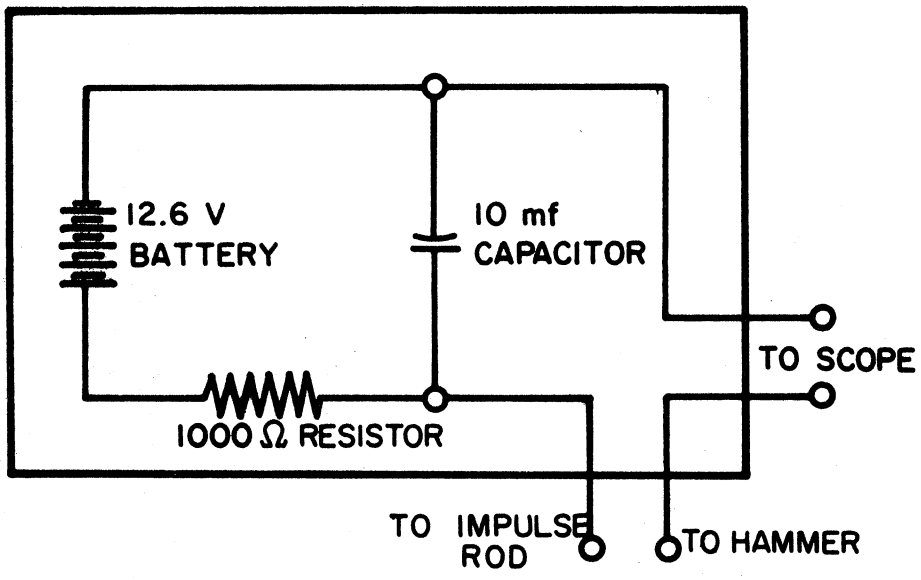

Figure 3.14. Modified triggering system for cross-hole tests.

Figure 3.15 shows the expansion-type impulse system. The expander was designed with the assistance of K. H. Stokoe. As its name implies, the expander operates by expanding two steel plates against the borehole wall. By using the expander, an impulse could be coupled into the surrounding soil at any elevation in a borehole. This capability eliminated the necessity of performing the cross-hole tests on the bottom of the borehole. The device expanded to an 8-in. diameter and collapsed to fit inside a 3.5-in. diameter pipe.

The expansion mechanism utilized the same principles as a scissors-type automobile jack. A 1/4-in. diameter inner rod turned a threaded bolt which forced the plates of the expander outward. A 3/4-in. diameter outer rod prevented the expander from rotating as the inner rod was twisted. The outer rod also served as the impulse rod during the test. Physical characteristics of the system such as weight and rod flexibility limited application to depths less than 30 ft.

(a)
Overall view of expansion-type impulse system.

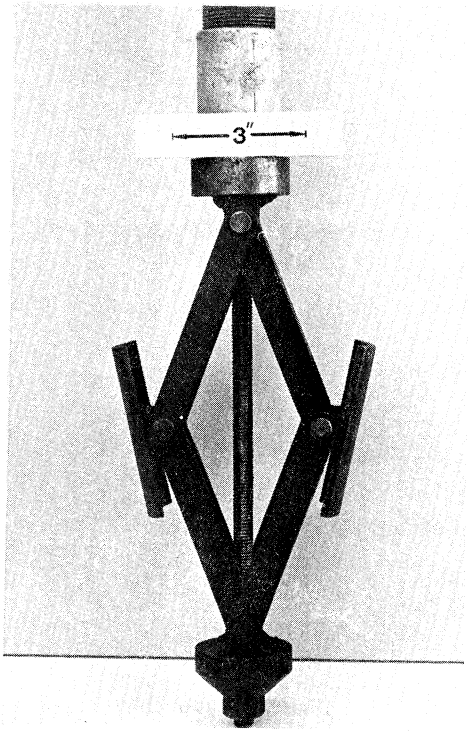

(b)
Close-up of expandable head

Figure 3.15. Expansion-type impulse system.

CHAPTER IV

TEST PROCEDURES

Each set of dynamic tests, whether it be conducted in the laboratory or in the field, incorporates a systematic sequence of steps. Laboratory tests commence with sample preparation and system alignment and end when the system is disassembled and final soil data are taken. The actual soil testing phase occurs between these two points. Field tests, in turn, involve a different sequence of steps. The test begins with borehole preparation and follows with data collection.

A. Laboratory Tests

Certain phases of the laboratory test procedure have been summarized before by other University of Michigan researchers, e.g., Drnevich (1967) and Afifi (1970). Other phases of the procedure are similar to methods commonly used in static testing of soils. The following paragraphs summarize standard tests methods and outline in detail modifications or changes in accepted procedure.

1. LOW AMPLITUDE RESONANT COLUMN TESTS

Over 30 Low Amplitude Resonant Column Tests were performed on 11 different soils. Each low amplitude test employed essentially the same sequence of steps; the sample was prepared and set up; the test was conducted; and the system was disassembled. The procedure was altered only

when the consistency of the material precluded the use of the standard sequence.

a. Sample Preparation and Test Setup

The first step in the sample preparation phase involved trimming the soil to the shape of a 3.57-cm diameter by 8.0-cm tall cylinder. The process conformed to that described by Lambe (1967) for preparation of triaxial test specimens. Excess material obtained from the top, bottom and side of the specimen was used for water content determinations. Following the trimming process, the total weight of the specimen was determined to the nearest 0.01 gram.

Once the sample was trimmed and weighed, the test setup phase began. A circular piece of saturated filter paper was placed on the bottom of the specimen. Specimen and filter paper were seated on a saturated porous stone that had previously been positioned on the base pedestal of the Hardin or Hall device. An aluminum top cap was placed directly on top of the cylindrical sample of soil. The sample was surrounded by filter paper drains (Bishop and Henkel, 1964) and enclosed in a rubber prophylatic membrane. At this point the diameter was measured at nine points around the sample circumference. The setup phase was completed by adding a second membrane and placing O-rings around the bottom and top ends of the membrane.

After the sample was set up, the water jacket was placed around the specimen and attached to the base plate. The water bath was then filled

with either distilled or salt water, depending upon the salt content of the soil's pore fluid.

It should be noted that filter paper was not placed between the top cap and the soil specimen. Direct contact produced a better coupling between the top cap and the soil, thereby reducing the possibility of slippage during torsional motion.

Following sample setup, the drive system was attached and tested. The attachment phase involved fastening the drive system to the top cap with two screws. When setting up a Hall test, attachment also included aligning the magnets about the coils and adjusting the length measuring apparatus. Once the system was attached and aligned, leads from the drive coil were connected to the signal source, and the output from the velocity coil in the Hall device or the accelerometer in the Hardin device was observed on an oscilloscope. If the oscilloscope displayed a good lissajous figure and if the frequency at resonance was realistic, the setup was considered ready for testing. The confining chamber was placed around the specimen, the final electrical connections were made and the system was sealed by placing a top plate on the confining chamber and tightening three threaded rods.

b. Test Procedure

Dynamic behavior was evaluated at three or four confining pressures: 10, 20, 40 and sometimes 60 psi. Figure 4.1 shows a typical pressure-time curve. The sequence differed when the initial pressure,

10 psi, exceeded the calculated overburden pressure and when certain stress conditions were desired.

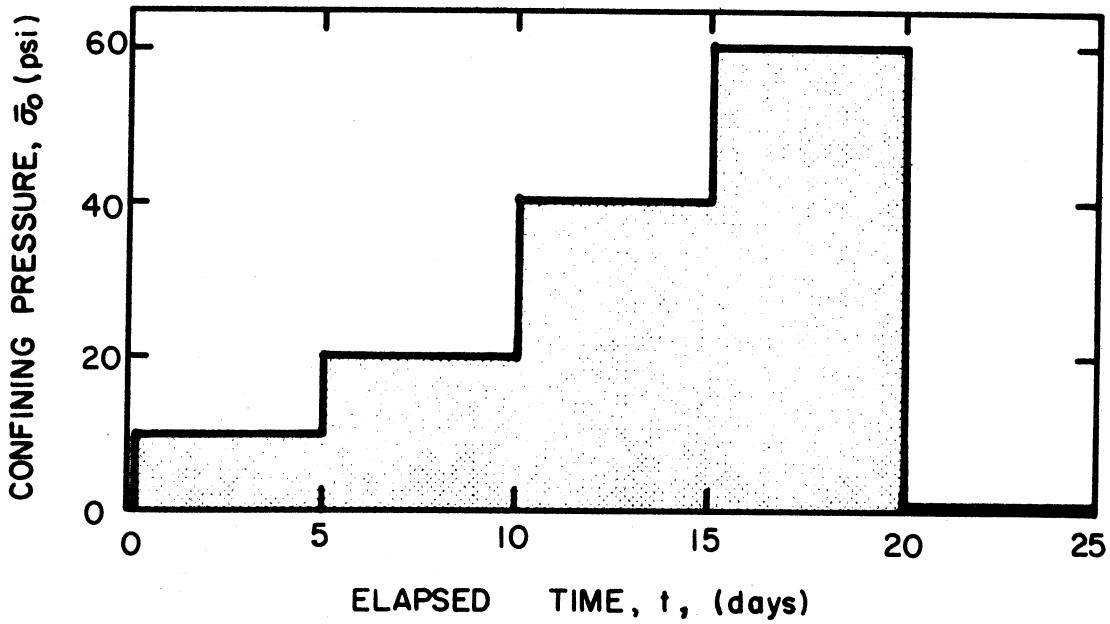

Figure 4.1. Typical pressure-time curve for a Low Amplitude Resonant Column Test.

After the test pressure was applied, the resonant frequency was measured at preselected intervals. The time intervals between readings were similar to those used during a consolidation test, i.e., 1,2,4,..., 1440 min. Readings, however, were continued for a minimum of five days (7220 min). Figure 4.2 illustrates a typical sequence of readings. If after 7220 min the shear wave velocity exhibited a constant increase when plotted against the logarithm of time, the chamber pressure was raised to the next pressure level. The sequence of readings was then repeated. For most soils the straight line portion of the V_s versus log time plot was well defined by 7220 min; however, in a few exceptional cases the relationship was not established. In these cases a longer

testing increment was used.

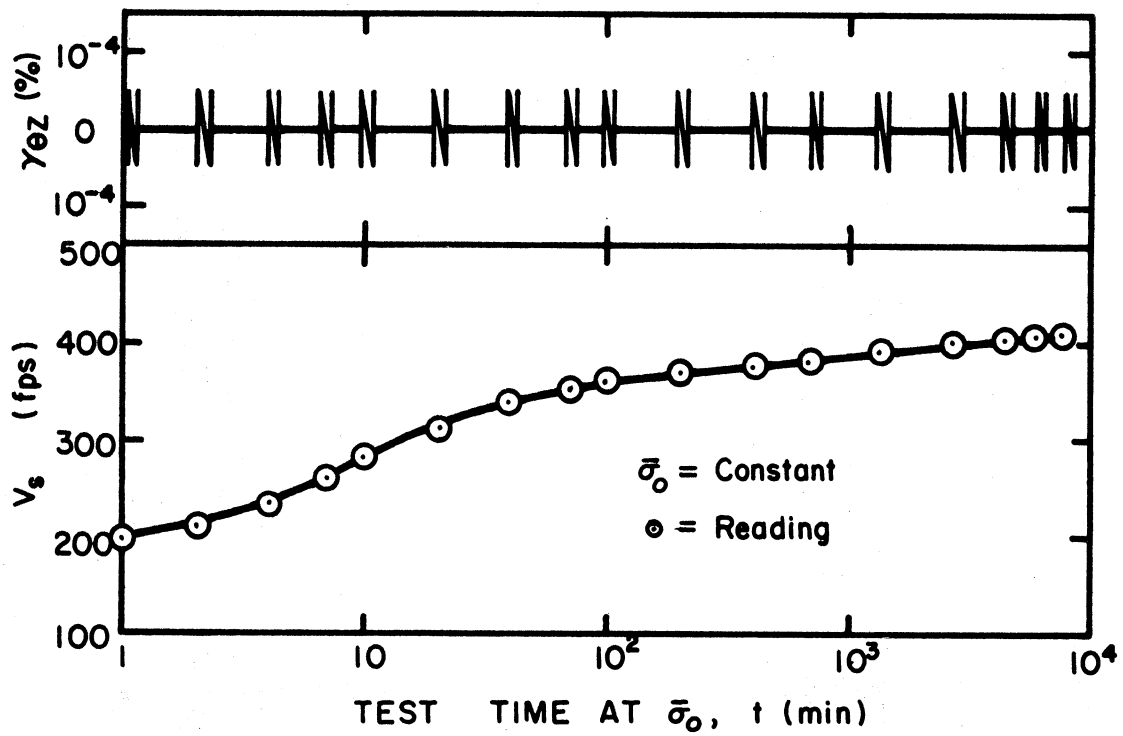

Figure 4.2. Typical sequence of readings for a Low Amplitude Resonant Column Test.

Sample drainage was permitted during the entire testing sequence. The pore fluid extracted during consolidation was collected in a 5 ml burette. Following each resonant frequency determination the burette and the strain indicator were read, thereby defining volume and height change of the specimen as a function of time.

c. Volume Change Determination

In certain situations the volume change calculation was of considerable importance. The volume change represented a change in the dimensions and weight of the soil specimen. These changes affected, in turn, the general velocity versus frequency relationship as defined by

Eq. (3.1). For most soils the weight and size changed slightly as the pressure increased from 0 to 60 psi. The magnitude of variation did not justify a recomputation in the frequency equation. But for soft materials the confining pressure caused significant sample consolidation. As the height and volume of the sample changed, the velocity-frequency relationship, Eq. (3.1), had to be recomputed.

Unfortunately a direct determination of volume change from the burette reading was impossible. It was found that after one day of testing air migrating through the rubber membrane, through the radial filter strips and finally into the drainage line displaced pore fluid in the burette to such an extent that any change in reading represented the amount of air migrating through the system and not the change in sample volume.

In view of this problem, an idealization was made to permit a theoretical determination of the volume change. The soil was assumed to be homogeneous and isotropic. It was possible, therefore, to define the volume change in terms of the height change. Air migration did not affect this determination.

This volume change computation did involve a trade-off. The development assumed that the soil was homogeneous and isotropic. Unfortunately most soils do not conform to this idealization. Chapter VII (Discussion of Results) considers the validity of the method in greater detail.

d. System Disassembly and Final Data Collection

The test was concluded when the rate of shear wave velocity increase had been well established at the highest pressure level. The confining pressure was reduced to zero, and a length change reading was taken. The zero pressure length reading was made after approximately one day. After the final height measurement was made, the confining chamber was removed and the drive system was disassembled.

Once the system was disassembled, final sample measurements were made. The sample diameter was measured at nine points around the circumference. The rubber membrane was removed, and the sample height was determined. After all filter paper had been removed, the sample was weighed to the nearest 0.01 gram. These properties, in conjunction with the average water content, defined the final total unit weight, final void ratio and final degree of saturation for the specimen.

The axial and radial variation in water content were also determined in the final phase of data collection. Since air migrated through the rubber membrane during long-duration testing, it was thought that the outside of the sample might exhibit lower water content than the inside of the sample. To prove or disprove this belief, an exact determination of axial and radial water content distribution was made. Each soil specimen was cut perpendicular to its axis into three cylindrical sections of equal lengths. The center of each section was then cored with a 2.54-cm diameter plastic tube. The outside portion gave an indication of the exterior water content; the portion from inside the corer

indicated the inner water content. The results of this comparison are included in Chapter VII with other comments regarding air migration effects.

2. HIGH AMPLITUDE RESONANT COLUMN TESTS

Six specimens were tested in the HATD. Data from these experiments helped establish the effect of high amplitude torsional shearing strains on the shear modulus, G, of soils. The data also defined the variation in response as the number of cycles increased at a constant strain amplitude and the rate of thixotropic regain in shear modulus after high amplitude straining ended. The following paragraphs review the preparation, testing and disassembly techniques utilized in this phase of testing.

a. Sample Preparation and Test Setup

As discussed in Chapter III, the HATD vibrated a hollow, cylindrical soil specimen in torsion. The outer and inner diameters of the cylindrical soil samples were 6.0 and 3.0 cm, respectively; the sample length was 12.0 cm.

The method for obtaining the outer dimensions was similar to that used during the preparation of Hall or Hardin specimens. After obtaining the proper outer diameter, a 12.0-cm long, cylindrical mold was placed around the soil specimen. The ends of the sample were trimmed flush with the ends of the mold.

A different procedure was used to trim-out the center of the

cylinder. The first step involved boring a 0.5-cm diameter hole down the vertical axis of the specimen. Either a small wood drill or a small rubber stopper corer was used to bore this preliminary hole. The drilling process required extreme care since any excursion from the axis could disturb the final dimension of the specimen. Once the small hole was drilled, a piece of wire was threaded through the hole and connected to a wire saw. The hole was then enlarged by trimming small strips of soil from the inner wall of the cylinder. An annular plate with a 3.0-cm inner diameter had been placed on each end of the mold to prevent trimming beyond the desired dimension. Figure 4.3 illustrates part of the trimming process. The final inner diameter was obtained by inserting a straight edge through the hole and twisting it against the inner diameters of the annular, end plates.

At this point certain sample parameters were established. Water content samples were taken from top, bottom, side and center trimmings. The trimmed sample was weighed to the nearest 0.01 gram. These values in conjunction with sample dimensions defined the total unit weight, void ratio and degree of saturation of the soil.

After weighing the sample, the setup phase of the procedure commenced. A saturated piece of filter paper was placed on the bottom of the specimen. Five strips of filter paper, 0.5 cm wide, were carefully spaced around the interior wall of the cylinder. The specimen was lowered over the inner membrane and positioned on an annular porous stone. The porous stone had previously been fixed to the base pedestal of the

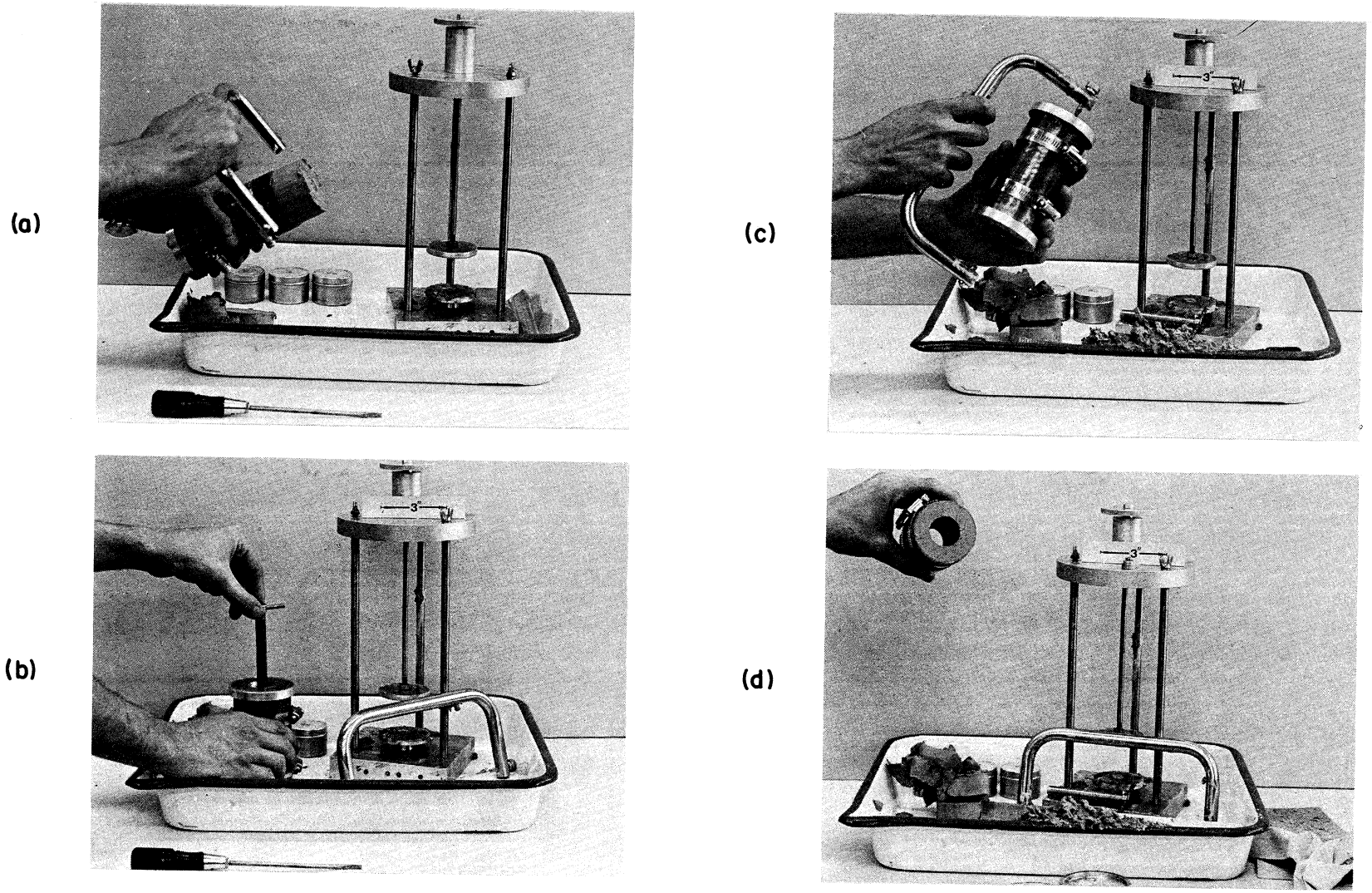

Figure 4.3. Trimming out the inner diameter of the hollow, cylindrical soil specimen.

HATD. An aluminum top cap with a serrated bottom surface was placed directly on top of the soil specimen.

The 3.0-cm diameter inner membrane, which was made at The University of Michigan (Afifi, 1970), fit through a hole in the top cap. An upper section of the top cap, when attached to the lower section, sealed the membrane against the top cap (Figure 3.8). Once the inner membrane was sealed, the mold around the specimen was removed. The setup was completed by surrounding the periphery of the sample with saturated, strips of filter paper and enclosing the sample in a single rubber membrane. The filter paper extended from the bottom to the top of the sample and covered every other 0.5-cm space around the circumference. The rubber membrane (purchased from Soil Test, Inc.) was 6.0 cm in diameter and had a 0.01-cm wall thickness. Four O-rings placed around the top cap and bottom pedestal sealed this membrane against the top cap and base pedestal.

Once the sample was set up, final specimen dimensions were determined. The outer diameter of the sample was measured at 12 points. These measurements included the thickness of the membrane. At a later stage in the computations, twice the thickness, 0.02 cm, was subtracted from the average diameter. The configuration of the specimen precluded a direct measurement of the inner diameter.

Drnevich (1967) suggested an indirect method for determining the inner volume of the cylinder. That method involved measuring the amount of water required to fill the inner volume. Although the procedure gave

good results for cohesionless soils, it was felt that the technique failed to indicate the true volume of the hole when cohesive soils were involved. The method performed satisfactorily for cohesionless soils because an internal vacuum held the membrane tightly against the wall of the soil cylinder. The cohesive setup could not utilize the same procedure because an internal vacuum would cause premature consolidation of the soil. If the membrane did not conform to the wall, inaccurate volume measurements resulted. It was finally decided to assume that the inner diameter equalled the inner diameter of the annular end plates, i.e., 3.0 cm.

The water jacket was attached to the base plate and filled with either distilled or salt water. The hollow portion of the cylinder was also filled with similar fluid.

The next phase of the test setup involved attachment and alignment of the drive coils. Magnet alignment required particular care because the gap between the poles of each magnet was only 0.2 in. in the vertical direction. As the soil specimen consolidated, the coil moved vertically in this gap, thereby decreasing the amount of clearance. If the magnets were not properly aligned, the effective travel distance of the coil in the magnet's gap would have been reduced, and more frequent adjustment of the base pedestal would have been necessary.

Once the drive system was aligned, the LVDT axial measuring device was attached and tested. The LVDT indicated the position of the coil within the magnet's gap. By raising and lowering the pedestal, thus

raising and lowering the drive coils, a relationship was determined between coil position in the gap and meter reading. The calibration procedure established the upper and lower meter reading that could be used without the coils touching the magnet. During a test the LVDT reading had to fall within these limits, or the system generated erroneous results.

All electrical connections were made, and the system was tested. If the oscilloscope displayed a good closure of the lissajous figure, the setup was assumed to be functioning properly. The chamber was sealed by placing a top plate on the confining chamber and tightening four threaded rods. At this point the testing phase commenced.

b. Test Procedure

During the initial phase of the test program the shear wave velocity versus time relationship was established at low amplitude torsional strains (approximately 0.001 percent). The procedure utilized in this phase of testing conformed with that previously described for low amplitude testing.

Low amplitude testing was conducted at two pressure levels. The first level was maintained for a minimum of 7220 min. If the V_s versus log time plot exhibited a constant secondary slope after 7220 min, the confining pressure was increased to the next pressure level. The second level was maintained for a minimum of 10,000 min. Once again the slope of the V_s versus log time plot was observed. If the slope was linear

at the higher pressure, the high amplitude test sequence was initiated.

The high amplitude testing sequence commenced at a low strain amplitude and progressed to a maximum value. Although the specific sequence varied from test to test, the general pattern increased in the following manner: 0.001, 0.004, 0.01, 0.04, 0.1 and 0.4 percent shearing strain. This distribution gave a good spread in data points when V_s was plotted as a function of the logarithm of strain amplitude.

To produce high amplitude straining, the power of the input signal was increased. The frequency of the input signal was then varied until resonance occurred. The process generally involved simultaneously adjusting both the power and the input frequency because as resonance was approached the power required to achieve resonance at a given strain amplitude decreased. Unfortunately the ratio between power and resonance at a given strain amplitude was nonlinear; therefore, a search procedure was necessary at the start of each amplitude series. Subsequent to the first test at any given strain amplitude, the power was reset at the level noted during the previous test. Only slight adjustments were, therefore, necessary.

The magnitude of top cap movement was determined by observing the output voltage from the Type 0 Operational Amplifier on an RMS voltmeter, see Chapter III. A computation had been made prior to commencing the high amplitude cycling to determine the magnitude of voltage which corresponded to a desired strain amplitude. The computation was based

on calibration data given in Appendix B. This level of voltage was sought during the previously described search procedure. When the lissajous figure closed and the RMS voltmeter indicated the desired voltage, then the shear wave velocity was defined at the preselected amplitude.

The effect of cycles on V_s was also evaluated for each strain amplitude. This evaluation involved cycling the sample at a constant strain amplitude for a certain number of cycles. Soil response was monitored during and after 1000, 10,000, 50,000 and 100,000 cycles. Figure 4.4 shows a typical test sequence. After the entire cycle spectrum had been applied, the strain amplitude was increased to the next higher level. The sequence was then repeated.

A desired number of cycles was applied by carefully controlling the duration that the high amplitude signal drove the coils. The length of signal application depended on the frequency at resonance. If 5000 cycles of strain were desired and if the resonant frequency were 50 Hz, then the number of cycles would have been divided by the frequency to define the length of signal application, i.e., 100 sec.

The resonant frequency for the desired strain level was estimated before applying the cycles. In most cases the actual frequency differed from the estimate; therefore, it was necessary to calculate the actual number of cycles at the conclusion of the test. The actual number of cycles was computed by multiplying the measured frequency by the elapsed cycling time. When the resonant frequency varied during the test, the

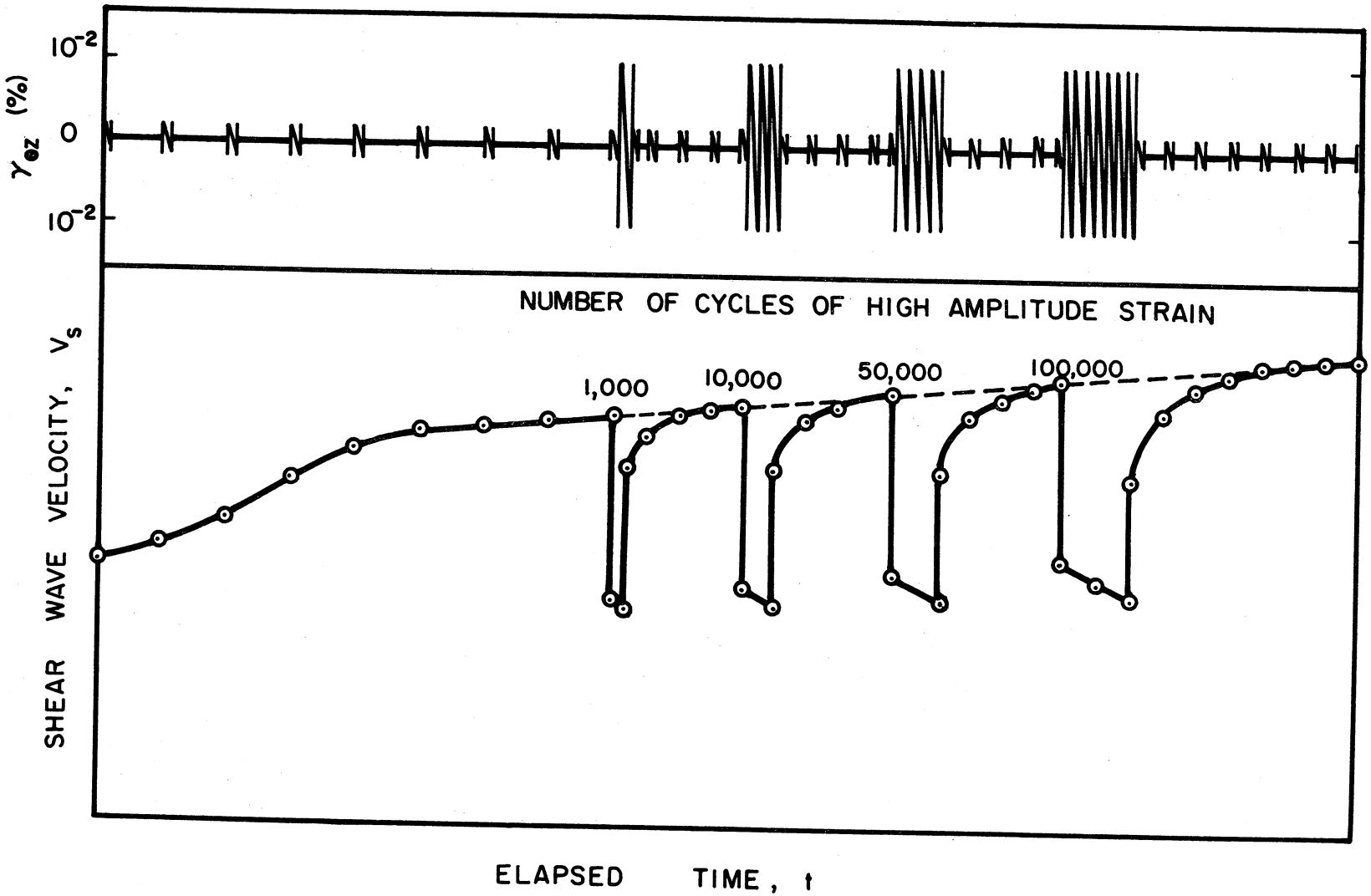

Figure 4.4. Typical high amplitude test sequence.

total number of cycles was determined by summing the incremental products of frequency and time.

Two persons were required when performing the high amplitude test. One individual adjusted the power to the coils and changed the input frequency to maintain resonance at the desired strain amplitude. The second person recorded the period of the input signal as it was displayed on the digital counter. Readings were taken every 3 sec at the start of the test. The interval between readings was gradually increased as the duration of testing increased.

The effect of high amplitude cycling on the low amplitude shear wave velocity was determined after each high amplitude test. In general high amplitude cycling caused a temporary reduction in the low amplitude velocity (Figure 4.4). As long as no additional high amplitude cycles ensued, then V_s at the low amplitude increased with time and ultimately reached the level recorded before high amplitude cycling. When regain in low amplitude velocity was complete, another test was conducted.

During several tests, the standard test procedure was altered. The change involved performing another high amplitude test before 100 percent regain of low amplitude velocity (Figure 4.5). The test was conducted at a strain amplitude equal to that used in the previous test. The percent regain (PR) that had occurred at the time of testing was determined by the ratio of moduli regained to the moduli lost. (Note that the same ratio would be defined by the ratio of shear wave velocities. PR is reported in terms of G for convenience.) Equation (4.1)

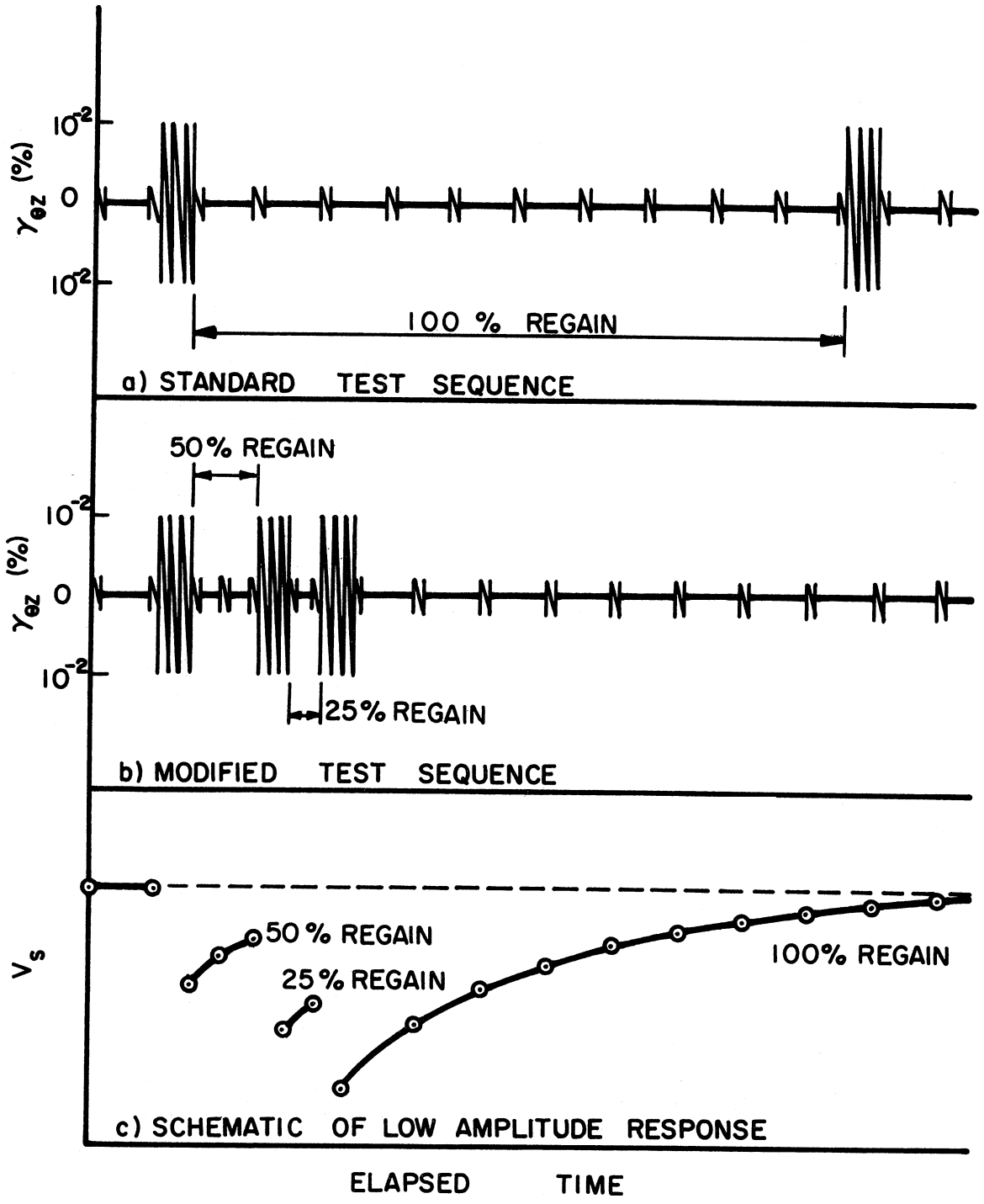

Figure 4.5. Schematic diagram of high amplitude cycling before 100 percent regain.

defines this relationship

$$PR = \frac{G_t - G_{after}}{G_{before} - G_{after}} * 100\% \qquad (4.1)$$

where G_t = shear modulus at time, t, after high amplitude cycling

G_{after} = shear modulus at 1 min after high amplitude cycling

G_{before} = shear modulus before high amplitude cycling

Tests were conducted at either 25, 50 or 75 percent regain. The high amplitude strains were applied for 1000 cycles during these tests.

c. System Disassembly and Final Data Collection

High amplitude cycling was concluded when tests had been performed at the maximum strain amplitudes. The power required to achieve resonance at high amplitudes generally determined the level of maximum strain amplitude. For the tests described herein the maximum amplitude varied from a high of 1.0 percent to a low of approximately 0.2 percent.

After the confining pressure was released and the system was disassembled, final specimen measurements were made. The rubber membrane, filter paper strips, and top cap were removed from the sample, and the total weight of the specimen was determined. The average inner and outer diameters and the specimen height were also measured. Following these measurements, the sample was sliced into pieces for water content determination.

3. LOW AMPLITUDE TEMPERATURE TESTS

The procedure utilized during low amplitude temperature tests conformed, in general, to that described for Low Amplitude Resonant Column Tests. The procedure differed only in the beginning and ending phases of testing.

The beginning phase of testing involved sample preparation and setup and system testing. The specimen was trimmed and set up in the previously described manner. The water bath and temperature coils within the water bath were attached to the appropriate connectors (Figure 3.11), the water bath was filled with distilled or salt water and the thermocouple was carefully positioned between the sample and the temperature coil. Upon completion of these steps, a single layer of fiberglass insulation was wrapped around the base pedestal and the water bath. The drive mechanism was placed over the insulated water bath, attached to the top cap and aligned. If the system performed satisfactorily during a preliminary test, the confining chamber was placed around the sample and drive system. The chamber was then sealed by placing a top plate on the chamber and tightening three threaded rods. Finally the entire system was covered with pipe insulation.

Before pressurizing the system, the sample was cooled to the test temperature. The cooling process was accomplished by circulating cold fluid through the temperature coils. Chapter III provides a description of the mechanism which cooled and circulated the fluid to the temperature coils. The soil was subjected to this temperature for at least

8 hr before applying a confining pressure.

The temperature in the water bath was determined by monitoring the output of the thermocouple. Results of these readings showed that the water in the water bath reached a new equilibrium in approximately 10 min when the temperature was changed 18°C. For tests described herein the temperature in the water bath was always lowered to 4°C, a drop of approximately 18°C from the laboratory temperature.

After the 8-hr period of equilibration, the actual testing sequence commenced. The procedure was very similar to that used for low amplitude tests. The specimen was subjected to a confining pressure, and the V_s versus log time relationship was established. If the secondary slope for this data exhibited a constant rate of increase after 7220 min, the confining pressure was increased to the next level. The testing sequence was repeated at three or four pressure levels: i.e., 10, 20, 40 and sometimes 60 psi.

Following the last V_s measurement at the highest pressure level, the temperature of the specimen was quickly increased to room temperature, about 22°C. Shear wave velocity and length change were monitored during and subsequent to the temperature change. The test was continued at room temperature until the V_s versus log time response was well defined.

The concluding phase of the temperature test was the same as that described for Low Amplitude Resonant Column Tests. The confining pressure was reduced; the system was disassembled; the specimen was weighed

and measured; and the water content distribution was determined.

B. Field Tests

The dynamic characteristics of cohesive soils were defined at several field test sites by performing cross-hole tests. The primary objective of these tests was to determine the dynamic characteristics of the soil in situ; i.e., in its original state. Subsequent to the in situ tests, representative samples of the material were removed from the site and transported to The University of Michigan for testing in resonant column devices.

The cross-hole test procedure was the same as that described by Stokoe and Woods (1972). In that procedure, two holes were bored by hand or by power to a certain depth. An impulse rod was placed on the bottom of one hole; a pickup transducer was positioned on the bottom of the other. By striking the impulse rod, compression and shear waves were created in the soil. As these waves propagated past the pickup transducer, the wound wire coil in the transducer vibrated. The vibrating coil generated an output voltage which was recorded on an oscilloscope.

For this study the depth and spacing of the boreholes differed from case to case. The holes at two locations were bored by hand; therefore, the maximum depth of testing was approximately 15 ft. At the other two sites where mechanized drilling equipment was utilized, boreholes were

drilled to 30 and 90 ft. The horizontal spacing between holes varied from a minimum of 3.5 ft to a maximum of 15 ft.

In most cases the impulse rod was positioned on the bottom of the borehole. When the impulse rod was struck, the disturbance traveled down the rod, into the soil and across to the pickup transducer. Once a satisfactory set of results was obtained, the two holes were extended to the next depth, and the process was repeated.

This procedure was altered when it was necessary to create the impulse at an intermediate depth in the borehole. To accomplish this, the previously described expander impulse mechanism was utilized. The impulse borehole was drilled to the maximum depth prior to testing, whereas the pickup hole was drilled only to the first test depth. The expander mechanism was lowered to the level of the first test depth and expanded against the wall until it supported itself. Once the pickup transducer had been positioned at the bottom of the other hole, a set of cross-hole tests was performed. Upon conclusion of the test series, the pickup transducer was removed from the borehole, and the borehole was drilled to the next test depth. In the meantime the expander was retracted, lowered to the next depth and expanded again. The test procedure was then repeated.

Figure 4.6 shows a typical set of traces from a standard cross-hole test. The first excursion on the trace, as the trace moves from left to right, defines the compression wave arrival. The shear wave arrival is located 3.7 divisions after the start of the trace. The upper and lower

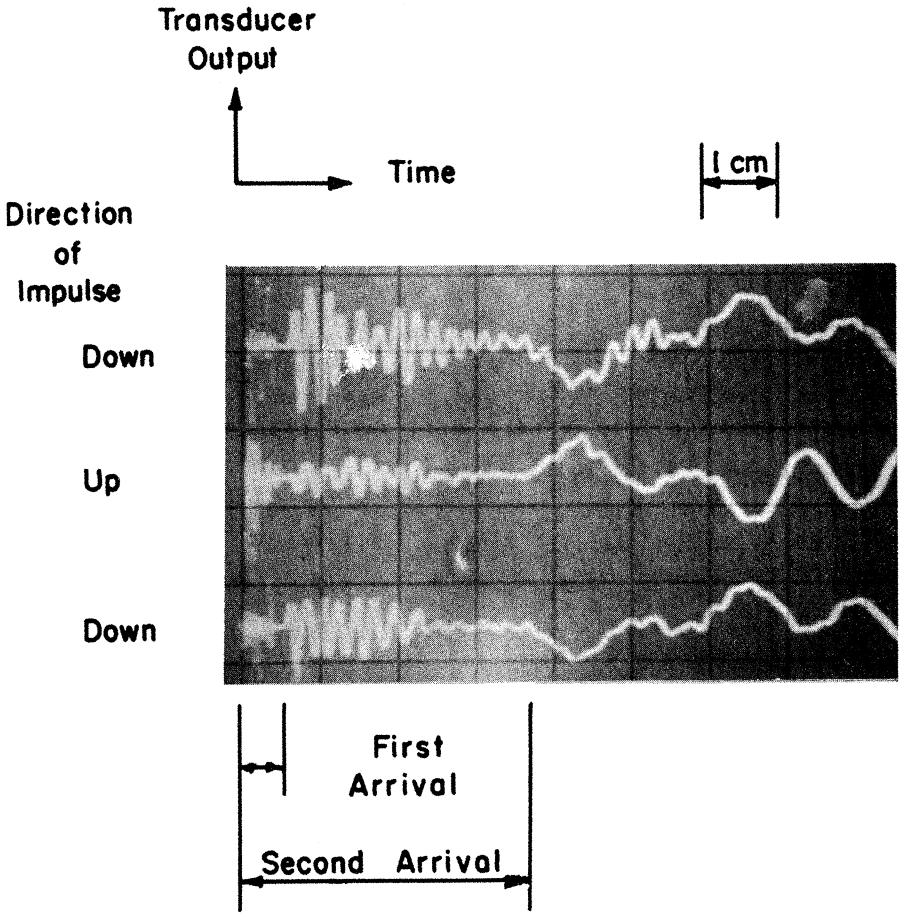

TEST DATA

Avg. Depth	=	4.7 ft
Path Length	=	10.0 ft
Sweep Rate	=	5.0 msec/cm
Rod Calibration Factor	=	0.7 msec

TEST RESULT

V_p = 4800 fps

V_s = 560 fps

Figure 4.6. Typical set of traces from a standard cross-hole test.

traces in the photograph show that the first shear wave motion was downward. The first shear wave motion in the middle trace was upward. The difference in direction of motion was due to the direction of impulse on the impulse rod. A downward blow was used in the upper and lower traces; the middle blow was caused by an upward blow.

CHAPTER V

TEST MATERIALS

A variety of cohesive soils were tested during this investigation. Characteristics of these materials varied greatly—from highly overconsolidated glacial clays to extremely soft, bentonite-silica flour mixtures. The following paragraphs identify these materials and then classify them with respect to index properties, strength values and consolidation characteristics. The final paragraph in the chapter summarizes the nature of dynamic tests performed on each soil.

A. Soil Types

Dynamic tests were conducted on two general types of soil: artificially prepared soil and naturally occurring, undisturbed material. The former type was prepared in the Soil Mechanics Laboratory at The University of Michigan; the latter originated from various field sites.

1. ARTIFICIAL SOILS

Two artificial soils were tested. Both materials exhibited uniform, but different, physico-chemical properties. Because properties were uniform, specific soil or equipment parameters could be isolated for detailed investigation. The results from tests on these two soils also supplied valuable information for general parametric studies.

a. Ball Kaolinite

The first artificial soil was prepared from powdered Ball Kaolinite. The material was purchased in powdered form from the Kentucky-Tennessee Clay Company (located in Mayfield, Kentucky). The powdered clay was mixed with sufficient amounts of distilled water to give a water content of approximately 40 percent.

After storing the mixture for 24 hr, the material was molded into cylindrical samples in a Vac Aire extruding device. Matlock, et al. (1951), described the general characteristics of soils molded in this manner. Although the molding method produced a helical structural orientation within the material, this orientation was similar from specimen to specimen. Material prepared in this manner exhibited a high degree of saturation, e.g., between 97 and 100 percent.

Material was extruded from the Vac Aire device in continuous 2.0- or 3.0-in. diameter bars, depending on the die size. As the material was extruded, it was cut into 3- or 6-in. lengths, covered with a layer of Saran Wrap, dipped in wax and stored. When a test was to be performed, the wax and Saran Wrap were removed, and the sample was trimmed to the desired diameter.

Kaolinite samples were stored for approximately three months to allow for thixotropic strength regain. Kashmeeri (1969) observed that for most compacted clays thixotropic regain occurred in the first 20 days after remolding. In view of these findings, it was thought that a three-month interval was sufficiently long to allow for the thixotropic

regain within the vacuum extruded material. It should be noted that although the formation process differed from that reported by Kashmeeri, the same physico-chemical properties governed regain. The rate of regain for the two formation processes should, therefore, be approximately the same.

b. Bentonite-Silica Flour

The second artificial material was formed by consolidating a slurry comprised of Wyoming Bentonite, AGSCO No. 140 Silica Flour and salt water (35 grams per liter). The American Colloid Company of Skokie, Illinois supplied the bentonite; AGSCO Corporation, a division of the American Graded Sand Company (located in Paterson, New Jersey), supplied the silica flour. When forming the slurry, equal parts of bentonite and silica flour were mixed with sufficient amounts of salt water to give a water content of approximately 150 percent. This water content was about 1.5 times the mixture's liquid limit; consequently, the mixture was liquid in consistency. The slurry was vacuum deaired for approximately 1 hr and then carefully poured into one of three Plexiglas consolidometers.

The consolidometers, which were designed and fabricated at The University of Michigan, are 4.0 in. in diameter and 24 in. tall (Figure 5.1). The lower end of each consolidometer contains a 2.5-in. diameter porous stone. A one-eighth inch, drainage line between the porous stone and the outside of the consolidometer allows the slurry to drain through

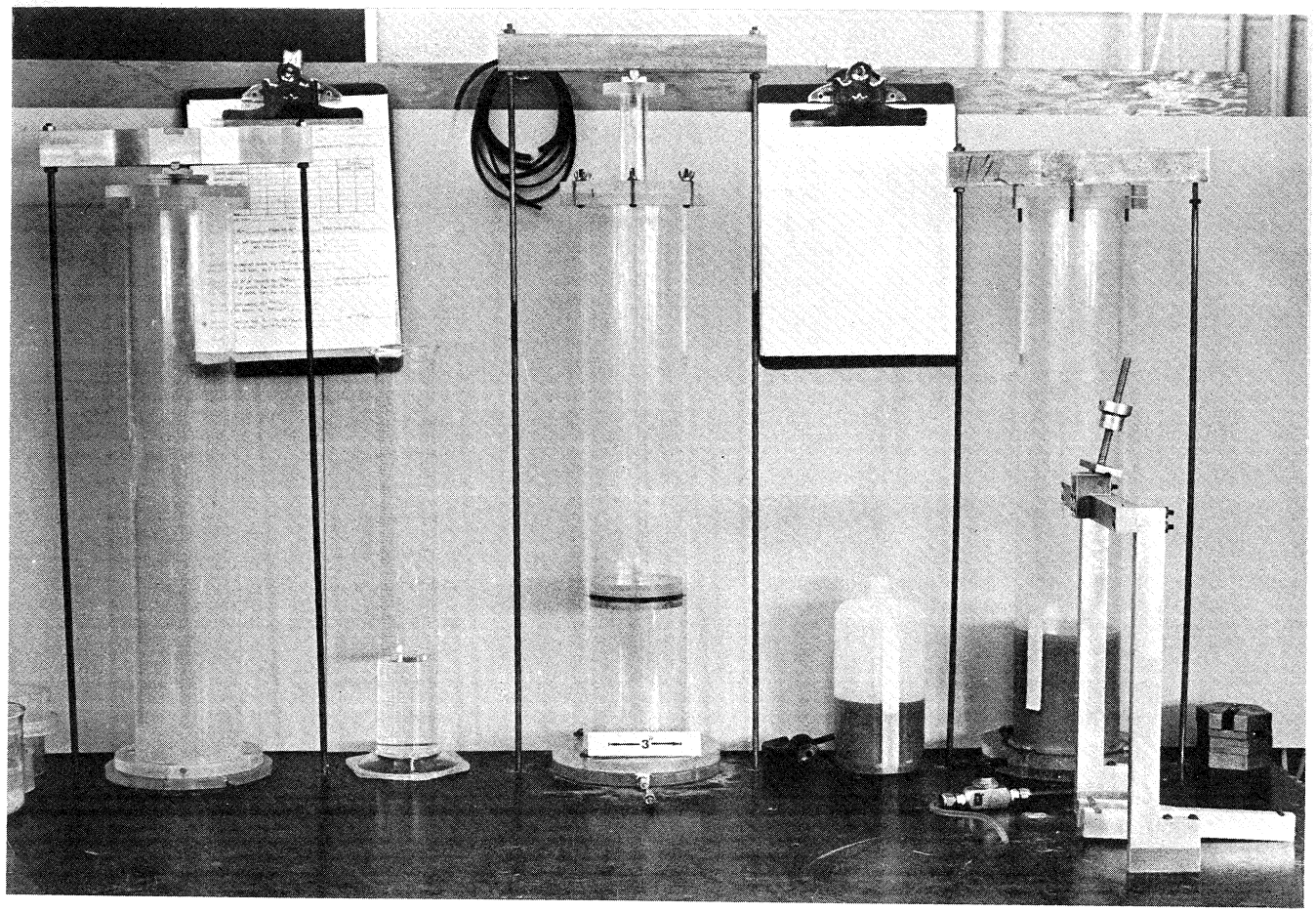

Figure 5.1. Slurry consolidometers.

the bottom during the loading process. The consolidometer utilizes a Plexiglas piston with a porous stone to load the slurry. A Quad-ring positioned around the perimeter of the piston limits extrusion of the mixture during loading.

The slurry was poured into the consolidometer in such a manner that a minimum amount of air was introduced into the mixture. The mixture was allowed to consolidate under its own weight for approximately one month. During the consolidation period, the slurry drained in two directions: through the drainage line in the base and through the porous stone at the soil-water interface.

Once the elevation of the soil-water interface reached equilibrium, the slurry was loaded through the piston in gradual increments until the pressure on the slurry was approximately 0.2 kg/cm^2. The loading interval lasted approximately one month. Drainage was permitted in both directions. After axial deformation ceased at the maximum pressure, the material was extruded from the consolidometer, covered with Saran Wrap, coated with wax and stored for approximately two months at laboratory temperature and humidity.

2. UNDISTURBED SOILS

Undisturbed soils are derived from various natural weathering processes. The properties of these materials differ according to their environment during and after formation. Climate, age, geologic events and a myriad other factors determine the final characteristics of these

materials. As a consequence, it is virtually impossible to duplicate all characteristics of undisturbed soils by utilizing laboratory formation processes. In view of the complexity of natural soils, it can be concluded that the behavior of undisturbed soils can best be determined by testing undisturbed soils.

Nine different undisturbed soils were tested during this investigation. Table 5.1 gives a tabulation of the geographic origins, natural environments, ground water conditions, sampling methods, depths, soil types and general consistency of the materials.

B. Soil Properties

Both index properties and consolidation and strength characteristics of the artificial and undisturbed soils were used to categorize the soils used during this test program. The index properties were determined by performing routine classification tests (Lambe, 1967) on trimmings from samples. The strength and consolidation characteristics were determined by testing undisturbed portions of the soil specimens.

1. INDEX PROPERTIES

The index properties for soils tested during this investigation are summarized in Table 5.2. These results define certain soil characteristics which influence or determine undisturbed soil behavior. The results also assist in delineating one material from the other. Representative grain size distribution curves for the materials are shown in Appendix D.

TABLE 5.1. IDENTIFICATION OF UNDISTURBED SOILS

Soil Name	Geographic Origin	Geographic Environment	Water Elevation (ft)	Sampling Method	Sample Depths (ft)	Soil Type	General Consistency	Remarks
Detroit Clay	East Side of Detroit, MI	Adjacent to Detroit River	-3.0	3" Shelby tube	10 thru 90	Gray silty clay w/some mottling and fine sand seams	Varies w/ depth. In general material is soft	
Ford Clay	Near Dearborn, MI	Clay pit owned by Ford Motor Company	≈ 4.0 below original ground surface	Block sample 1' x 1' x 1'	6	Gray brown silty clay w/ some coarse material	Relatively soft	Difficult to establish exact water table due to clearing and digging in area
Eaton Clay	Southfield, MI	Beneath brake testing facility owned by Eaton Corp.	Approximately 2.5 ft. May be perched above clay layer	3" Shelby tube	10 thru 22	Silty gray clay	Medium stiffness	Clay layer overlain by 10 ft sand layer. Upper portion of clay may be dessicated.
Chevy Clay	Hamtramck, MI	Beneath proposed stamping forge location in Chevrolet Division of GMC Stamping Forge Plant	Unknown	3" Shelby tube	20 thru 50	Gray-brown silty clay w/trace of sand and gravel	Stiff to very stiff. Softer w/ depth	
Leda Clay I	Montreal, Quebec	Unknown	Unknown	2.6" ϕ by 6" Undisturbed jar sample	10 thru 20	Gray silty clay	Medium stiffness	Very sensitive
Leda Clay II	Saint-Jean Vianney, Canada	Trench about 6 ft below failue plane of landslide	Unknown	Block Sample 1' x 1' x 1'	Unknown (probably less then 10 ft)	Gray silty clay	Very stiff	Very overconsolidated but also very sensitive
Gulf of Mexico Clay	Main Pass area off mouth of Mississippi River	Borings from 140 ft of water-obtained by McClelland Engineers	140 ft of water	2.125" Liner sample from wire line sampler	1.5 thru 70	Gray-green silty clay	Soft to medium, varies w/ depth	Marine orgin. Likely to be underconsolidated at shallow depths
Santa Barbara Clay	Santa Barbara Channel off coast of S. California	Borings from approximately 800 ft of water	800 ft of water	2.5" diameter samples	25	Gray silty clay	Varies w/ depth	Marine origin, very soft
Ostiglia Silt	Milan, Italy	Site of Power Station. Studied by Studio Geotechnical Italiano	Unknown	3" Shelby tube	15 thru 21	Tan to brown sandy silt w/ brown to gray mottling	Medium	

TABLE 5.2. INDEX PROPERTIES OF SOILS

Soil Name	Sample Depth (ft)	Unified Classif-ication	e_o	ω_o (%)	γ_t (pcf)	G_s	S_r (%)	$\omega_{\ell\ell}$ (%)	I_p (%)	D_{50} (mm)	%< 2μ	Test No
Ball	-	CH	1.11	41	110	2.65	97	71	39	0.00025	84	K3
Kaolinite	-	CH	1.09	40	111		97	71	39			K4
Bentonite-	-		1.88	70	99		100					BS1
Silica	-	CH	1.87	70	100	2.70	100	96	64	0.003	47	BS2
Floor	-		2.01	73	97		100					BS3
Detroit	10	CL	0.89	33	120		100	30	12	0.002	49	R2-1
Clay	14	CL	0.82	28	119		92	36	15	0.002	51	R3-3
	26	CL	1.24	45	109		98	44	20	0.009	26	R3-8a
	26		1.09	42	115		100					R3-8b
	32.5	CH	1.45	52	105		97	55	30	0.04	12	R3-11a
	32.5		1.25	46	109		98					R3-11b
Ford			0.88	31	117		94					F1
Clay	≈6	CL	0.75	28	123	2.71	100	37	19	0.0035	42	F2
			0.82	30	121		99					F3
Eaton	14	CL	0.62	23	128		100	35	17	0.004	40	E1
Clay	20		0.70	27	126		100			0.002	50	E2
	20	CL	0.72	27	125		100	40	20			E3
Chevy	21	CL	0.46	14	132		81	25	10	0.01	27	C3
Clay	21		0.38	14	139	2.71	96					C5
	35		0.41	16	138		100			0.01	27	C1
	35		0.39	14	138		100					C2
	51	CL	0.50	16	131		86	25	10	0.018	20	C4
Leda Clay	14.2	CH	2.19	79	96		99	69	44	0.0005	78	L1
I	15.5		2.14	78	97		97					L4a
	15.5		2.04	74	98	2.74	98					L4b
	16		2.18	76	95		96					L3
	17	CH	2.05	74	96		97	67	37			L2
Leda Clay			1.13	38	110	2.74	93			0.0015	55	LB1
II			1.12	39	112		95					LB2
Gulf of	22	CH	2.13	79	96	2.70	100	89	54	0.0011	55	M1
Mexico Clay	25	CH	1.98	71	97		97	85	50			M2
Santa Barbara Clay	25	MH	2.28	80		2.72	96	83	44			A1
Ostiglia	16.4		0.69	25	125		98			0.040	13	I1
Silt	16.5		0.77	28	122		99			0.026	14	I2
	23		0.74	27	123		98			0.024	16	I3

2. CONSOLIDATION AND STRENGTH CHARACTERISTICS

Undrained shear strength and consolidation characteristics for the previously mentioned soils are tabulated in Table 5.3. The undrained shear strength was defined by performing either unconfined compression tests (UC), consolidated undrained triaxial tests (CU) or vane shear tests (VS). Lambe (1967) described the method for performing unconfined compression and consolidated undrained tests while Bowles (1968) described the vane shear test procedure. Consolidation characteristics were established by performing uni-directional odeometer tests. The procedure for the odeometer tests conformed to standard practice (Lambe, 1967).

C. Test Program

Five different types of dynamic tests were conducted. Four of the tests were performed in the laboratory while the fifth was conducted in situ. Some soils were tested by more than one technique. Table 5.4 gives a summary of the types of tests performed on each soil.

TABLE 5.3. UNDRAINED SHEAR STRENGTH AND CONSOLIDATION CHARACTERISTICS

Soil Name	Sample Depth (ft)	Consolidation Characteristics		Undrained Shear Strength, S_u		
		Preconsolidation Pressure P_c (kg/cm^2)	Compression Index C_c	Unconfined Compression UC, (kg/cm^2)	Consolidated Undrained, CU (kg/cm^2)	Vane Shear, VS (kg/cm^2)
Ball Kaolinite	-	1.4	0.31	0.4	-	0.4
Bentonite Silica Floor	-	< 0.2	0.57	-	-	0.045
Detroit Clay	9	1.0	0.16	0.09	-	0.20
	11	1.1	0.21	0.29-0.43	-	-
	15	1.9	0.17	1.5	-	-
	18	2.7	0.22	0.65-0.74	-	1.1
	33	< 2.0	0.44	-	-	-
	35	< 2.0	0.38	0.44-0.45	-	0.33-0.35
Ford Clay	≈6	3.3	0.20	1.95	1.73 ($\bar{\sigma}_o$ = 20 psi)	-
Eaton Clay	14	1.7	0.13	-	1.71	-
	20	2.2	0.20	-	($\bar{\sigma}_o$ = 20 psi)	-
Chevy Clay	21	-	-	3.5	-	-
	35	-	-	2.3	-	-
	51	-	-	1.5	-	-
Leda Clay I	14	-	-	0.53	-	-
	17	2.2	0.59	-	1.0 at ($\bar{\sigma}_o$ = 20 psi)	0.2
Leda Clay II	-	3.2	0.44	2.5-3.0	-	-
Gulf of Mexico Clay	22	-	-	-	-	0.08
	25	-	-	-	-	0.11
Santa Barbara Clay	25	0.46	0.68	-	0.152 at ($\bar{\sigma}_o$ = 7.2 psi)	-

TABLE 5.4. SUMMARY OF DYNAMIC TESTS

Soil Name	Sample Depth (ft)	Laboratory Tests				Cross-Hole
		Hall	Hardin	HATD	Temp.	
Ball Kaolinite	--	x	x		x	
Bentonite-Silica Flour	--	x		x	x	
Detroit Clay	10		x			x
	14	x				
	26	x			x	
	32	x		x		
Ford Clay	≈ 6	x		x	x	x
Eaton Clay	14	x				x
	20	x		x		x
Chevy Clay	21	x	x			x
	35	x				x
	51	x				x
Leda Clay I	14			x		
	15.5	x			x	
	16		x			
	17	x				
Leda Clay II	--	x			x	
Gulf of Mexico Clay	22				x	
	25	x				
Santa Barbara Clay	25		x	x		
Ostiglia Silt	16.4		x			
	16.5		x			
	23		x			

CHAPTER VI

TEST RESULTS

The results of this investigation, as summarized in the following four sections, established the effects of time, amplitude and temperature on the dynamic behavior of cohesive soils. Chapters III and IV described in detail equipment and procedures used to determine these test results. Although a limited number of materials were tested, the spectrum of samples was such that the results characterize qualitatively the behavior of many cohesive soils.

Most of the test results are reported in terms of shear wave velocity. High amplitude data are, however, defined in terms of shear modulus. This form was used because it conformed with that reported in the literature. It should be noted that shear wave velocity is directly related to shear modulus by

$$G = \rho V_s^2 \tag{6.1}$$

where G = shear modulus

ρ = soil mass density

V_s = shear wave velocity

A. Low Amplitude Test Results

Low amplitude laboratory tests were performed to evaluate the effects of time on the behavior of cohesive soils. During these tests,

specimens of soil were subjected to constant confining pressures for extended lengths of time. The variation in V_s was monitored throughout the test interval.

Data from tests on five different cohesive soils are reported. These results show that after a certain interval of time at a constant confining pressure, V_s for a material increased linearly as the logarithm of time increased. Figure 6.1 illustrates this increase for Detroit Clay. Appendix E contains similar curves for the other clay soils. The magnitude of velocity increase per unit time at a given pressure is a quantitative measure of the time effects. The general form of the behavior is commonly referred to as the secondary increase in velocity or modulus (Afifi, 1970).

The experimental results also show that the change in V_s per logarithmic cycle of time increases as the average confining pressure, $\bar{\sigma}_o$, increases. To remove this pressure effect, the secondary increase is normalized by dividing the secondary increase per logarithmic cycle of time by the shear wave velocity at 1000 min, i.e.,

$$\frac{\Delta V_s \text{ per log cycle}}{V_{s1000}} * 100\% \qquad (6.2)$$

and expressing the result in percent. The result is called the normalized secondary increase and is abbreviated as $\Delta V_s/V_{s1000}$.

The shear wave velocity at 1000 min and the normalized secondary increase are tabulated for the five soils in Figures 6.2 and 6.3. These data show that the velocity and the normalized secondary increase depend

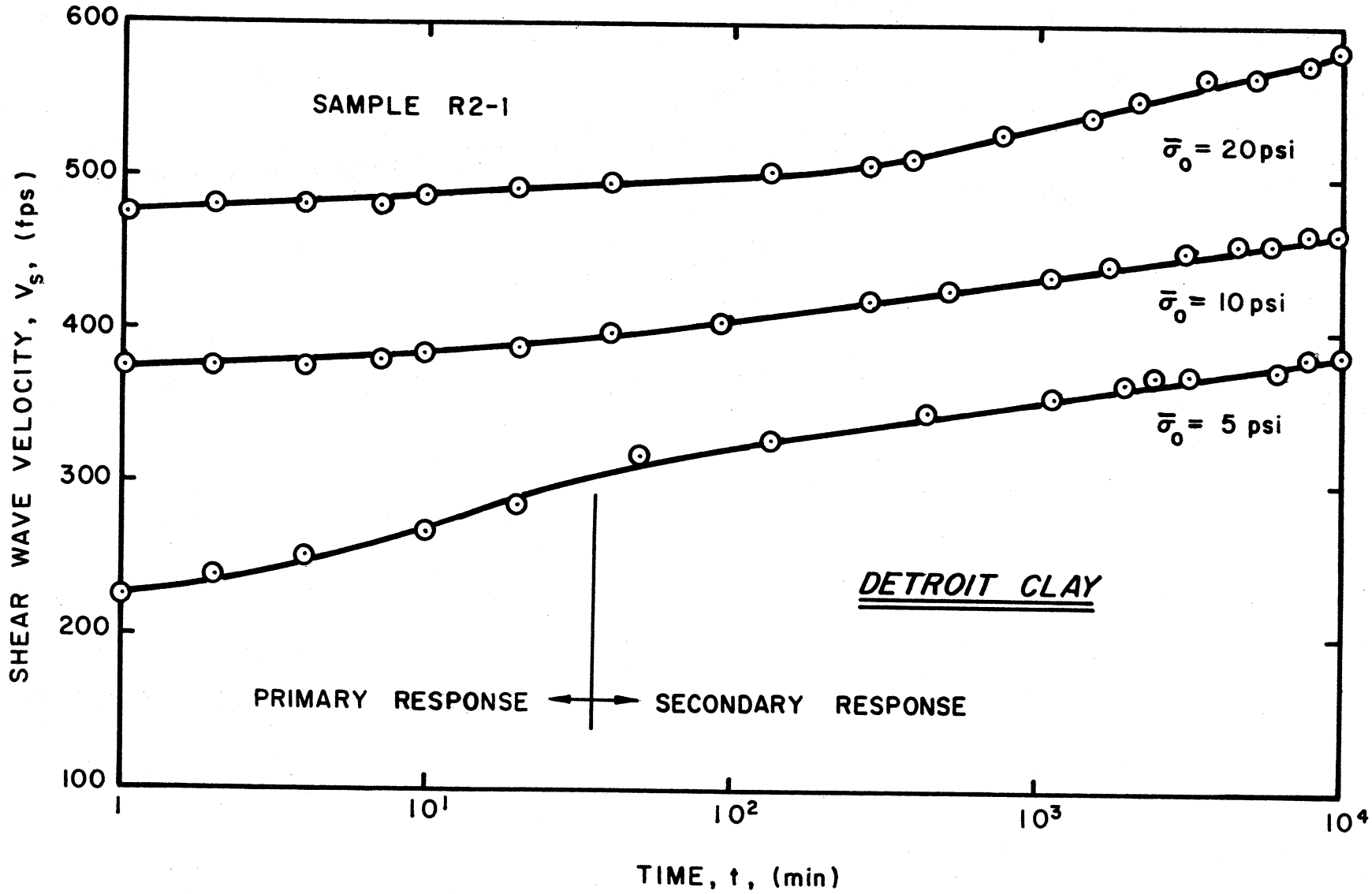

Figure 6.1. Comparison of V_s with time for Detroit Clay.

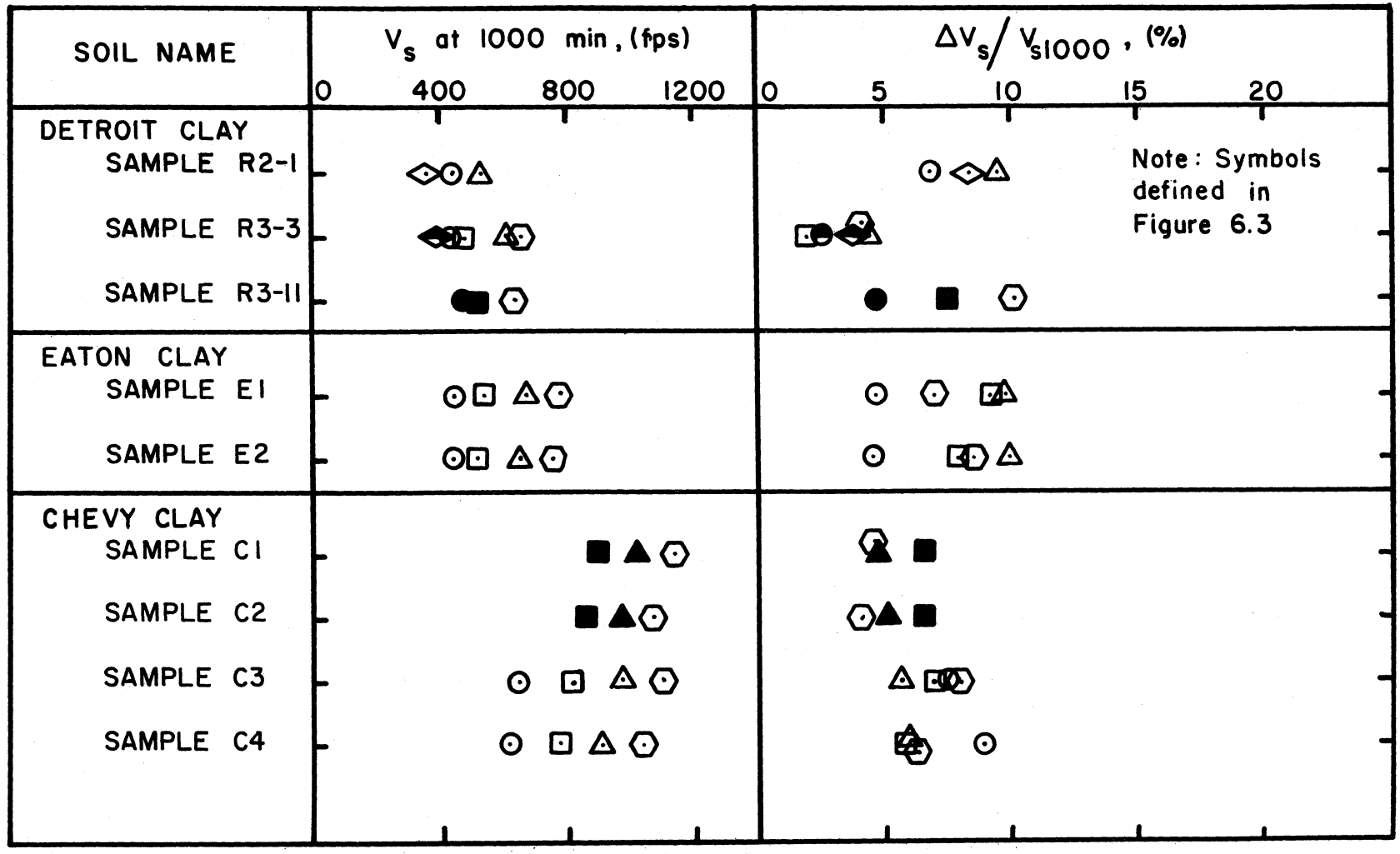

Figure 6.2. Tabulation of V_s and $\Delta V_s/V_{s1000}$ for Detroit, Eaton and Chevy Clays.

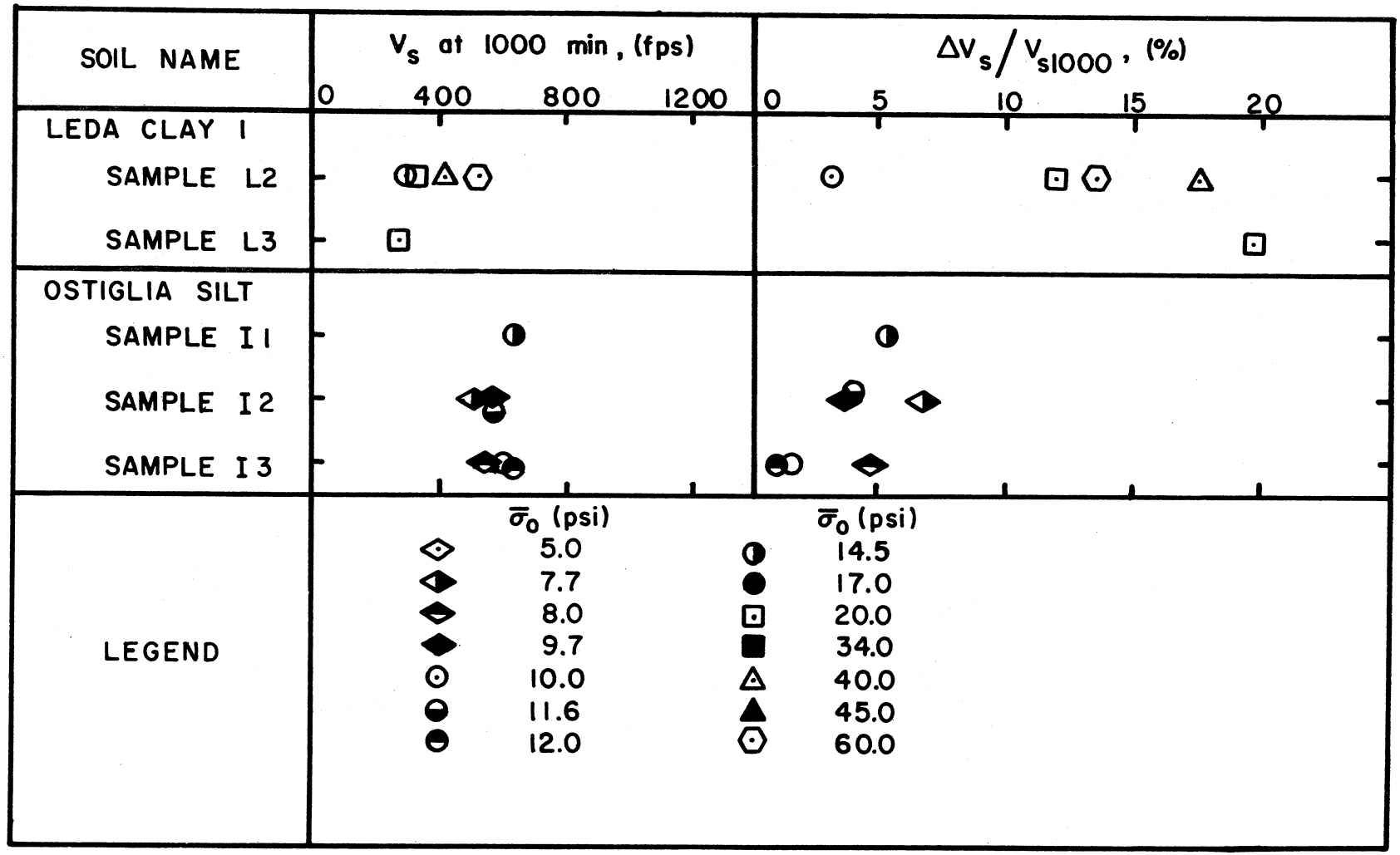

Figure 6.3. Tabulation of V_s and $\Delta V_s/V_{s1000}$ for Leda Clay and Ostiglia Silt.

on soil type and confining pressure. Shear wave velocities for the soils varied from 200 to 1100 feet per second (fps); the normalized secondary increase ranged from less than 2.0 to 20 percent.

B. High Amplitude Test Results

High amplitude laboratory tests were conducted to determine the effect of strain amplitude on the dynamic characteristics of clays. The high amplitude test series was also used to evaluate the effect of cycles of constant strain on the dynamic response and the effect of high amplitude straining on low amplitude modulus, G_{max}.

Six different cohesive soils were tested. These soils were subjected to a constant confining pressure for an extended time interval. During this interval, the modulus was monitored at low strain amplitudes. Once the secondary response was well established, a series of high amplitude tests were performed.

Figures 6.4 through 6.6 show G_{max} as a function of time for each of these materials. As observed in the previous section, a constant secondary increase in G_{max} occurred as the logarithm of time increased. All six material exhibited this characteristic. One soil, Bentonite-Silica Flour, showed a change in secondary behavior after the start of high amplitude tests.

To compare the effects of high amplitude straining for the six soils, the following ratio was defined

$$\frac{G}{G_{max}}$$

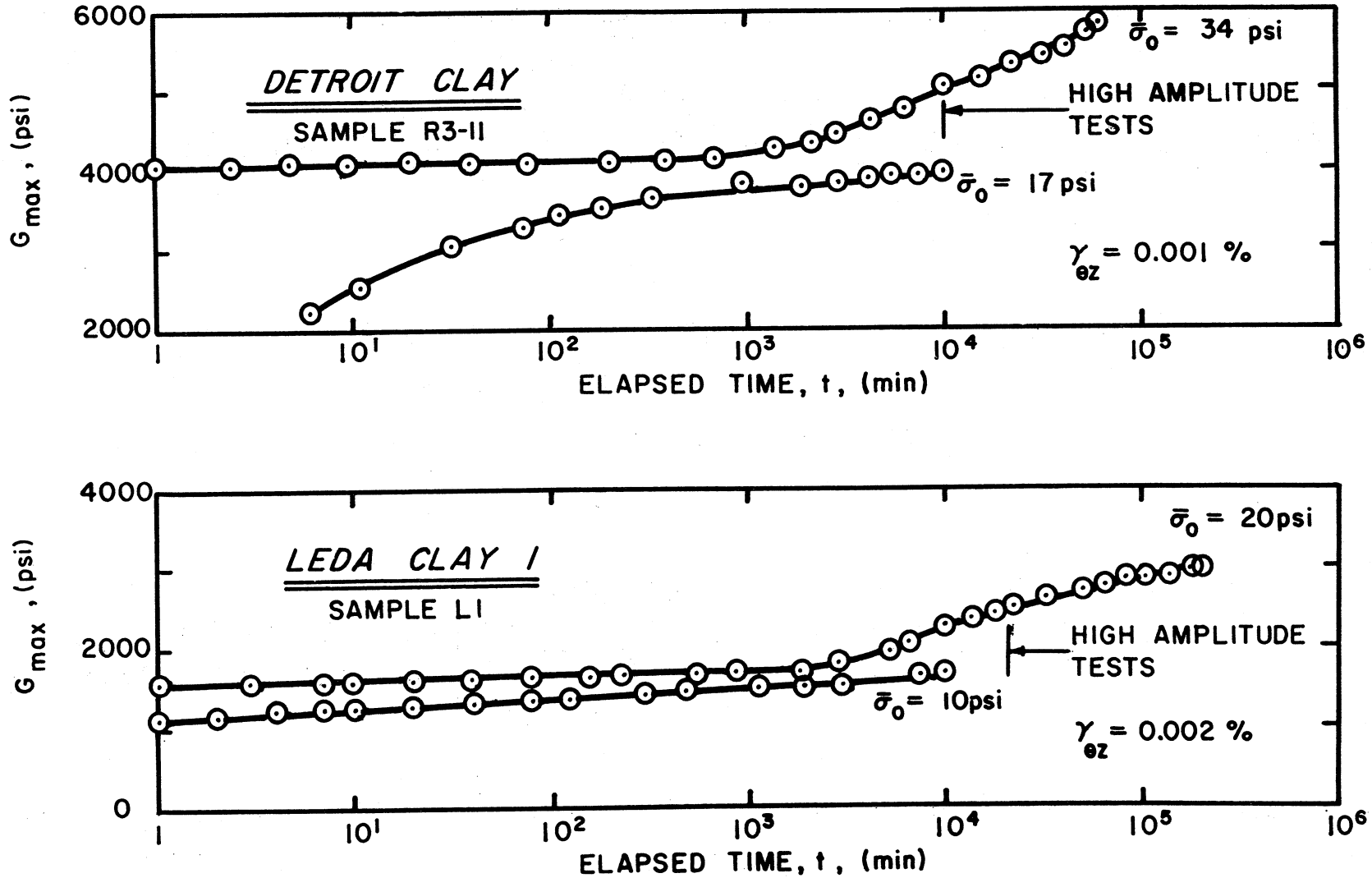

Figure 6.4. Variation in G_{max} with time for Detroit Clay and Leda Clay I.

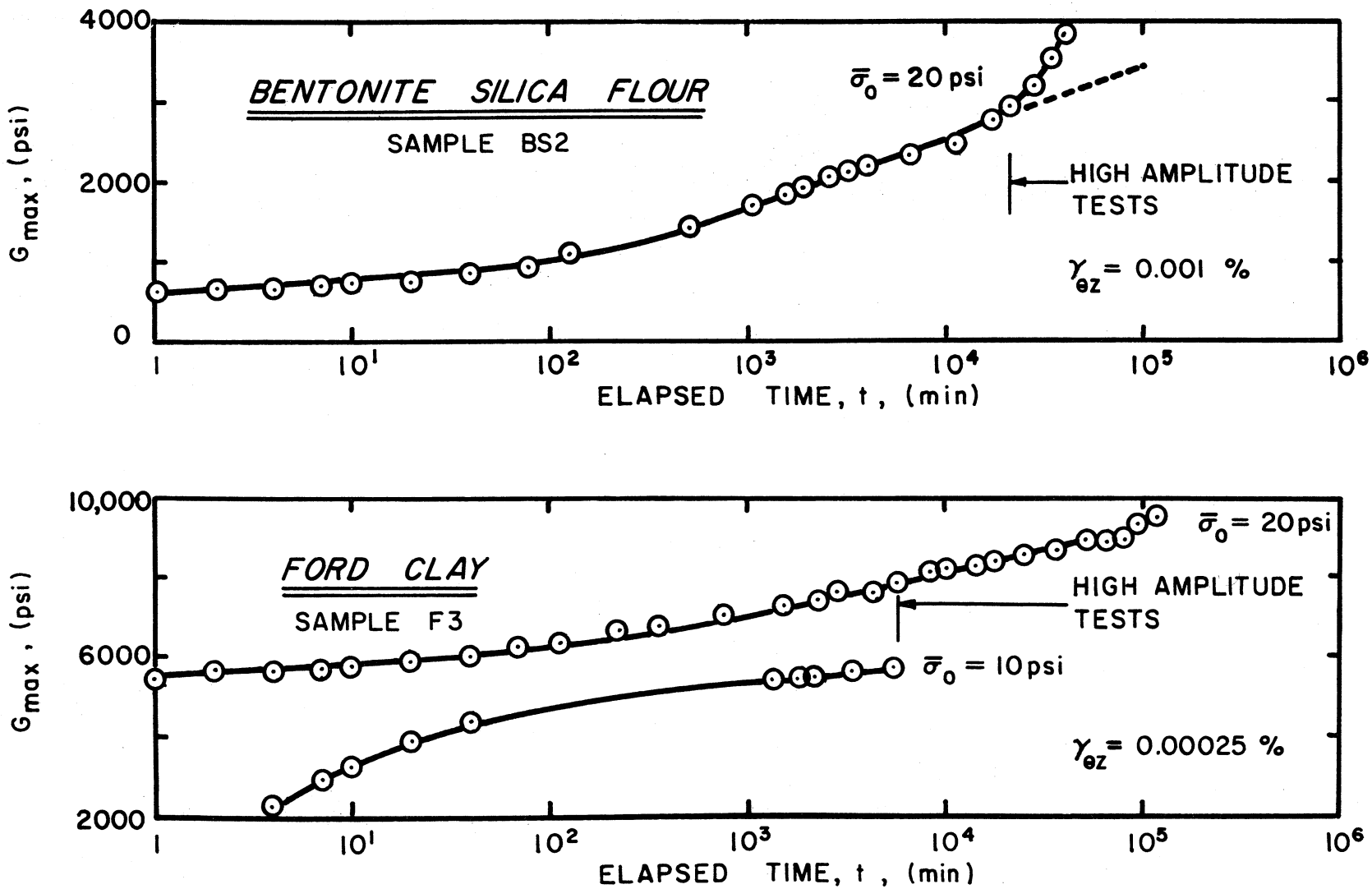

Figure 6.5. Variation in G_{max} with time for Bentonite-Silica Flour and Ford Clay.

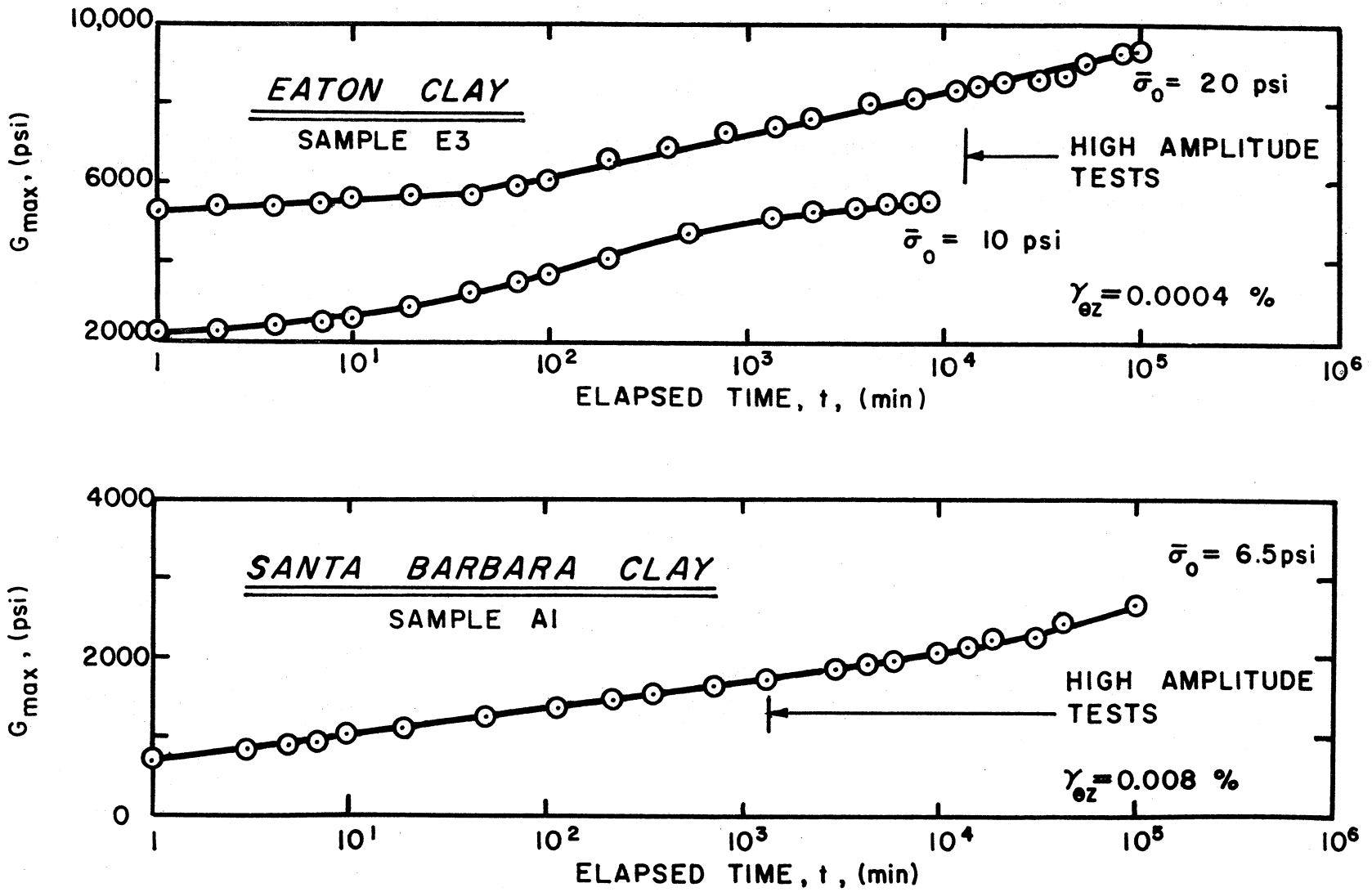

Figure 6.6. Variation in G_{max} with time for Eaton Clay and Santa Barbara Clay.

where G = shear modulus measured at high strain amplitude

G_{max} = shear modulus measured at low strain amplitude just before high amplitude cycling

This ratio indicated the percent reduction in G due to high amplitude straining. For the comparison G was defined at the 1000th cycle of strain.

The ratio of G/G_{max} is plotted as a function of the logarithm of strain amplitude in Figure 6.7. This figure shows that when strains did not exceed approximately 0.01 percent, variations in strain had little affect on G/G_{max}. Once strains exceeded 0.01 percent, G/G_{max} decreased as the strain amplitude increased. It was concluded, therefore, that for a constant G_{max}, the modulus at high amplitude decreased in some nonlinear manner once strains exceeded some threshold level.

As noted previously, G_{max} increased with time during secondary response. It was also observed that G measured at high amplitudes increased with time (Figure 6.8). In this test G was defined at each amplitude before thixotropic regain was permitted. After the last amplitude reading, regain was allowed to occur. Once regain was completed, G was defined again at each amplitude. Figure 6.8 shows that G at each amplitude increased as a function of time at about the same rate as G_{max} increased. The ratio of G/G_{max} for any strain amplitude remained approximately constant. It was concluded, therefore, that secondary time effects influenced high amplitude results absolutely, as defined by G, but not relatively, i.e., G/G_{max} remained constant.

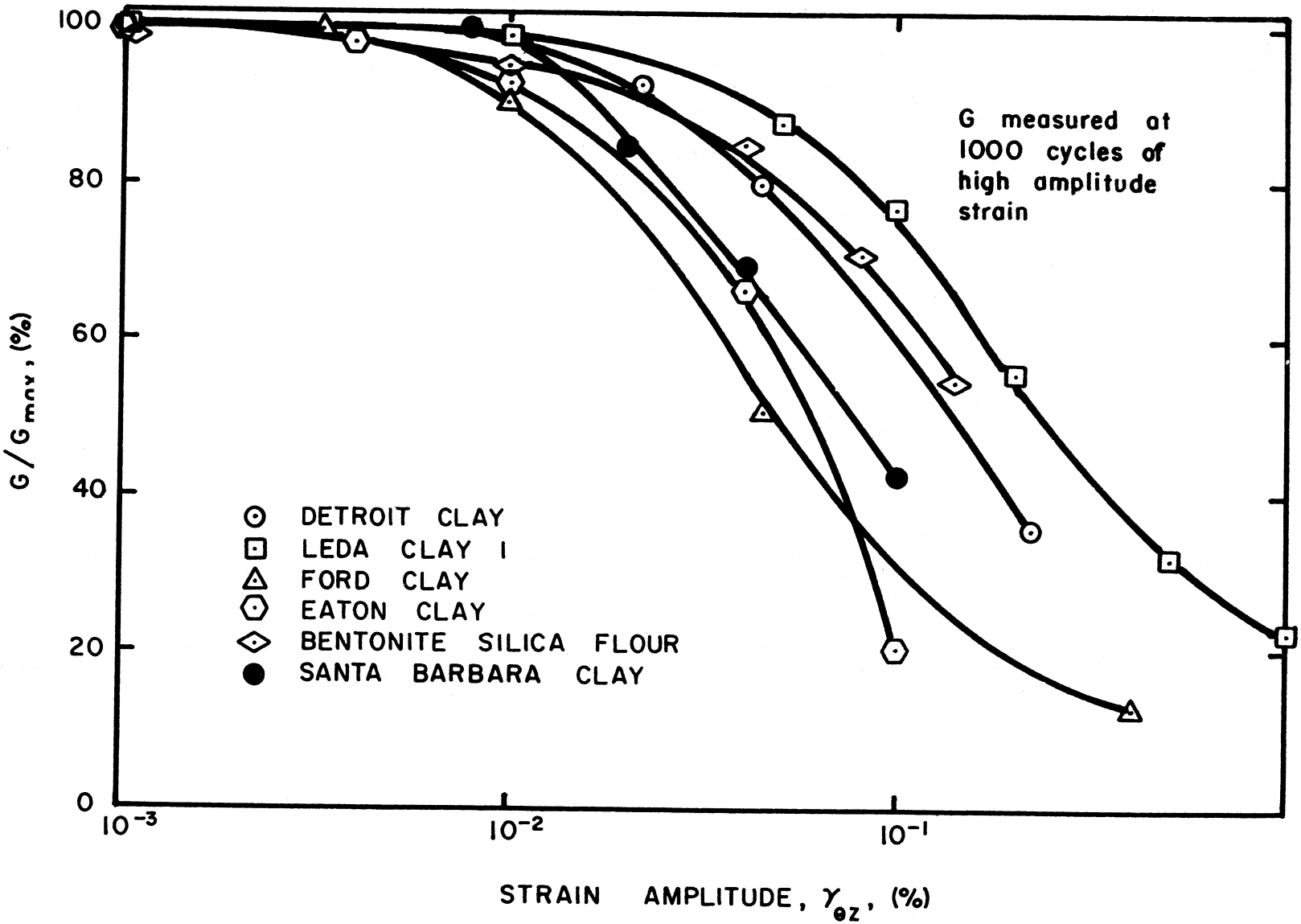

Figure 6.7. Effect of strain amplitude on G/G_{max}.

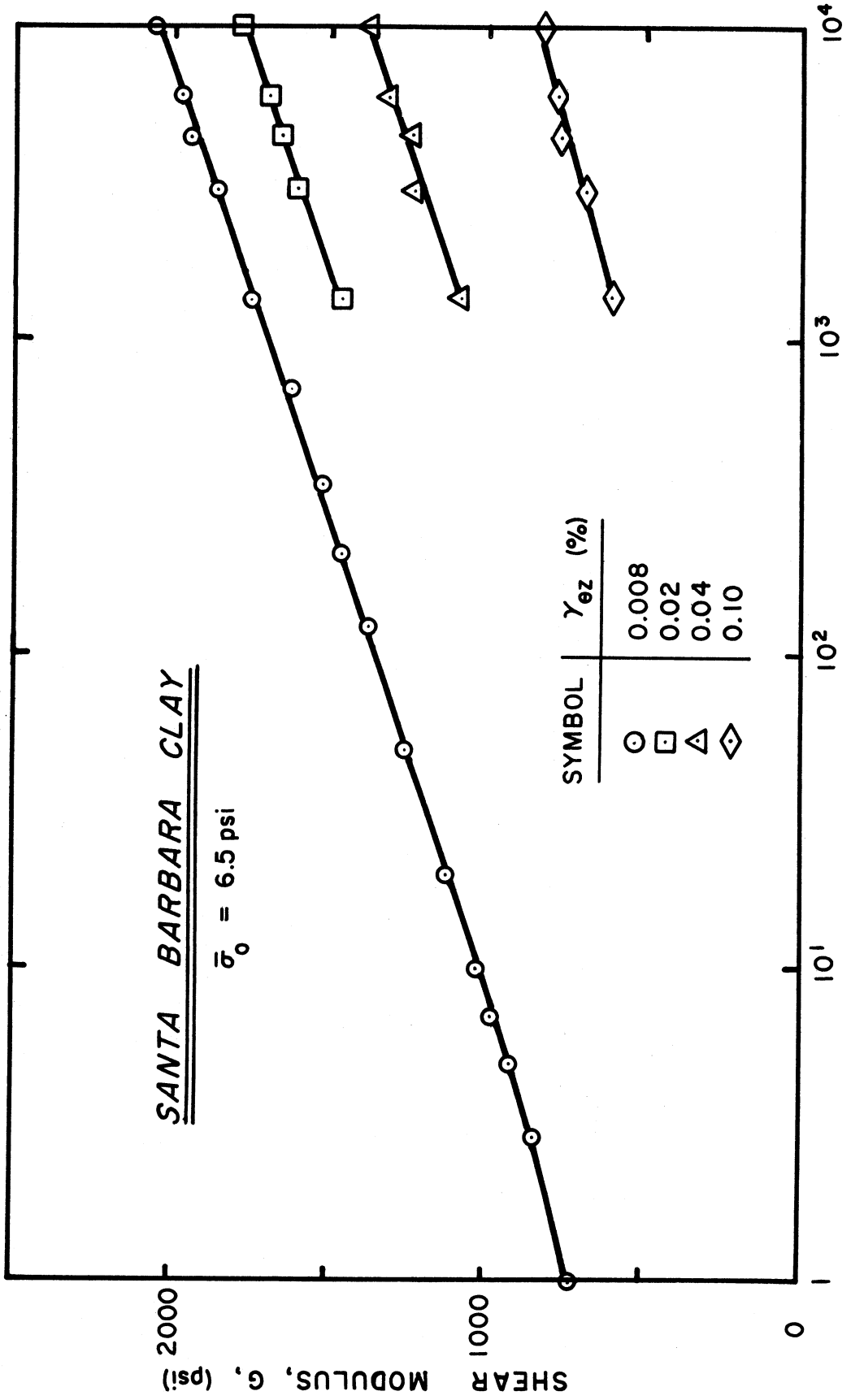

Figure 6.8. Variation in high amplitude G with time for Santa Barbara Clay.

Figures 6.9 and 6.10 show the effect of cycling on the modulus measured during high amplitude straining. The modulus decreased as the number of cycles of strain increased. It is apparent from these plots that the effect of cycles was more important at higher levels of strain amplitude. The magnitude of modulus reduction between the 500th and 1000th cycle was consistently about 5 percent while the reduction between the 500th and 100,000th cycle varied from less than 5 to over 40 percent, depending on the strain amplitude. The nature of the laboratory test procedure was such that the effect of fewer than 500 cycles could not be evaluated.

High amplitude straining affected the low amplitude modulus measured immediately after high amplitude cycling. Figure 6.11 illustrates this effect for five of the test materials. The magnitude of reduction was normalized by dividing the low amplitude modulus measured 1 min after high amplitude cycling (G_{after}) by the low amplitude modulus measured immediately before high amplitude cycling (G_{before}). This normalization was performed for comparative purposes. The horizontal axis of Figure 6.11 indicates the strain amplitude during high amplitude cycling.

Figure 6.11 shows that 1000 cycles of high amplitude strain had little effect on G_{max} as long as the strain amplitude was less than 0.01 percent. If strain amplitudes exceeded 0.01 percent, a significant reduction in G_{max} occurred. The magnitude of reduction increased as the strain amplitude increased.

Figures 6.12 and 6.13 show that the number of cycles of high

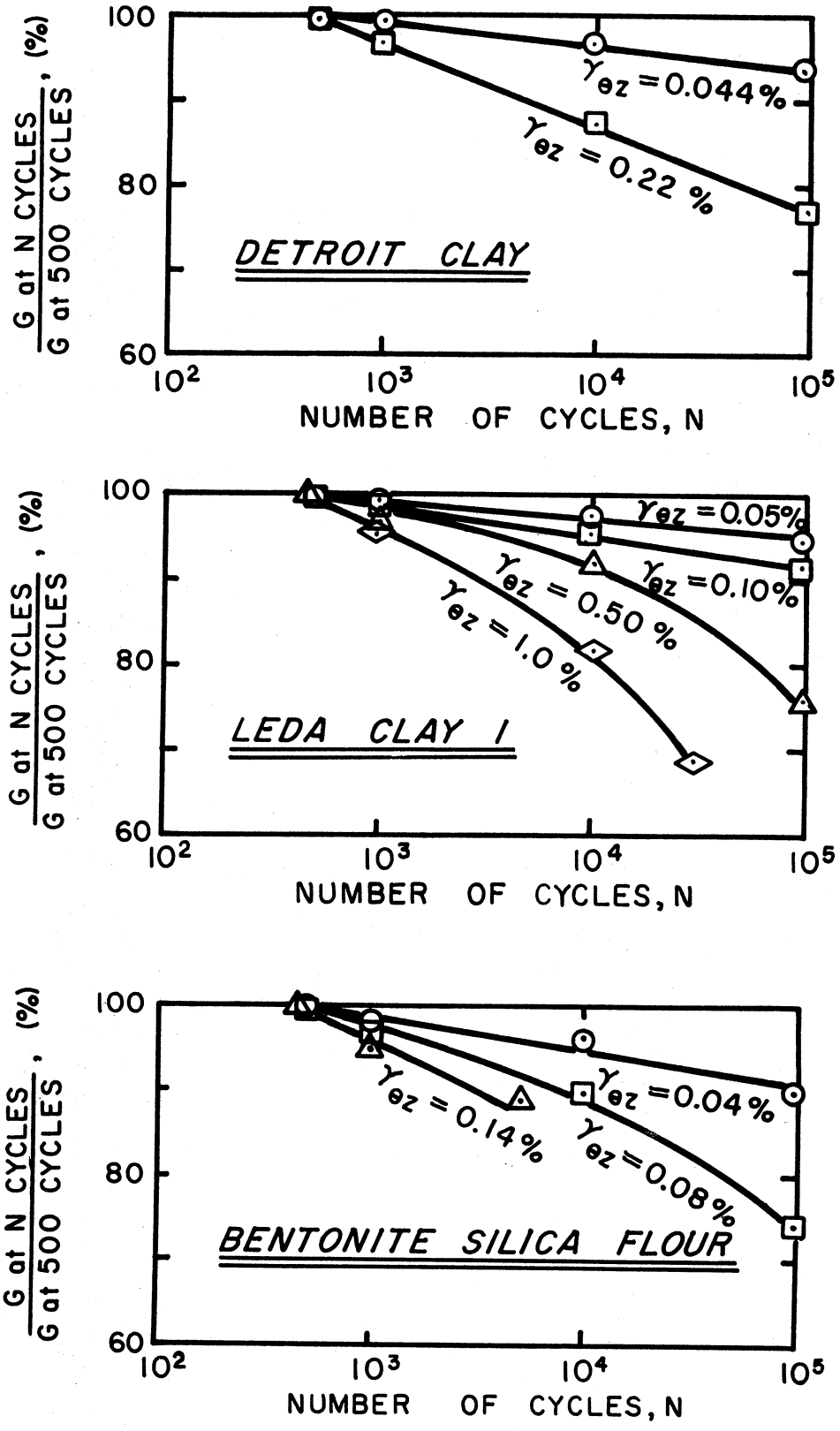

Figure 6.9. Effect of cycling on high amplitude G for Detroit Clay, Leda Clay I and Bentonite-Silica Flour.

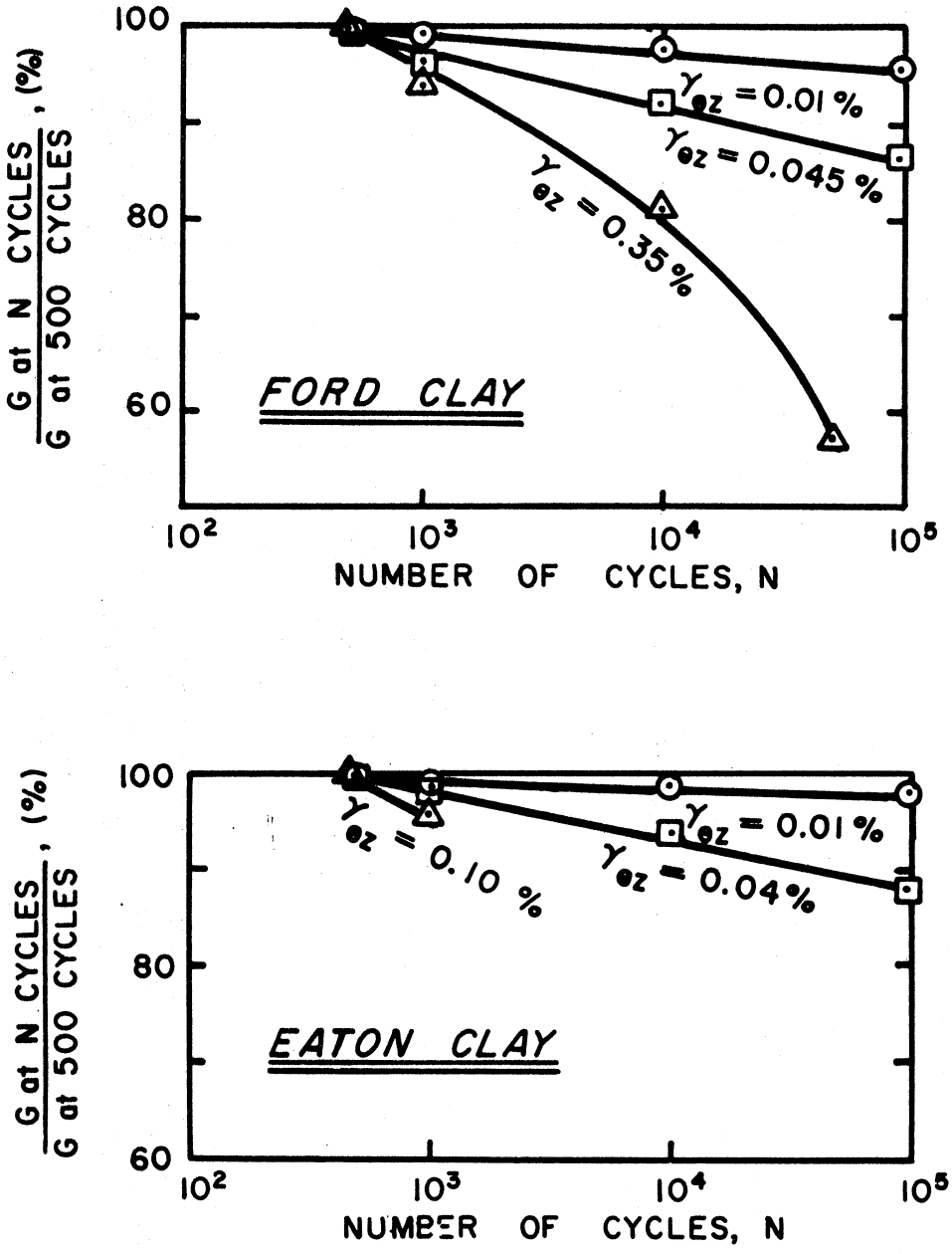

Figure 6.10. Effect of cycling on high amplitude G for Ford Clay and Eaton Clay.

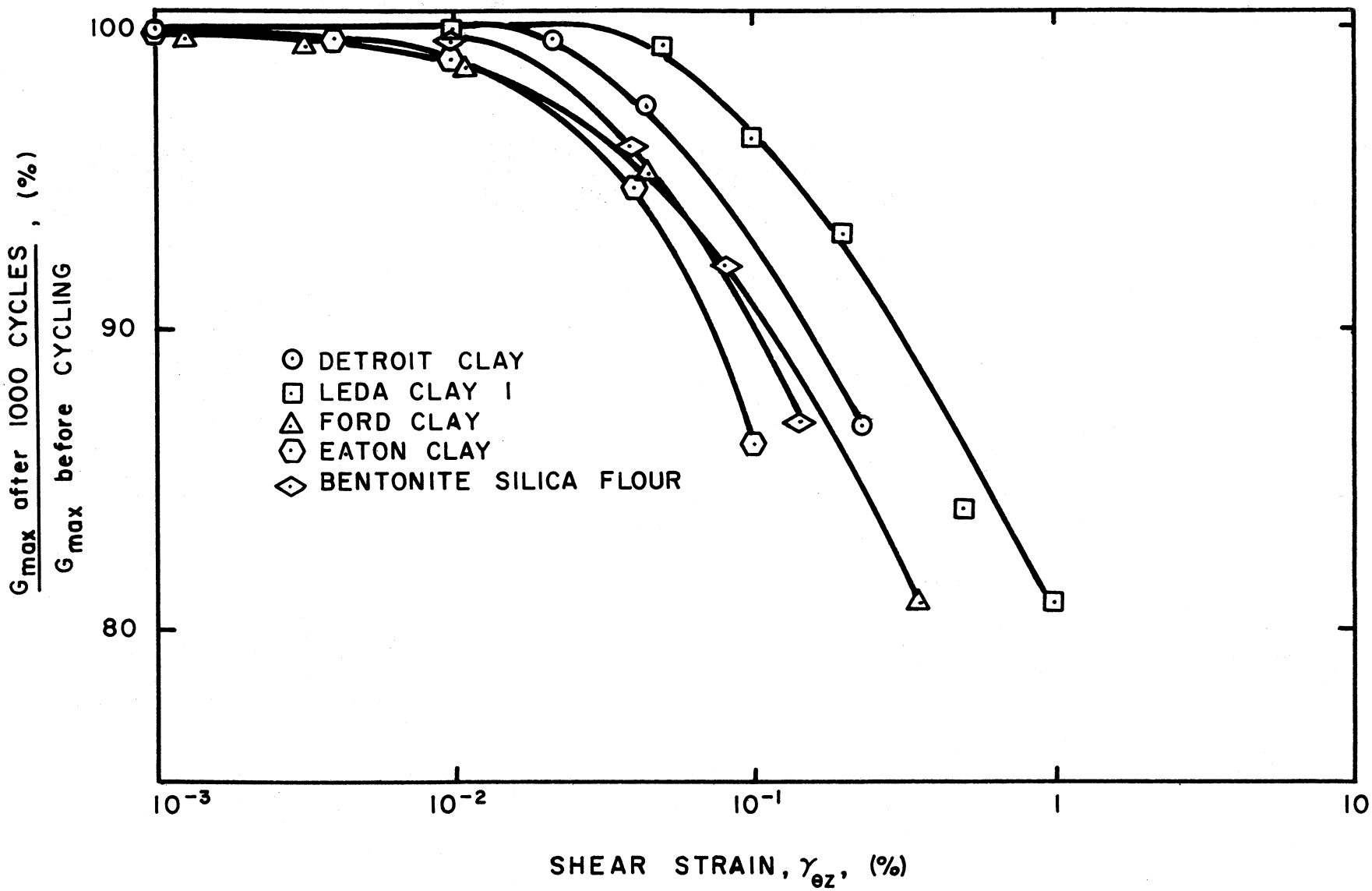

Figure 6.11. Variation in G_{max} measured 1 min after high amplitude straining.

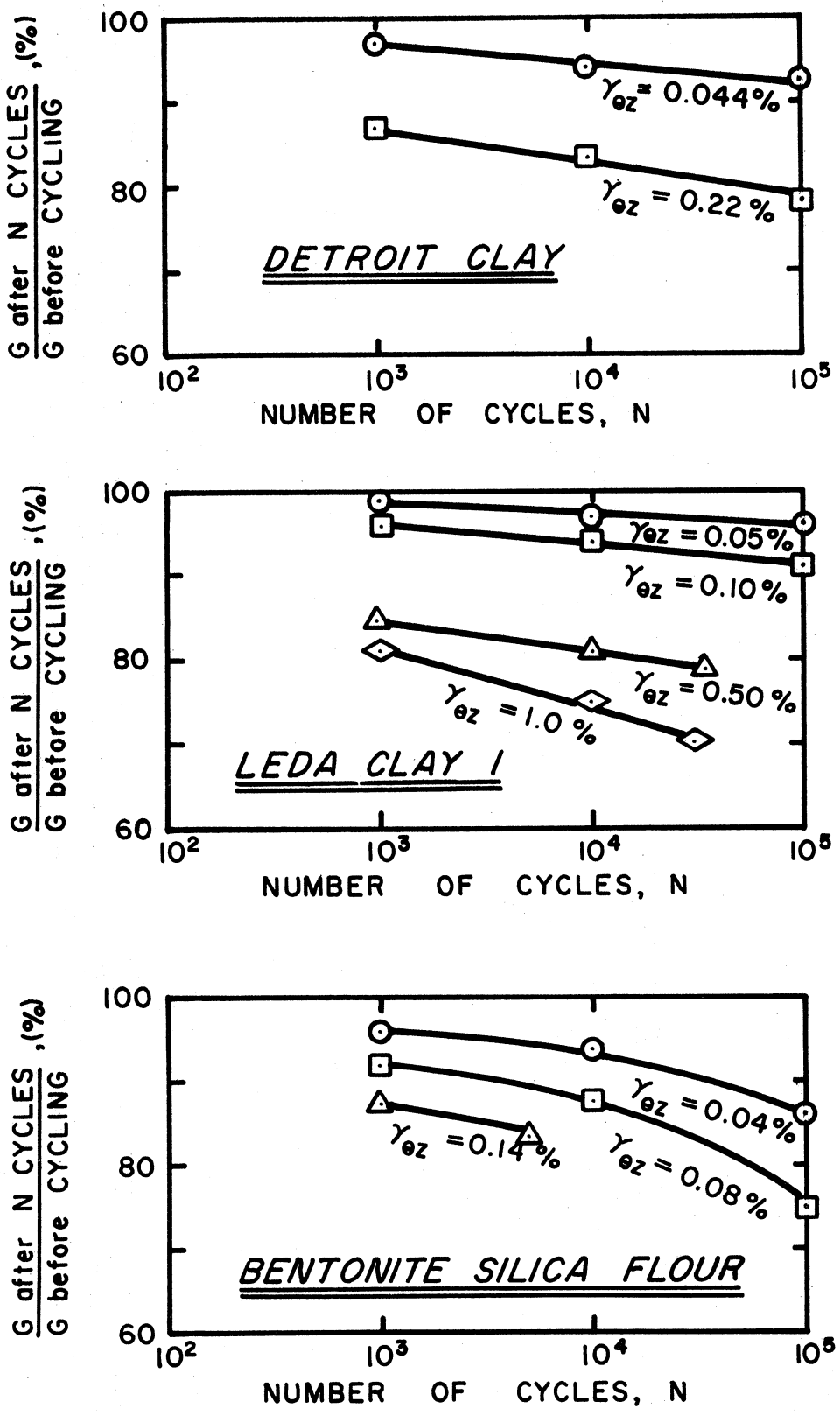

Figure 6.12. Effect of repetitions of high amplitude strain on G_{max} for Detroit Clay, Leda Clay I and Bentonite-Silica Flour.

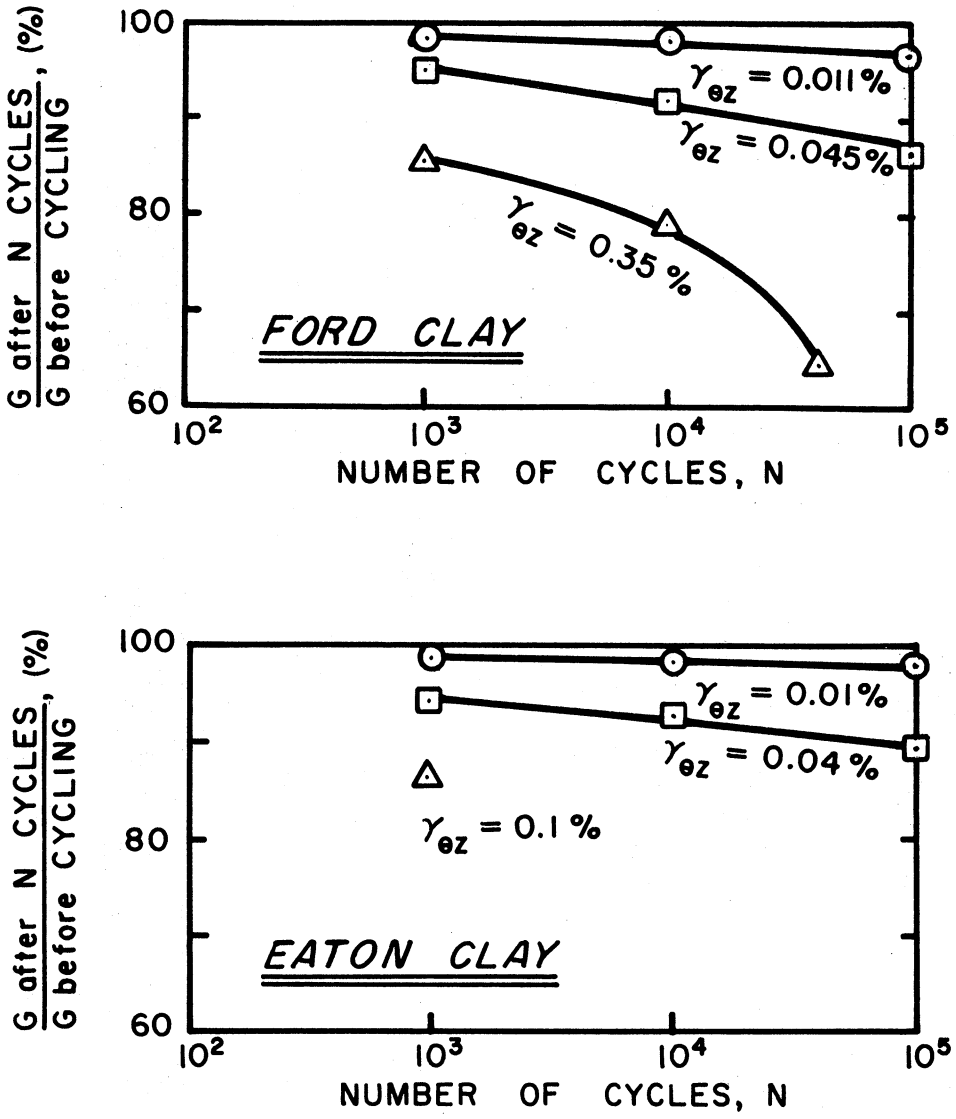

Figure 6.13. Effect of repetitions of high amplitude strain on G_{max} for Ford Clay and Eaton Clay.

amplitude strain affects G_{max} measured 1 min after high amplitude testing. The magnitude of decrease in G_{max} increased as the number of cycles of high amplitude strain increased. The number of cycles affected behavior more noticeably when the soil was cycled at high levels of strain amplitude.

The reduction in G_{max} as described above was temporary. In every test series, the modulus increased with time and eventually reached the level measured before high amplitude cycling. The general pattern of increase is shown in Figure 6.14. In this test a predetermined number of cycles of high amplitude strain (0.5 and 1.0 percent) were applied to the specimen. A reduction in G_{max} occurred. Subsequently the magnitude of G_{max} increased with time. Once the modulus reached the level measured prior to high amplitude cycling, another high amplitude test involving more cycles was performed.

The time in minutes necessary to regain 100 percent of the low amplitude modulus loss is plotted in Figures 6.15 and 6.16 as a function of strain amplitude during high amplitude cycling. The general pattern of plots shows that when the strain amplitude increased beyond a certain level, a significantly longer interval of time was required for 100 percent regain of G_{max}. It should be noted that the number of cycles of high amplitude strain did not appreciably influence the time for 100 percent regain, as seen in Figure 6.14.

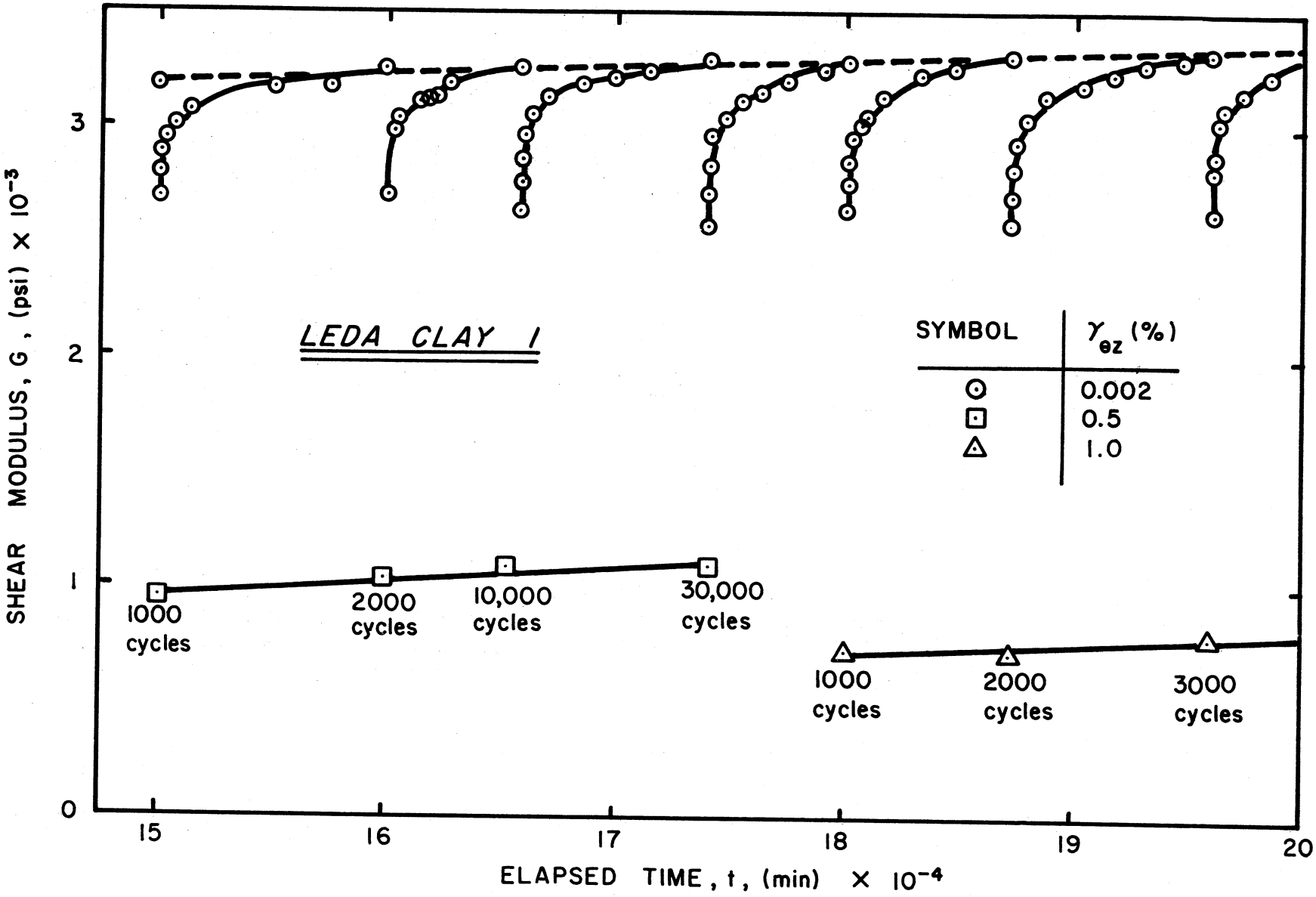

Figure 6.14. Regain in G_{max} after high amplitude cycling for Leda Clay I.

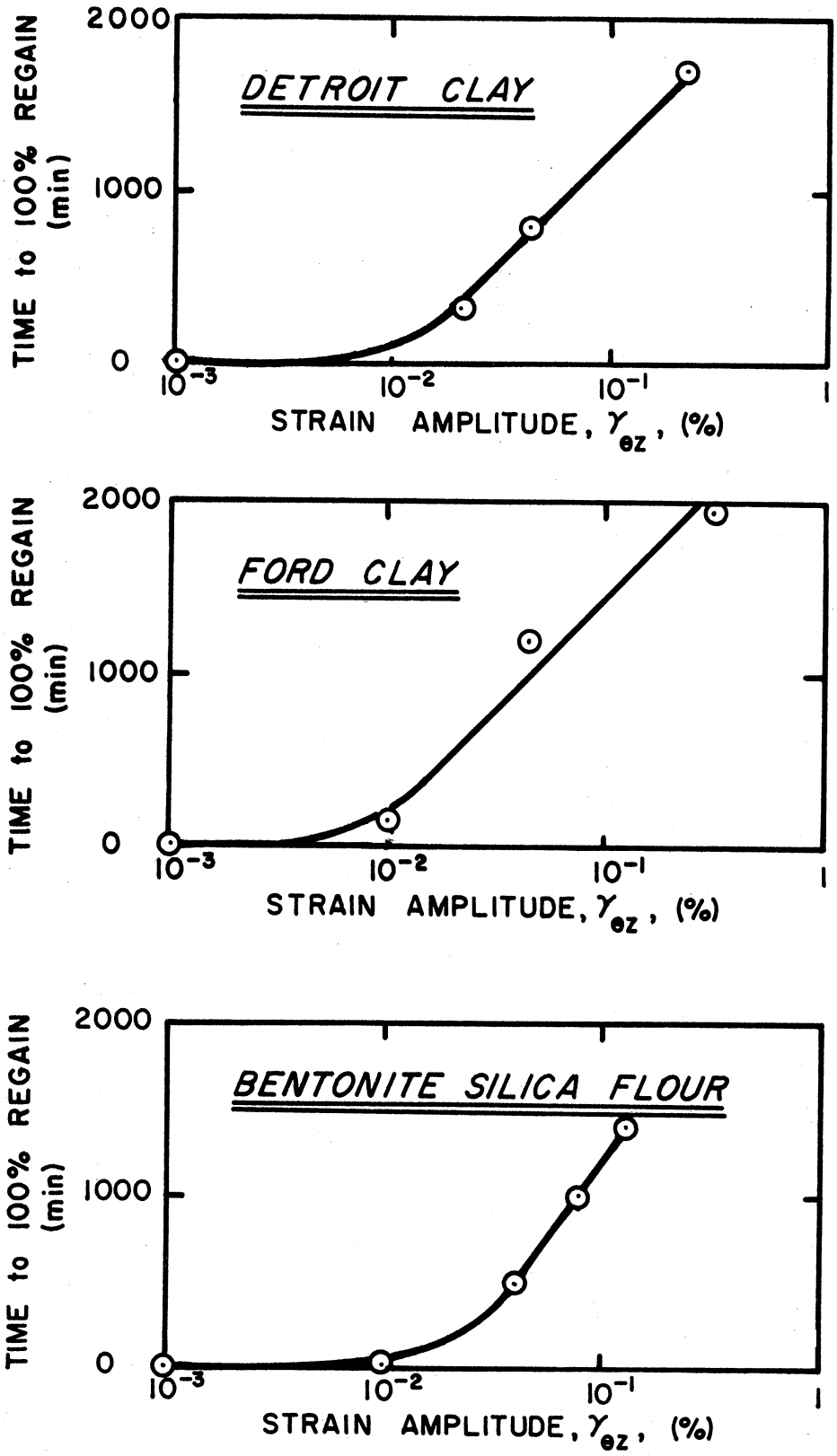

Figure 6.15. Time to 100 percent regain in G_{max} for Detroit Clay, Ford Clay and Bentonite-Silica Flour.

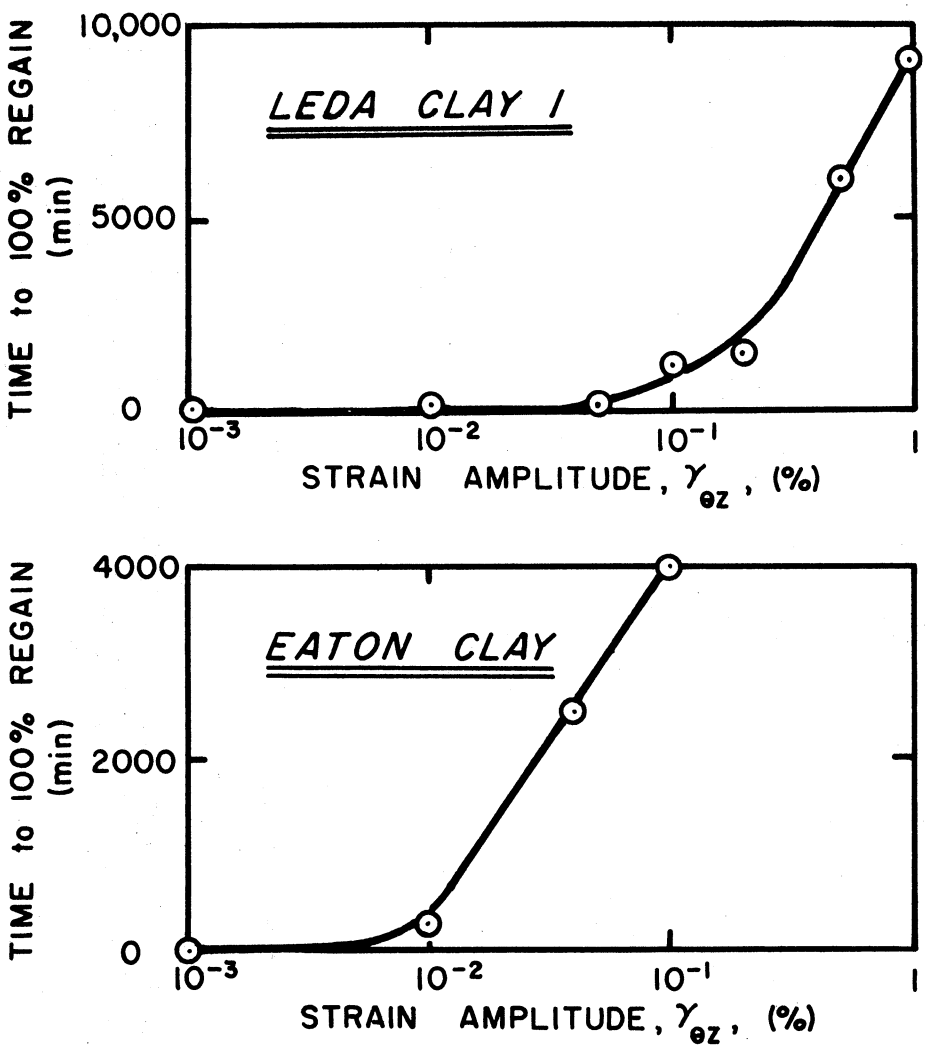

Figure 6.16. Time to 100 percent regain in G_{max} for Leda Clay I and Eaton Clay.

C. Temperature Test Results

Laboratory tests were performed to determine the effect of temperature on the dynamic characteristics of cohesive soil. Two conditions were evaluated during each test series: response at room temperature (22°C) and response at a cooler temperature (4°C). Response was determined by using the same procedure as used for low amplitude tests.

Temperature test results are presented for seven different types of cohesive soils. The general characteristics of the V_s versus log time response are similar to those described for low amplitude tests. Each velocity versus time plot includes, however, data from two test conditions, one obtained at 4°C and the other obtained at 22°C. Figure 6.17 shows the temperature response of Ball Kaolinite—which is considered a representative response. The other six plots are found in Appendix F.

The magnitude of shear wave velocity at 1000 min and the normalized secondary increase are tabulated for the seven materials in Figures 6.18 and 6.19. These figures show that velocity and normalized secondary increase varied with temperature as well as material properties and pressure.

Values of V_{s1000} at 4°C are compared to values of V_{s1000} at 22°C in Figure 6.20. This plot gives a good visual indication of temperature effects. Figure 6.20 shows that V_s was consistently higher when tested at 4°C. In general, V_s at the colder temperature exceeded V_s measured at room temperature by 0 to 13 percent. The magnitude of difference decreased as the velocity of the material increased.

Figure 6.21 shows that ΔV_s per log cycle of time for many cohesive soils depended on the test temperature. Most data points on this plot fell to the right of the 45-degree line. This trend suggested that secondary behavior increased as the temperature increased. The secondary behavior of Leda Clay I was observed to be significantly affected by change in temperature.

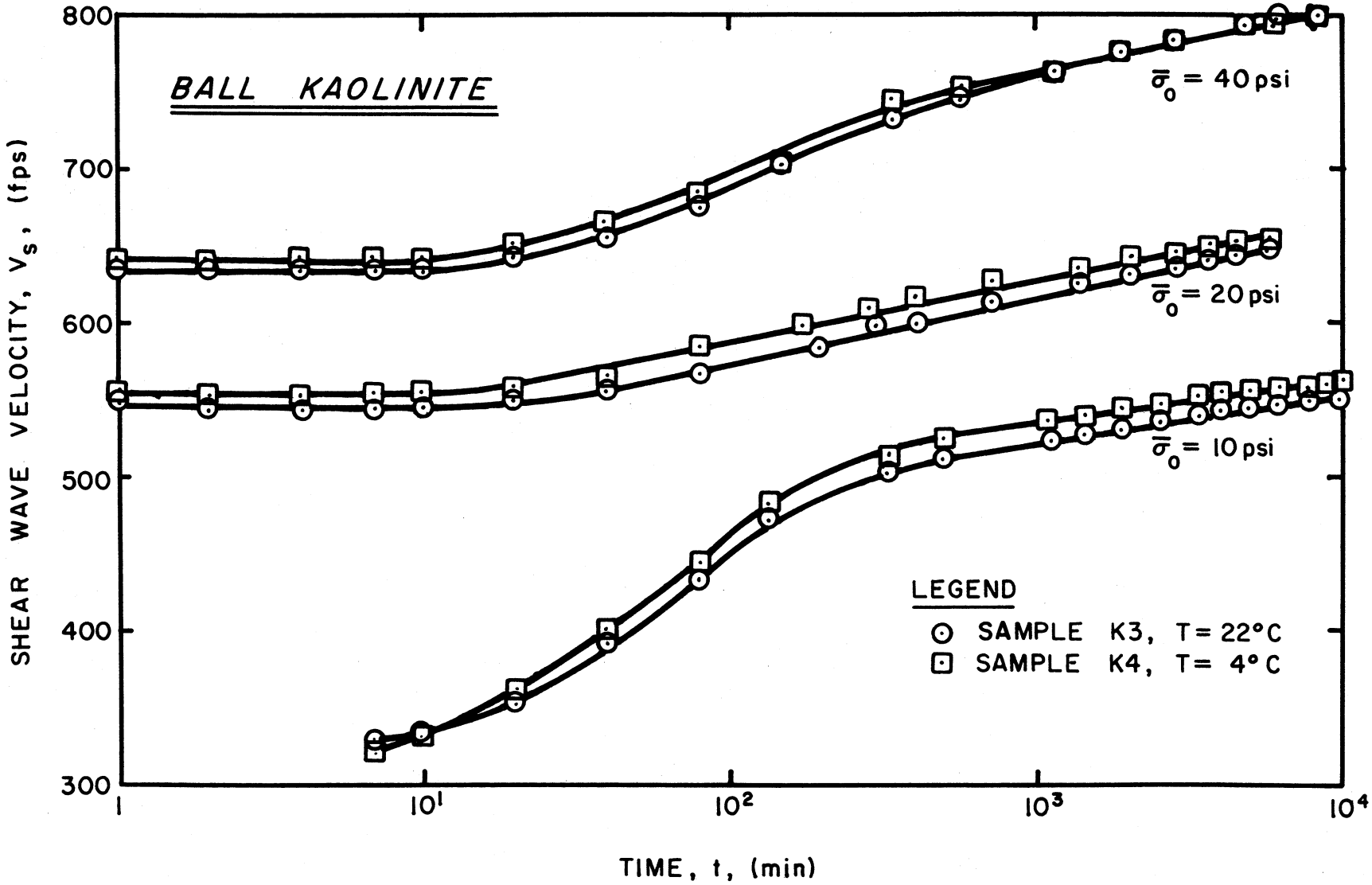

Figure 6.17. Variation in V_s with time and temperature for Ball Kaolinite.

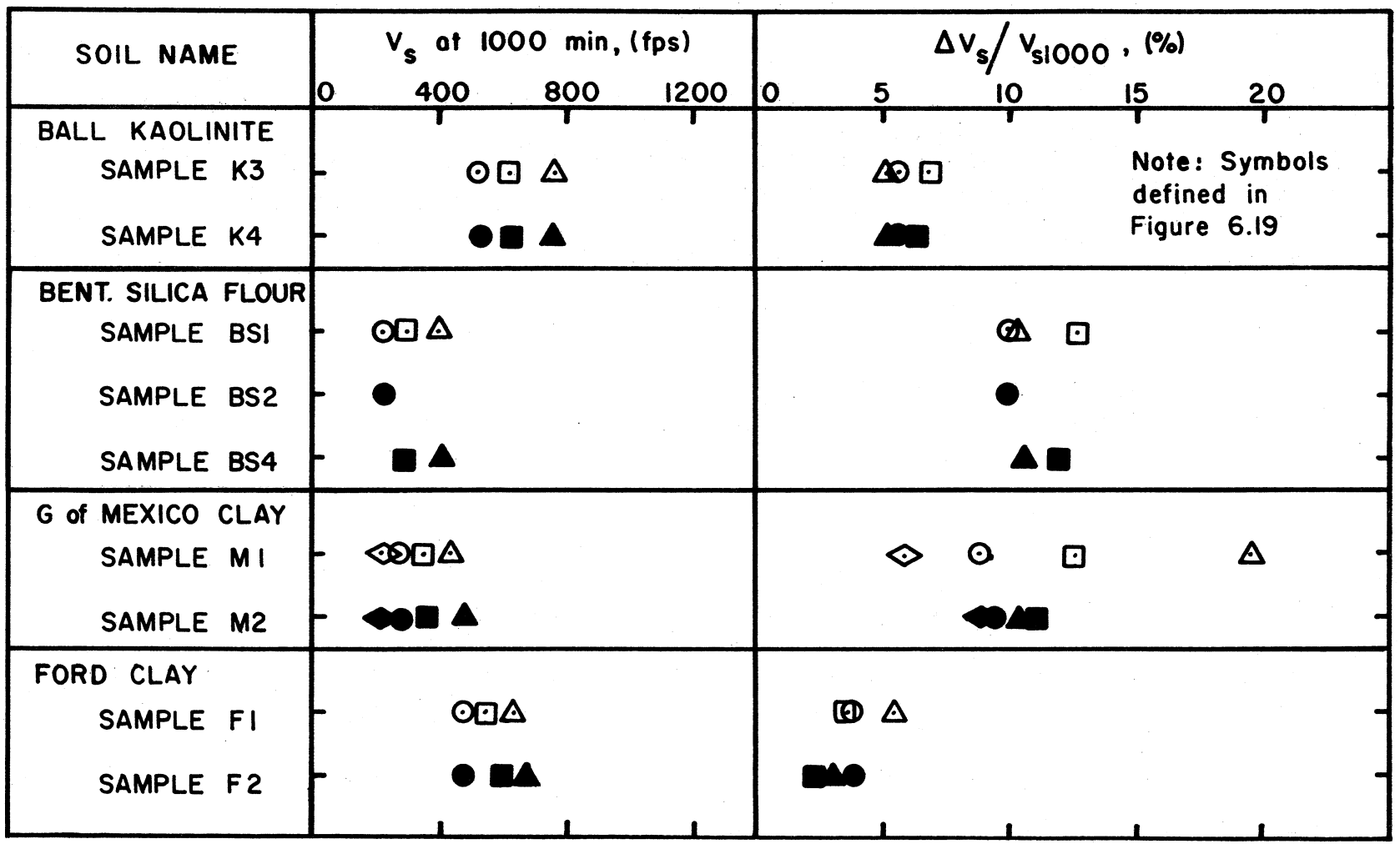

Figure 6.18. Tabulation of V_s and $\Delta V_s/_{s1000}$ at 4° and 22°C for Ball Kaolinite, Bentonite-Silica Flour, Gulf of Mexico Clay and Ford Clay.

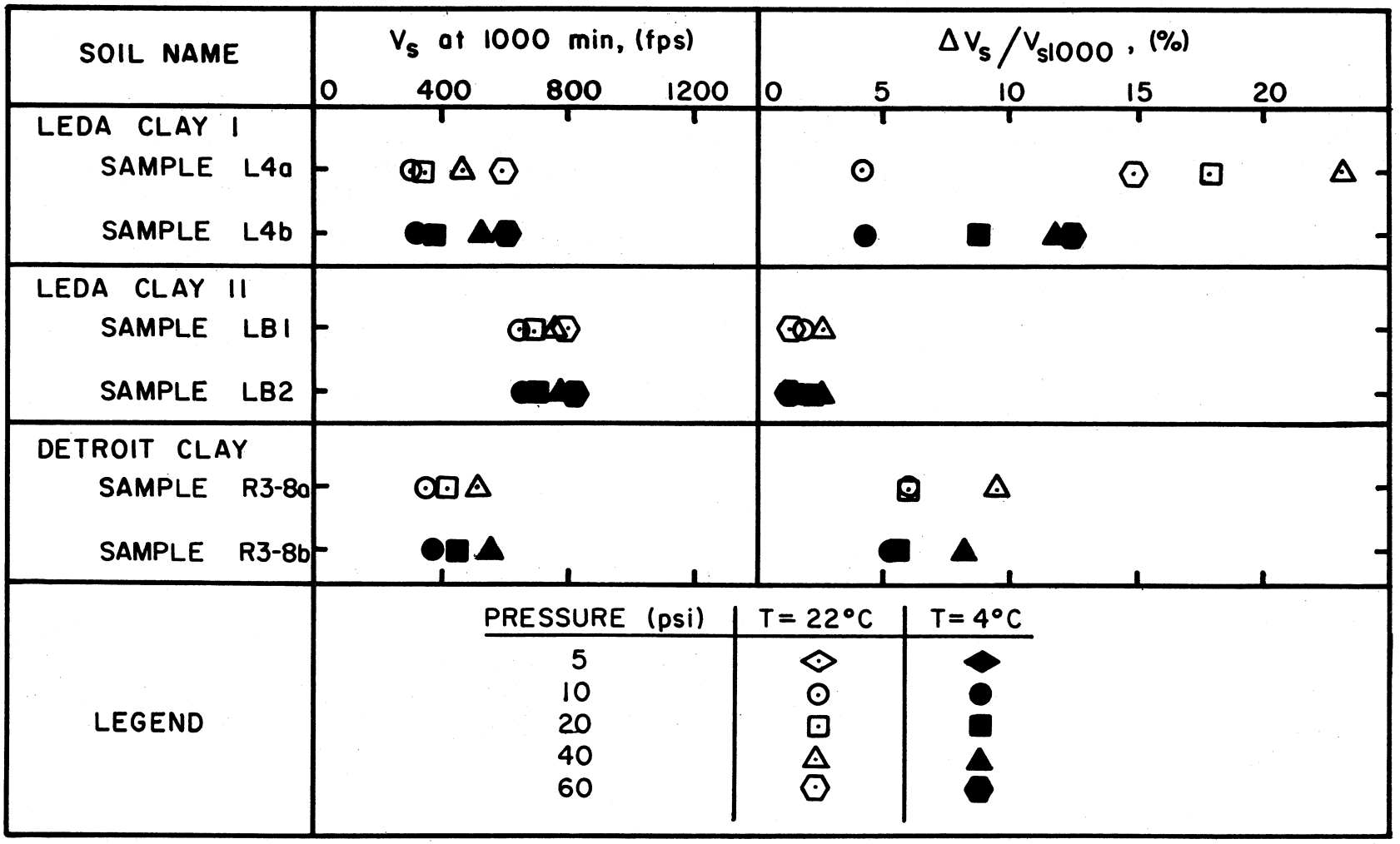

Figure 6.19. Tabulation of V_s and $\Delta V_s/V_{s1000}$ at 4° and 22°C for Leda Clay 1, Leda Clay II and Detroit Clay.

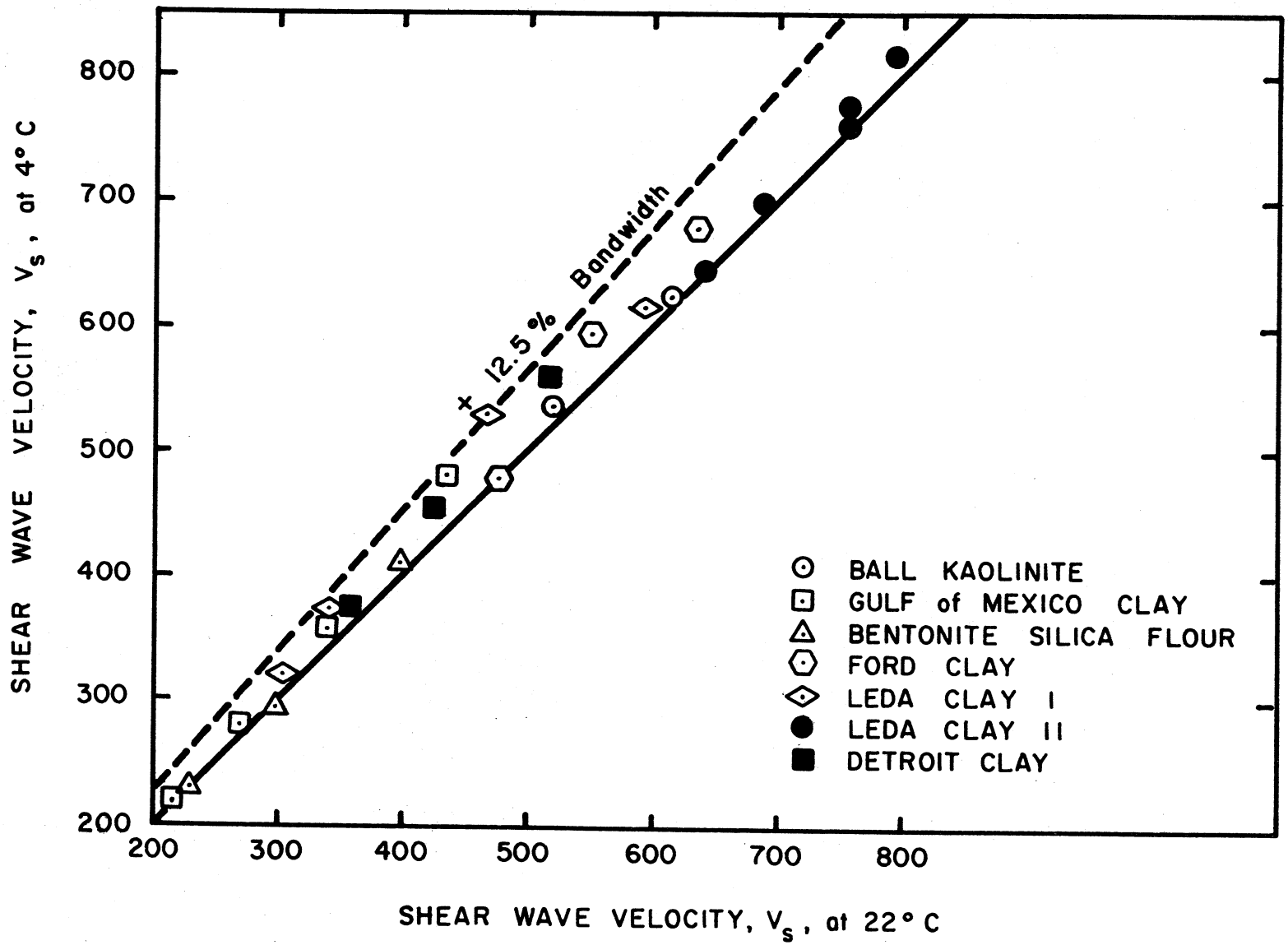

Figure 6.20. Relationship between V_{s1000} at 4°C and V_{s1000} at 22°C.

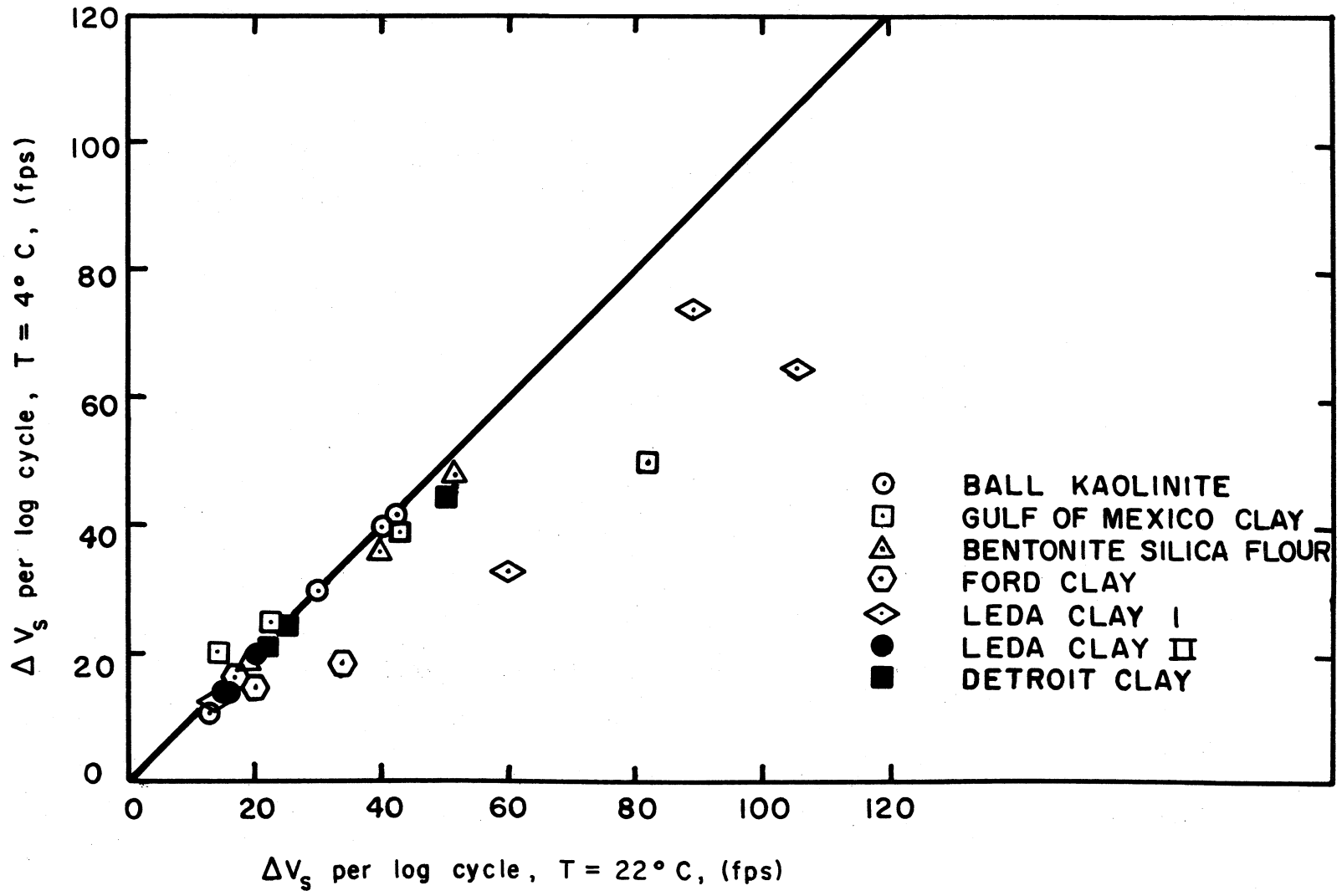

Figure 6.21. Relationship between ΔV_s per log cycle at 4°C and ΔV_s per log cycle at 22°C.

D. Field Versus Laboratory Test Results

In one phase of this investigation, shear wave velocities were measured *in situ* and then compared to values obtained by performing laboratory tests on specimens from the field site. The *in situ* values were determined by utilizing the cross-hole test procedure. Low amplitude resonant column tests were conducted to determine the laboratory results.

The values of V_s determined by field methods are plotted in Figures 6.22 and 6.23 as a function of depth. These plots show that V_s varied significantly with test location and, in two cases, with depth.

The results of the field tests are compared to the results from laboratory tests in Table 6.1. The field results were selected from Figures 6.22 and 6.23. The laboratory test results were obtained from the low amplitude tests performed at the probable overburden pressure. K_o varied according to the soil's plasticity and stress history. The actual V_s versus log time plots for the samples are found in either Appendix E or F, with the reference locations noted in Table 6.1.

Two values of V_s are given in Table 6.1 for each laboratory test. The first velocity was reported for 1000 min duration of confining pressure. This value included very little, if any, secondary velocity increase. The second value gives the 20-year velocity. This value was obtained by projecting the secondary increase approximately four logarithmic cycles beyond the 1000-min reading to a time of 20 years.

The results of the laboratory and field tests are compared in

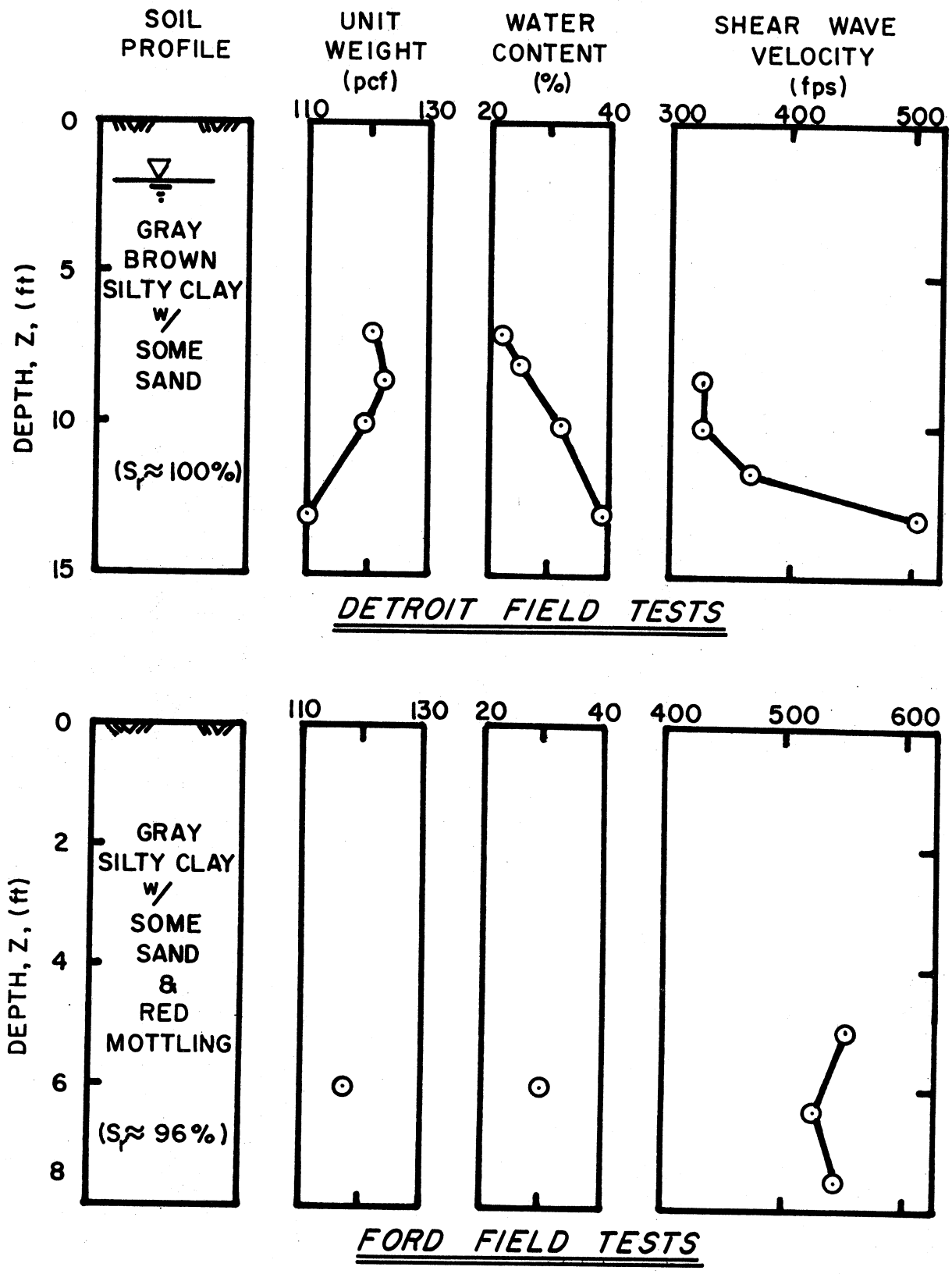

Figure 6.22. Shear wave velocity and soil data for Detroit and Ford Field Test Sites.

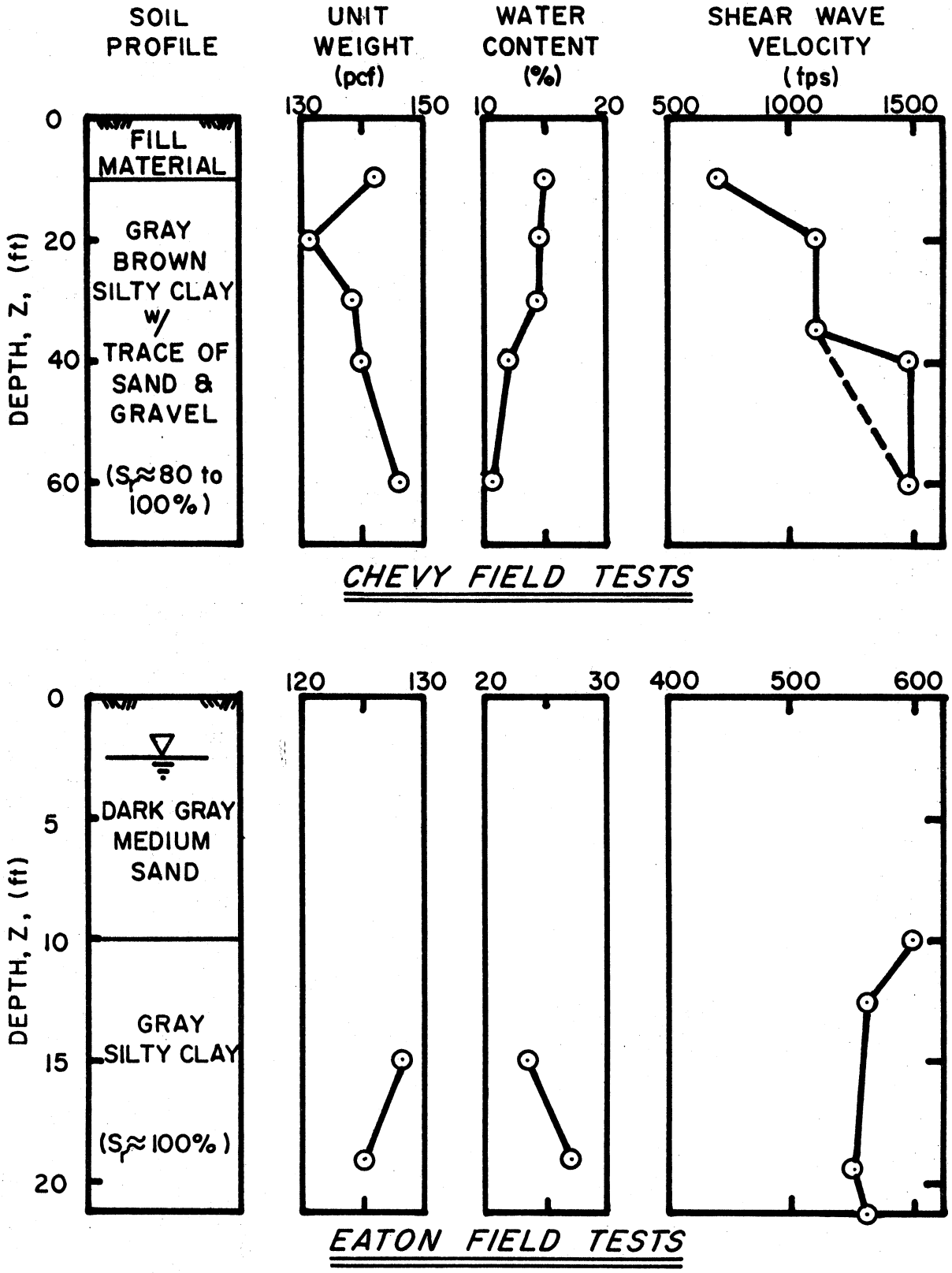

Figure 6.23. Shear wave velocity and soil data for Chevy and Eaton Field Test Sites.

TABLE 6.1. RESULTS OF LABORATORY VERSUS FIELD COMPARISON

Test Site	Field Tests		Laboratory Tests				
	Depth (ft)	V_s (fps)	Sample Number	Pressure (psi)	V_s 1000 min (fps)	V_s 20 yr (fps)	Figure Number
Detroit	10	330	R2-1	5	350	470	6.1
Ford*	6	550	F1	10	480	540	F.4
Chevy	20	1100	C3	17	810	1050	E.7
	35	1100	C1 & C2	24	880	1120	E.5 & E.6
	50	1500	C4	33	970	1230	E.8
Eaton	15	565	E1	6	380	520	E.3
	19	550	E2	8	390	550	E.4

*NOTE: Originally 18 ft of overburden. Approximately 12 ft removed prior to cross-hole test. Laboratory results extrapolated from test data obtained at 10 and 20 psi.

Figure 6.24. At three of the four sites, V_s from the field test exceeded V_s measured in the laboratory after 1000 min of testing. However, when the comparison was made between the field and the 20-year laboratory velocities, the difference decreased noticeably. In several of the tests, the 20-year velocity was virtually equal to the field result. Variations in data are discussed in detail in Chapter VII, Discussion of Results.

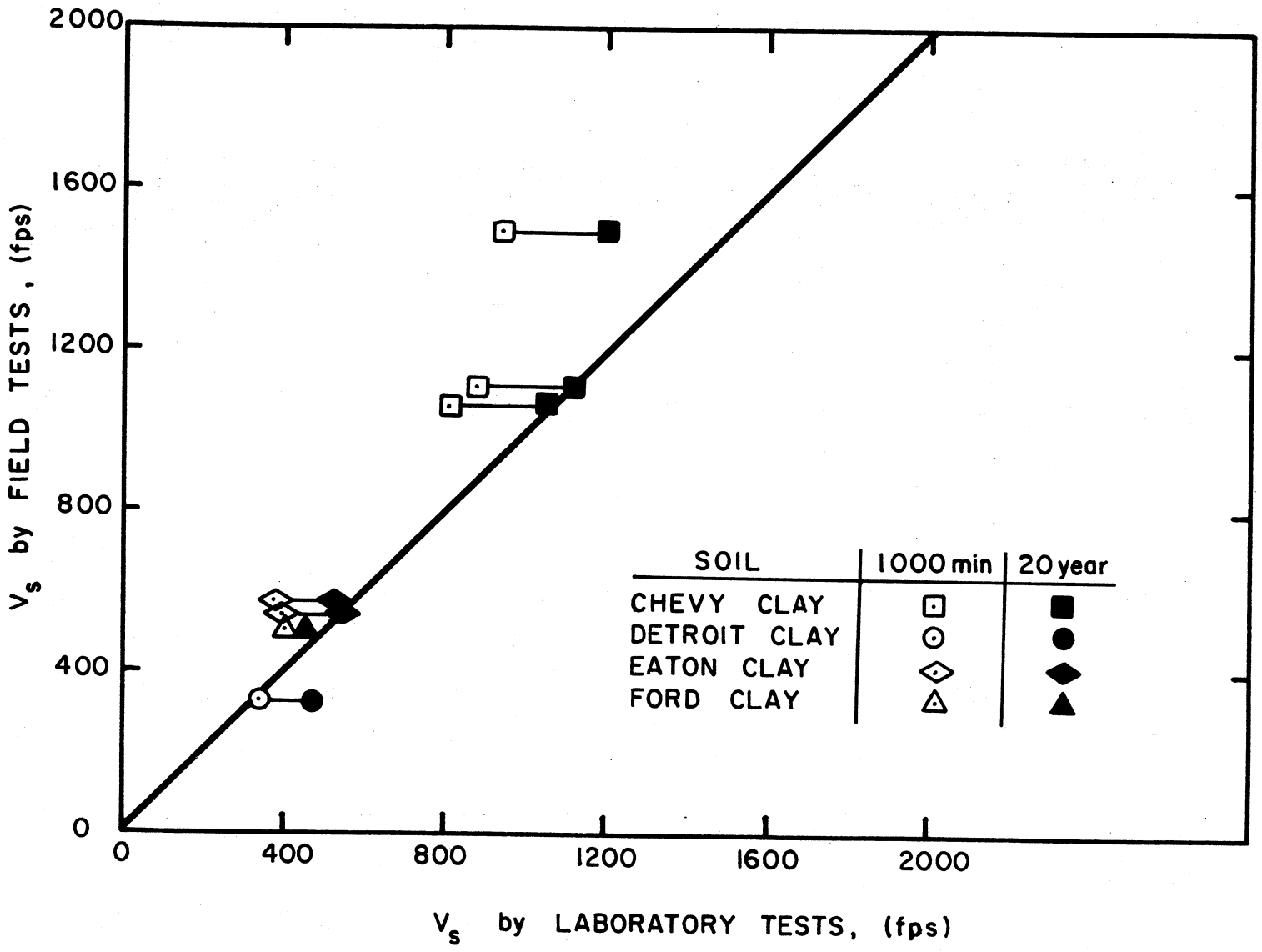

Figure 6.24. Comparison between V_s defined by laboratory testing and V_s measured in situ.

CHAPTER VII

DISCUSSION OF RESULTS

The following sections present a detailed review of test results. During the review, emphasis is placed on trends established by data, chemical and physical mechanisms governing response, absolute comparison of behaviors and overall validity of results. When appropriate, test results are compared to experimental, empirical and analytical results presented by others.

A. Low Amplitude Test Results

A number of important observations can be made about the low amplitude test data presented in Chapter VI. The most important of these observations involves the effects of confining pressure on shear wave velocity, the effects of time on long-term sample response and the repeatability of test data.

1. EFFECTS OF CONFINING PRESSURE

During the low amplitude tests described herein, the shear wave velocity, V_s, increased as the confining pressure increased. The increase occurred when the sample was permitted to drain. Various other researchers (Hardin and Black, 1968; Humphries and Wahls, 1968) observed similar behavior. The increase in V_s was generally attributed to the increase in effective stress and the decrease in void ratio. The

stress effect was considered the more important of the two parameters.

Two empirical methods were described in Chapter II for predicting the low amplitude shear modulus, G_{max}, on the basis of the confining pressure, the void ratio and the overconsolidation ratio. The results determined during this investigation were compared with the results predicted by a modified version of the Hardin and Black equation, i.e.,

$$V_s = (159 - 53.5e)\, OCR^{K/2}\, \bar{\sigma}_o^{\,0.25} \qquad (7.1)$$

where V_s = shear wave velocity (fps)

e = void ratio

OCR = overconsolidation ratio

K = plasticity factor (Figure 2.2)

$\bar{\sigma}_o$ = confining stress (psf).

The comparison is shown in Figure 7.1.

The shear wave velocity measured in the laboratory test after 1000 min of confinement was used as the comparison value. The velocity defined by Eq. (7.1) and called hereafter the empirical result or empirical velocity was modified to compensate for changes in void ratio which occurred during the test interval and adjusted to include the effects of overconsolidation. All empirical results were corrected for change in void ratio; approximately one-third of the data points were adjusted for overconsolidation.

As indicated in Figure 7.1, the empirical velocities were consistently greater than V_s determined during the laboratory test. The

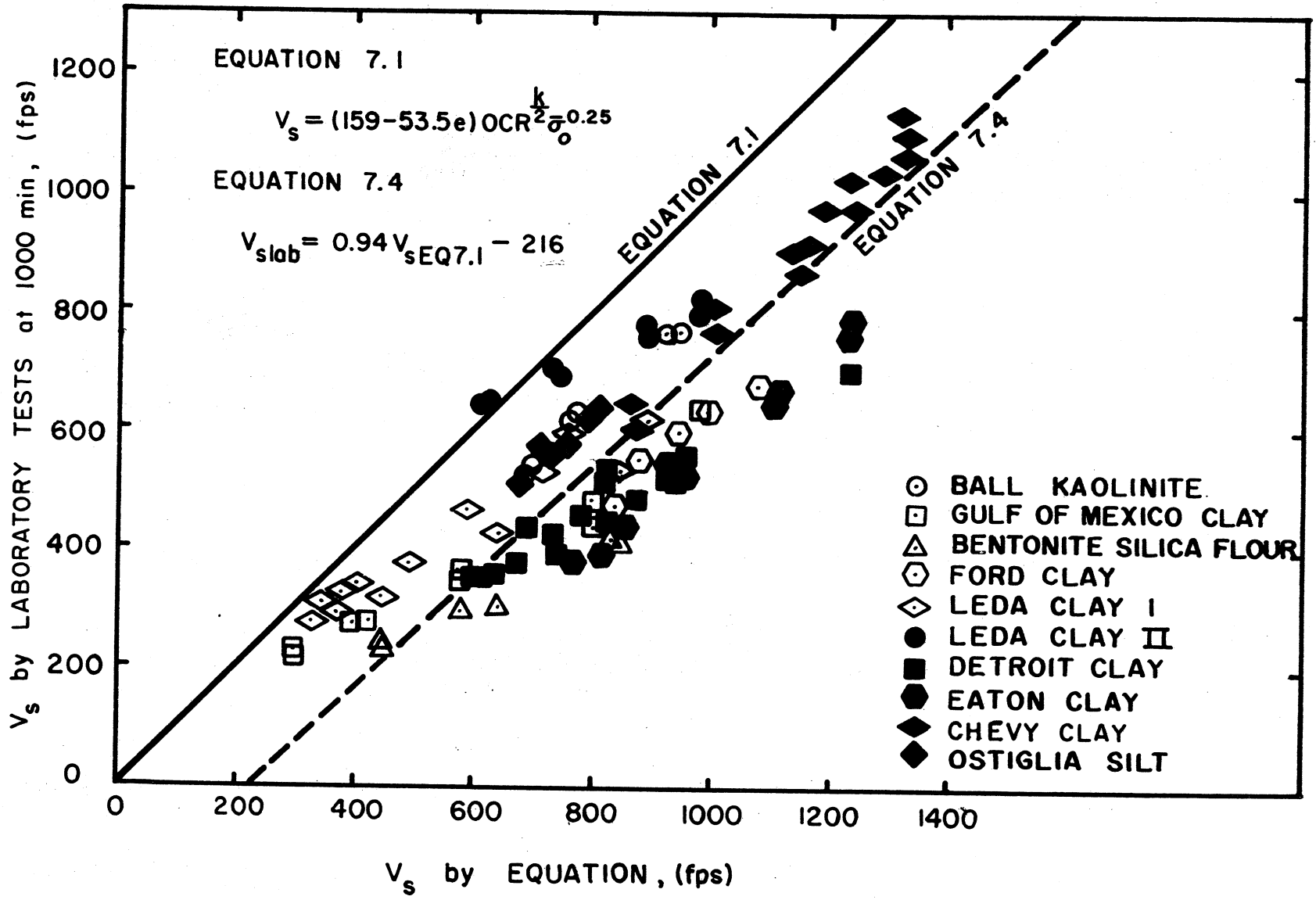

Figure 7.1. Relationship between V_s defined in the laboratory and V_s predicted by Eq. (7.1).

magnitude of the discrepancy ranged from 15 to 100 percent. A majority of the laboratory values were, however, within 40 percent of the predicted values. It was concluded that, in general, the Hardin and Black equation did not adequately predict V_s measured in the laboratory resonant column device after 1000 min of confinement.

The difference between the laboratory and the empirical result was related to certain assumptions and simplifications made during analyses. Three of the more apparent factors contributing to the difference included the method used to adjust the void ratio at each pressure level, the overall applicability of the empirical equation and the time, following the application of the confining pressure, when the laboratory value of V_s was selected.

a. Void Ratio Adjustment

The empirical velocity was computed on the basis of the void ratio of the soil specimen at the particular confining pressure. When estimating the laboratory test result, it was necessary, therefore, to substitute not only the correct confining pressure but also the appropriate void ratio at that confining pressure.

The void ratio of the specimens changed as the confining pressure changed. During a standard triaxial test the magnitude of void ratio change is calculated on the basis of the measured change in height and volume of the test specimen. The volume change is indicated by the amount of pore water extruded from the sample during drainage. Unfortunately the standard method of determining void ratio change could not

be used. Air migrated through the system and out the drainage line to such an extent that all volume readings were erroneous. It was necessary, therefore, to use an indirect method to calculate the void ratio change.

The basic premise of the indirect solution was that the material was homogeneous and isotropic; consequently, for hydrostatic confinement lateral strains equalled axial strains. Once this assumption was made, the following relationship between axial strain and change in void ratio was developed

$$\Delta e = \epsilon_a(1 + e_o)(3 - 3\epsilon_a + \epsilon_a^2) \qquad (7.2)$$

where Δe = change in void ratio

ϵ_a = axial strain (in./in.)

e_o = initial void ratio

This derivation is subject to justified criticism because few soils are homogeneous and isotropic in character. Equation 7.2 is particularly questionable when soils are stratified or varved.

The general validity of this adjustment technique was checked by comparing void ratio changes predicted by Eq. (7.2) on the basis of axial strain to similar quantities measured during a triaxial consolidation test performed in a triaxial apparatus (Figure 7.2). Water was used as a confining medium during the consolidation test; therefore, air migration was not a problem. Ball Kaolinite, as described in Chapter V, was employed as the test material.

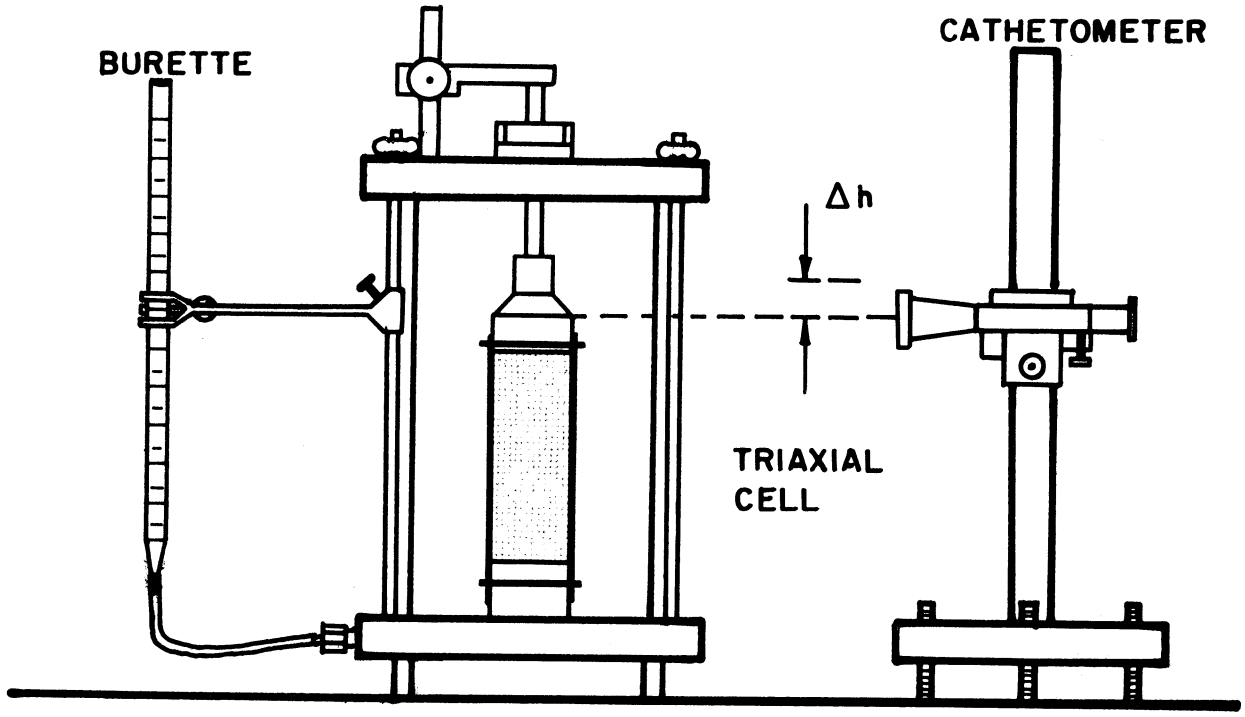

(a) Schematic diagram

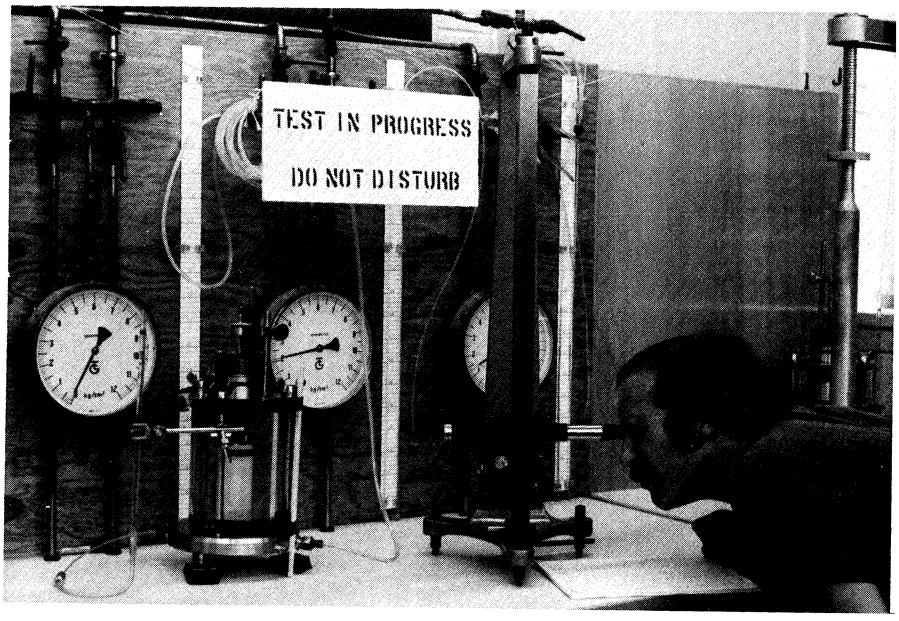

(b) Photograph

Figure 7.2. Triaxial consolidation test setup.

The results of this comparison are shown in Table 7.1. The theoretical method gave a reasonably close approximation of the void ratio calculated by direct methods. It must be emphasized that this close correlation does not necessarily hold for all other soils. The Ball Kaolinite sample should have conformed reasonably well to the homogeneous, isotropic criteria.

TABLE 7.1. COMPARISON OF VOID RATIOS DETERMINED BY THEORETICAL METHODS AND BY DIRECT MEASUREMENTS

Confining Pressure $\bar{\sigma}_o$ (psi)	Test Specimen 1			Test Specimen 2		
	Axial Strain (%)	Measured Void Ratio	Calculated Void Ratio	Axial Strain (%)	Measured Void Ratio	Calculated Void Ratio
0	0	1.12	--	0	1.14	--
10	1.1	1.07	1.05	0.9	1.05	1.08
20	1.8	1.02	1.01	1.5	1.01	1.04
40	3.3	0.93	0.92	3.6	0.92	0.92

If the void ratio adjustment method overestimated the actual void ratio change, then a higher value for the empirically derived V_s would have been defined. The magnitude of this overestimation would not, however, have caused the magnitude of differences noted in Figure 7.1.

b. General Validity of Hardin-Black Equation

Equation (7.1), without the OCR term, was originally derived by Hardin and Richart (1963) to predict V_s for angular grained sands. In a more recent investigation, Hardin and Black (1968) found that the same equation gave a good indication of V_s for clays with low surface

activity as long as the vibration amplitude was less than 0.01 percent. This information was documented in the text, Vibrations of Soils and Foundation, by Richart, Hall and Woods (1970).

In the closure to their 1968 paper, Hardin and Black (1969) concluded that although the general form of Eq. (2.2) (and consequently Eq. (7.1)) was correct, the absolute magnitude was better predicted by

$$G = C \frac{(2.973 - e)^2}{1 + e} OCR^K \bar{\sigma}_o^{0.5} \qquad (7.3)$$

where the constant, C, varied from 600 to 1230. This conclusion was based on laboratory tests results for 10 different cohesive soils. Soils tested by Hardin and Black exhibited a wide range of properties: plasticity indices (I_p) varied from 2 to 85 percent, void ratios ranged from 0.5 to 1.7 and activities varied from 0.29 to 2.13. The scope of the Hardin and Black comparison was limited to a single pressure, 2 kg/cm^2.

The magnitude of difference noted by Hardin and Black was similar to that shown in Figure 7.1. The obvious conclusion was that Eq. (7.1) should be modified to account for the discrepancy. However, before making such a modification, the effects of time were considered.

c. Time Effects

The empirical velocity was compared to the 1000-min laboratory value of V_s. The selection of the 1000-min time for defining V_s was based on precedent established by others (Afifi and Woods, 1972). Various V_s versus log time plots show, however, that a constant increase in

V_s occurs after 1000 min. If the 10,000-min velocity had been compared to the empirical velocity, then the agreement would have been better.

It seems apparent that the difference between V_s defined by the laboratory resonant column device and V_s defined by Eq. (7.1.) depended primarily on the time at which the laboratory value was selected. In general the comparison between the two velocities improved as more secondary increase in velocity was included within the laboratory result. This secondary increase effect can be related to the variations noted in Eq. (7.3). The lowest value of C, 600, might be used to define G without secondary increase while the highest value, 1230, might be used to define G with secondary increase. Unfortunately Hardin and Black did not report the time at which the laboratory value of V_s was recorded.

2. PROPOSED EMPIRICAL EQUATIONS

In certain situations the shear modulus before or during secondary increase is desired. Equation (7.3) encompasses such a wide range of possible values, depending upon the selection of the constant C, that it does not adequately satisfy prediction requirements. In view of this deficiency, three new empirical equations are proposed. These equations were derived from laboratory results measured after 1000-min of confinement and, consequently, give a better prediction of V_s (and therefore G_{max}) at the beginning of secondary increase.

The proposed equations were developed by statistically evaluating the results given in Chapter VI. The evaluation involved over 90 data points for nine different clays and one silty material. The engineering

properties of these materials are summarized in Chapter V. Prior to the statistical analyses, data were adjusted for overconsolidation effects and for change in void ratio due to confinement. Techniques used to make these adjustments were described in the previous section.

a. Proposed Equation (1)

The first proposed relationship was simply a best fit line drawn through the plotted data. Linear regression techniques were used to define the constants for the line. On the basis of this analysis, the average V_s at 1000 min was given by

$$V_{s1000} = 0.94\, V_{sEQ} - 216 \qquad (7.4)$$

where V_{sEQ} = the shear wave velocity (fps) determined by Eq. (7.1). The correlation coefficient for this line was 0.87. The coefficient defines the "goodness" of the fit, with 1.0 being a perfect fit and 0.0 being no correlation. As can be seen in Figure 7.1, the data are within plus or minus 100 fps of the line.

Obviously a significant variation in results occurred even with this modified equation. The magnitude of variation suggested that factors other than void ratio, overconsolidation ratio and confining pressure influenced V_s of cohesive soils.

b. Proposed Equations (2) and (3)

The second and third proposed equations were developed to give a better overall approximation of dynamic response. In Figure 7.1,

results at low velocities tended to deviate in a consistent manner from the line representing Eq. (7.4). Apparently a different mechanism governed the response of materials at high void ratios.

The second and third empirical equations were derived by reanalyzing the relationship between confining pressure, void ratio and V_s. Appendix G provides a detailed description of the analysis procedure.

The first of the two equations was bilinear in form. The equation was developed by separating test results into two groups: data with void ratios above 1.25 and data with void ratios equal to or less than 1.25. By performing a linear regression analysis on each data group, the following two equations were defined

$$\text{for } e > 1.25$$

$$V_s = (75 - 17e)\, OCR^{K/2}\, \bar{\sigma}_o^{\,0.25} \qquad \text{(a)}$$

$$\text{for } e \leq 1.25$$

$$V_s = (117 - 48e)\, OCR^{K/2}\, \bar{\sigma}_o^{\,0.25} \qquad \text{(b)} \qquad (7.5)$$

where V_s is defined in feet per second (fps) and $\bar{\sigma}_o$ is defined in pounds per square foot (psf).

Velocities calculated by Eqs.(7.5) are compared to laboratory velocities in Figure 7.3. A fairly good correlation occurs. The mean difference between laboratory data and the proposed equations is 77 fps; the standard deviation is 50 fps.

The second equation related V_s to the overconsolidation ratio, the confining stress and the logarithm of the void ratio. This comparison

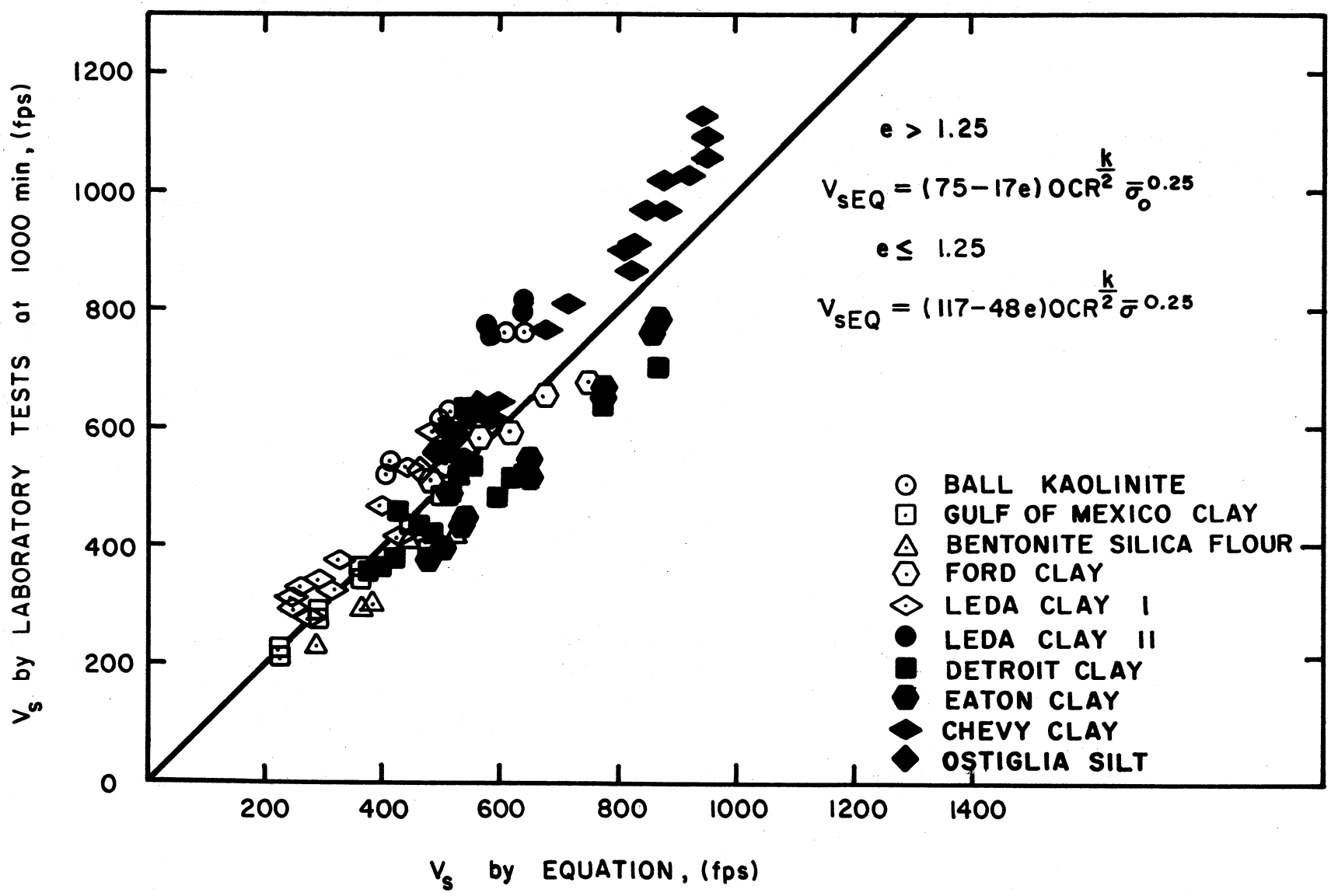

Figure 7.3. Comparison of V_s defined in the laboratory and V_s predicted by Eq. (7.5).

also adjusted for variations in V_s observed at high void ratios.

On the basis of a linear regression analysis the following relationship was defined

$$V_s = (66 - 123 \log e)\, OCR^{K/2}\, \bar{\sigma}_o^{0.25} \qquad (7.6)$$

units for this equation are the same as those units used in Eqs. (7.5). The velocity, as defined by Eq. (7.6), is compared to the laboratory results in Figure 7.4. Despite a significant amount of scatter, a definite correlation occurs. The mean difference between laboratory data and Eq. (7.6) is 85 fps; the standard deviation is 60 fps.

Equations (7.5) were judged slightly better than Eq. (7.6). This decision was based on a comparison of mean differences and standard deviations. The difference was, however, slight. Both equations gave a better average indication of response than did Eq. (7.4). The scatter in data for all cases was attributed to various factors not included in the equations.

The apparent nonlinear relationship between V_s and void ratio merits some additional discussion. Such behavior suggests that strength does not decrease in direct proportion to void ratio increase. Two possible explanations are proposed for this behavior.

The first explanation is based on the size of the soil particles. It was observed that two materials, Leda Clay I and Gulf of Mexico Clay, departed noticeably from the linear relationship. Both soils had a substantial proportion of particles less than the 2-μ size. Although

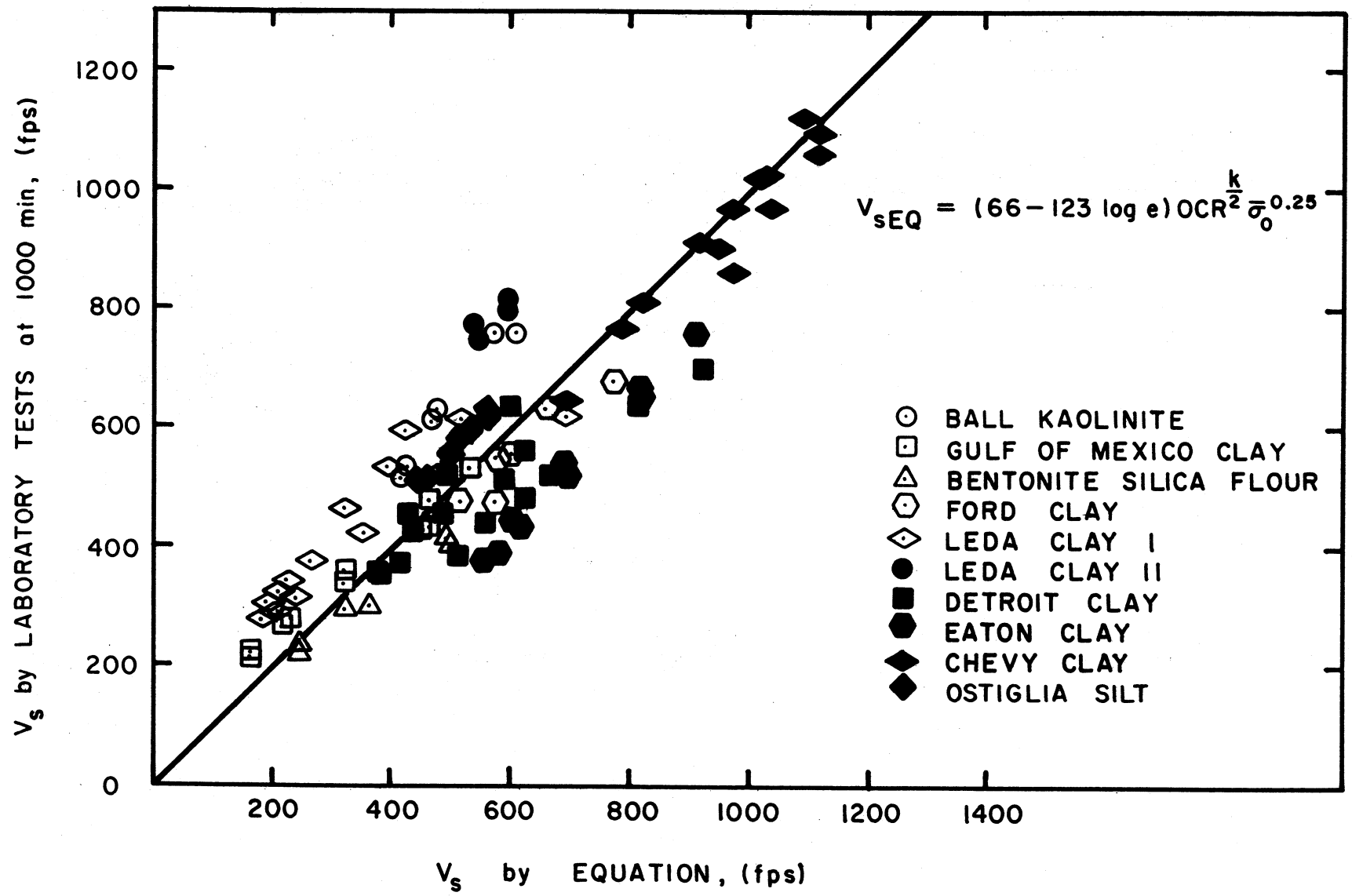

Figure 7.4. Comparison of V_S defined in the laboratory and V_S predicted by Eq. (7.6).

the volume of these materials was low, the surface area was high, and consequently the potential contribution of interparticle forces was large. The value of V_s was expected to differ according to the contribution of interparticle forces. It was thought, therefore, that these two soils may have exhibited higher values of V_s because interparticle forces were larger.

The second explanation is related to the origin of the materials. The geologic background of the Leda Clay and the Gulf of Mexico Clay was similar. Both materials were originally deposited at very slow rates in seawater. Noorany and Gizienski (1970) noted that soils deposited in marine environments often exhibit a high undrained strength to overburden pressure ratio without being overconsolidated. The high strength to pressure ratio is attributed to the slow consolidation process. A "reserve" strength or pseudo overconsolidation condition occurs. The same explanation might be used to account for the high velocities observed for Leda Clay and Gulf of Mexico Clay.

3. SECONDARY INCREASE IN VELOCITY

The results of this investigation show that V_s increased as time increased beyond the 1000-min interval. All ten soils exhibited this type of response. The rate of increase was linear on a semi-logarithmic plot. Various other researchers (Hardin and Black, 1968; Marcuson and Wahls, 1972; Afifi and Richart, 1973) observed similar behavior in cohesive soils.

A method of predicting the rate of secondary increase was desired.

It was thought that such a relationship could be derived on the basis of material properties. Normalized secondary increase, $\Delta V_s/V_{s1000}$, for the test data was, therefore, compared to various soil parameters: for example, the percent less than the 2-μ size, liquid and plastic limits, plasticity and liquidity indices, and soil activity. Although all these parameters represented physical characteristics of the materials, none gave a satisfactory correlation when compared to $\Delta V_s/V_{s1000}$. A certain amount of correlation was found to exist between $\Delta V_s/V_{s1000}$ and mean particle diameter, initial void ratio and undrain shearing strength.

Figure 7.5 shows the relationship between $\Delta V_s/V_{s1000}$ and the logarithm of the mean particle diameter, D_{50}. Although the data were very scattered, in general, it can be seen that $\Delta V_s/V_{s1000}$ increased as log D_{50} decreased. A straight line defined by performing a linear regression analysis on data had a very low correlation coefficient, i.e., 0.27.

The logarithm of $\Delta V_s/V_{s1000}$ was replotted as a function of log D_{50} (Figure 7.6). Once again data were scattered. However, the straight line for this data had a correlation coefficient of 0.47. This improvement suggests that the secondary increase was better approximated by the log-log relationship. Such behavior tends to confirm the general form of the nonlinear relationship proposed by Afifi and Richart (1973).

Figure 7.7 shows the relationship between the logarithm of $\Delta V_s/V_{s1000}$ and the initial void ratio, e_o. The plot indicates that secondary behavior increased as the initial void ratio increased. The correlation coefficient for the lines is 0.77.

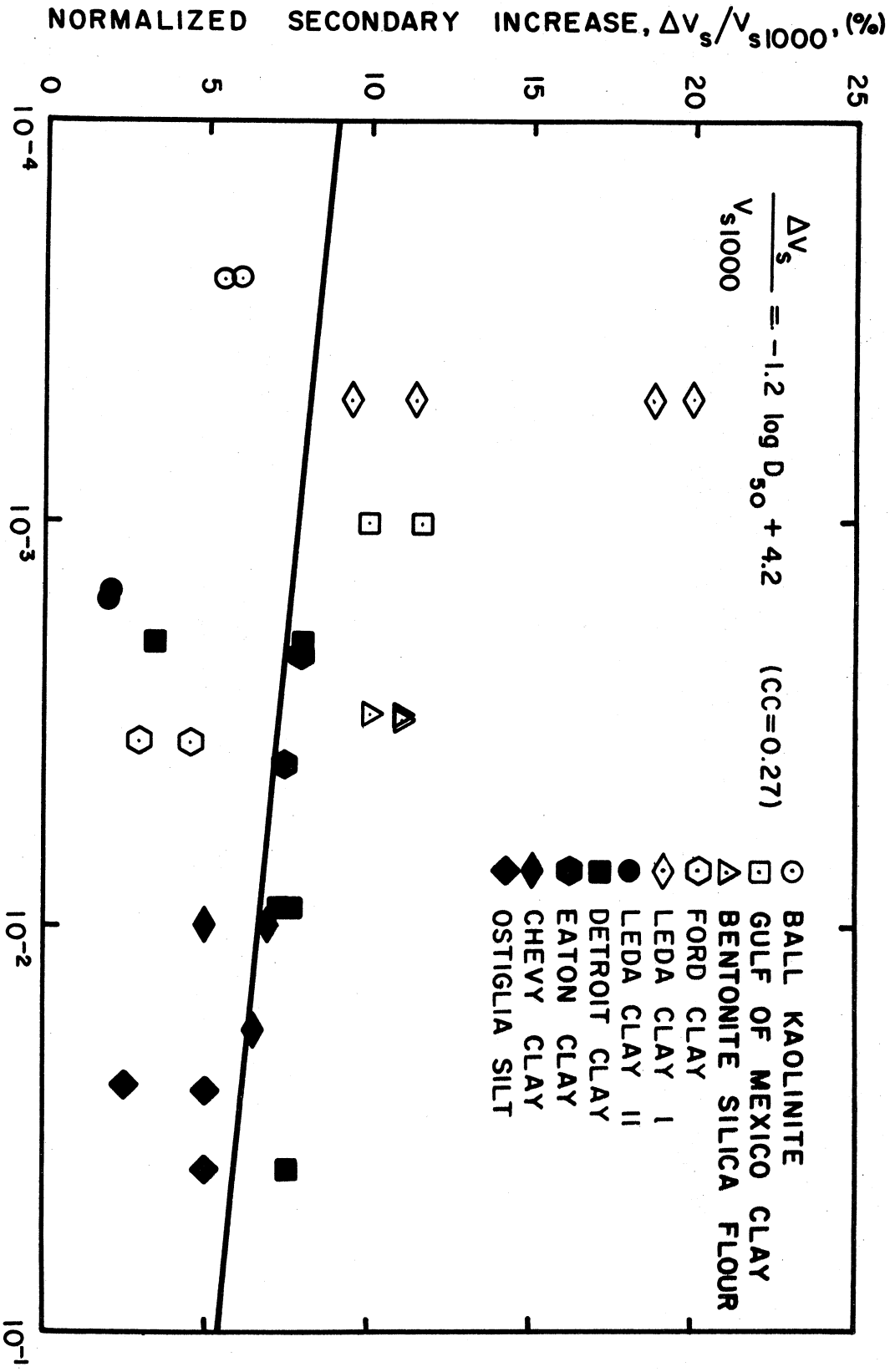

Figure 7.5. Relationship between $\Delta V_s/V_{s1000}$ and the logarithm of the mean particle diameter.

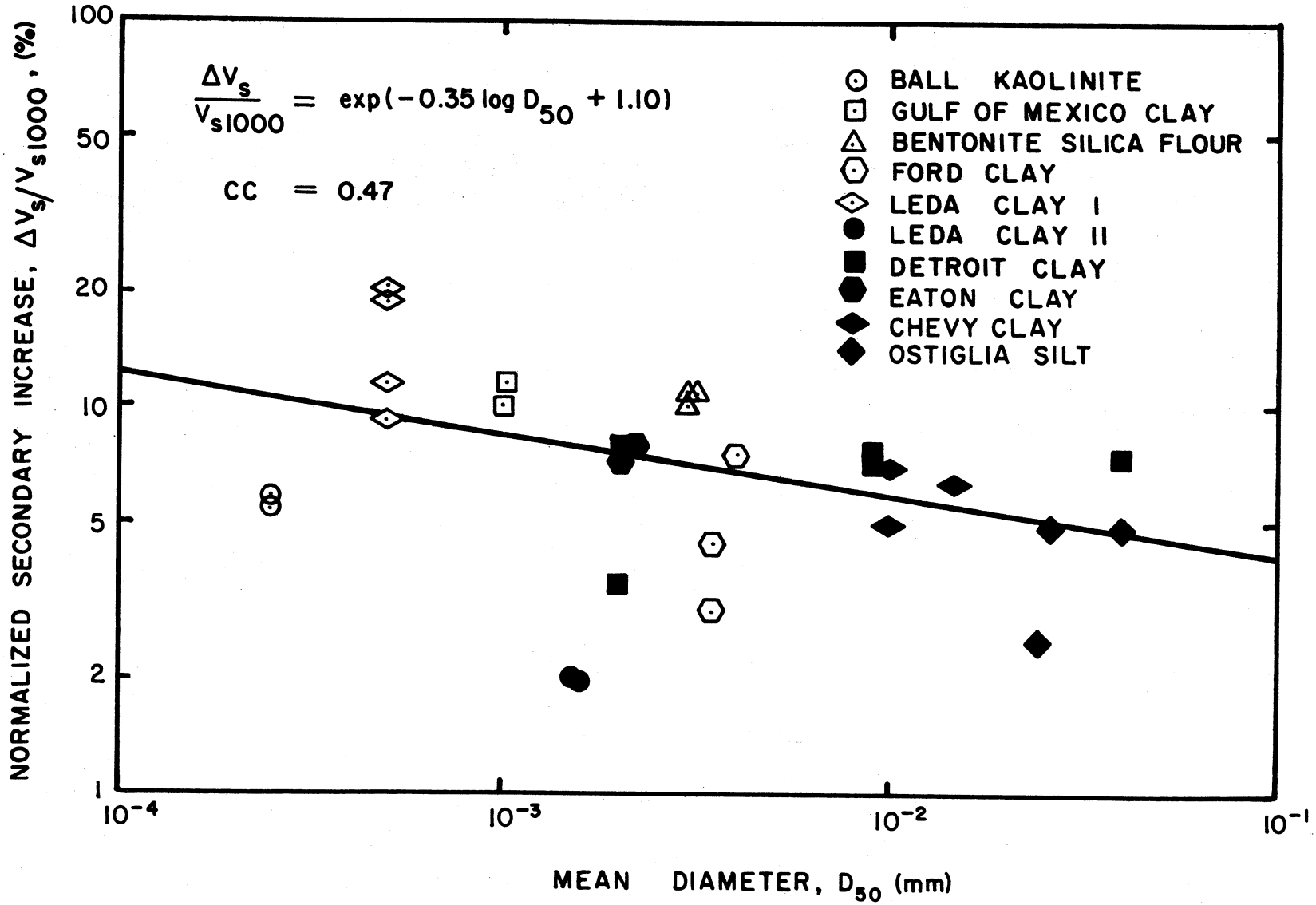

Figure 7.6. Relationship between the logarithm of $\Delta V_s/V_{s1000}$ and the logarithm of the mean particle diameter.

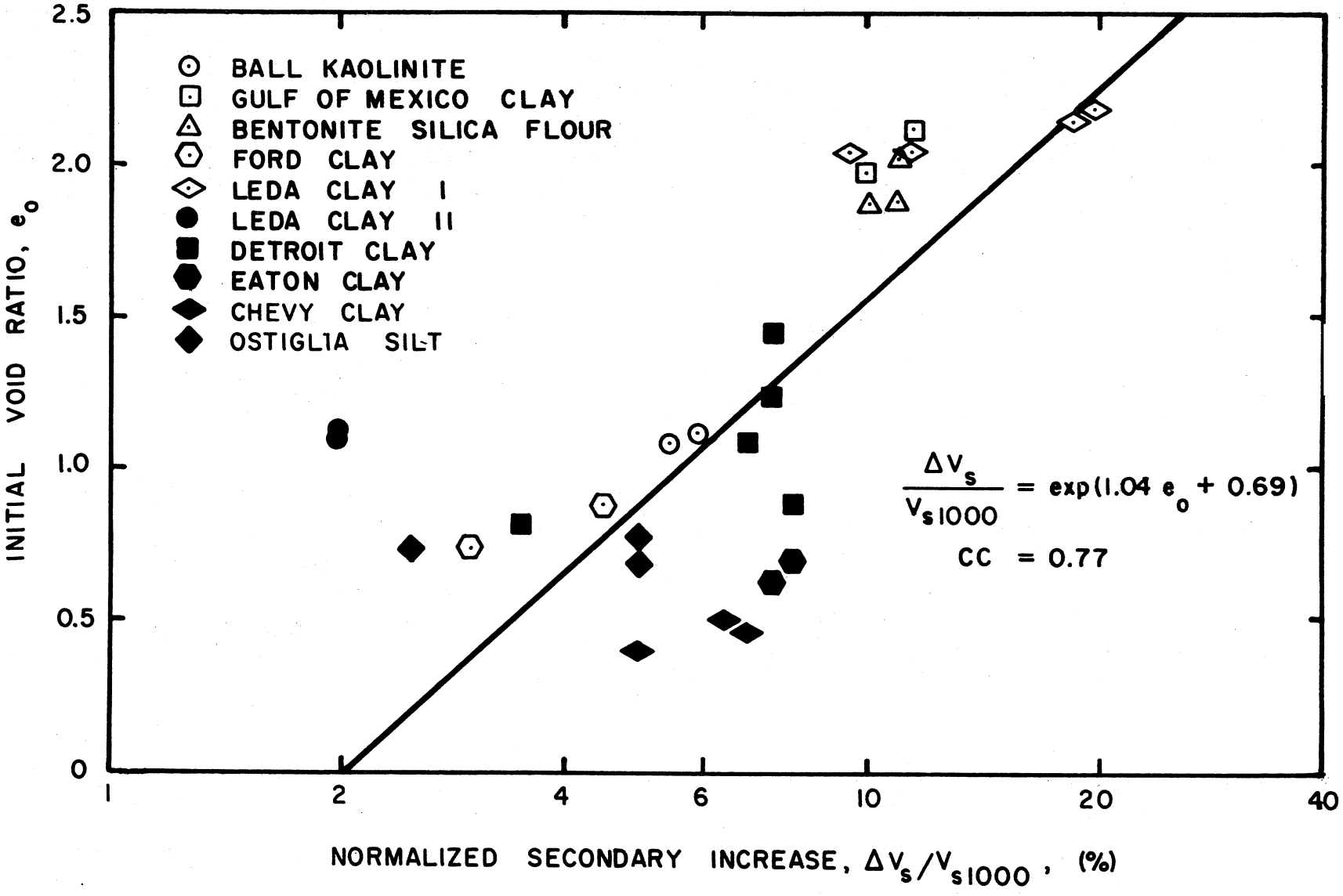

Figure 7.7. Relationship between the logarithm of $\Delta V_s/V_{s1000}$ and the initial void ratio.

The relationship between the logarithm of $\Delta V_s/V_{s1000}$ and the undrained shearing strength, S_u, is plotted in Figure 7.8. The secondary response decreased as the strength of the material increased. A fairly good correlation coefficient occurred for the best fit line through the data (CC = 0.87). The equation of this line was of limited use because most data points were distributed about one end of the plot. The plot did, however, describe a significant trend.

4. PROPOSED EMPIRICAL EQUATIONS

In view of the apparent correlation between log $\Delta V_s/V_{s1000}$, e_o and S_u, a multi-linear regression analysis was performed to obtain a functional relationship between these three parameters. The resulting relationship was defined as

$$\frac{\Delta V_s}{V_{s1000}} = \exp(2 - 0.46S_u + 0.25e_o) \qquad (7.7)$$

where S_u = the undrained shearing strength (kg/cm^2)

e_o = the initial void ratio

The laboratory value of $\Delta V_s/V_{s1000}$ is compared to the results defined by Eq. (7.7) in Figure 7.9. The correlation is relatively good.

A similar statistical analysis was made using the relationship between $\Delta V_s/V_{s1000}$, D_{50} and e_o. The functional relationship as defined by a multi-linear regression analysis was

$$\frac{\Delta V_s}{V_{s1000}} = \exp(1.2 + 0.06 \log D_{50} + 0.68e_o) \qquad (7.8)$$

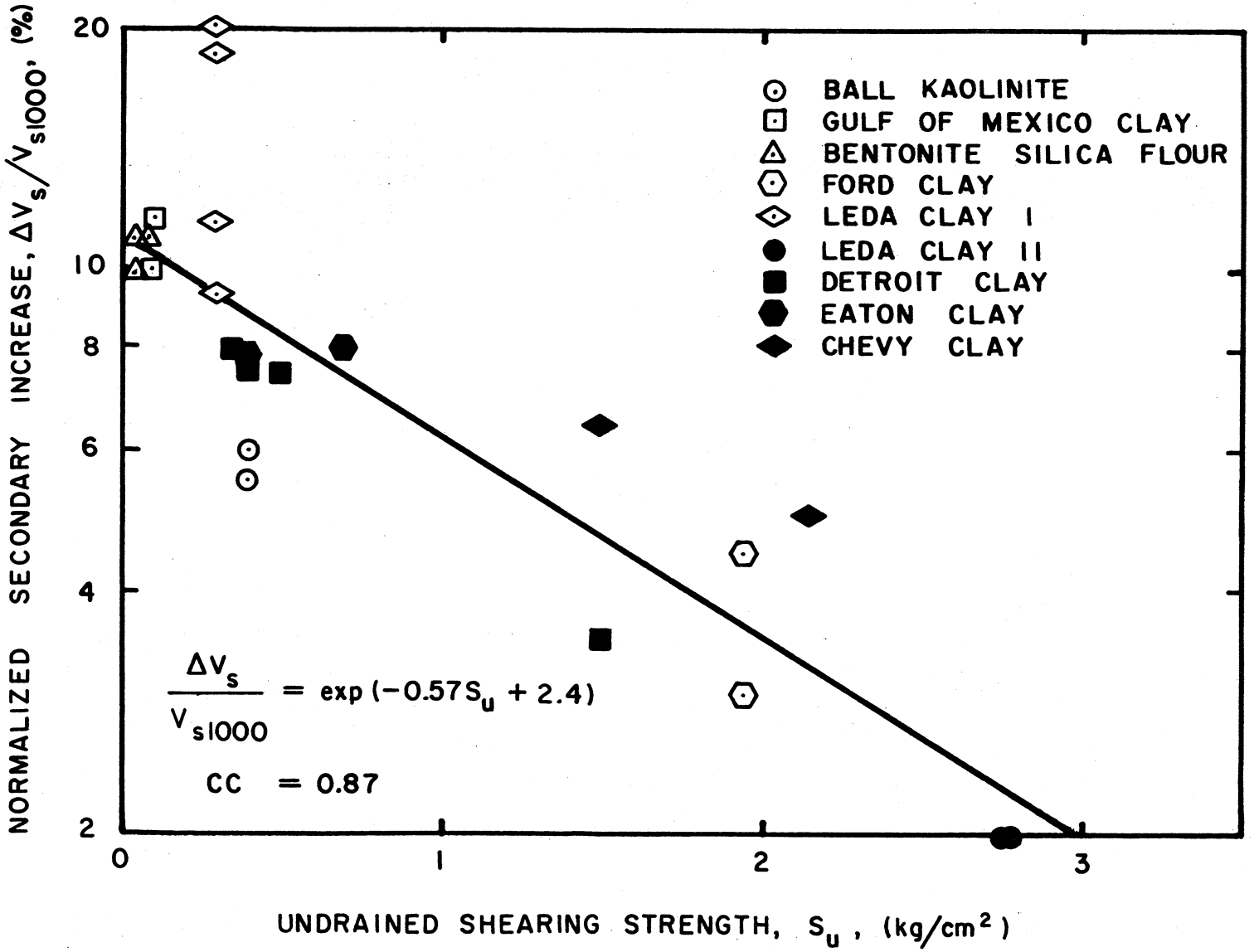

Figure 7.8. Relationship between the logarithm of $\Delta V_s/V_{s1000}$ and the undrained shearing strength

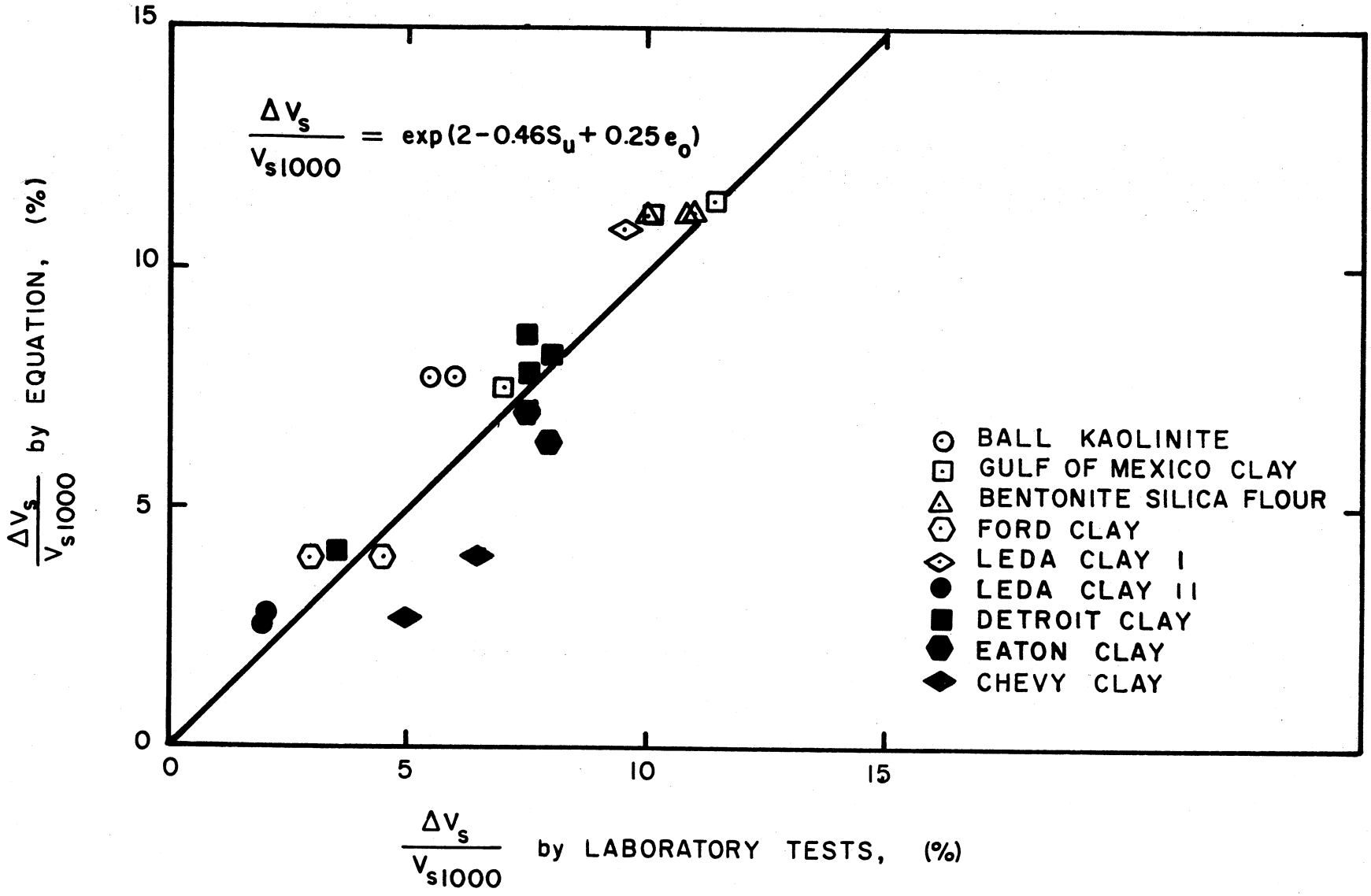

Figure 7.9. Comparison of $\Delta V_s/V_{s1000}$ from laboratory tests to $\Delta V_s/V_{s1000}$ predicted by Eq. (7.7).

where D_{50} = the mean grain diameter (mm)

e_o = the initial void ratio.

The laboratory value of $\Delta V_s/V_{s1000}$ is plotted against the results defined by Eq. (7.8) in Figure 7.10. Although a correlation seems to exist, the scatter is greater than that shown in Figure 7.9. This variation might have been expected because the two parameters, e_o and D_{50}, do not adequately reflect the stress history effects; whereas the undrained strength term does include these effects.

5. LOW AMPLITUDE BEHAVIOR

The behavior of cohesive materials during Low Amplitude Resonant Column Tests is controlled by a phenomenological mechanism which governs the behavior of all cohesive soils. This mechanism can be used to explain the functional relationships established in Sections 2 and 4 of this chapter. It must be recognized that the behavior of cohesive soils is complex, to say the least. The phenomenological mechanism involves, therefore, a certain amount of speculation.

a. Phenomenological Mechanism

The phenomenological mechanism and the particular components influencing the mechanism can best be described by following a typical set of response curves, such as shown in Figure 7.11.

At time equal to zero, a 5 psi confining stress was applied to the soil specimen. The confining stress was hydrostatic and, therefore, imposed a uniform stress on all surfaces. The effective stress in the

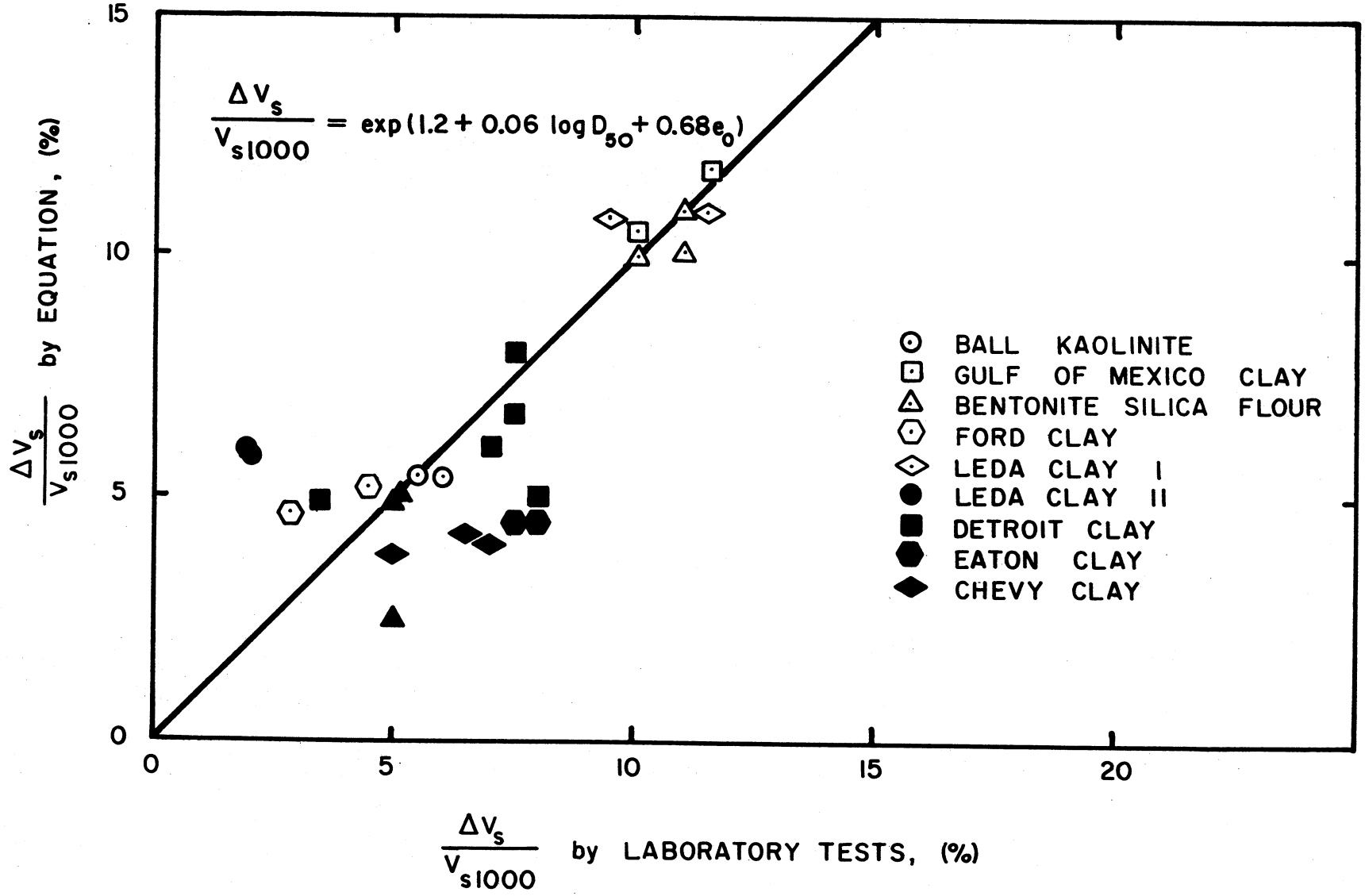

Figure 7.10. Comparison of normalized secondary increase from laboratory tests to $\Delta V_s/V_{s1000}$ predicted by Eq. (7.8).

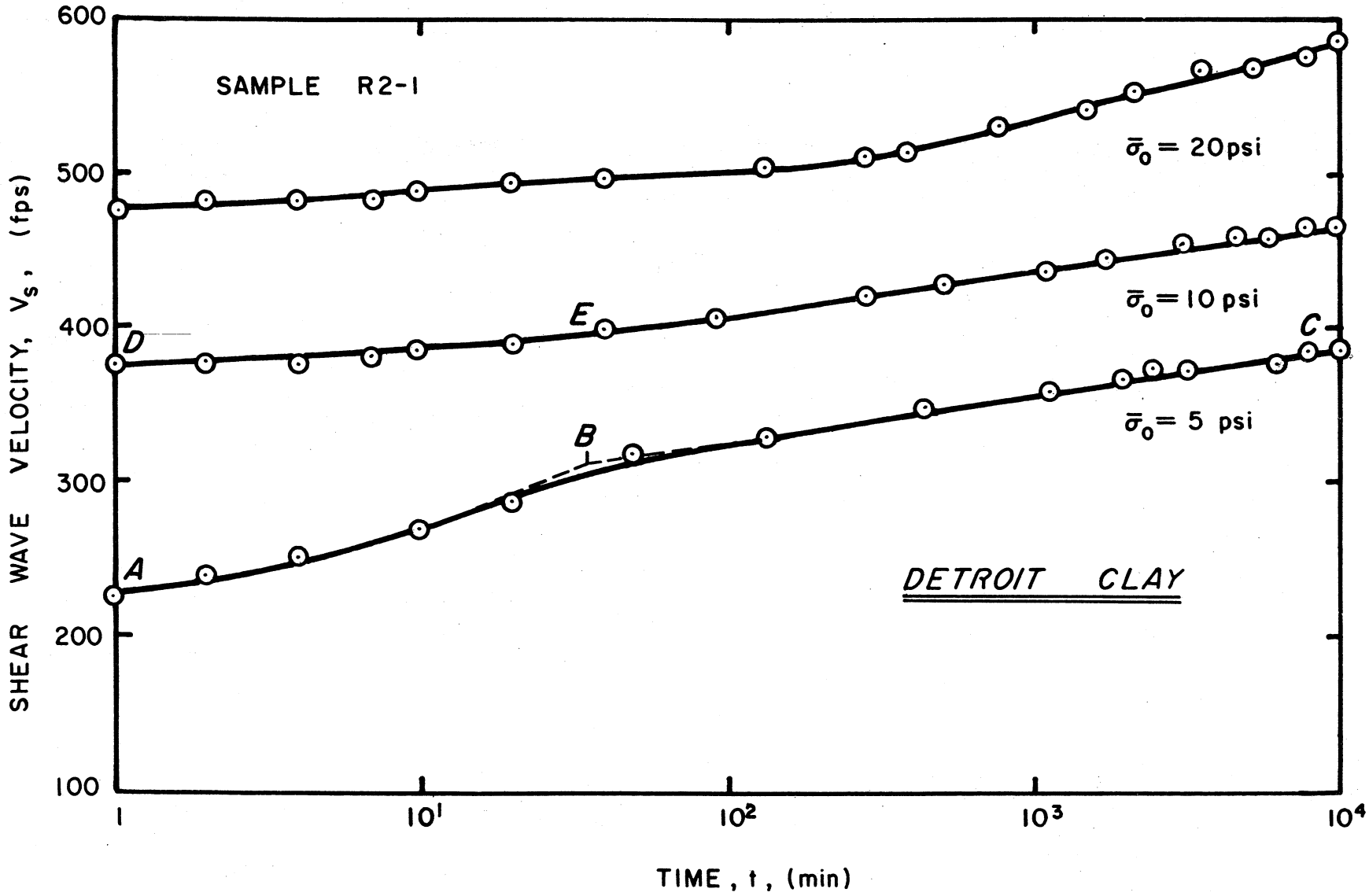

Figure 7.11. Typical relationship between V_S and time for a standard pressure sequence.

sample increased with time as might be expected from the theory of consolidation.

The specimen underwent volumetric straining during primary phase of behavior (time interval between Points A and B). The rate of volumetric straining was dictated by the rate of pore pressure dissipation and the ability of particles to resist very small shearing stresses. As individual particles deformed during volumetric straining, a gradual decrease in void ratio and increase in particle interference occurred. The value of V_s increased accordingly.

A number of existing physico-chemical bonds may have been ruptured during the primary phase of volumetric straining. Although such ruptures tended to reduce V_s for the specimen, the process of void ratio decrease-particle interference increase exerted more influence in the zone between Points A and B. Consequently, a net increase in V_s occurred.

Point B defined the approximate time at which pore pressures were completely dissipated, and total stress within the system equalled effective stress. The location of Point B was determined by the intersection of two tangent lines as shown in Figure 7.11. This procedure was substantiated by determining the end of primary consolidation on the basis of a $\Delta h - \sqrt{time}$ plot (Bishop and Henkel, 1964). At Point B the system was theoretically in equilibrium; and therefore, volumetric straining should have ceased.

Despite this apparent state of equilibrium, a noticeable increase

in V_s occurred between Points B and C. This increase in V_s was attributed to a thixotropic regain in strength. The next subsection reviews the concept of thixotropic regain in greater detail. It should be noted that a small change in void ratio occurred between Points B and C; however, the magnitude of void ratio change was too small to cause the observed change in V_s. The small change in void ratio was due to secondary compression of the soil.

At Point C the confining pressure was increased to 10 psi. The velocity after 1 min was plotted at Point D. A very slight decrease in V_s occurred. The decrease reflected a decrease in bond strength within the material. These bonds were either developed during thixotropic strength gain at the previous confining pressure or were fundamental bonds characteristic to the material. It should be noted that there was a void ratio decrease and interference increase during the same time interval. However, the magnitude of V_s decrease exceeded that gained by particle interference.

The value of V_s remained relatively constant during the time interval between D and E. It was presumed that in this region the sample was subjected to opposing forces which balanced out. For example as the void ratio decreased, bonds were broken and thus V_s decreased. But as the void ratio decreased, particle interference increased and V_s increased. The thixotropic regain of broken bonds also contributed to a potential increase in V_s.

During the initial phase of primary behavior either process may

have dominated, i.e., either loss exceeded gain or gain exceeded loss. At some stage most bonds that could have been broken were broken, and the interference phenomena began to dominate. Once this process commenced, V_s increased and continued to increase until the end of primary behavior (Point E). Subsequent to Point E, the interference process ceased but thixotropic regain continued.

b. Thixotropic Regain Concept

Thixotropic increases in V_s are governed by the balance of interparticle forces. If attractive forces exceed repulsive forces, then a microscopic rearrangement of particles occurs until a force balance is achieved. As the particles are rearranged, a stronger, more rigid system results. The balancing process is time dependent; the rate of increase is greatest when the imbalance is greatest.

The thixotropic concept requires, therefore, that a net state of energy attraction existed at Points B and E in Figure 7.11. Mitchell (1960) suggested that a temporary displacement from a net state of energy attraction could be caused by an exterior straining process. Consolidation is volumetric straining; consequently, it might be assumed that during consolidation the total energy of interaction (e.g., the balance of attractive forces, double layer repulsion forces and repulsion caused by straining) is repulsive as shown in Figure 7.12a. When consolidation ceases, energy of repulsion decreases, and a net attraction results (Figure 7.12b). Figure 7.13 shows Mitchell's proposed schematic diagram of the thixotropice regain process for fine grained soils.

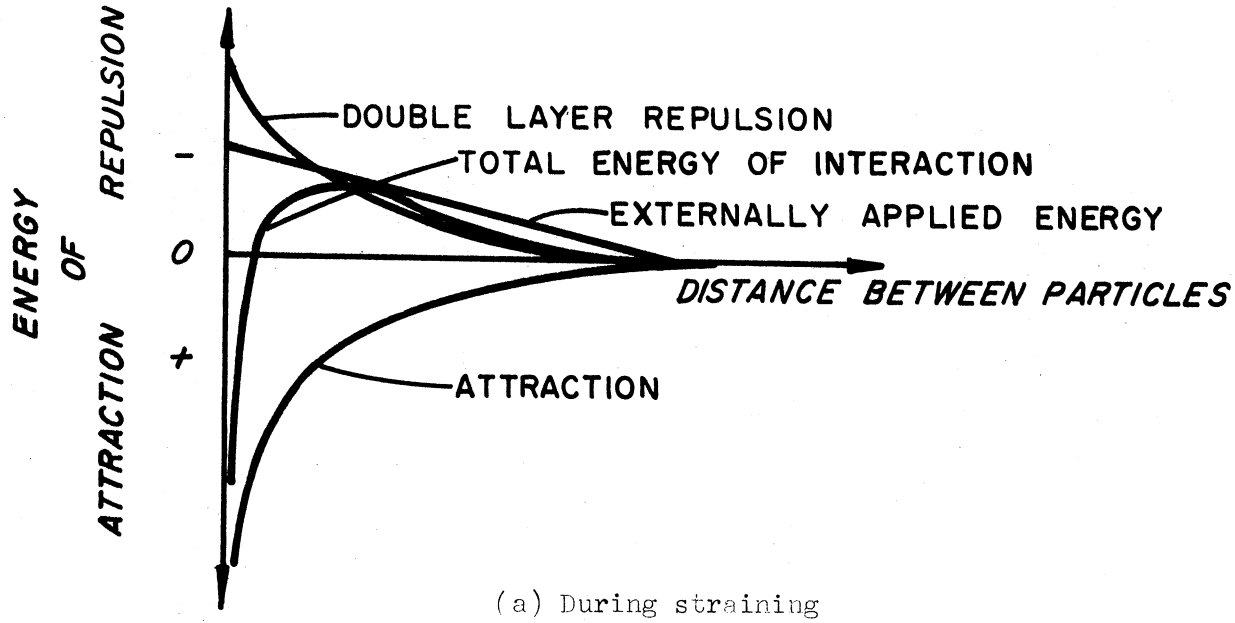

(a) During straining

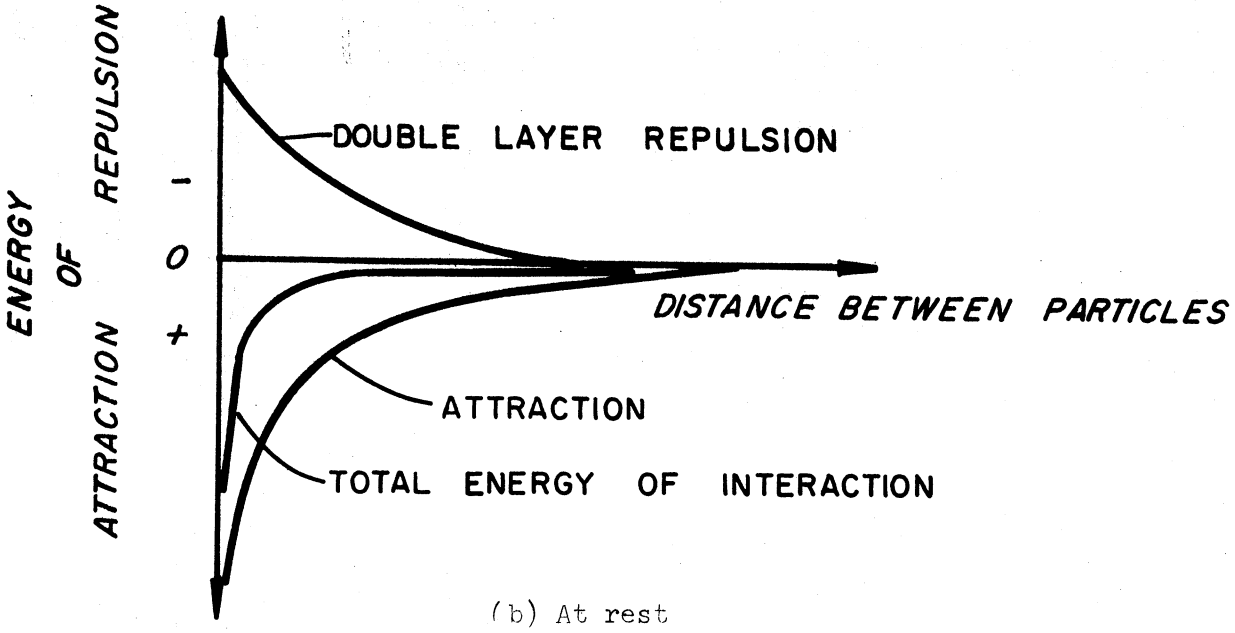

(b) At rest

Figure 7.12. Energy distance curves for thixotropic soils illustrating shift in net energy of particle interaction curves (after Mitchel, 1960).

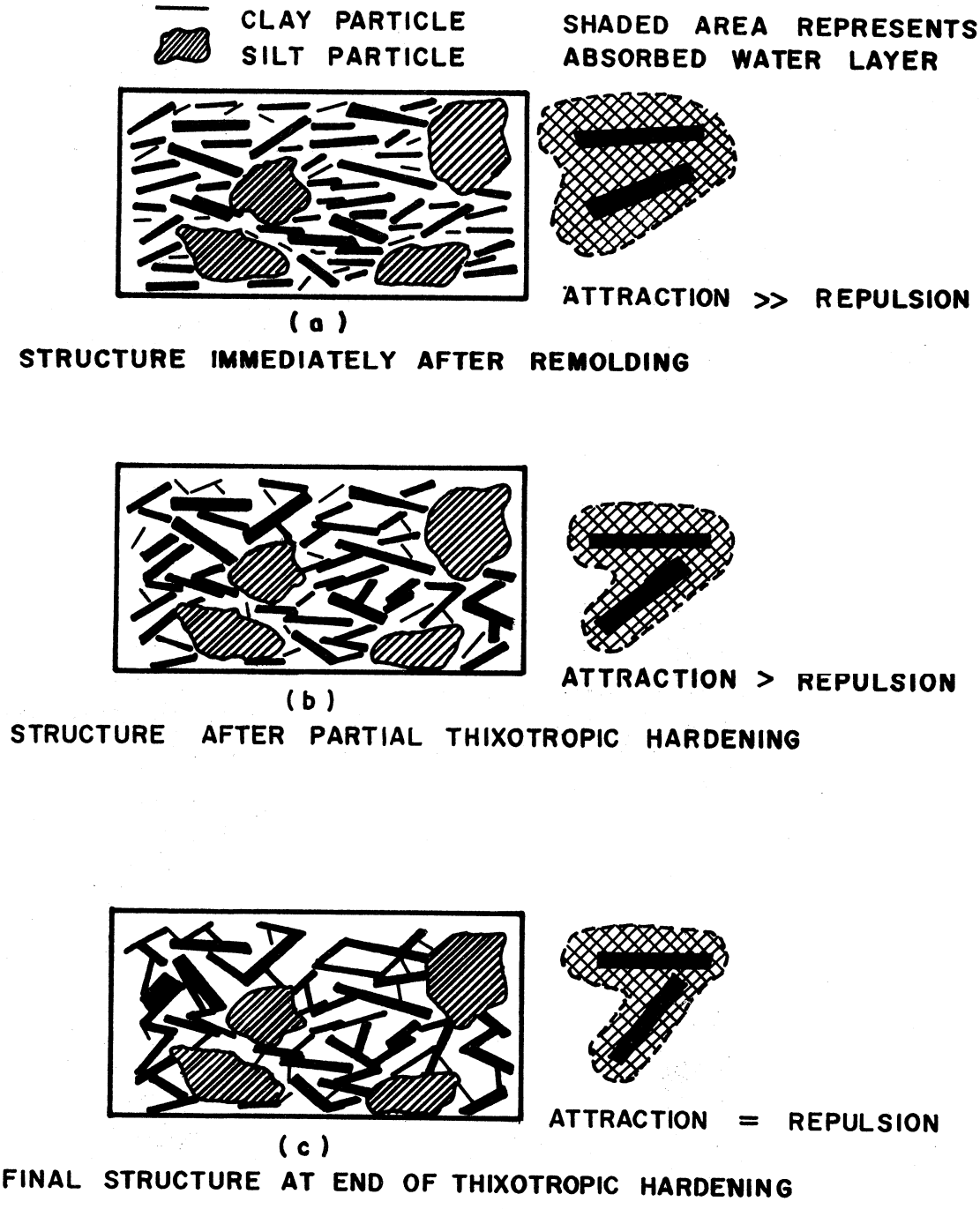

Figure 7.13. Schematic diagram of thixotropic structure change in fine grained soils (after Mitchell, 1960).

c. Laboratory Evaluation

An attempt was made to verify the thixotropic regain concept by performing two controlled duration, resonant column tests on specimens of Ball Kaolinite. The test procedures conformed to standard procedure with one exception: the durations of testing were less than five days. The shorter durations at each confining pressure were intended to allow different amounts of secondary increase in V_s to occur. If the proposed phenomenological explanation were correct, the shape of the primary phase of specimen response for the short duration tests would become more similar to the shape of the primary phase of the initial pressure curve. This behavior was expected because, as the duration of confinement decreased, the number of thixotropic bonds developed during secondary response would decrease. If fewer bonds existed, then the previously described interference process would dominate at an earlier stage.

Figure 7.14 shows the results of this experiment. As the pressure duration decreased, the shape of the primary response curve conformed more to the shape of the primary phase at the initial pressure. During the 200-min pressure sequence, the 1 min velocity was still slightly less than the velocity at the end of the previous stress level. However, the velocity increased steadily thereafter. The initial decrease was attribute to the breaking of primary bonds developed during primary response at the lower pressure level. The influence of this decrease was significantly less than subsequent increase in V_s due to particle interference. The phenomenological model as presented in the previous

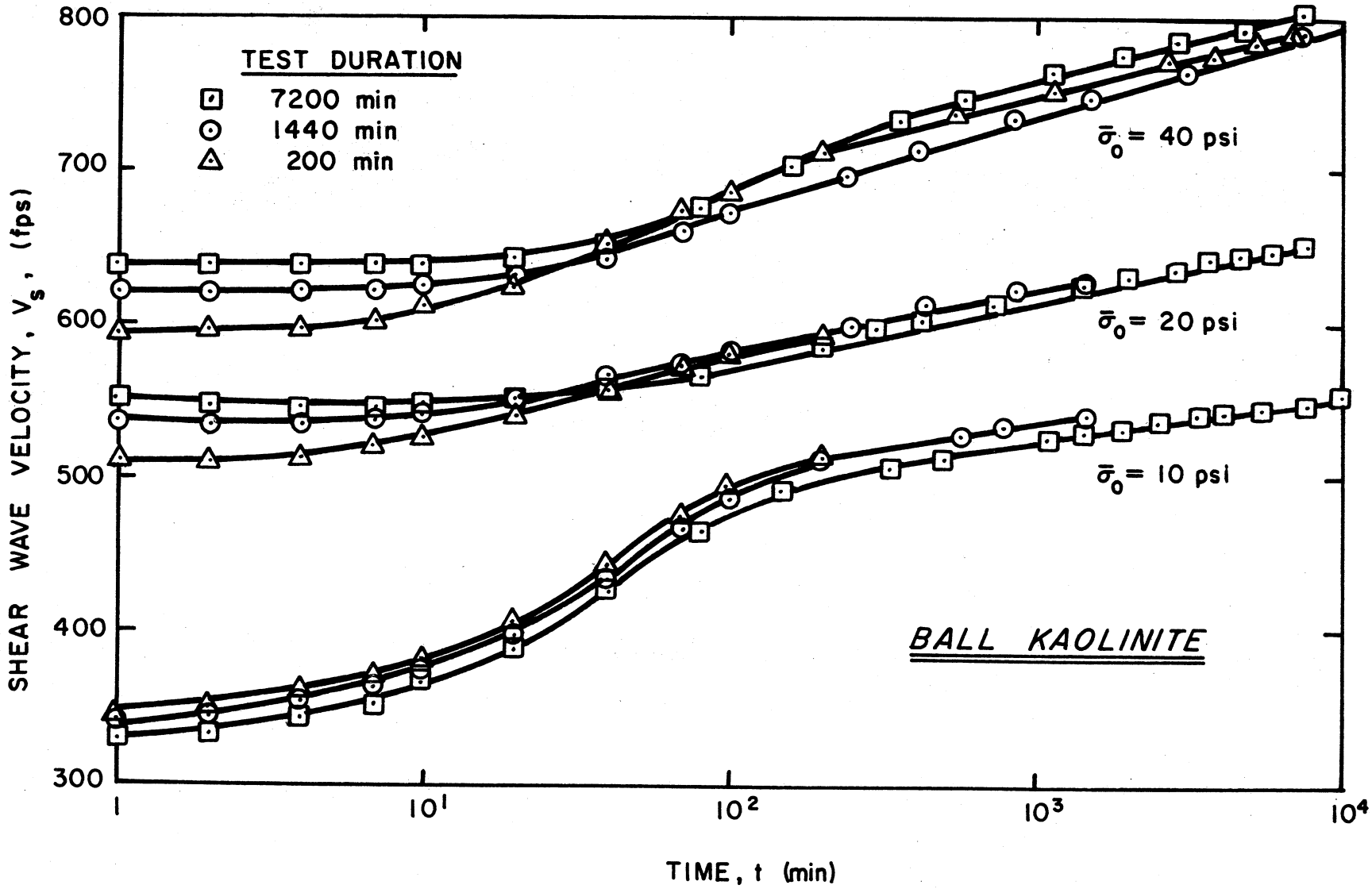

Figure 7.14. Variation in V_s with time for different durations of confinement.

section was, thereby, verified in principle.

It is interesting to note that despite the different durations of confinement at a particular pressure, the V_s values were nearly identical after approximately 40 min. Such behavior suggested that test duration did not affect the general characteristics of the dynamic response of soils.

d. Correlation to Empirical Results.

The phenomenological mechanism proposed in the previous paragraphs established a reasonable explanation for the empirical trends noted in Sections 2 and 4.

The magnitude of the low amplitude test result obviously depended on the amount of secondary or thixotropic increase included in the measurement. Any empirical equation must take this fact into consideration. Equations (7.4) through (7.6) were written explicitly for determining V_s at the beginning of secondary increase. The general characteristics of these equations show that V_s is determined by the stress transferred at points of particle contact ($\bar{\sigma}_o$), the amount of particle interference (e) and stress history of the specimen (OCR).

Two relationships were proposed for predicting $\Delta V_s/V_{s1000}$. The first, as defined by Eq. (7.7) suggested that the secondary increase was related to the undrained strength and the initial void ratio of the soil specimen. This relationship can be justified in the following manner. The void ratio term determined the amount of particle interference at a given structural configuration. The undrained strength

established the rigidity of the bonds in this configuration. It was expected, therefore, that a combination of the two terms would indicate the strength of interparticle forces. The interparticle forces would, in turn, determine the amount of straining which would occur for a given stress level. As noted previously, straining causes a temporary displacement from a net state of energy attraction which results in regain.

The statistical correlation between secondary increase and void ratio-particle diameter (Eq. (7.8)) is justified in the following manner. Interparticle forces, which as noted above determine $\Delta V_s/V_{sl000}$, depend on particle spacing; particle spacing varies according to the void ratio and the specific surface of the particles; and the specific surface is a function of the size of the particle. These functional relationships can be idealized as follows:

$$\begin{aligned} IF &= g(d) \\ d &= h(S,e_o) \\ S &= j(D_{50}) \end{aligned} \qquad \frac{\Delta V_s}{V_{sl000}} = f(IF) \qquad (7.9)$$

where IF = interparticle force

d = particle spacing for parallel arrays of platelets

S = specific surface

e_o = initial void ratio

D_{50} = mean particle diameter

When functions were combined to give a single relationship,

$$\frac{\Delta V_s}{V_{sl000}} = J(e_o,D_{50}) \qquad (7.10)$$

it is apparent that $\Delta V_s/V_{s1000}$ is a function e_o and D_{50}.

6. EFFECTS OF AIR MIGRATION ON LOW AMPLITUDE TEST RESULTS

It was noted in previous chapters that air migrated through the rubber membrane surrounding the specimen during low amplitude tests. The amount of leakage depended on the type of confining medium and on the magnitude of the confining pressure. In particular the rate of migration increased significantly when air was in direct contact with the rubber membrane. Leakage decreased when water separated the membrane from the compressed air.

The effects of air migration are subject to considerable speculation. A comprehensive investigation performed by Poulos (1964) showed that air and water migration could cause a 20 to 30 percent decrease in effective stresses measured during an undrained triaxial test. Poulos attributed this decrease to an increase in pore pressure during a state of constant total stress. Poulos also noted that errors caused by leakage during the consolidation phase of triaxial testing and during a drained triaxial test were small. Furthermore, he suggested that these errors affected only the volume computations. If the quantity of leakage were determined, then Poulos believed that errors could be handled with a simple volume correction for leakage.

Poulos did not, however, consider the possibility that the sample might dry because of air migration. If the sample dried, as indicated by a change in the degree of saturation, it would have exhibited greater stiffness and, consequently higher V_s. If drying did not occur, then

only volume measurements would have been affected by air migration.

It was not immediately apparent whether or not sample drying occurred during the air migration process. The air could have stayed in solution, passed through the radial filter strips and come out of solution in the drainage line. Such behavior would not have altered the water content of the material. On the other hand the air could have come out of solution, penetrated voids in the material and caused a reduction in the degree of saturation. The latter case, i.e., air penetrating voids, required that sufficiently large voids were present to accept the air bubble, points of nucleation occurred and various other unknown factors existed simultaneously around the periphery of the specimen.

In view of the apparent complexity and possible consequences of air leakage, three tests were performed to evaluate the effects of air migration. The three studies were conducted to ascertain the influence of air migration on water content distribution and the influence of air migration on the shear wave velocity of the material. Appendix H contains a detailed summary of general procedures for performing tests and of results defined during tests.

The results of the air migration tests, as summarized in Appendix H, suggested that air migration, which occurred during resonant column tests, caused only minor variations in the degree of saturation and V_s as long as a water bath surrounded the specimen. When air was permitted to migrate directly through the membrane (i.e., water bath not used), V_s

still was not affected as long as the duration of the pressure increment was less than five days. Such behavior implied either that the air stayed in solution as it passed through the filter paper or that the air passed directly through the filter paper without drying the sample. It was concluded on the basis of these tests that for most soils of low permeability air migration was not a serious problem. If, however, the permeability of the soil approached or exceeded that of the filter paper, then significant drying could have occurred. This drying would have altered dynamic characteristics of the material.

7. COMPARISON OF TEST RESULTS

Three different types of test devices were used to determine low amplitude test results. It was assumed throughout the investigation that these devices would define the same velocity or modulus if tests were performed on identical test specimens.

The validity of this assumption was questioned recently after the results of a study performed by the U.S. Army Engineer Waterways Experiment Station (WES) were released. WES contracted six groups to evaluate the dynamic response of artificially compacted sand and silty clay. The results of the WES study (Cunny, et al., 1973) suggested that the Hall resonant column device, utilized at The University of Michigan, defined shear moduli which were 17 to 28 percent above the average results defined by the others. The other groups used the Hardin device, the HATD and various versions of the Wilson device.

Such findings obviously would affect the validity of results for

this investigation. If the Hall device overestimated V_s or G, then most of the previously reported low amplitude test results would have been too high. In view of the WES study, it was decided that the results of the Hall test should be examined in greater detail.

A series of tests were performed at The University of Michigan on similar specimens of Ball Kaolinite using three of the four previously mentioned test devices: the HATD and the Hall and Hardin devices. As noted in Chapter V, Ball Kaolinite exhibited very uniform material properties. The stress history for different specimens of this material was also very similar.

Specimens of Ball Kaolinite were trimmed, set up and tested in the previously described manner (Chapter IV). Pressure increments were 10, 20, 40, and 60 psi. Each pressure increment was maintained for at least five days.

The results of three tests are shown in Figure 7.15. This distribution of data suggests that results defined by different devices are very similar. The difference in V_s at 1000 min varied from 4 to 8 percent. The rate of secondary increase for the three specimens was virtually the same. It should be noted that a significant difference in velocity occurred at the initial stage of the lowest pressure increment. This difference was attributed to variations in drainage characteristics, influence of temperature and seating of the drive system. The difference was minor after about 100 min.

On the basis of this study, it was concluded that all three devices

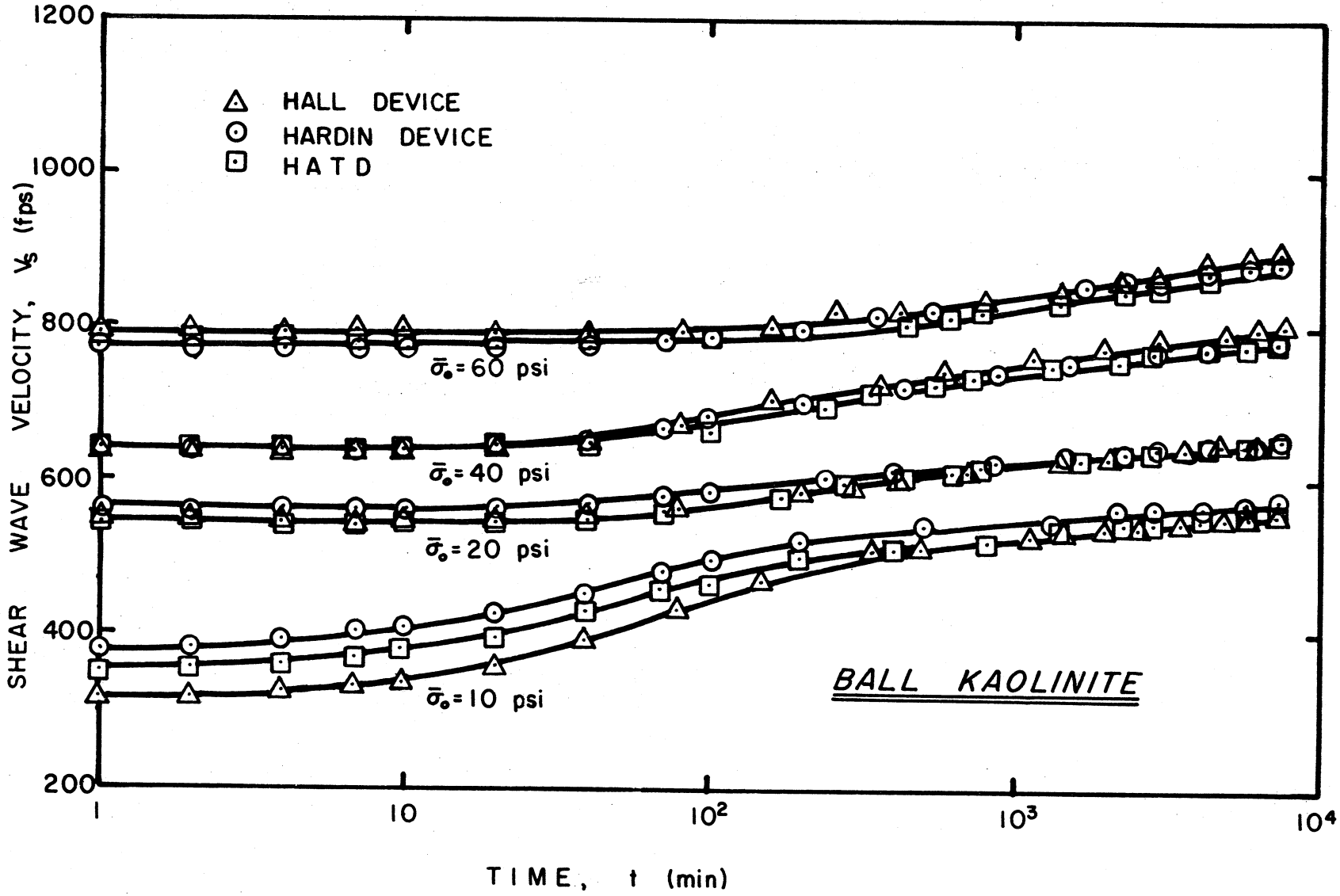

Figure 7.15. Comparison of test results from three different test devices.

were capable of defining similar results as long as material properties were similar. The variation noted by Cunny, et al., were probably due to variations in certain material properties such as residual stresses developed during preparation. Cunny, et al., states that each group used a different compaction technique. If the materials had all been prepared in a similar manner, as was done in The University of Michigan study, a better correlation would have been expected.

B. High Amplitude Test Results

High amplitude test results, as summarized in Chapter VI, show that strain amplitude and number of cycles were the fundamental parameters controlling the dynamic response of cohesive soils. These two parameters affected not only the shear modulus of the material during cycling but also introduced certain effects that continued after the end of cycling. The significance of these effects varied according to the magnitude and the number of cycles of strain.

The results of high amplitude test are analyzed in three sections. These sections review the general characteristics of dynamic response before, during and after high amplitude cycling.

1. DYNAMIC RESPONSE BEFORE HIGH AMPLITUDE CYCLING

Figures 6.4 and 6.6 show G_{max} versus log time curves for the six cohesive soils measured prior to high amplitude cycling. The general form of these plots is similar to that recorded for Low Amplitude

Resonant Column Tests.

The similarity between results defined by the HATD at low amplitudes and results determined with the Hall and Hardin devices was expected because the soil specimens were subjected to similar types of dynamic loads during the respective tests series. Strain amplitudes were approximately the same, and boundary conditions and methods of analyzing results were similar. Only the test devices differed.

An additional observation was made. In two of the materials, Detroit Clay and Leda Clay I, secondary response commenced at some point beyond 1000 min. This time was substantially greater than that noted for similar specimens tested in the Hall and Hardin devices. The difference was attributed to variations in drainage conditions.

Although the explanation of the difference was not particularly noteworthy, the fact that primary response had not been completed at the end of approximately one day was of importance. This behavior demonstrated that dynamic response must be plotted when performing a low amplitude test. The end of primary behavior can then be selected on the basis of sample behavior rather than some predetermined time interval.

2. DYNAMIC RESPONSE DURING HIGH AMPLITUDE CYCLING

The introductory paragraph of this section noted that strain amplitude and number of cycles of strain influenced to a great degree the dynamic response of cohesive soils. The influence was particularly noticeable when specimens were subjected to high amplitude, cyclic strains.

a. Strain Amplitude Effect

The effect of strain amplitude on shear modulus, G, is clearly illustrated in Figure 6.7. This plot shows that for the six materials, G/G_{max} began to decrease once shearing strains exceeded 0.01 percent. At any point in time G_{max} was constant; therefore, it can be concluded that G decreased once shearing strains exceeded 0.01 percent. The decrease in G/G_{max} became significant when strain amplitudes exceeded approximately 0.1 percent. For the six test materials, the ratio of G/G_{max} varied from 25 to 80 percent at 0.1 percent strain; the average decrease was about 50 percent. As the strain amplitudes approached 1.0 percent, the general trend in data suggested that G/G_{max} approached 20 percent for all soils examined.

These data indicate that any dynamic analysis involving strains greater than 0.01 percent must incorporate a nonlinear modulus versus strain relationship to accurately model field conditions. It is also obvious that the Low Amplitude Resonant Column Test by itself does not provide enough information for conducting a high amplitude study. Either varying amplitude tests must be performed to define the nonlinear zone, or an analytical procedure must be utilized to extrapolate the low amplitude results to some high amplitude, nonlinear form.

Before concluding this discussion on dynamic response, a comment must be made about secondary increase and its effect on high amplitude response. Figure 6.8 shows that secondary increase also affected G recorded at high strain amplitudes. In general G increased in

approximately the same proportion as the increase in G_{max}. This trend can be verified by comparing the ratio of G/G_{max} at various time intervals.

b. Modelling Strain Amplitude Effect

As noted in Chapter II, two models have been proposed to account for the nonlinear response of cohesive soils. The first, as defined by Hardin and Drnevich, utilized a modified hyperbolic relationship. The second, as suggested by Seed and Idriss, was based on an analysis of various test data.

The results of this investigation were compared to the two relationships (Figure 7.16). The modified hyperbolic line was evaluated at 1000 cycles and at a reference strain of 0.3 percent. This reference strain was selected on the basis of the average plasticity indices for the materials and the average effective stress conditions utilized during tests described herein. These results illustrate that a modified hyperbolic relationship was a better model of the data defined by this investigation.

Figure 7.16 shows a comparison between the results from this investigation and an average hyperbolic representation. A certain amount of variation was expected because of differences in soil properties. A more accurate comparison was made by incorporating soil strength and secant modulus data in the modified hyperbolic equation. These comparisons are shown in Figures 7.17 and 7.18.

A Ramberg-Osgood relationship is also plotted in Figures 7.17 and

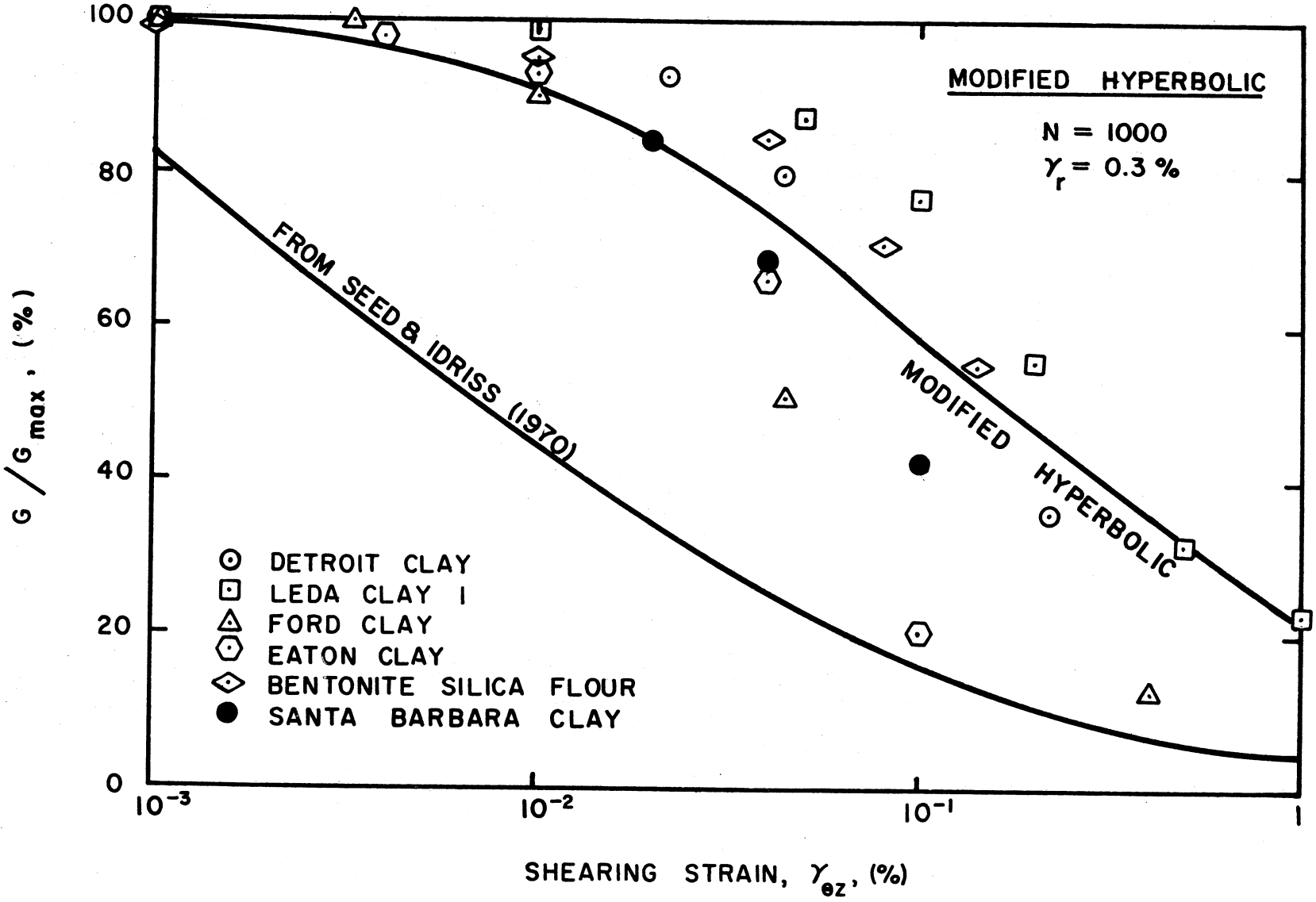

Figure 7.16. Comparison of high amplitude test results to nonlinear relationships proposed by Seed and Idriss (1970) and Hardin and Drnevich (1972b).

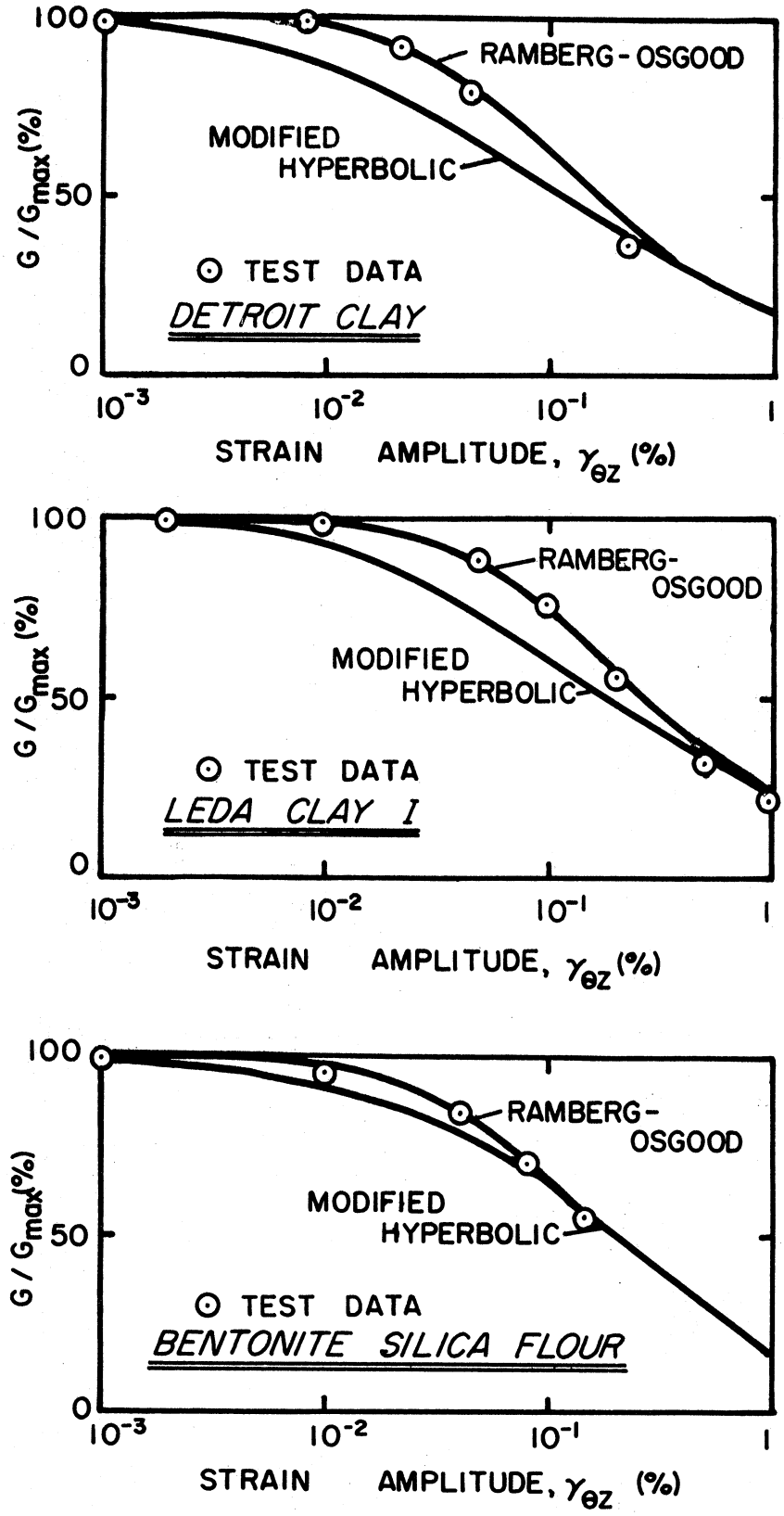

Figure 7.17. Comparison of high amplitude test results to modified hyperbolic and Ramberg-Osgood relationships for Detroit Clay, Leda Clay I and Bentonite-Silica Flour (α = 1.0, τ_y = 0.4 τ_{max}, R = 3).

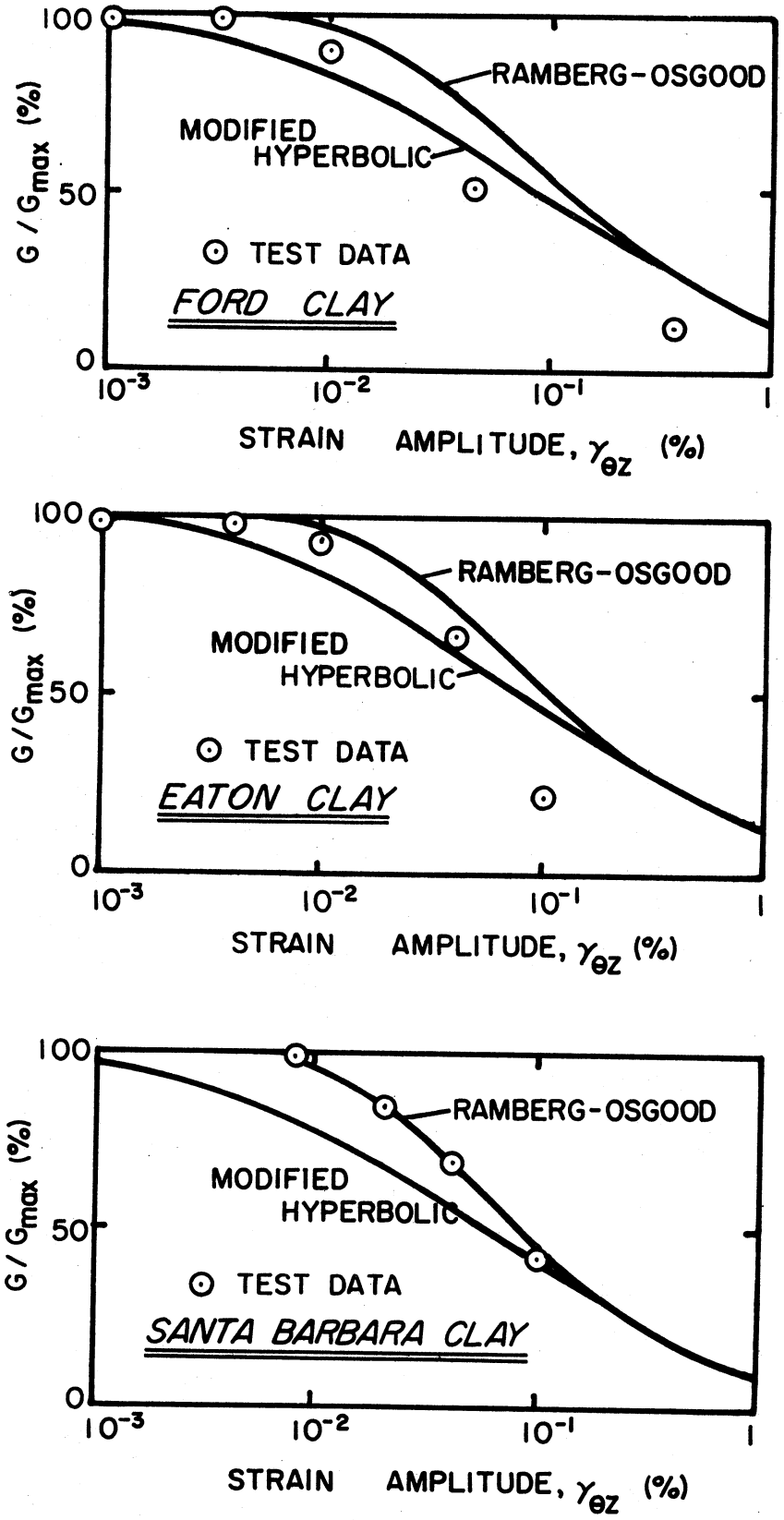

Figure 7.18. Comparison of high amplitude test results to modified hyperbolic and Ramberg-Osgood relationships for Ford Clay, Eaton Clay and Santa Barbara Clay (α = 1.0, τ_y = 0.4 τ_{max}, R = 3).

7.18. This relationship was suggested by Jennings (1964) and used by Streeter, Wylie and Richart (1974) for modelling the nonlinear behavior of soils during dynamic response. The general form of the Ramberg-Osgood relationship given in terms of secant shear moduli was defined by

$$\frac{G}{G_{max}} = \frac{1}{1 + \alpha\left(\frac{\tau}{\tau_y}\right)^{R-1}} \qquad (7.11)$$

where α = shape factor (1.0)

τ = shearing stress at strain amplitude

τ_y = shearing stress at yield

R = correlation number for the Ramberg-Osgood curve

G_{max} = shear modulus at low amplitude shearing strains.

The parameters used in Eq. (7.11) are adjusted to describe typical soil response. The yield stress is assumed to be between 40 and 80 percent of the undrained shearing strength of the soil. The correlation number, which defines the sharpness of the bend in the curve, is typically between three and five. The curves plotted in Figures 7.17 and 7.18 were developed for a yield stress equal to 40 percent of the undrained strength and a correlation number of three.

Figures 7.17 and 7.18 show that no single relationship, whether it be Ramberg-Osgood or modified hyperbolic, consistently predicts the results of laboratory tests. The plots do illustrate, however, that in most cases the Ramberg-Osgood equation with R = 3, α = 1 and τ_y = 0.4 τ_{max} gives a better indication of the variation of G with shearing strain. This is particularly true when strain amplitudes are less than

0.1 percent. The Ramberg-Osgood and the modified hyperbolic equations define approximately the same G when strain amplitudes are between 0.1 percent and 1.0 percent shearing strain. Unfortunately very little laboratory data are available in this range to verify either of the empirical equations.

A certain amount of discrepancy was observed between the Ramberg-Osgood curve and the laboratory data for the Ford and Eaton clays. The difference may have been related to the determination of τ_{max}. If τ_{max} were approximately one-half the valued measured during undrained triaxial tests, then a better correlation would have occurred. The difference may also have indicated that stiffer materials do not conform to previously noted modelling scheme.

It seems apparent that either the modified hyperbolic or the Ramberg-Osgood equations can be used to approximate nonlinear response of soil. If either representation is incorporated within an analysis, then a certain amount of variation must be expected. In this investigation the magnitude of difference exceeded 20 percent in several cases; however, in general the difference was less than 10 percent.

c. Cycle Effect

The effect of the number of load repetitions on G was shown in Figures 6.9 and 6.10. These curves indicated that a decrease in the ratio of the modulus at the Nth cycle of high amplitude strain, G_N, to the modulus at the 500th cycle of high amplitude strain, G_{500}, occurred as the number of repetitions of high amplitude strain increased. For a

given G_{500}, it was apparent that G decreased as cycling continued. The magnitude of decrease in G_N/G_{500} increased as the strain amplitude during cycling increased. When strain amplitudes were less than about 0.2 percent, then the decrease in G_N/G_{500} was relatively linear on a semi-logarithmic plot. Once strains exceeded 0.2 percent, the decrease tended to be nonlinear.

The magnitude of decrease due to high amplitude cycling depended on the strain amplitude and the number of repetitions of strain. In situations that involved a large strain amplitude and a large number of cycles, a 50 percent decrease in G_N/G_{500} occurred between the 500th and the 100,000th cycle. In other situations where strain amplitudes were small, the decrease in G_N/G_{500} was less than 1.0 percent per logarithmic cycle and, therefore, could be ignored if the event causing the load were of short duration, i.e., less than several million cycles.

d. Modelling Cycle Effect

Hardin and Drnevich introduced a correction factor in the modified hyperbolic equation to include the effect of the number of repetitions of strain. They showed, in general, that the decrease in G was related to the logarithm of the number of repetitions. They did not show, however, that strain amplitude influenced this correction factor.

In view of the apparent deficiency of the Hardin and Drnevich correction technique, the results of this investigation were reanalyzed to include a strain amplitude effect. The average decrease in G_N/G_{500} per logarithmic cycle of repetitions, $\Delta(G_N/G_{500})$, was compared to the

logarithm of the strain amplitude. This comparison, as plotted in Figure 7.19, shows that a correlation exists between the two parameters. A least square fit for the data points defined the power curve

$$\Delta\left(\frac{G_N}{G_{500}}\right) = 459\ \gamma_{\theta z}^{0.64} \tag{7.12}$$

where the strain amplitude, $\gamma_{\theta z}$, is defined in radians. The correlation factor for the data is 0.89.

The power curve is plotted in Figure 7.19. A significant amount of variation occurs between the data points and the statistical representation. Although the difference exceeds 100 percent in several cases, Eq. (7.12) does define the general trend of data.

If should be noted that Eq. (7.12) did not account for the nonlinear behavior of some data. The equation was developed for an average straight line drawn through the nonlinear zones. A more thorough analysis was not possible because of the limited amount of data.

Equation (7.12) is used in the following manner. The modulus is defined at the 1000th cycle of high amplitude strain by performing a high amplitude torsional test or by utlizing an empirical equation. The decrease in G after the 1000th cycle of strain is then estimated by Eq. (7.12) on the basis of the strain amplitude. Once the decrease per logarithmic cycle is defined, the modulus after N cycles is determined from

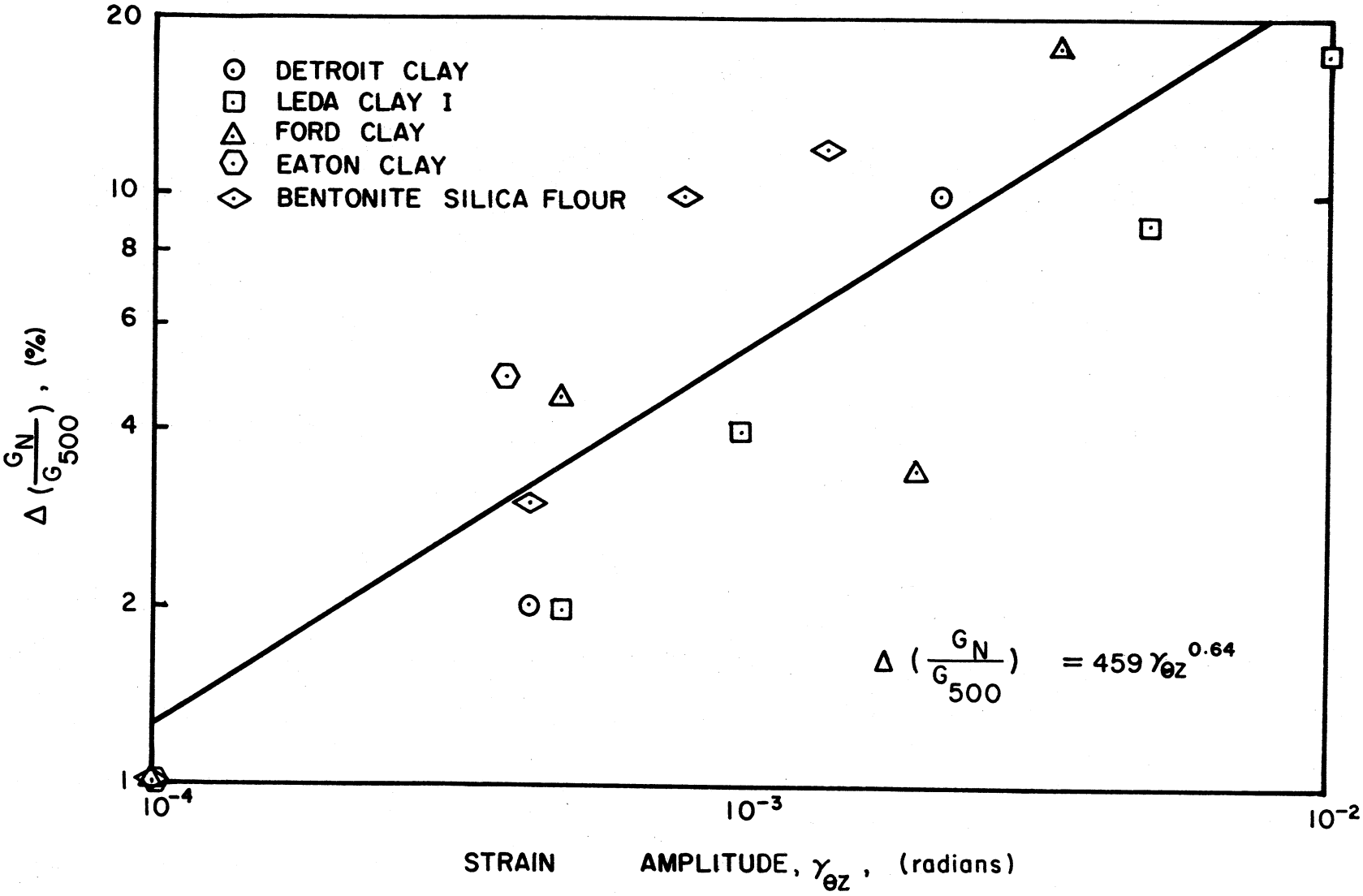

Figure 7.19. Comparison between the change in G/G_{max} per logarithmic cycle of repetitions and strain amplitude.

$$G_N = \left[\left(\frac{G}{G_{max}} \right)_{1000} - .459\, \gamma_{\theta z}^{0.64} * (\log N - 3) \right] * G_{max} \qquad (7.13)$$

where the number of cycles, N, is greater than 1000. This solution applies to cases where strain amplitudes exceed 0.01 percent. It also assumes that the torsional test or the empirical equation gives G after 1000 repetitions of strain.

e. Phenomenological Mechanism

The nonlinear relationship between G and strain amplitude reflects the general nonlinear characteristics of soil. Such behavior is attributed to the progressive decrease in the ability of soil to resist increased stresses at points of particle contact. The magnitude of decrease in G depends on the amount of deformation that occurs before new positions of force equilibrium are established. At low stresses a constant factor, G, relates shearing stress to shearing strain. As the shearing stress increases, then G decreases, and consequently greater strain occurs for the same change in stress.

Repetitions of constant strain amplitude cause a gradual reduction in G when the amplitude of strain exceeds some threshold level. This reduction implies that the stress-strain characteristics for the soil are gradually changed by each increase and decrease in deformation. Such behavior suggests that remolding of the soil is occurring. The remolding is attributed to a gradual weakening of interparticle bonds.

3. DYNAMIC RESPONSE AFTER HIGH AMPLITUDE CYCLING

The low amplitude modulus measured 1 min after the end of high amplitude cycling, G_{after}, was less than that recorded before cycling. The magnitude of reduction depended on the amplitude and number of repetitions of strain. The initial loss was followed by a period of modulus regain.

a. Reduction in Modulus

Figure 6.11 shows that the ratio of G_{after}/G_{before} decreased when the strain amplitude during cycling increased. As long as strain amplitudes did not exceed 0.01 percent, the amount of reduction for 1000 cycles of strain was relatively small, i.e., less than 1.0 percent. Once the strain amplitude exceeded this level, a significant decrease in G_{after}/G_{before} occurred. The magnitude of decrease approached 20 to 30 percent when the results in Figure 6.11 were extrapolated to 1.0 percent strain amplitude.

Figure 6.12 and 6.13 show that the ratio of G_{after}/G_{before} decreased as the number of repetitions increased. The decrease in G_{after}/G_{before} per logarithmic cycle of repetitions increased as the strain amplitude during cycling increased.

b. Modelling Amplitude and Cycle Effect

The effects of high amplitude cycling on low amplitude modulus were noted by other researchers, but a quantitative analysis of these effects had not been presented in the literature. The following

paragraphs introduce one possible prediction scheme.

High amplitude cycling may or may not affect the low amplitude modulus. If strain amplitudes do not exceed approximately 0.02 percent, then the effect of high amplitude cycling on G_{after} is minor and can probably be neglected. When amplitudes exceed 0.02 percent, the decrease in G_{after}/G_{before} is more significant and should be considered.

When a linear regression analysis was performed on data points shown in Figure 6.11 for strain amplitudes greater than 0.02 percent, the following equation was defined.

$$\frac{G_{after}}{G_{before}} = \left[-12.6 \log \gamma_{\theta z} + 53.6\right] \qquad (7.14)$$

where strain amplitude was defined in radians. Fifteen data points were analyzed during the derivation of this equation. The correlation coefficient is 0.89. As shown in Figure 7.20 actual data fall within plus or minus 5.0 percent of this line. The equation gives, therefore, a reasonable approximation of the decrease in G_{after}/G_{before} to be expected after 1000 repetitions of high amplitude strain.

The ratio of G_{after}/G_{before} also decreased as the number of cycles increased. Figure 7.21 shows a comparison between the decrease in G_{after}/G_{before} per logarithmic cycle of repetitions, $\Delta(G_{after}/G_{before})$, and the strain amplitude. When a least square fit for the data points was performed, the following power curve was derived

$$\Delta\left(\frac{G_{after}}{G_{before}}\right) = 60.2\ \gamma_{\theta z}^{0.41} \qquad 7.15)$$

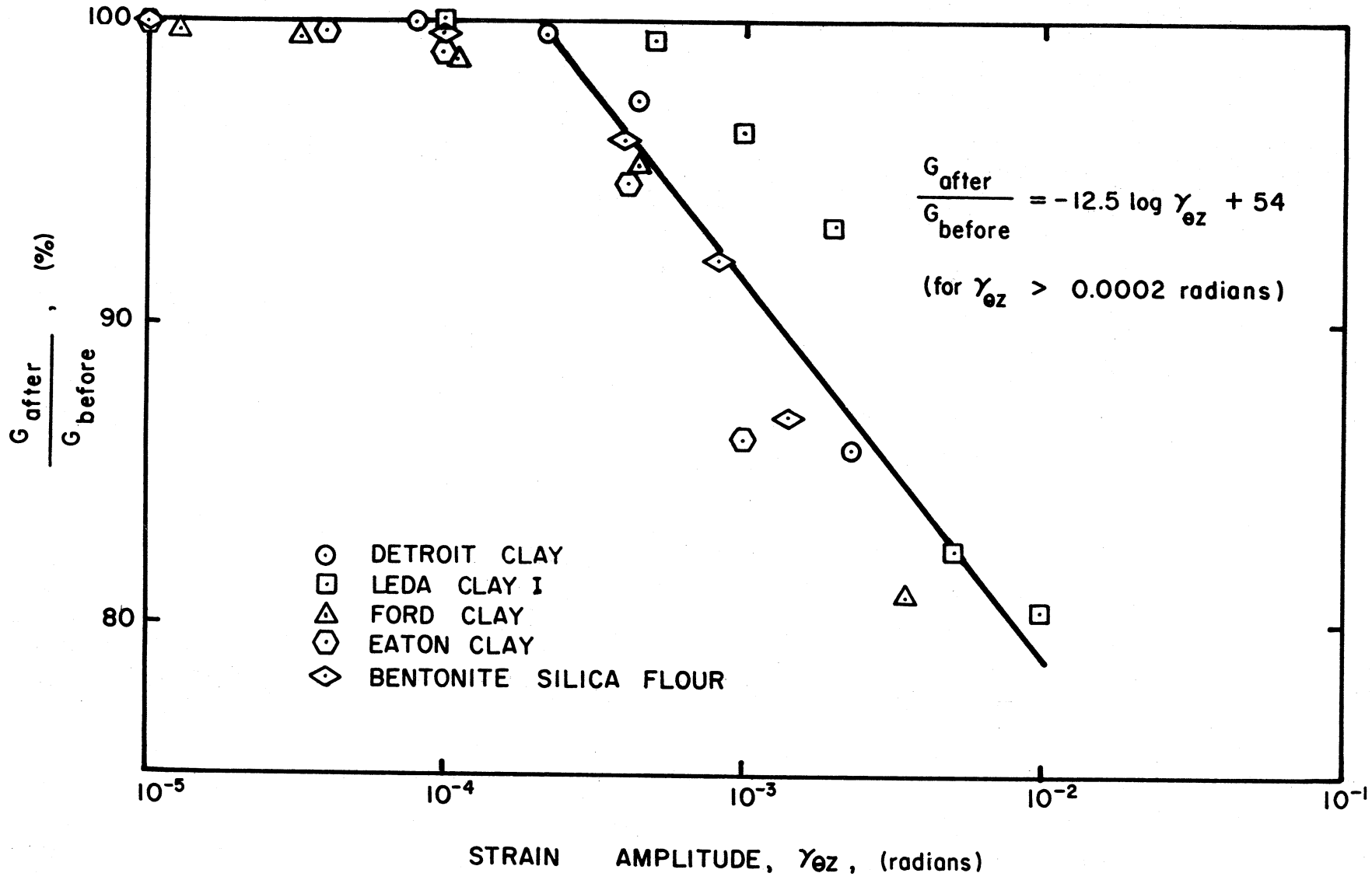

Figure 7.20. Comparison between G_{after}/G_{before} and strain amplitude.

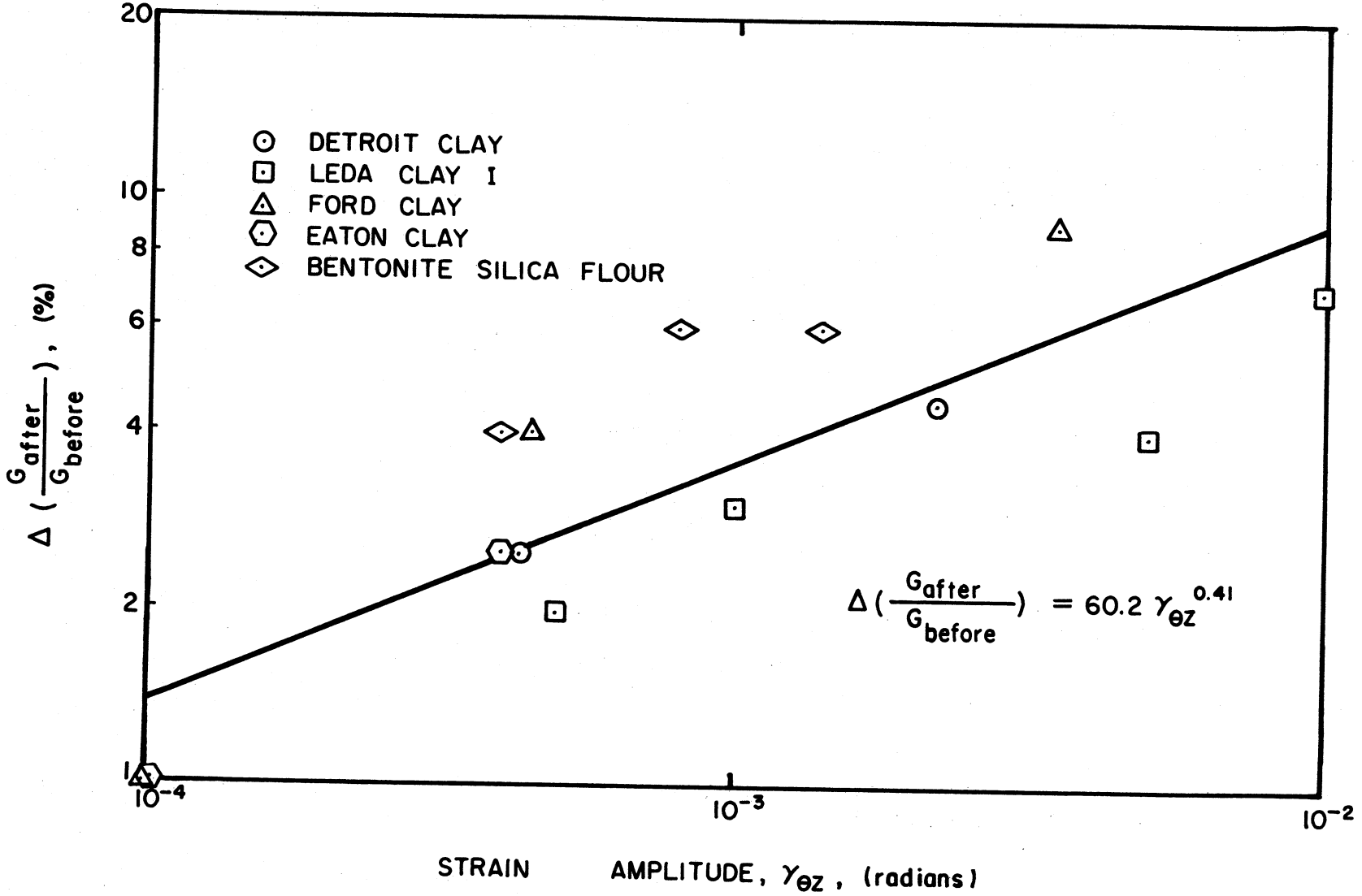

Figure 7.21. Comparion between the change in G_{after}/G_{before} per logarithmic cycle of repetitions and strain amplitude.

where the strain amplitude was defined in radians. The correlation factor for this equation is 0.85.

A certain amount of variation can be observed between data points and the power curve. The maximum difference approached 100 percent in two cases. Despite the variation, Eq. (7.1) appeared to give a reasonable estimate of the change in G per change in the number of repetitions at a given strain amplitude.

Equations (7.14 and (7.15) can be used in the following manner. If a cohesive soil were subjected to a number of cycles, N, of high amplitude strain, then the immediate decrease in G_{after} would have been given by

$$G_{after} = 60.2 \left[0.9 - \gamma_{\theta z}^{0.41} * (\log N - 3) - 0.21 \log \gamma_{\theta z}\right] * G_{before} \quad (7.16)$$

This solution assumes that the strain amplitude exceeds 0.02 percent and that the number of cycles, N, is greater than 1000. It should be noted again that G_{after} begins to increase immediately after the end of high amplitude cycling. Equation (7.16) defines, therefore, the maximum measureable decrease in modulus.

c. Regain in Modulus

As noted in previous paragraphs, high amplitude cycling caused a decrease in the low amplitude modulus, G_{max}, when the strain amplitude during cycling exceeded a threshold limit. This reduction in modulus was, however, temporary. A time dependent regain in modulus commenced immediately after the end of high amplitude cycling. The time dependent

increase is defined in terms of G_{max}.

Figure 6.14 illustrates this increase in G_{max} for Leda Clay I. The plot shows the increase in G_{max} for two strain amplitudes, 0.5 and 1.0 percent, and for various numbers of cycles. These data are typical for all six test materials. Figure 6.14 also shows that the rate of G_{max} increase was greatest immediately after the end of high amplitude cycling. As time elapsed, the rate of increase in G_{max} decreased and eventually became tangent to the secondary slope for G_{max} extended from before high amplitude cycling commenced. The point at which tangency occurred was designated as the time to 100 percent regain. It is important to note that for the six cohesive materials tested each eventually regained 100 percent of the decrease in G_{max}.

Figures 6.15 and 6.16 show that the time to 100 percent regain of G_{max} differed according to the strain amplitude imposed during high amplitude cycling. When the high amplitude strain was less than 0.02 percent, regain of G_{max} occurred within several hundred minutes. As the strain amplitude during cycling increased, the time to 100 percent regain of G_{max} became progressively greater.

The number of cycles at a particular strain amplitude had little influence on the time to 100 percent regain of G_{max} after cessation of high amplitude straining. Figure 7.22 illustrates this behavior. In this figure the percentage regain in G_{max} as given by Eq. (4.1) in the Chapter IV, was plotted against elapsed time after the end of high amplitude cycling. It can be observed that the percentage regain, PR,

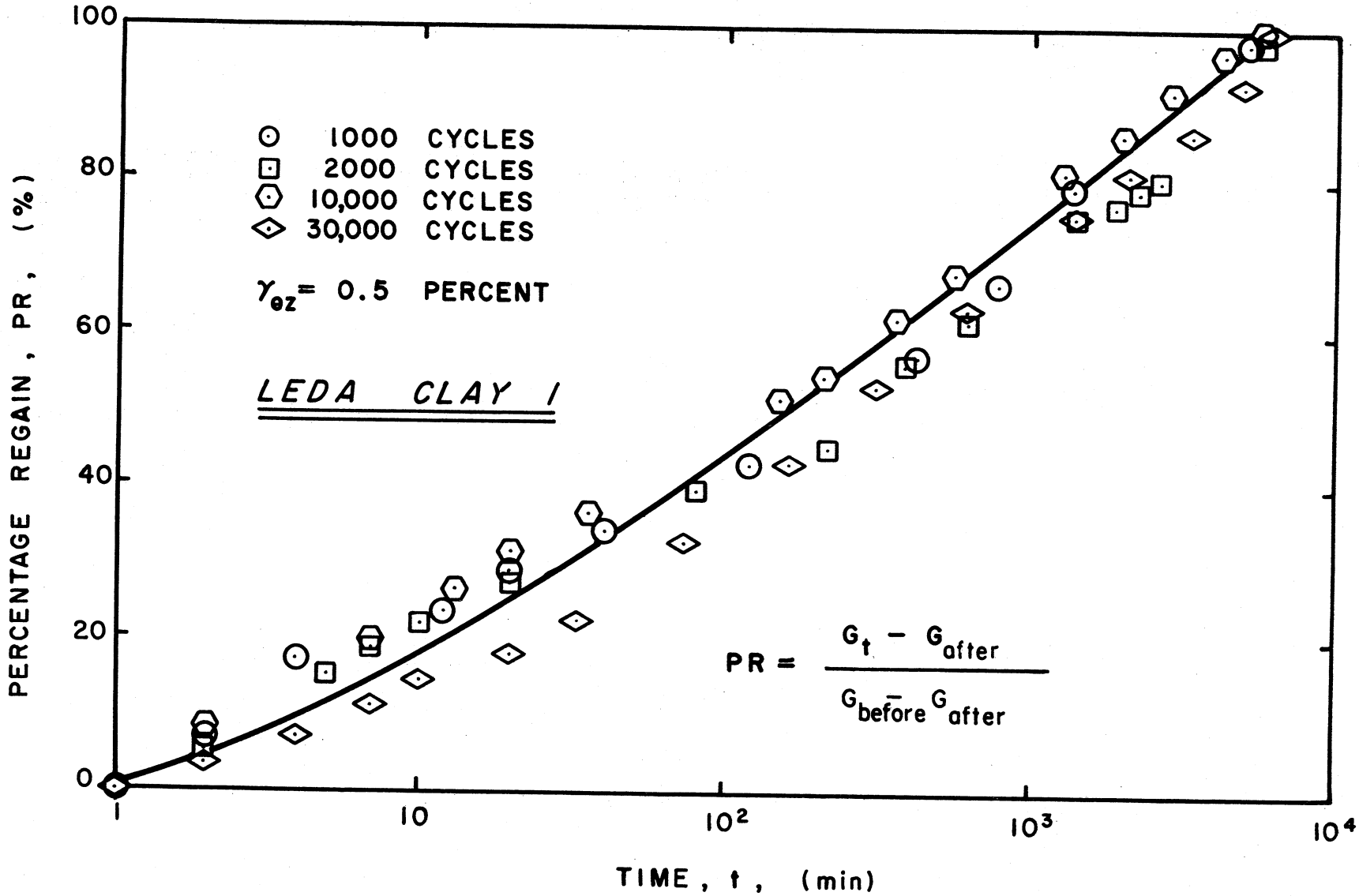

Figure 7.22. Comparison between percentage regain in G_{max} after high amplitude cycling and time for Leda Clay I.

was relatively similar for different numbers of cycles of strain. The data in Figure 7.22 are, admittedly, better than that recorded for some tests; however, all tests exhibited the same general characteristics. Figure 7.22 also shows that after about 10 min PR was relatively linear on a semi-logarithmic plot.

d. Modelling of Modulus Regain

As noted in a previous paragraph, the time to 100 percent regain in G_{max} increased as the strain amplitude during high amplitude cycling increased. Figure 7.23 shows that a relatively consistent trend in data occurs if the logarithm of the time to 100 percent regain in G_{max} is plotted against the logarithm of the strain amplitude. When a least squares fit was performed for the data points, the following power curve was obtained.

$$t_{100} = 201{,}000\ \gamma_{\theta z}^{0.72} \qquad (7.17)$$

where t_{100} is the time in minutes and $\gamma_{\theta z}$ is the strain amplitude in radians. The correlation factor for this equation is 0.87.

Once again the power curve approximated the test data reasonably well. Two data points exceeded the predicted value by more than 100 percent. Other points, however, were considerably closer to the proposed line.

Equation (7.17) can also be used to approximate the time necessary for any percentage regain. The percentage regain, as defined by Eq. (4.1) was in general proportional to the logarithm of time after the end

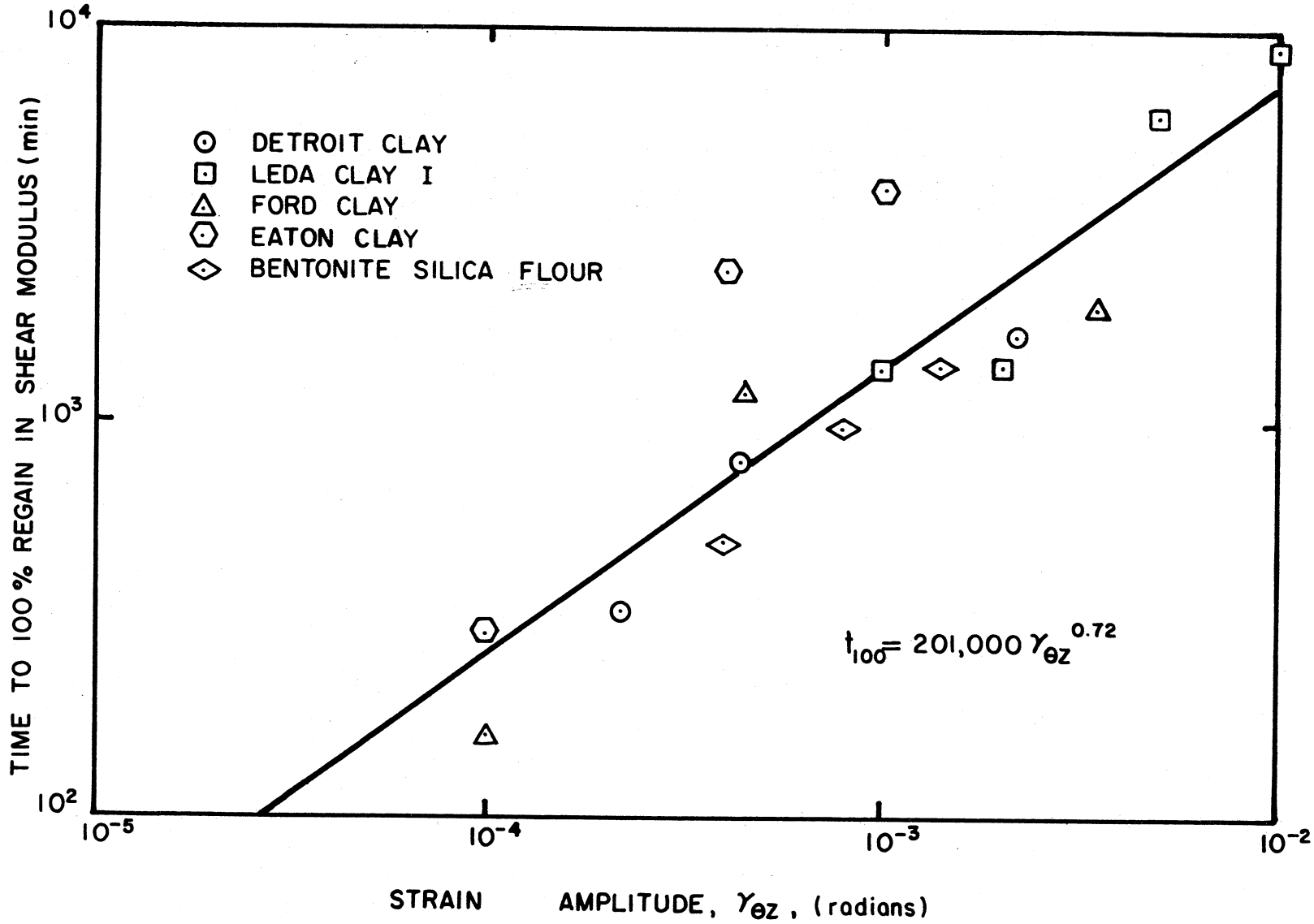

Figure 7.23. Typical comparison between time to 100 percent regain in G_{max} and strain amplitude.

of high amplitude cycling. On the basis of this proportionality the following expression was formulated

$$\frac{\log t_{100}}{(PR = 100\%)} = \frac{\log t_a}{(PR)_t} \tag{7.18}$$

The percentage regain in modulus at any time, $(PR)_t$, was given by

$$(PR)_t = \frac{\log t_a}{\log t_{100}} * 100\% \tag{7.19}$$

where t_{100} is defined by Eq. (7.17) and t_a is the number of minutes after high amplitude cycling. Once again, a certain amount of variation should be expected when utilizing this relationship.

e. High Amplitude Cycling Before 100 Percent Regain

During several high amplitude tests, additional cycles of high amplitude strain were applied to the specimen before PR equalled 100 percent. The object of these tests was to simulate a condition that might occur during earthquake or water wave loading. The test series modelled field conditions by first imposing a number of cycles of high amplitude strain to a test specimen. After high amplitude cycling ceased, thixotropic regain was allowed to occur for a certain period of time. Then before PR equalled 100 percent, the test specimen was subjected to another series of high amplitude strains. The process was repeated for various degrees of PR. In each test the amplitude and number of cycles of strain were held constant. Tests of this nature were intended to demonstrate whether or not the ratio of the high to low amplitude moduli (G/G_{max}) was affected when PR was less than 100 percent.

Figure 7.24 shows typical results of one of these experiments. When the average modulus measured after 1000 cycles of high amplitude strain, G, was divided by the low amplitude modulus, G_{max}, measured just prior to cycling, a nearly constant ratio was defined. This ratio was independent of PR, i.e., the same G/G_{max} occurred when PR was 25, 50 and 100 percent. This behavior was also characteristic of the behavior for other materials tested.

An important conclusion can be made about these results. The test series suggest that the same empirical prediction technique can be used despite past stress history. Proper evaluation requires only that G_{max} be identified. This conclusion is based on a limited amount of data, and therefore, additional verification is required.

f. Phenomenological Mechanism for Modulus Reduction and Regain

High amplitude cycling caused a decrease in the low amplitude modulus measured just after the end of high amplitude cycling. This decrease in G_{max} was temporary. In all cases reported herein, G_{max} ultimately returned to its original level.

Such behavior tended to verify the phenomenological mechanism suggested for determining high amplitude behavior. In that mechanism high amplitude cycling was assumed to cause rearrangement of the clay structure at the microscopic level. In these positions the particles exhibited lower values of G. Once cycling stopped, however, particles were no longer in positions of energy balance. Microscopic readjustments occurred until an equilibrium of attractive and repulsive forces existed.

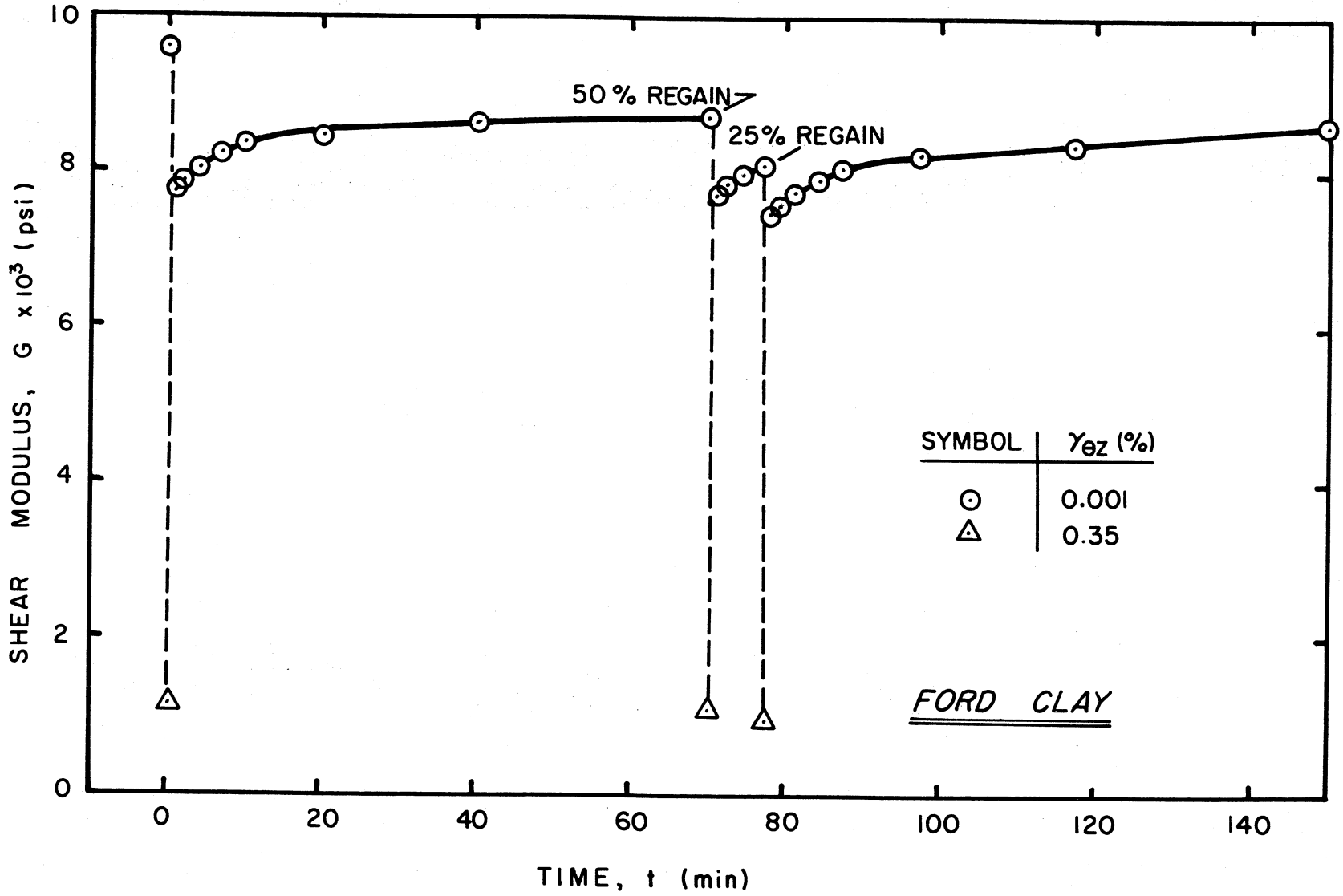

Figure 7.24. Variation in G_{max} when percentage regain is less than 100 percent.

As particles readjusted, bond strength and, consequently, G_{max} increased.

As noted in previous paragraphs, when the magnitude of strain utilized during high amplitude cycling was increased, the decrease in modulus measured after high amplitude cycling increased. This behavior occurred because large strains introduced large internal stresses which, in turn, altered the state of energy equilibrium. Particles readjusted to equilibrate various forces. Larger strains caused greater reorientation of the soil fabric. As reorientation occurred, bonds were weakened, and a smaller value of G_{max} resulted. This condition persisted immediately after the end of high amplitude cycling.

It was also noted that when strains did not exceed certain threshold levels, then negligible reduction in G occurred. This behavior suggested that the bond strength was sufficient to resist tendencies for reorientation during high amplitude cycling. When reorientation was negligible, the decrease in G_{max} was negligible.

Repetition of high amplitude strain also caused a decrease in G_{max}. A similar explanation can be used to define the phenomenological mechanism associated with this behavior. Each cycle of strain altered the position of particles at the microscopic level. The more cycles introduced, the greater was the tendency for reorientation and subsequent reduction in modulus. The effect of cycles was expected to be strain dependent because strains introduced the shearing forces that caused reorientation of soil structure. When strains were low, there was little tendency to rearrange the structure despite the number of cycles. A

large number of low amplitude cycles might, however, alter rigidity by initiating a creeping mechanism. Such behavior was not noted in this test program.

Figure 7.22 shows that the rate of thixotropic regain was approximately linear on a semi-logarithmic plot. This behavior was also expected because the degree of particle-force imbalance was greatest immediately after the end of high amplitude cycling. As particles were reoriented, the degree of imbalance decreased and, thus, the tendency to readjust decreased. The net effect was a decreasing rate of modulus regain with time. When plotted on semi-logarithmic coordinates, the decreasing rate of increase in modulus approximated a straight line. Mitchell (1960) suggested similar behavior for strength regain after a soil is remolded.

A previous paragraph noted that in five of the six soils high amplitude cycling did not alter the long-term rate of increase in G_{max}, i.e., secondary increase. For the five materials high amplitude cycling apparently did not introduce macroscopic changes in structure. This behavior tended to verify the concept that rearrangement in soil structure introduced by high amplitude cycling was on the microscopic level.

In the case of Bentonite-Silica Flour, a noticeable change in secondary increase occurred after the start of high amplitude cycling. It appears that a strain hardening condition existed. The strain hardening behavior suggested that high amplitude cycling caused a macroscopic reorientation of particles in this material. The new structure exhibited

more particle interference and, therefore, higher G_{max}.

Despite this apparent change in the structure of Bentonite-Silica Flour, the ratio of G/G_{max}, was predicted very well by the basic Ramberg-Osgood equation. This rather good correlation implied that the yield strength was not altered by the variation in structure. The two conclusions appear to be contradictory. No other explanation was, however, readily apparent.

C. Temperature Effects

The results of the temperature test series suggested that temperature influenced both the magnitude and rate of secondary increase in shear wave velocity. Other temperature data showed that the long-term effect of temperature on V_s differed from the short-term effect. These results and trends in results are reviewed in greater detail in the ensuing paragraphs. A short section is also devoted to consequences of temperature variation.

1. LONG-TERM TEMPERATURE EFFECTS

The long-term effect of temperature on V_s is considered in two parts: its effect on the magnitude of V_s and its effect on $\Delta V_s/V_{s1000}$. A third section is included to explain the responses in terms of physico-chemical behavior of soils.

a. Effect on Magnitude

Figure 6.20 shows that V_s measured at 4°C was consistently greater

than V_s measured at 22°C. The velocities were compared after 1000 min of confinement.

Figure 6.17 and the figures in Appendix F also show that for the seven test materials primary response had ended at about 1000 min. Although the absolute amounts of secondary increase for the seven materials differed at 1000 min, the relative amounts of secondary occurring at the two temperatures for the same material was approximately the same. On the basis of this observation, the velocity comparisons at 1000 min should give a valid indication of the temperature effect on the magnitude of V_s.

Figure 6.20 also shows that the effect of an 18°C temperature change was rather small. A line drawn at + 12.5 percent from the 45-degree, or equality, line encompassed all data points. Most of the points fell within 7.0 percent of the equality line. This magnitude of variation was approximately within the accuracy of the test method.

When a linear regression analysis was performed on the data, the following equation was defined

$$V_{s4} = 1.02\, V_{s22} + 8.5 \qquad (7.20)$$

where V_{s4} = shear wave velocity at 4°C (fps)

V_{s22} = shear wave velocity at 22°C (fps)

The correlation coefficient for the equation is 1.0. Temperature effect apparently became more significant as the V_s increased. The amount of data at high V_s was limited; therefore, such behavior must be regarded

as only a trend rather than absolute fact.

b. Effect on Secondary Increase

The rate of secondary increase, as defined by ΔV_s per log cycle of time, was also affected by varying the test temperature. Figure 6.21 shows that in general ΔV_s per log cycle for specimens tested at 22°C exceeded the same change for specimens tested at 4°C. The difference was, however, small for most data.

This observation was not, however, absolute. The Gulf of Mexico clays actually exhibited greater ΔV_s per log cycle when tested at the cooler temperature. Leda Clay I was, in turn, sensitive to temperature changes. For this material the secondary increase at 22°C exceeded that at 4°C by 20 to 90 percent. Most other data fell within 10 percent of the equality line.

Two linear regression analyses were performed. When all data was considered, the following relationship was defined

$$\left(\Delta V_{s4}\right)_{\text{log cycle}} = 0.72 \left(\Delta V_{s22}\right)_{\text{log cycle}} + 4.3 \qquad (7.21)$$

where $\left(\Delta V_{s4}\right)_{\text{log cycle}}$ = the change in shear wave velocity per log cycle of time at 4°C (fps)

$\left(\Delta V_{s22}\right)_{\text{log cycle}}$ = the change in shear wave velocity per log cycle of time at 22°C (fps).

The correlation coefficient for this equation is 0.93. When the Leda Clay I data was excluded from the analysis, the following equation was defined

$$\left(\Delta V_{s4}\right)_{\text{log cycle}} = 0.96 \left(\Delta V_{s22}\right)_{\text{log cycle}} + 0.55 \qquad (7.22)$$

where the terms were the same as defined in Eq. (7.21). The correlation coefficient improved to 0.95.

Equation (7.22) was considered more representative of soils typically encountered at field sites. This relationship shows that the secondary increase did vary slightly with temperature. The effect also appeared more pronounced at higher magnitudes of secondary increase.

Another observation can be made about the rate of secondary increase. Figures 6.18 and 6.19 show that the scatter of data for $\Delta V_s/V_{s1000}$ was considerably greater when the temperature during testing was 22°C. This trend was particularly true for Gulf of Mexico Clay and Leda Clay I. For the Gulf of Mexico Clay $\Delta V_s/V_{s1000}$ varied by 14 percent at 22°C and by only 4 percent at 4°C. The variation was 20 percent for Leda Clay at 22°C and 7 percent at 4°C. Other materials exhibited the same general trend but at considerably reduced magnitudes. It was also interesting to note that the two materials with large scatter of $\Delta V_s/V_{s1000}$, i.e., Gulf of Mexico Clay and Leda Clay I, also departed most from the trend in data shown in Figure 6.21.

c. Phenomenological Mechanism

Various studies are cited in Chapter II which explain why temperature affects the behavior of soil. These explanations are generally based on the molecular and atomic behavior of the soil structure or

inferred from the behavior of other solid materials. The complexity of soils is such that these studies normally involve many simplifications or assumptions and, consequently, are of limited quantitative use. The studies do however, define useful trends which can be compared to the results of this investigation.

Mitchell (1960) performed a comprehensive study of double layer attractive and repulsive forces in soils. He concluded that if the dielectric constant of soil varied with temperature, as it probably does, then repulsive forces are unchanged as the temperature varies from 0° to 100°C. Mitchell added that the interparticle contact structure may be weakened because of increased thermal activity of constituent atoms and thus cause a reduction in bond strength. Increased thermal activity is, of course, associated with higher temperatures.

The magnitude of V_s measured after 1000 min of confinement was higher at the lower temperature. Such behavior conformed to Mitchell's statement regarding the thermal activity of constituent atoms. It seems reasonable that thermal activity was lower at 4°C than at 22°C and, consequently, the amount of interparticle weakening was less. If bond weakening were less, then V_s should have been higher.

Murayama (1969) recalled that the elastic properties of most engineering materials are temperature dependent and then proposed the use of a rheological model to evaluate soil response. The model showed that as temperature increased elastic moduli decreased. Data from a series of relaxation tests substantiated these results. Murayama attributed the

temperature effect to the physico-chemical characteristics of the soil.

Modulus versus temperature trends defined in this investigation are similar to those proposed by Murayama. The magnitude of change per unit change in temperature, however, differed noticeable. Data from Murayama suggested that the decrease in modulus exceeded 25 percent when temperature was increased from 4°C to 25°C. Except for Leda Clay I data, results of this investigation indicated less than a 14 percent change for the same temperature variation. Such behavior implied that the model proposed by Murayama was not applicable to most of the soils described herein.

Both Mitchell and Murayama's results can be compared qualitatively to the variations in the magnitude of V_s determined in this investigation. None of the aforementioned result, however, explains directly the secondary increases in ΔV_s per log cycle noted during this investigation.

As noted previously, secondary increase is attributed to thixotropic regain. If Mitchell's comments are adjusted somewhat, then it can be assumed that temperature change causes a change in strength of certain bonds. At higher temperatures the thermal activity is greater and more of the interparticle contact structure is weakened. Consequently, a larger energy imbalance occurs than would occur for the same conditions at lower temperatures. As was discussed previously, the rate of regain in modulus or velocity increases as the degree of energy imbalance increases.

2. SHORT-TERM TEMPERATURE EFFECTS

Temperature fluctuations caused immediate variations in V_s. The following paragraphs show that these variations were due to pore pressure changes within the soil specimen. As long as drainage was permitted, these effects were temporary.

a. Effect on Magnitude and Rate of Secondary Increase

The short-term effect of temperature on V_s was discovered by accident. During the performance of a high amplitude test the air conditioner which maintained the laboratory at a constant temperature failed. The room gradually warmed from 23°C to 31°C in a 12-hr period. Figure 7.25 illustrates the relationship between V_s and temperature during that period. Despite the immediate decrease in velocity, the change in temperature had no permanent affect on the long-term behavior of the soil.

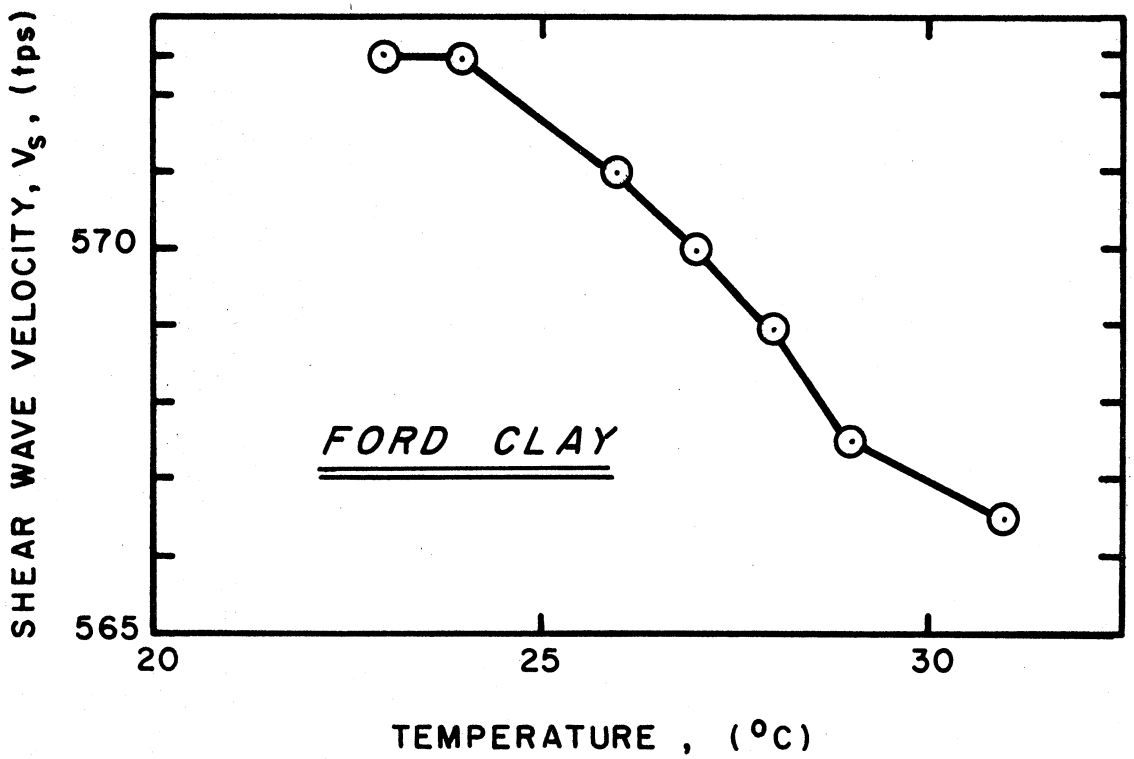

Figure 7.25 Shear wave velocity measured during temperature change.

Subsequent to this observation, similar data were gathered from low amplitude temperature tests. Once ΔV_s per log cycle of time was well established for the cooled sample at the final confining pressure, the temperature in the water bath was suddenly increased to 22°C. The water in the bath reached the higher temperature in approximately 10 min. During and following the temperature change, V_s of the specimen was monitored.

Figure 7.26 shows how Detroit Clay responded to the increase in temperature. This behavior was considered typical for all test data. An immediate decrease in V_s occurred as the sample began to warm. During the same interval, the axial length of the sample increased and pore water began flowing out the drainage line. Figure 7.26 also shows that after a short period of time the behavior reversed. Velocity began to increase.

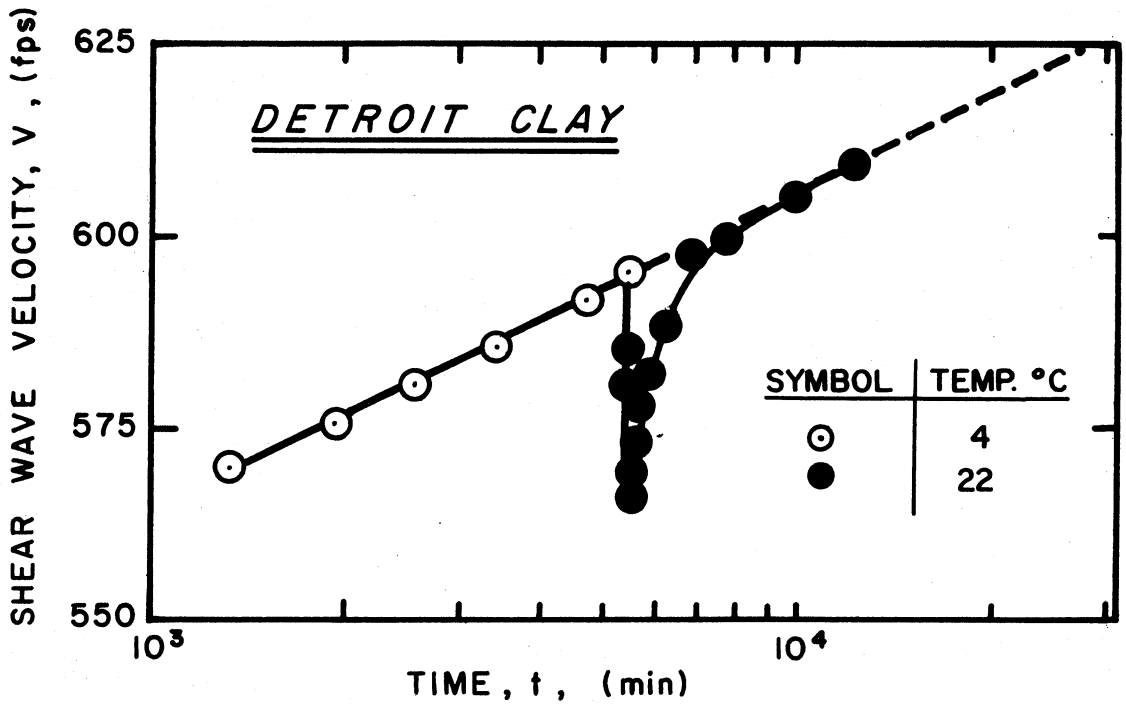

Figure 7.26. Effect of rapid temperature change on V_s.

The shear wave velocity eventually reached the level measured prior to the temperature change. When the secondary slope was extended, regain approached the extended line tangentially. The secondary slope, ΔV_s per log cycle, did not appear to change after changing the temperature.

The magnitude of V_s decrease due to the 18°C temperature change typically varied from 2 to 8 percent for the seven materials. For the data shown in Figure 7.26, the decrease is 4.2 percent of V_s measured before temperature change. It took between 1000 and 5000 min after the time of the temperature change to regain 100 percent of the decrease in V_s.

b. Phenomenological Mechanism

Mitchell (1960) provided a reasonable explanation for the previously described short-term temperature response. According to Mitchell, a change in temperature caused an immediate expansion of the pore-water. The expansion in pore-water volume created excess pore pressures which, in turn, reduced the effective stress transferred at points of particle contact. As the effective stress decreased, V_s decreased. Eventually excess pore pressures decreased because of drainage from the sample, and effective stresses increased. As effective stresses increased, V_s increased.

This explanation assumes that two conditions occurred. It assumes first that excess pore pressures developed. Excess pore pressures develop when volumetric expansion of the pore fluid is restricted by the

soil structure and when the rate at which fluids flows out of the material does not exceed the rate of volumetric increase in pore fluid due to temperature change. If these conditions were satisfied, then excess pore pressures would have developed. The explanation also assumes that drainage was permitted. Excess pore pressures could, therefore, dissipate at some rate determined by the permeability of the material. The characteristics of the soil and the test devices are such that these conditions existed at the time of the temperature change. Mitchell's explanation appears, therefore, to be valid.

Mitchell also showed that a permanent volume decrease occurred as result of temperature change. In test results reported herein, the axial height did decrease below that measured prior to temperature change. Although the permanent change in height indicated a volume decrease, neither V_s nor ΔV_s per log cycle changed appreciably.

3. Practical Aspects of Temperature Change

The previous paragraphs reviewed the short- and long-term effects of temperature changes on V_s for cohesive soils. Both conditions are important from a laboratory testing standpoint.

Long-term response approximates the conditions that occur when samples are removed from the ground and are tested in the laboratory at normal laboratory temperatures. A temperature change of 10°C to 20°C generally occurs within the soil. Pore pressures probably increase, but by the time the samples are tested total dissipation of excess pore pressures undoubtedly occurs. The change in soil structure during

stress relief also tends to compensate for any increase in pore fluid volume. On the basis of these observations and results of this investigation, it can be concluded that the sample tested at laboratory temperatures will give a slightly lower V_s and a slightly greater ΔV_s per log cycle than samples tested at in situ temperatures. Neither of these changes is, however, of sufficient magnitude to warrant either changes in test procedure or inclusion of temperature correction terms in empirical prediction methods.

The short-term response to temperature variation is noticeable. As reported previously, the typical cause of such variations is the inability to maintain laboratory temperatures at some constant level. If test temperature variations do occur, then V_s may vary by 10 percent or more. The actual magnitude of variation will depend on the magnitude of the temperature change and drainage conditions within the sample. In certain situations the presence of excess pore pressures might influence results. This would be particularly true if excess pore pressures exist when high amplitude response is being monitored. Furthermore, excess pore pressures may induce permanent volume changes which may alter the dynamic behavior of the soil.

D. Field Versus Laboratory Test Results

It was found during this investigation that laboratory and field test results differed. In general V_s determined by field test methods exceeded V_s determined by laboratory methods. The difference was

attributed to inaccuracies associated with test procedures and to incorrect interpretation of test results.

1. VALIDITY OF FIELD TEST RESULTS•

The ability of the field test to accurately indicate in situ characteristics depends on soil conditions at the test site, the test procedure and the interpretation of test data. A certain amount of variation in test results is always expected because of inaccuracies introduced by variations in making distance and time measurements. Each field site had a different set of problems; therefore, each site will be discussed separately.

a. Detroit Field Test Site

The Detroit field test involved a variation from accepted test procedure which may have influenced test results. During these tests, the distance between the impulse and pickup points was only 3.5 ft. This short distance resulted in very short travel times. Consequently, any small error in selecting the shear wave arrival time introduced noticeable error in the shear wave velocity determination. Furthermore, any small error made in measuring the distance between impulse and pickup points added to the error.

At the 10-ft depth the expected variations in measured distance and travel time were 0.5-ft and 1.0-msec, respectively. When these factors were introduced into a standard error equation, a maximum velocity difference of approximately plus or minus 80 fps was defined, i.e.,

$$V_s = \frac{L}{t}$$

$$\Delta V_s = \left|\frac{\partial}{\partial L}\ \frac{L}{t}\right| \Delta L + \left|\frac{\partial}{\partial t}\ \frac{L}{t}\right| \Delta t$$

$$\Delta V_s = \frac{\Delta L}{t} + \frac{L}{t^2}\,\Delta t \qquad (7.23)$$

$$= \frac{0.5 \text{ ft}}{10.6 \text{ msec}} + \frac{3.5 \text{ ft}}{(10.6 \text{ msec})^2} * 1 \text{ msec}$$

$$\cong 80 \text{ fps}$$

where V_s = shear wave velocity (fps)

L = travel path (3.5 ft)

t = shear wave arrival time (10.6 msec)

ΔL = expected variation of L (0.5 ft)

Δt = expected variation of t (1.0 msec)

Note that if the velocity of the material were the same and if the travel path were increased to 15 ft, the expected variation would have decreased to plus or minus 18 fps. It is apparent, therefore, that the magnitude of possible variation increases substantially as the travel time decreases.

Table 6.1 shows that V_s measured in the field at the Detroit site was substantially below the 1000-min laboratory reading. However, the field value of V_s exceeds the laboratory value of V_s if the 80 fps variation is added to the field value of V_s. The higher value falls within the range of expected behavior.

A second source of error may be related to common difficulties

associated with borehole excavation. Borehole drilling operation creates a zone of disturbance around the borehole. If excessive disturbance of the soil occurs, V_s in the disturbed zone would undoubtedly be lower than that in the undisturbed zone. In cases where the borehole spacing is 10 ft or greater the zone of lower V_s has little overall effect, but when the travel path is short the effect may be substantial. There is no data to estimate the extent of the disturbed zone, however, this hypothesis seems to justify adjusting V_s upward.

It is also noted in Figure 6.22 that a rapid transition in V_s occurred between the 10- and 13-ft depths. The magnitude of change did not seem reasonable in view of the soil properties. An abrupt variation in velocity is generally associated with either a change in soil type or a change in soil properties. Neither condition occurred.

On the basis of this discussion, it seems that higher velocities could be justified at the site.

b. Ford Field Test Site

Several factors influenced the validity of the Ford field test results. These factors involved stress conditions at the site, pore-water conditions at the site and homogeneity of soil at the site.

The stress conditions at the site as controlled by the overlying material are subject to some question. Approximately 5 hr prior to performing the cross-hole test, 12 ft of overburden were removed from the test site. The excavation was performed as part of the daily enlargement of a debris pit. This excavation caused a reduction in

confining stress.

The change in overburden pressure allowed stress relief in the soil. In most situations stress relief introduces no serious problems. The soil is considered to be overconsolidated and appropriate adjustments are made. However, in the particular test the time element associated with stress relief may have added certain unknown factors. If insufficient time elapsed after stress relief, then negative residual pore pressures would have existed. These pore pressures would have caused unknown effective stress conditions to exist within the soil. About 5 hr separated the start of stress relief (removal of overburden) and the time of cross-hole testing; and pressure variations may have still existed in the soil.

The second possible source of error involved the location of the ground water table at the site. The location was not precisely known. It was assumed to be about 4 ft below the location of the original soil surface, i.e., the surface before excavation. This assumption was based on the elevation of water in nearby pits. The level of water in these pits varies somewhat according to time and duration of rainfall; however, the variation probably does not exceed a foot. If the assumption about water level were incorrect, then stress computations would have been in error.

Another uncertainty involved the homogeneity of soil at the test site. In this study the soil specimen obtained for laboratory testing originated from a point located about 10 ft horizontally from the point

of cross-hole testing. The elevations of the field test and the laboratory test specimen were approximately the same. It was assumed, therefore, that the material was homogeneous in the lateral direction.

These three factors introduced potential sources of error. It was thought that the magnitude of these errors probably falls within the expected velocity variation, as defined by Eq. (7.23). When $\Delta L = 0.5$ ft and $\Delta t = 1$ msec, ΔV_s is approximately 50 fps or 10 percent of the measured value.

c. Chevy Field Test Site

The results of the Chevy field tests were somewhat difficult to interpret. When cross-hole tests were repeated at some elevations, V_s varied by several hundred feet per second. Also the velocity at the 50-ft depth appeared to be too high when compared to empirical and laboratory data. These behaviors may be attributed to several factors.

For depths less than 35 ft, the expansion-type impulse system was used. This system may have introduced inaccuracies because of the mechanical coupling involved. If a time lag occurred as the impulse passed through the expandable coupling, the apparent velocities would have decreased. The decrease would have varied according to the energy of the blow and the rigidity of the expansion system at the time of the impulse. The rigidity of the expansion system depended on the torque used to force the expansion plates into the side of the borehole. It was generally necessary to re-tighten the plates after each series of blows. A variation in results might, therefore, have occurred.

Despite the previously noted variation, the average data for all but the 50-ft depth appear consistent with empirical and laboratory results. It should also be noted that the expected variation for data, as defined in Eq. (7.23) (where Δt = 0.5 msec and ΔL = 0.5 ft) was approximately 200 fps. A noticeable scatter of results was therefore, to be expected.

As mentioned previously, V_s at the 50-ft depth appeared to high when compared to empirical and laboratory data. This apparent discrepancy may be associated with the interpretation of data. The velocity was obtained by interpolating between results measured at 40 and 60 ft. The velocities at these two depths were the same; consequently, V_s was assumed to be uniform in this range.

The assumption of a uniform velocity profile was not necessarily substantiated by other soil data. Although soil properties changed gradually below 20 ft, V_s changed noticeably between 35 and 40 ft. This behavior could imply that the velocity at 40 ft was invalid. If V_s at 50 ft were determined by interpolating between 35- and 60-ft readings, a lower, more representative value would have been defined.

d. Eaton Field Test Site

No unusual behaviors were noted for the Eaton field test. Procedures conformed to accepted methods; results were interpreted with relative ease. A certain amount of variation occurred but the variation could be accounted for in the error analysis. The expected variation as defined by the error equation was plus or minus 40 fps.

2. VALIDITY OF LABORATORY RESULTS

Two factors determined the validity of the laboratory test results: the degree to which the small volume of soil represented in situ conditions and the ability of the laboratory test to approximate or simulate field conditions. The former factor depended on the amount of disturbance associated with the sampling process and on the homogeneity of the soil at the test site. The ability of the laboratory test to approximate field conditions depended on not only how accurately the test method modelled in situ conditions but also on the interpretation of test results.

a. Quality and Homogeneity

Laboratory tests were performed on small volumes of soil obtained from the field test site. It was assumed that the properties of a small volume of soil represented the general properties at the site. The validity of this assumption was determined in part by the amount that soil properties varied at the site. For the four test sites described herein, it was believed that the samples did represent the average properties of the in situ test zones because the geologic methods of forming these soils generally gave fairly good lateral homogeneity within the limited areas of interest.

Whenever soil is removed from the ground, certain amount of disturbance is inevitable. The disturbance is attributed to the removal process. In three of the four comparisons, laboratory tests were performed on samples obtained in thin-wall Shelby tubes. These samples were

regarded as the best possible samples that could be obtained by commercial means. Area ratios associated with the sampling method were small (i.e., less than 10 percent) and disturbance was believed to be restricted to a thin zone around the wall of the sampling tube. The fourth comparison utilized material trimmed from a 1 ft^3 block of soil. The block was disturbed to a lesser extent than the thin-wall Shelby tube samples. In view of these methods, it seems reasonable to believe that these samples were relatively undisturbed and, therefore, gave a fairly good indication of in situ properties.

Laboratory specimens were trimmed from the inner 1.4 in. of the 3-in. Shelby tube sample and from the inner portion of the 1 ft^3 block. It was assumed that the 1.4-in. size was still representative of in situ conditions because coarse soil particles were absent. If the material were comprised of large sand or gravel sized particles, this assumption would have been questionable. The Chevy Clay samples were the only materials with a noticeable proportion of coarse particles; however, a visual inspection performed subsequent to testing found no particles greater than 1/4 in. in diameter.

The last major factor which may have affected sample quality involved stress changes. Stresses were removed during sampling and then reapplied during the laboratory test. It was assumed that the initial stress relief did not permanently alter the soil structure and that when pressures were reapplied, field conditions were recreated. Both of these assumptions are subject to criticism.

b. Simulating Field Conditions

The resonant column device was used to measure V_s as a function of confining pressure and time. When comparing laboratory values of V_s to *in situ* values, the laboratory velocity was determined at the confining pressure which would come closest to simulating *in situ* stress conditions. Once data were defined at this pressure, it was necessary to include appropriate increases in velocity due to time effects.

During laboratory tests, the *in situ* stress conditions were approximated by the average ochtahedral confining stress, i.e.,

$$\bar{\sigma}_o = \frac{\bar{\sigma}_1 + 2\bar{\sigma}_3}{3} \tag{7.24}$$

where $\bar{\sigma}_1$ = vertical effective stress

$\bar{\sigma}_3$ = horizontal effective stress

The vertical effective stress and the horizontal effective stress are related by the coefficient of earth pressure at rest, K_o.

$$K_o = \frac{\bar{\sigma}_3}{\bar{\sigma}_1} \tag{7.25}$$

By substituting Eq. (7.25) into Eq. (7.24), the following relationship was derived

$$\bar{\sigma}_o = \bar{\sigma}_1 \frac{(1 + 2K_o)}{3} \tag{7.26}$$

Therefore, the confining pressure for the laboratory test was determined once the vertical overburden pressure and the coefficient of earth pressure at rest were defined.

The coefficient of earth pressure at rest was determined from a relationship suggested by Lambe and Whitman (1969). These individuals plotted K_o as a function of overconsolidation ratio and plasticity index, I_p (Figure 7.27). The overconsolidation ratios, K_o values and the average confining stresses are summarized in Table 7.2.

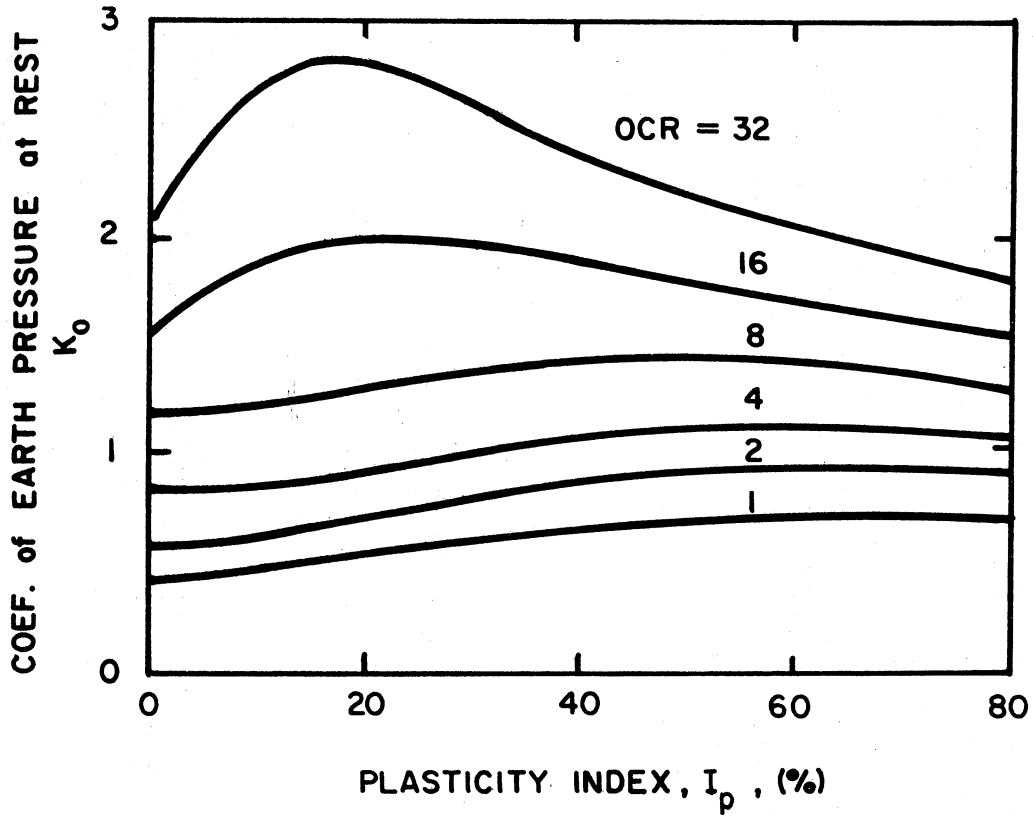

Figure 7.27. Variation in K_o with I_p and overconsolidation ratio (OCR).

TABLE 7.2. SUMMARY OF COEFFICIENTS OF EARTH PRESSURES AT REST AND OVERCONSOLIDATION RATIOS FOR FIELD TESTS

Soil	Depth (ft)	$\bar{\sigma}_o$ (psi)	K_o	OCR
Detroit Clay	10	5	0.8	2.8
Ford Clay	6	10	2.3	20
Chevy Clay	20	17	0.7	3
	35	24	0.6	2
	50	33	0.5	1
Eaton Clay	15	6	0.8	3.5
	19	8	0.8	3.6

It was also shown previously that after a certain time interval V_s defined in the laboratory resonant column device increased linearly as the logarithm of time increased. The secondary increase in velocity varied from 5 to 50 fps per logarithmic cycle of time. Obviously the comparison of laboratory to field results depended on the time at which the velocity was defined.

Figure 6.24 shows that most laboratory values of V_s approached field values of V_s when the secondary increase in velocity was extrapolated to the 20-year date. This point was four logarithmic cycles beyond the 1000-min reading. A 10 to 40 percent increase in V_s occurred during the four log cycle interval. If the data were extrapolated to 200,000 years, the increase in V_s would have varied from 20 to 80 percent for most materials. The extrapolation procedure was based on the assumption that a linear relationship existed between V_s and log time during secondary response. Afifi (1970) showed that this assumption was correct for a one-year extrapolation (about three log cycles of time).

The most logical time for comparing results seems to be at the geologic age of the material. Mitchell (1960) suggested such an approach for estimating the time at which thixotropic regain ceased after remolding of soils. It would be difficult, however, to verify this theory in a laboratory test because the age of the material may exceed tens of thousands of years. Abdel-razzak (1973) has a limited amount of data that tends to substantiate the idea for man-made embankments. In Abdel-razzak's study, laboratory values of V_s equalled field values of V_s at the approximate age of the embankment. It seems, therefore, that three to six logarithmic cycles of extrapolation (2 to 2000 years) would be appropriate for most field comparisons.

For the four case studies reported herein, a 20-year extrapolation was used. It was believed that in these cases stress conditions would have probably changed recently and, consequently, justified a shorter regain interval.

3. COMPARISON OF RESULTS

Now that the validity of laboratory and field test results have been discussed, velocity measurements can be compared on a more quantitative basis. These velocities can also be compared with velocities predicted by the Hardin empirical equation.

a. Field to Laboratory Comparison

Figure 6.24 illustrates the comparison of V_s defined by laboratory test to V_s defined by field methods. The data for this comparison are

given in Table 6.1. In three out of the four investigations, field values of V_s exceeded laboratory values of V_s. This behavior was expected. It probably represented minor amounts of strength loss due to alterations in soil fabric. When secondary regain in V_s was introduced into the comparison, the discrepancy between laboratory and field values of V_s decreased. In several cases there was virtually no difference in velocities.

The Detroit Clay data did not develop expected behavior. However, it was noted previously that the field value of V_s was of questionable validity. The discrepancy was probably related to the close spacing of the boreholes.

A significant difference between laboratory and field velocities was also observed for the Chevy data at the 50-ft depth. This difference was thought to be associated with improper interpretation of data. However, it could have reflected disturbance to the laboratory sample. Sample disturbance would have reduced the V_s measured in the laboratory test.

Figure 6.24 also shows that a 20-year extrapolation of secondary increase in V_s provided an adequate representation of field V_s in most cases. The 20-year duration seems reasonable because all data having a close correlation originated from within 30 ft of the ground surface. Because of the nature of each site, the 30 ft zone probably has undergone recent stress change; therefore, the interval of time during which secondary increase in velocity occurred would have been relatively short.

b. Comparison With Empirical Results

Table 7.3 gives a comparison between V_s measured by laboratory and field techniques and V_s computed by Eq. (7.1). In several cases the empirical equation gave a fairly good indication of field and laboratory velocities. In other situations a noticeable disparity occurred.

Several factors may have contributed to the apparent inaccuracies of the empirical equation. In general Eq. (7.1) defined V_s in terms of void ratio, overconsolidation ratio and average effective octahedral stress. Other factors, however, may have influenced V_s. Furthermore the three previously mentioned paramenters were not always easily defined.

4. APPLICATION OF FIELD AND LABORATORY DATA

Both the field and the laboratory test methods were used to establish dynamic characteristics of the soil. The field test gave a good indication of in situ properties. The laboratory test was best suited for determining how those in situ properties changed with changes in parameters such as pressure, temperature and time.

The field test had certain advantages and limitations. Its prime advantage was that it measured soil properties without removing samples from the ground. Soil disturbance was, therefore, minimized. The principal disadvantage of the field test was that the soil along the travel path could not be seen. Consequently, layering or obstructions might have existed which significantly altered velocity values. The accuracy of the method was determined by the accuracy of distance and

TABLE 7.3. COMPARISON OF LABORATORY, FIELD AND ANALYTIC TEST RESULTS

Soil	Depth (ft)	Void Ratio	$\bar{\sigma}_o$ Confining Pressure (psi)	Shear Wave Velocity (fps)		
				Empirical	Laboratory (20 year)	Field
Detroit Clay	8.5	0.74	4	630		330
	10	0.86	5	630	474	330
	11.5	0.98	5	600		370
	13	1.14	5	550		500
Ford Clay	6	0.87	10	730	540	550
Chevy Clay	20	0.49	17	1050	1050	1100
	35	0.40	24	1090	1120	1100
	50	0.32	33	1180	1230	1500
Eaton Clay	15	0.62	6	750	523	565
	19	0.71	8	780	550	550

time measurements.

Laboratory tests also had advantages and disadvantages. Obviously the prime disadvantage was that results depended on the quality of the soil specimen. Furthermore, the laboratory tests are dependent on the ability to reproduce field conditions. Despite these limitations the laboratory method was ideal for performing parametric studies. The laboratory result was also used to verify irregular field values of V_s.

CHAPTER VIII

CONCLUSIONS

The primary conclusions of this investigation are concerned with the influence of time, strain amplitude, number of repetitions at a given strain amplitude and testing temperature on the dynamic properties of cohesive soils. Additional conclusions were derived from studies which described the effects of stress history, the relationship between laboratory and field shear wave velocity and the development of empirical equations to approximate the influence of parameters studied.

A. Low Amplitude Response

The shear wave velocities established during low strain amplitude tests showed a time-dependent variation throughout the duration of the load application. The time-dependent behavior could be divided into portions corresponding to primary and secondary consolidation, with a distinct break in the velocity-logarithm of time curve occurring at about 1000 min. In the secondary range, the magnitude of V_s depended on the confining pressure, void ratio, overconsolidation pressure and, of course, time (Eqs. (7.1, 7.5 and 7.6)).

The rate of secondary increase in V_s was found to be nearly constant with the logarithm of time. To facilitate presentation of data, the parameter, ΔV_s per log cycle of time, was divided by V_s measured

after 1000 min. This ratio increased as the mean particle diameter decreased and as the initial void ratio increased or the undrained shearing strength decreased. Empirical equations (Eqs. (7.7) and (7.8)) were formulated to relate the influences of these quantities.

B. Test Conditions

Careful observation of air leakage through the rubber membrane showed that no noticeable effects of air migration occurred on either V_s or the water content of the samples. Using three different types of resonant column devices, it was shown that device variables did not introduce a difference in measured material properties.

C. High Amplitude Response

High amplitude straining caused a decrease in V_s (or G) when the strain amplitude exceeded about 0.01 percent. At a strain amplitude of 1.0 percent, the shear modulus, G, was reduced to 20 percent of the low amplitude value measured immediately before the start of high amplitude cycling. The reduction of G with shearing strain amplitude could be approximated by empirical curves based on the hyperbolic relationship (Eq. (2.7)) or the Ramberg-Osgood equations (Eq. (7.11)).

Sustained repetitions of high amplitude strain caused further decrease in G. The cycle effect was studied for the range from 500 to 100,000 cycles. An empirical equation (Eq. (7.12)) was developed to

describe this response.

D. Stress History Effects

Stress history effects were studied by evaluating the low amplitude shear modulus after a series of high amplitude stresses had been applied. Immediately following high amplitude straining, the low amplitude modulus was reduced (Figure 6.11). Subsequently, a time-dependent regain occurred. Ultimately G reached its original value. The time required for complete regain could be estimated by Eq. (7.17).

E. Temperature Effects

The effect of testing temperature was investigated because of the possible influences it might have on the magnitude of V_s and the rate of secondary increase in V_s. A typical laboratory temperature of 22°C and a probable extreme field temperature of 4°C were chosen. The long-term effect of the change in temperature indicated that the magnitude of V_s was from zero percent to 12.5 percent higher at 4°C than it was at 22°C (Figure 6.20). The rate of secondary increase increased slightly as the temperature increased. Short-term effects of temperature variation resulted in immediate changes in V_s. This variation essentially disappeared when pore pressures, which were caused by the temperature change, equalized.

F. Field Comparison

It was found that the laboratory values of V_s corresponding to 1000-min test duration were appreciably lower than field values of V_s. However, if the secondary increase in V_s were included, a better agreement resulted. When laboratory values of V_s were modified by adding a 20-year extrapolation of the secondary effects, then the modified V_s corresponded, in most cases, with the field value.

CHAPTER IX

REFERENCES

1. Abdel-razzak, K. G., (1973), "In Situ and Laboratory Shear Wave Velocities of Two Compacted Soils," thesis presented to the University of Massachusetts, at Amherst, Massachusetts, in partial fulfillment of the requirements for the degree of Master of Science in Civil Engineering.

2. Afifi, S.E.A., (1970), "Effects of Stress History on the Shear Modulus of Soils," thesis presented to The University of Michigan, at Ann Arbor, Michigan, in partial fulfillment of the requirements for the degree of Doctor of Philosophy.

3. Afifi, S.E.A., and Woods, R. D., (1971), "Long-term Pressure Effects on Shear Modulus of Soils," Journal of the Soil Mechanics and Foundations Division, ASCE, Vol. 97, No. SM10, October, pp. 1445-1460.

4. Afifi, S.E.A., and Richart, F. E., Jr., (1973), "Stress-History Effects on Shear Modulus of Soils," Soils and Foundations (Japan), Vol. 13, No. 1, March, pp. 77-95.

5. Andresen, A., and Simons, N. E., (1960), "Norwegian Triaxial Equipment and Technique," Proceedings of the Research Conference on Shear Strength of Cohesive Soils, sponsored by the Soil Mechanics and Foundations Division, ASCE, Boulder, Colorado, June, pp. 695-709.

6. Bamert, E., Schnitter, G., and Weber, M., (1965), "Triaxial and Seismic Laboratory Tests for Stress-Strain Time Studies," Proceedings of the Sixth International Conference on Soil Mechanics and Foundation Engineering, Vol. 1, Montreal, pp. 151-154.

7. Bishop, A. W., and Henkel, D. J., (1964), The Measurement of Soil Properties in the Triaxial Test, Edward Arnold, Ltd., London, 228 pp.

8. Bowles, E. E., (1968), Foundation Analysis and Design, McGraw-Hill, New York, 659 pp.

9. Bowles, E. E., (1970), Engineering Properties of Soils and Their Measurement, McGraw-Hill, New York, 187 pp.

10. Buisman, A. S., (1936), "Results of Long-Duration Settlement Tests," Proceedings of the First International Conference on Soil Mechanics and Foundation Engineering, Vol. 1, Cambridge, pp. 103-106.

REFERENCES (Continued)

11. Calhoun, D. E., and Triandafilidis, G. E., (1969), "Dynamic Odeometer Study of Lateral Yield Effects," Proceedings of the Seventh International Conference on Soil Mechanics and Foundation Engineering, Vol. 1, Mexico City, pp. 65-72.

12. Campanella, R. G., and Mitchell, J. K., (1968), "Influence of Temperature Variations on Soil Behavior," Journal of the Soil Mechanics and Foundations Division, ASCE, Vol. 94, No. SM3, May, pp. 709-733.

13. Converse, F. J., (1961), "Stress Deformation Relations for Soft Saturated Silt Under Low-Frequency Oscillating Direct-Shear Forces," Symposium on Soil Dynamics, ASTM STP 305, American Society for Testing Materials, pp. 15-19.

14. Cunny, R. W., and Fry, Z. B., (1973), "Vibratory In Situ and Laboratory Soil Moduli Compared," Journal of the Soil Mechanics and Foundations Division, ASCE, Vol. 99, No. SM12, December, p. 1055-1076.

15. Cunny, R. W., Marcuson, W. F., III, and Skoglund, G. R., (1973), "Evaluation of Resonant Column Dynamic Test Devices," Draft Report, U.S. Army Engineer Waterways Experiment Station, July, 11 pp.

16. Delflanche, A. P., Bryant, W. R., and Cernock, P. J., (1971), "Determination of Compressibility of Marine Sediments from Compression-Wave Velocity Measurements," Preprints from the 1971 Offshore Technology Conference, Vol. 1, April, pp. 33-42.

17. Drnevich, V. P., (1967), "Effects of Strain History on the Dynamic Properties of Sand," thesis presented to The University of Michigan, Ann Arbor, Michigan, in partial fulfillment of the requirements for the degree of Doctor of Philosophy.

18. Drnevich, V. P., Hall, J. R., Jr., and Richart, F. E., Jr., (1967), "Effects of Amplitude of Vibration on the Shear Modulus of Sand," Proceedings of the International Symposium on Wave Propagation and Dynamic Properties of Earth Materials, University of New Mexico, Albuquerque, N.M., pp. 189-199.

19. Finn, F. N., (1951), "The Effect of Temperature on the Consolidation Characteristics of Remolded Clay," Symposium on Consolidation Testing of Soils, ASTM STP 126, American Society for Testing Materials, pp. 65-71.

REFERENCES (Continued)

20. Fisher, F. E., and Alvord, H. H., (1971), "Instrumentation for Mechanical Analysis," Engineering Summer Conferences Publication, The University of Michigan, Ann Arbor, Michigan, 179 pp.

21. Gray, H., (1936), "Progress Report on Research on the Consolidation of Fine-Grained Soils," Proceedings of the First International Conference on Soil Mechanics and Foundation Engineering, Vol. 2, Cambridge, pp. 138-141.

22. Gray, D. H., and Kashmeeri, N. A., (1971), "Thixotropic Behavior of Compacted Clays," Journal of the Soil Mechanics and Foundations Division, ASCE, Vol. 97, No. SM1, January, pp. 193-207.

23. Hall, J. R., Jr., and Richart, F. E., Jr., (1963), "Dissipation of Elastic Wave Energy in Granular Soils," Journal of the Soil Mechanics and Foundations Division, ASCE, Vol. 89, No. SM6, November, pp. 27-56.

24. Hardin, B. O., and Black, W. L., (1966), "Sand Stiffness Under Various Triaxial Stresses," Journal of the Soil Mechanics and Foundations Division, ASCE, Vol. 92, No. SM2, March, pp. 27-42.

25. Hardin, B. O., and Black, W. L., (1968), "Vibration Modulus of Normally Consolidated Clay," Journal of the Soil Mechanics and Foundations Division, ASCE, Vol. 94, No. SM2, March, pp. 353-368.

26. Hardin, B. O., and Black, W. L., (1969), Closure to "Vibration Modulus of Normally Consolidated Clay," Journal of the Soil Mechanics and Foundations Division, ASCE, Vol. 95, No. SM6, November, pp. 1531-1539.

27. Hardin, B. O., and Drnevich, V. P., (1972a), "Shear Modulus and Damping in Soils: Measurement and Parameter Effects," Journal of the Soil Mechanics and Foundations Division, ASCE, Vol. 98, No. SM6, June, pp. 603-624.

28. Hardin, B. O., and Drnevich, V. P., (1972b), "Shear Modulus and Damping of Soils: Design Equations and Curves," Journal of the Soil Mechanics and Foundations Division, ASCE, Vol. 98, No. SM7, July, pp. 667-692.

29. Hardin, B. O., and Mossbarger, W. A., Jr., (1966), "The Resonant Column Technique for Vibration Testing of Soils and Asphalts," Proceedings, Instrument Society of America, October.

REFERENCES (Continued)

30. Hardin, B. O., and Music, J., (1965), "Apparatus for Vibration of Soil Specimens during the Triaxial Test," Symposium on Instrumentation and Apparatus for Soils and Rocks, ASTM STP 392, American Society for Testing Materials, pp. 55-74.

31. Hardin, B. O., and Richart, F. E., Jr., (1963), "Elastic Wave Propagation in Granular Soils," Journal of the Soil Mechanics and Foundations Division, ASCE, Vol. 89, No. SM1, February, pp. 33-65.

32. Haupt, W. A., (1973), Personal Communication, Research Engineer, University of Karlsruhe, Karlsruhe, West Germany.

33. Humphries, W. K., and Wahls, H. E., (1968), "Stress History Effects on Dynamic Modulus of Clay," Journal of the Soil Mechanics and Foundations Division, ASCE, Vol. 94, No. SM2, March, pp. 371-389.

34. Ishihara, K., and Li, S., (1972), "Liquefaction of Saturated Sand in Triaxial Torsion Shear Test," Soils and Foundations (Japan), Vol. 12, No. 3, June, pp. 19-39.

35. Jennings, P. C., (1964), "Periodic Response of a General Yielding Structure," Journal of the Engineering Mechanics Division, ASCE, Vol. 40, No. EM2, April, pp. 131-166.

36. Kashmeeri, N. A., (1969), "Thixotropic Behavior of Compacted Clays," thesis presented to The University of Michigan, at Ann Arbor, Michigan, in partial fulfillment of the requirements for the degree of Doctor of Philosophy.

37. Kovacs, W. D., Seed, H. B., and Chan, C. K., (1971a), "Dynamic Moduli and Damping Ratios for a Soft Clay," Journal of the Soil Mechanics and Foundations Division, ASCE, Vol. 97, No. SM1, January, pp. 59-75.

38. Kovacs, W. D., Seed, H. B., and Idriss, I. M., (1971b), "Studies of Seismic Response of Clay Banks," Journal of the Soil Mechanics and Foundations Division, ASCE, Vol. 97, No. SM2, February, pp. 441-445.

39. Krizek, R. J., and Franklin, A. G., (1967), "Energy Dissipation in a Soft Clay," Proceedings of the International Symposium on Wave Propagation and Dynamic Properties of Earth Materials, University of New Mexico, Albuquerque, N.M., pp. 797-807.

REFERENCES (Continued)

40. Krizek, R. J., and Franklin, A. G., (1968), "Nonlinear Dynamic Response of Soft Clays," Symposium on Vibration Effects of Earthquakes on Soils and Foundations, ASTM STP 450, American Society for Testing Materials, pp. 96-114.

41. Lambe, T. W., (1967), Soil Testing for Engineers, John Wiley, New York, 165 pp.

42. Lambe, T. W., and Whitman, R. V., (1969), Soil Mechanics, John Wiley, New York, 553 pp.

43. Lashine, A.K.A., (1973), "Deformation Characteristics of a Silty Clay Under Repeated Loading," Proceedings of the Eighth International Conference on Soil Mechanics and Foundation Engineering, Vol. 1, Part 1, Moscow, pp. 237-244.

44. Lawrence, F. V., Jr., (1963), "Propagation of Ultrasonic Waves Through Sand," Report No. 14, Response of Soils to Dynamic Loading, directed by R. V. Whitman, Massachusetts Institute of Technology, Cambridge, Massachusetts.

45. Lawrence, F. V., Jr., (1965), "Ultrasonic Wave Velocities in Sand and Clay," Report No. 23, Response of Soils to Dynamic Loadings, directed by R. V. Whitman, Massachusetts Institute of Technology, Cambridge, Massachusetts.

46. Lee, K. L., and Fitton, J. A., (1968), "Factors Affecting the Cyclic Loading of Soil," Symposium on Vibration Effects of Earthquakes on Soils and Foundations, ASTM STP 450, American Society for Testing Materials, pp. 71-95.

47. Lo, K. Y., (1961), "Secondary Compression of Clays," Journal of the Soil Mechanics and Foundations Division, ASCE, Vol. 87, No. SM4, August, Part 1, pp. 61-87.

48. Marcuson, W. F., III, and Wahls, H. E., (1972), "Time Effects on Dynamic Shear Modulus of Clays," Journal of the Soil Mechanics and Foundations Division, ASCE, Vol. 98, No. SM12, December, pp. 1359-1373.

49. Matlock, H., Jr., Fenske, C. W., and Dawson, R. F., (1961), "De-aired, Extruded Soil Specimens for Research and for Evaluation of Test Procedures," ASTM Bulletin No. 177, American Society for Testing Materials.

REFERENCES (Continued)

50. Miller, R. P., and Brown, F. R., (1972), "Shear Modulus Determination of Soils by In Situ Methods for Earthquake Engineering," Proceedings of the International Conference on Microzonation for Safer Construction, Research and Application, Vol. 2, Seattle, Washington, pp. 545-558.

51. Mitchell, J. K., (1960), "Fundamental Aspects of Thixotropy in Soils," Journal of the Soil Mechanics and Foundations Division, ASCE, Vol. 86, No. SM3, Part 1, June, pp. 19-52.

52. Mitchell, J. K., (1969), "Temperature Effects on the Engineering Properties and Behavior of Soils," Proceedings of an International Conference: Effects of Temperature and Heat on Engineering Behavior of Soils, HRB Special Report 103, Highway Research Board, pp. 1-28.

53. Murayama, S., (1969), "Effect of Temperature on Elasticity of Clays," Proceedings of an International Conference: Effects of Temperature and Heat on Engineering Behavior of Soils, HRB Special Report 103, Highway Research Board, pp. 194-203.

54. Murayama, S., and Shibata, T., (1960), "On the Dynamic Properties of Clay," Proceedings of the Second World Conference on Earthquake Engineering, Vol. 1, Tokyo and Kyoto, pp. 297-310.

55. Murphy, V. J., (1972), "Geophysical Engineering Investigation Techniques for Microzonation," Proceedings of the International Conference on Microzonation for Safer Construction, Research and Application, Vol. 2, Seattle, Washington, pp. 131-159.

56. Nacci, V. A., and Taylor, R. J., (1967), "Influence of Clay Structure on Elastic Wave Propagation," Proceedings of the International Symposium on Wave Propagation and Dynamic Properties of Earth Materials, University of New Mexico, Albuquerque, N.M., pp. 491-501.

57. Noorany, I., and Gizienski, S. F., (1970), "Engineering Properties of Submarine Soils: State-of-the-Art Review," Journal of the Soil Mechanics and Foundations Division, ASCE, Vol. 96, No. SM5, September, pp. 1735-1762.

58. Paaswell, R. E., (1967), "Temperature Effects on Clay Soil Consolidation," Journal of the Soil Mechanics and Foundations Division, ASCE, Vol. 93, No. SM3, May, pp. 9-22.

REFERENCES (Continued)

59. Pang, D. D-J, (1972), "Resonant Footing Test," Soil Mechanics Report No. 11, No. UKY TR61-72-CE22, University of Kentucky, 155 pp.

60. Plum, R. L., and Esrig, M. I., (1969), "Some Temperature Effects on Soil Compressibility and Pore Water Pressure," Proceedings of an International Conference: Effects of Temperature and Heat on Engineering Behavior of Soils, HRB Special Report 103, Highway Research Board, pp. 231-242.

61. Poulos, S. J., (1964), "Control of Leakage in the Triaxial Test," Harvard Soil Mechanics Series No. 71, Harvard University, Cambridge, Massachusetts, 230 pp.

62. Richart, F. E., Jr., (1961), Closure to "Foundation Vibrations," Journal of the Soil Mechanics and Foundations Division, ASCE, Vol. 87, No. SM4, Part 1, August, pp. 169-178.

63. Richart, F. E., Jr., Hall, J. R., Jr., and Woods, R. D., (1970), Vibrations of Soils and Foundations, Prentice-Hall, Inc., Englewood Cliffs, New Jersey, 414 pp.

64. Schwarz, S. D., and Musser, J. M., (1972), "Various Techniques for Making In Situ Shear Wave Velocity Measurements—A Description and Evaluation," Proceedings of the International Conference on Microzonation for Safer Construction, Research and Application, Vol. 2, Seattle, Washington, pp. 593-608.

65. Scott, R. F., and Ko, H-Y, (1969), "Stress-Deformation and Strength Characteristics," Proceedings of the Seventh International Conference of Soil Mechanics and Foundation Engineering, State-of-the-Art Volume, Mexico City, pp. 1-47.

66. Seed, H. B., (1960), "Soil Strength During Earthquakes," Proceedings of the Second World Conference on Earthquake Engineering, Vol. 1, Tokyo and Kyoto, pp. 183-194.

67. Seed, H. B., and Chan, C. K., (1966), "Clay Strength under Earthquake Loading Conditions," Journal of the Soil Mechanics and Foundations Division, ASCE, Vol. 92, No. SM2, March, pp. 53-78.

68. Seed, H. B., and Idriss, I. M., (1970), "Soil Moduli and Damping Factors for Dynamic Response Analyses," Report No. EERC 70-10, University of California, Berkeley, September.

REFERENCES (Continued)

69. Seed, H. B., and Wilson, S. D., (1967), "The Turnagain Heights Landslide, Anchorage, Alaska," Journal of the Soil Mechanics and Foundations Division, ASCE, Vol. 93, No. SM4, July, pp. 325-353.

70. Sherif, M. A., Wu, M. J., and Bostrom, R. C., (1972), "Reduction in Soil Strength Due to Dynamic Loading," Proceedings of the International Conference on Microzonation for Safer Construction, Research, and Application, Vol. 2, Seattle, Washington, pp. 439-454.

71. Shumway, G., (1960), "Sound Speed and Absorption Studies of Marine Sediments by a Resonance Method" (Parts I and II), Geophysics, Vol. 25, Nos. 2 and 3, pp. 451-467 and 659-682.

72. Silver, M. L., and Moore, C. A., (1972), "Shipboard Measurement of Acoustic Velocities in Sediment Cores," Preprints from 1972 Offshore Technology Conference, Vol. 1, May, pp. 342-352.

73. Stokoe, K. H., II, (1972), "Dynamic Response of Embedded Foundations," thesis presented to The University of Michigan, Ann Arbor, Michigan, in partial fulfillment of the requirements for the degree of Doctor of Philosophy.

74. Stokoe, K. H., II, and Richart, F. E., Jr., (1973a), "Shear Moduli of Soils: In Situ and from Laboratory Measurements," Proceedings of the Fifth World Conference on Earthquake Engineering, Vol. 1, Paper No. 41 (Preprint), Rome.

75. Stokoe, K. H., II, and Richart, F. E., Jr., (1973b), "In Situ and Laboratory Shear Wave Velocities," Proceedings of the Eighth International Conference on Soil Mechanics and Foundation Engineering, Vol. 1, Part 2, Moscow, pp. 403-409.

76. Stokoe, K. H., II, and Woods, R. D., (1972), "In Situ Shear Wave Velocity by Cross-Hole Method," Journal of the Soil Mechanics and Foundations Division, ASCE, Vol. 98, No. SM5, May, pp. 443-460.

77. Streeter, V. L., Wylie, E. B., Richart, F. E., Jr., (1974), "Soil Motion Computation by Characteristics Method," Journal of the Geotechnical Engineering Division, ASCE, Vol. 100, No. GT3, March, pp. 247-263.

78. Taylor, P. W., and Bacchus, D. R., (1969), "Dynamic Cyclic Strain Tests on a Clay," Proceedings of the Seventh International Conference on Soil Mechanics and Foundation Engineering, Vol. 1, Mexico City, pp. 401-409.

REFERENCES (Concluded)

79. Taylor, P., and Hughes, J., (1965), "Dynamic Properties of Foundation Subsoils as Determined from Laboratory Tests," Proceedings of the Third World Conference on Earthquake Engineering, Vol. 1, Vancouver, pp. 196-212.

80. Taylor, P. W., and Parton, J. M., (1973), "Dynamic Torsion Testing of Soils," Proceedings of the Eighth International Conference on Soil Mechanics and Foundation Engineering, Vol. 1, Part 2, Moscow, pp. 425-432.

81. Thiers, G. R., and Seed, H. B., (1968), "Cyclic Stress-Strain Characteristics of Clay," Journal of the Soil Mechanics and Foundations Division, ASCE, Vol. 94, No. SM2, March, pp. 555-569.

82. Thiers, G. R., and Seed, H. B., (1969), "Strength and Stress-Strain Characteristics of Clays Subjected to Seismic Loads," Symposium on Vibration Effects of Earthquakes on Soils and Foundations, ASTM STP 450, American Society for Testing Materials, pp. 3-56.

83. Woods, R. D., (1973), Personal Communication, Associate Professor of Civil Engineering, The University of Michigan, Ann Arbor, Michigan.

84. Yoshimi, Y., and OH-Oka, H., (1973), "A Ring Torsion Apparatus for Simple Shear Tests," Proceedings of the Eighth International Conference on Soil Mechanics and Foundation Engineering, Vol. 1, Part 2, Moscow, pp. 501-506.

85. Zeevaert, L., (1967), "Free Vibration Torsion Tests to Determine Shear Modulus of Elasticity of Soils," Proceedings of the Third Pan-American Conference on Soil Mechanics and Foundation Engineering, Vol. 1, Venezuela, pp. 111-129.

APPENDIX A

SUMMARY OF TESTS PERFORMED DURING INVESTIGATION

TABLE A.1. SUMMARY OF TESTS PERFORMED DURING INVESTIGATION

Test	Soil Name	Number of Specimens		Pressure Increments (psi)	Elapsed Testing Time (weeks)
Low Amplitude Resonant Column Tests	Ball Kaolinite	6		10,20,40,60	15
	Chevy Clay	4		10,20,40,60	12
	Detroit Clay	3		5-60	22
	Eaton Clay	2		10,20,40,60	8
	Leda Clay I	2		10,20,40,60	8
	Ostiglia Silt	3		5-15	7
High Amplitude Resonant Column Tests	Bent.-Silica Flour	1		10,20	4
	Detroit Clay	1		17,34	6
	Eaton Clay	1		10,20	10
	Ford Clay	1		10,20	10
	Leda Clay I	1		10,20	20
	Santa Barbara Clay	1		6.5	10
		4°C	22°C		
Temperature Controlled Low Amplitude Resonant Column Tests (T = 4°, 22°C)	Ball Kaolinite	1	1	10,20,40	6
	Bent.-Silica Flour	2	1	10,20,40	8
	Detroit Clay	1	1	10,20,40	4
	Ford Clay	1	1	10,20,40	7
	G. of Mexico Clay	1	1	5,10,20,40	9
	Leda Clay I	1	1	10,20,40,60	15
	Leda Clay II	1	1	10,20,40,60	6

APPENDIX B

CALIBRATION DATA

Certain calibration data played a significant part in establishing the type and level of system performance. The validity of calibration data depended on the test procedures utilized to define data.

1. CALIBRATION PROCEDURE

The next several paragraphs provide a brief review of procedures employed when calibrating the output signal from the velocity coil or accelerometer, when determining mass moment of inertia for the drive system and when establishing the calibration factors for the length measuring devices.

a. Signal Calibration for the HATD and the Hall Device

Signal calibration was essential for establishing the relationship between the voltage output from the velocity coil (or accelerometer) and the torsional displacement of the top cap. Figure B.1 illustrates the equipment employed when determining the calibration factors.

An optical following device was used to monitor the steady state displacement of the top cap due to a sinusoidal input signal. The actual displacement was compared to the voltage output from the velocity coil measured during torsional oscillation. In the case of the accelerometer, the comparison was made to the twice integrated acceleration signal. The constant factor derived during the comparison defined the

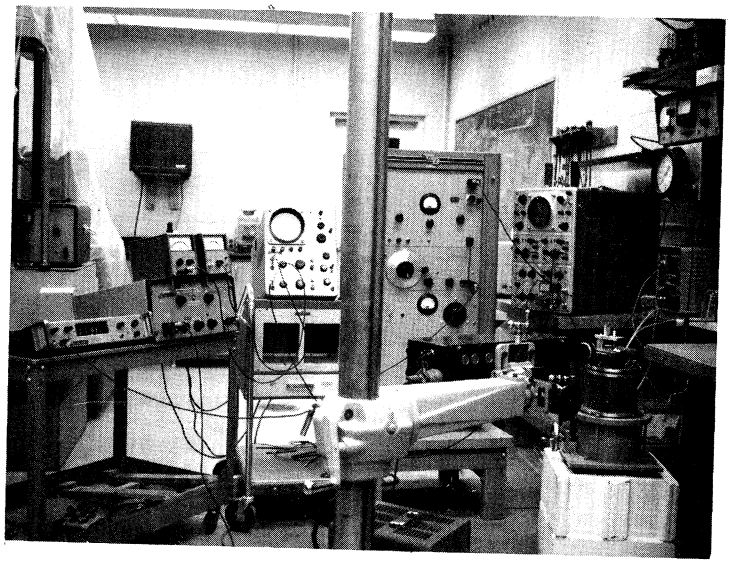

(a)
Optical following device (manufactured by OPTRON -- a division of Universal Technology, Inc.) aimed at HATD drive system. Photo also shows ancillary equipment used during signal calibration.

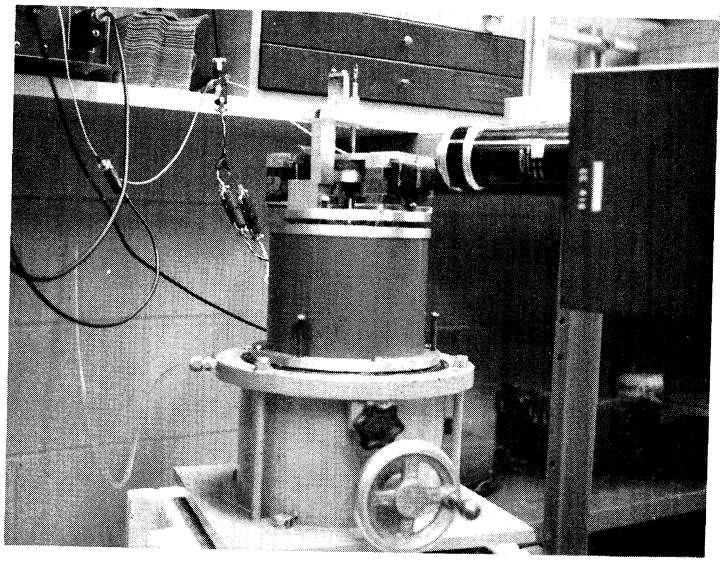

(b)
Close-up of OPTRON focused on HATD.

Figure B.1. Equipment used to calibrate HATD and Hall device.

calibration factor for the signal.

b. Mass Moment of Inertia for the HATD and Hall Device

The equations for determining the shear wave velocity on the basis of the resonant frequency depend on the mass moment of inertia of the top cap-drive system, as can be seen in Eqs. (3.1) and (3.2). The mass moment of inertia is determined, in turn, by the weight and configuration of the top cap-drive system. Any changes in the weight or configuration necessitate changes in the mass moment of inertia.

Chapter III describes several modifications that were performed on either the top cap or drive system. It was, therefore, necessary to redetermine the mass moment of inertia during this investigation. Unfortunately the configurations of the top cap and drive systems were such that the mass moment of inertia could not be calculated directly. An indirect procedure was used.

The mass moments of inertia for the HATD and the Hall device were established by using the three-wire pendulum technique. The primary component of the method is the three-wire pendulum. The three-wire pendulum was simply a platform supported by three strings equally spaced around the periphery of the platform. The item whose mass moment of inertia was to be determined was placed on the platform so that the center of gravity coincided with the center of the platform. By introducing a small initial deflection, the top cap and platform oscillated through a small angle in a horizontal plane.

The period of oscillation in conjunction with the characteristics of the platform determined the mass moment of inertia for the top cap and the platform. A similar determination was made without the top cap. The difference in results defined the mass moment of inertia for the top cap. Fisher and Alvord (1973) described in detail the procedure and mathematics to follow when using the method.

c. Strain Gage and LVDT Calibration

The LVDT and strain gage measuring device were calibrated to establish a relationship between readout data and the axial deformation of the soil sample. During calibration, the LVDT or the cantilever system was displaced a known distance and the change in output from the monitoring device was recorded. A dial indicator with a sensitivity of 0.0001-in. was used to define the magnitude of actual movement during the calibration process. The ratio of the readout data to the displacement determined the calibration factor.

2. CALIBRATION DATA

Table B.1 summarizes the calibration data pertinent to analysis of test data. It should be noted that the calibration factor for the HATD output signal is the calibration of the system as of October, 1973. The magnitude of this factor actually varied throughout the investigation.

TABLE B.1. CALIBRATION DATA FOR HATD AND HALL DEVICES

Factor \ Device	Hall Resonant Column Device (Single Coil Drive)				HATD
	#1	#2	#3	#4	
Signal Calibration Factor	4.5 mv/rad/sec	2.9 mv/rad/sec	2.7 mv/rad/sec	4.1 mv/rad/sec	20.7×10^{-3} rad/volt(rms)
Mass Moment of Inertia (gm cm sec^2)	0.56	0.41	0.52	0.43	21.2
Strain Gage or LVDT	$\frac{90\ \mu\ in./in.}{0.01\ in.}$	$\frac{90\ \mu\ in./in.}{0.01\ in.}$	$\frac{90\ \mu\ in./in.}{0.01\ in.}$	$\frac{60\ \mu\ in./in.}{0.01\ in.}$	0.01 in./div

APPENDIX C

STATIC LABORATORY TESTS

Consolidation and triaxial tests were performed during this investigation. The results of these tests established certain compressibility and strength characteristics of the test materials. This information assisted in defining the behavior of the soils during dynamic loading.

1. TEST DEVICES

Figure C.1 shows the consolidometers used in this test program. Karol Warner, Inc., manufactured the three consolidometers on the right-hand side and Anteus Laboratory Equipment, Inc., produced the device shown on the left-hand. The two systems differed in certain test capabilities. The Karol Warner devices could apply a maximum of 16 kg/cm^2 to a standard 2.5-in. diameter soil specimen. The Anteus device, however, applied up to 128 kg/cm^2 to the same size sample. The Anteus device also included a back pressuring capability which allowed *in situ* pore pressure conditions to be recreated. All three devices utilized the fixed ring configuration during the test. Lambe (1967) and Bowles (1970) described the typical characteristics of consolidometers.

The triaxial test equipment shown in Figure C.2 was manufactured by Geonor A/S Ltd. of Oslo, Norway. Andresen and Simon (1960) gave a detailed description of this equipment. The University of Michigan

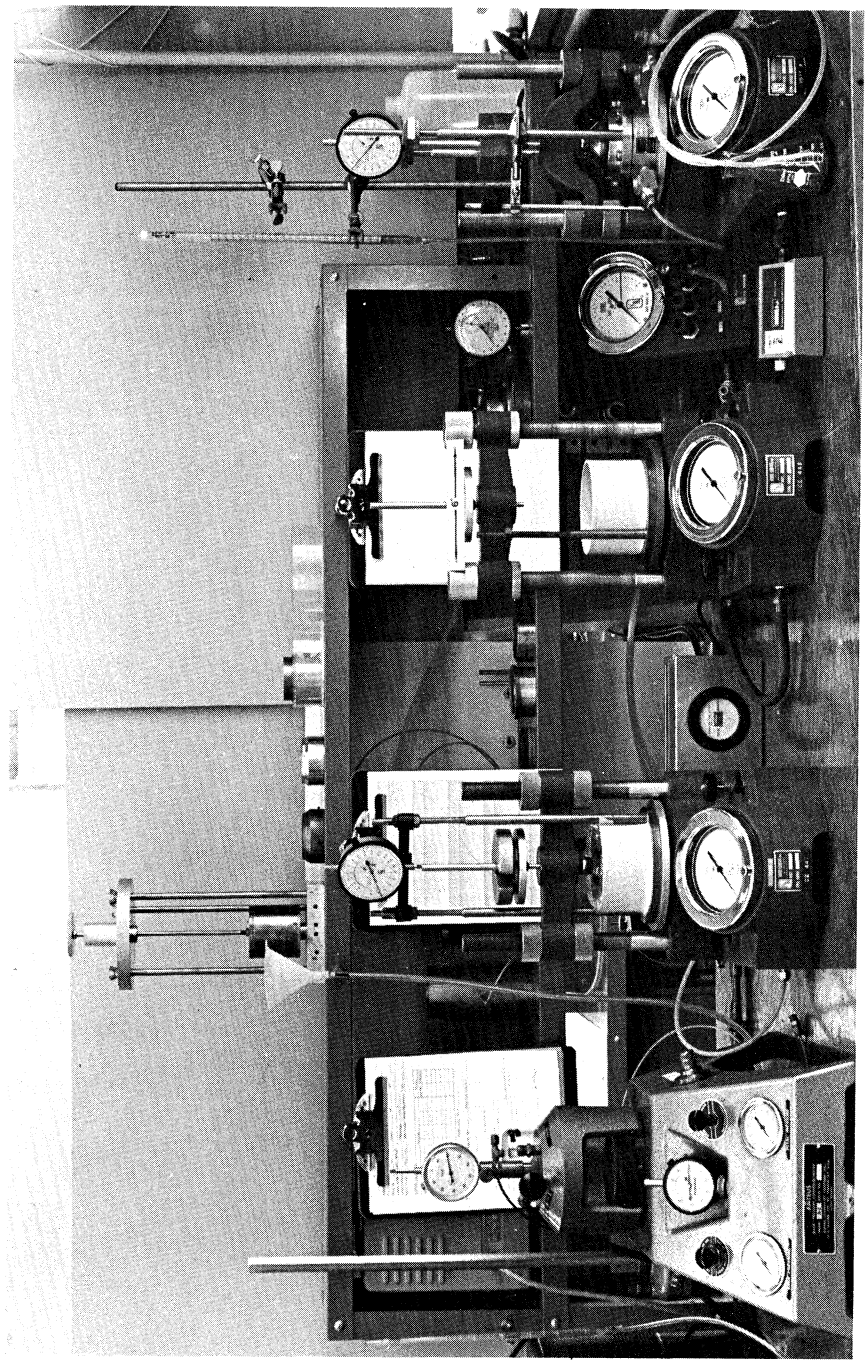

Figure C.1. Consolidation test equipment.

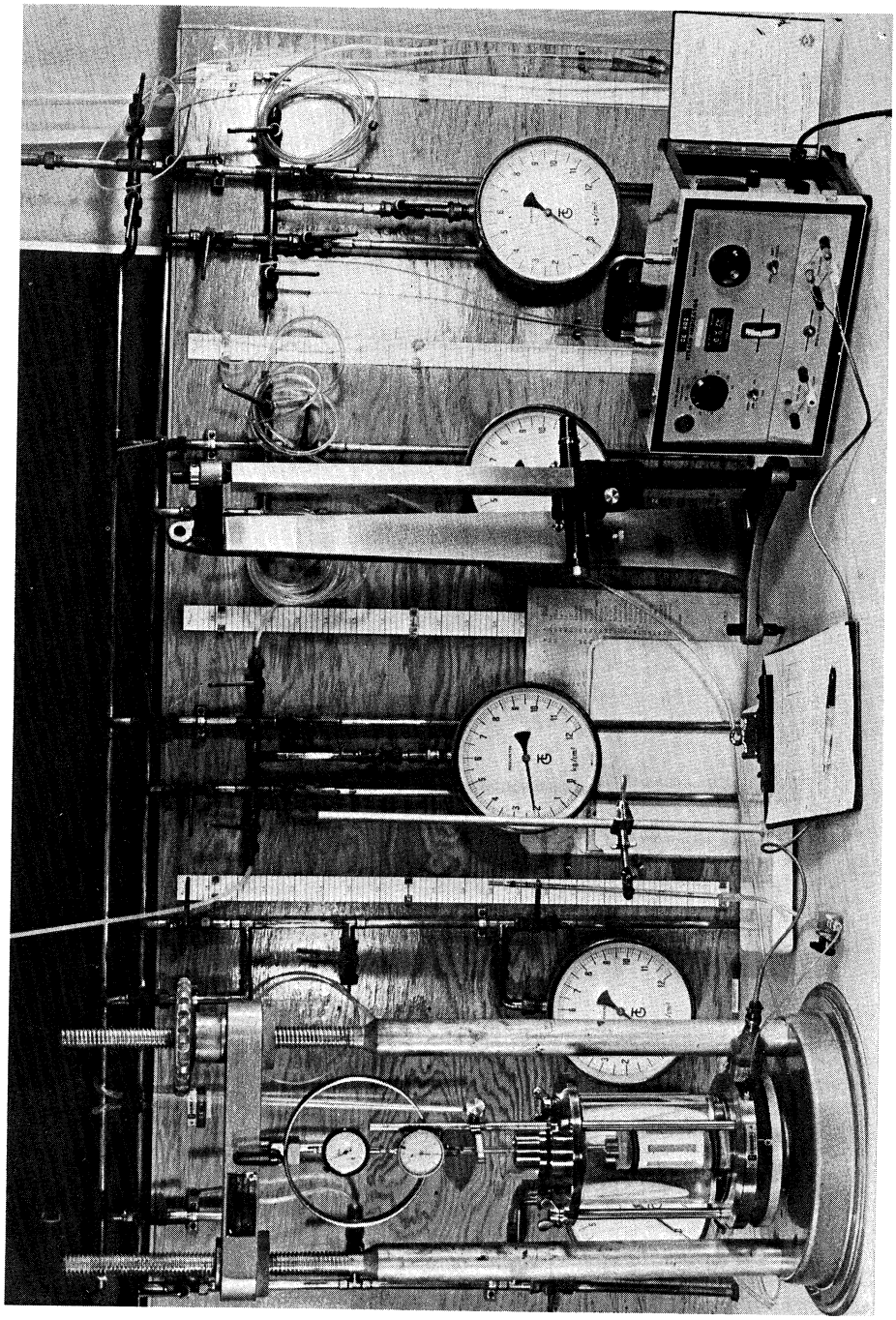

Figure C.2. Triaxial test equipment.

triaxial system differed from that described by Andresen and Simon at only one point. The University of Michigan device employed a Dynisco pressure transducer to monitor pore pressures rather than the null indicator system described by the authors. The pressure transducer recorded pore pressures up to 10 kg/cm^2. A temperature compensation arrangement within the transducer eliminated erroneous variations in transducer output due to temperature changes.

2. TEST SETUP

Figures C.1 and C.2 show the entire setup for the consolidation and triaxial tests. As seen in the photograph, the consolidation test required no ancillary equipment. The triaxial setup utilized two accessories. A BLH Strain Indicator registered changes in output from the pore pressure transducer. The strain indicator also supplied the input voltage to the bridge circuit in the transducer. An Ealing Half Meter Utility Cathetometer also was used in the triaxial setup. The cathetometer allowed axial deformations to be monitored during triaxial consolidation (Figure 7.2).

APPENDIX D

GRAIN SIZE CURVES

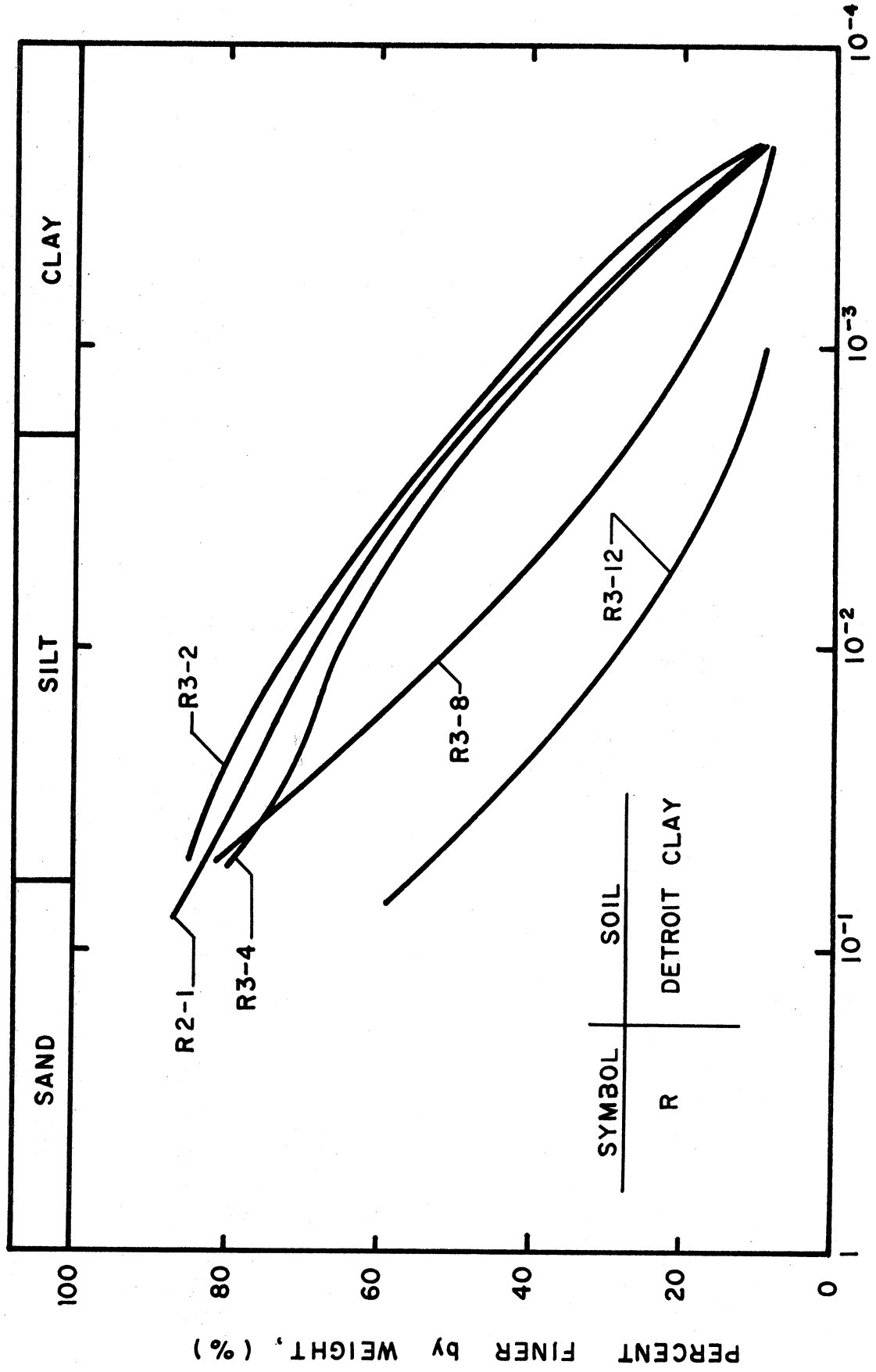

Figure D.1. Grain size curves for Detroit Clay (R2-1, R3-2, R3-4, R3-8 and R3-12).

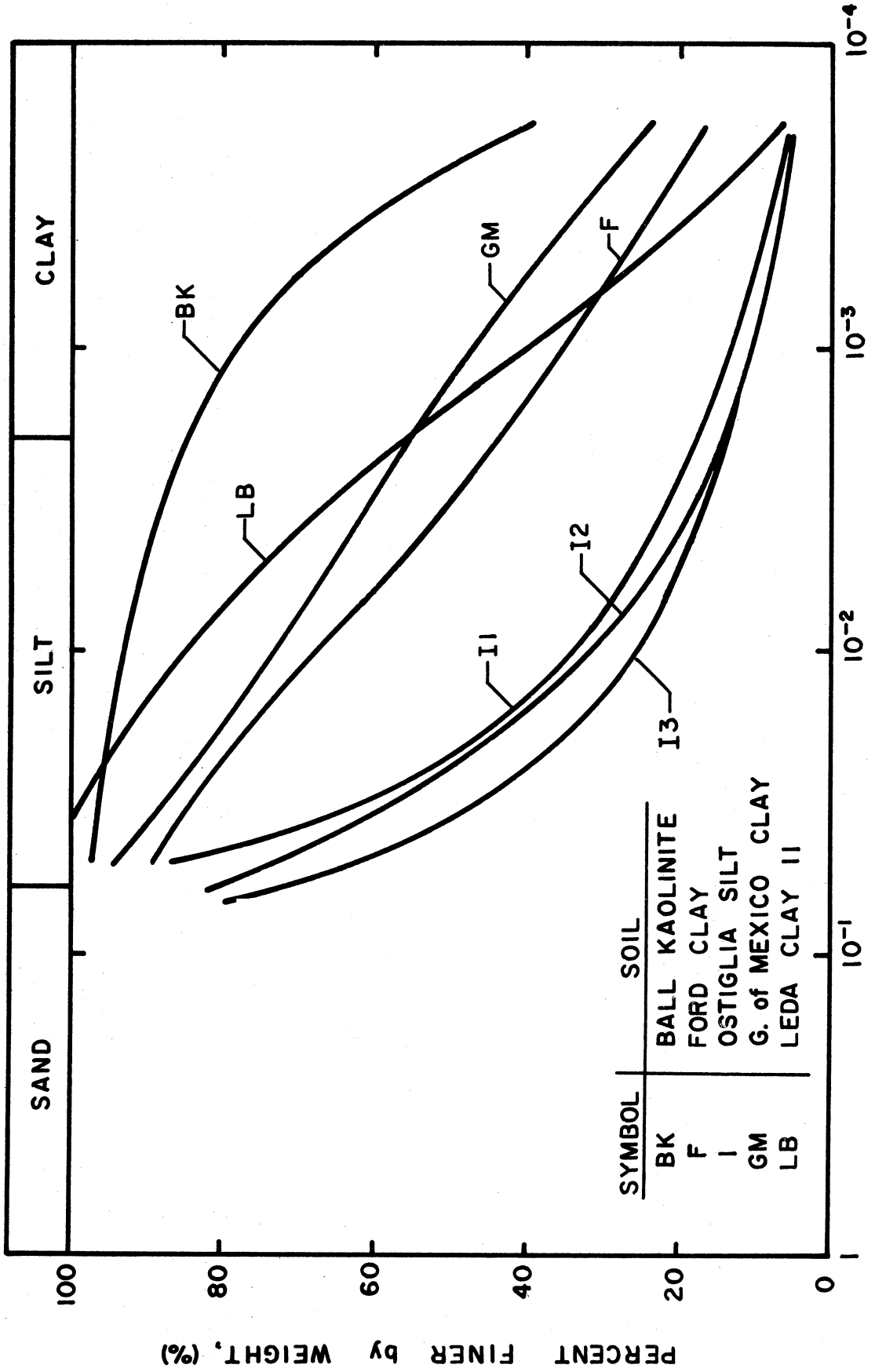

Figure D.2. Grain size curves for Ball Kaolinite (BK), Gulf of Mexico Clay (GM), Ford Clay (F), Leda Clay II (LB) and Ostiglia Silt (I1, I2 and I3).

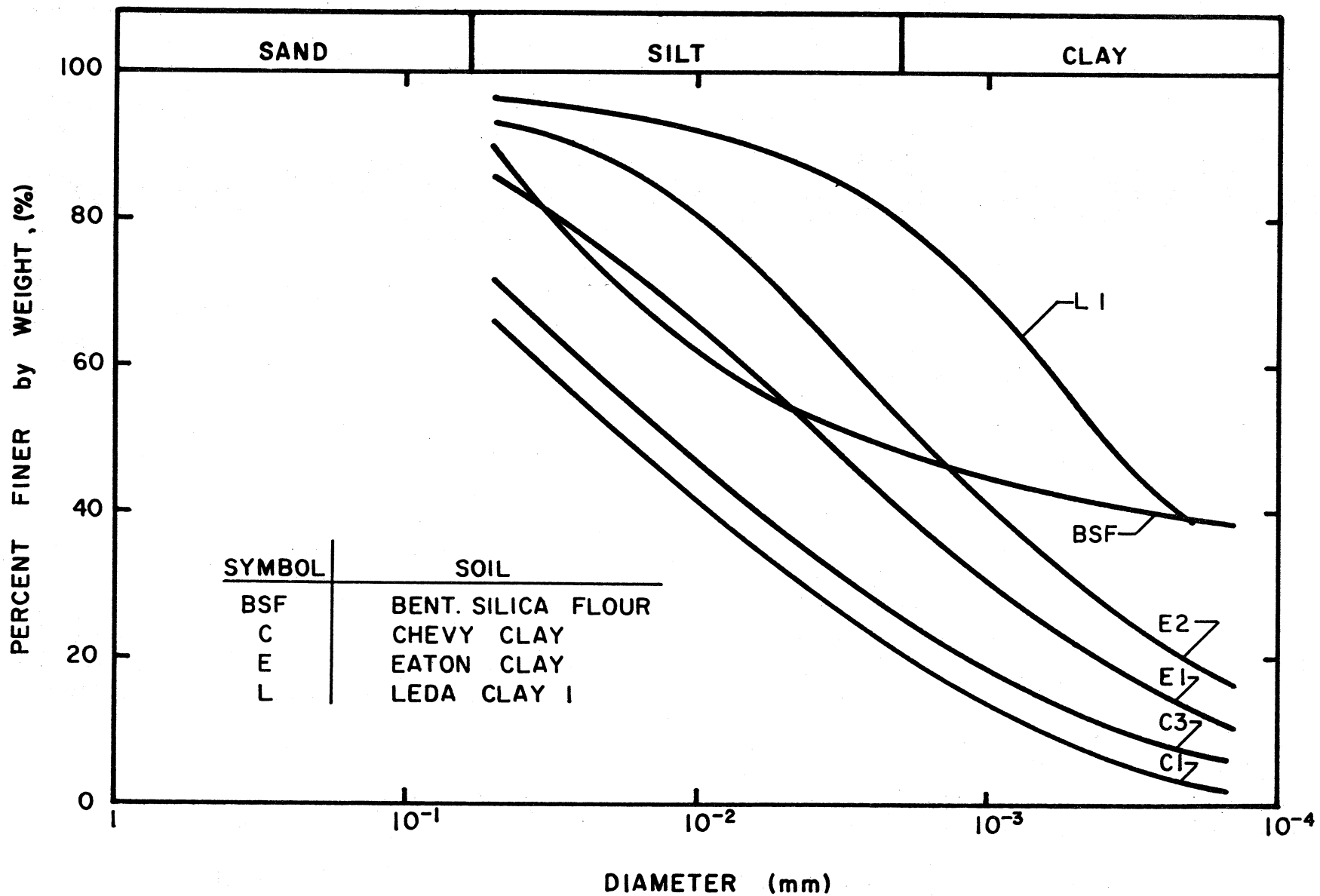

Figure D.3. Grain size curves for Leda Clay I (L1), Bentonite-Silica Flour (BSF), Eaton Clay (E1 and E2) and Chevy Clay (C1 and C3)

APPENDIX E

LOW AMPLITUDE PLOTS

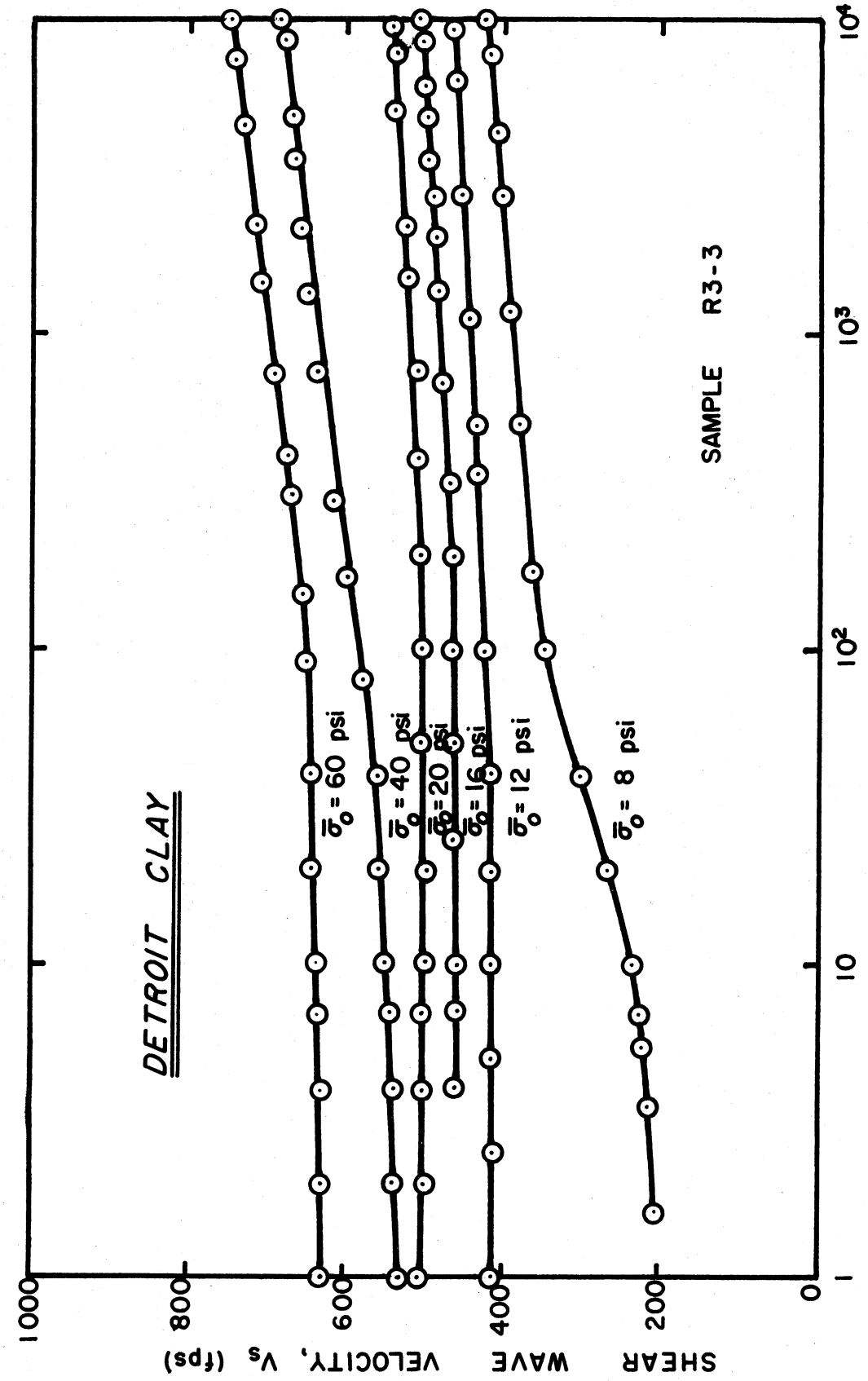

Figure E.1. Comparison of V_s with time for Detroit Clay (R3-3).

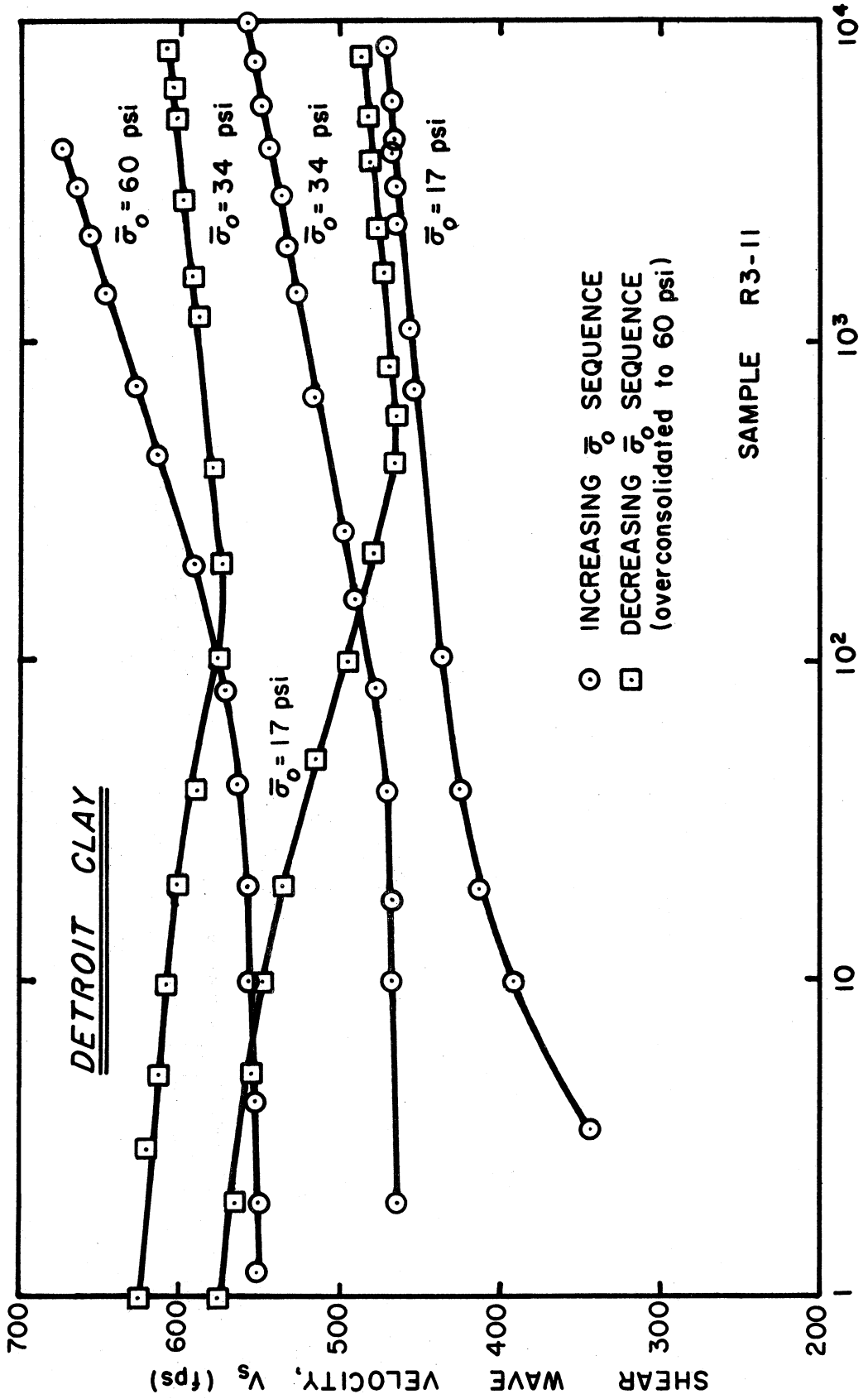

Figure E.2. Comparison of V_s with time for Detroit Clay (R3-11).

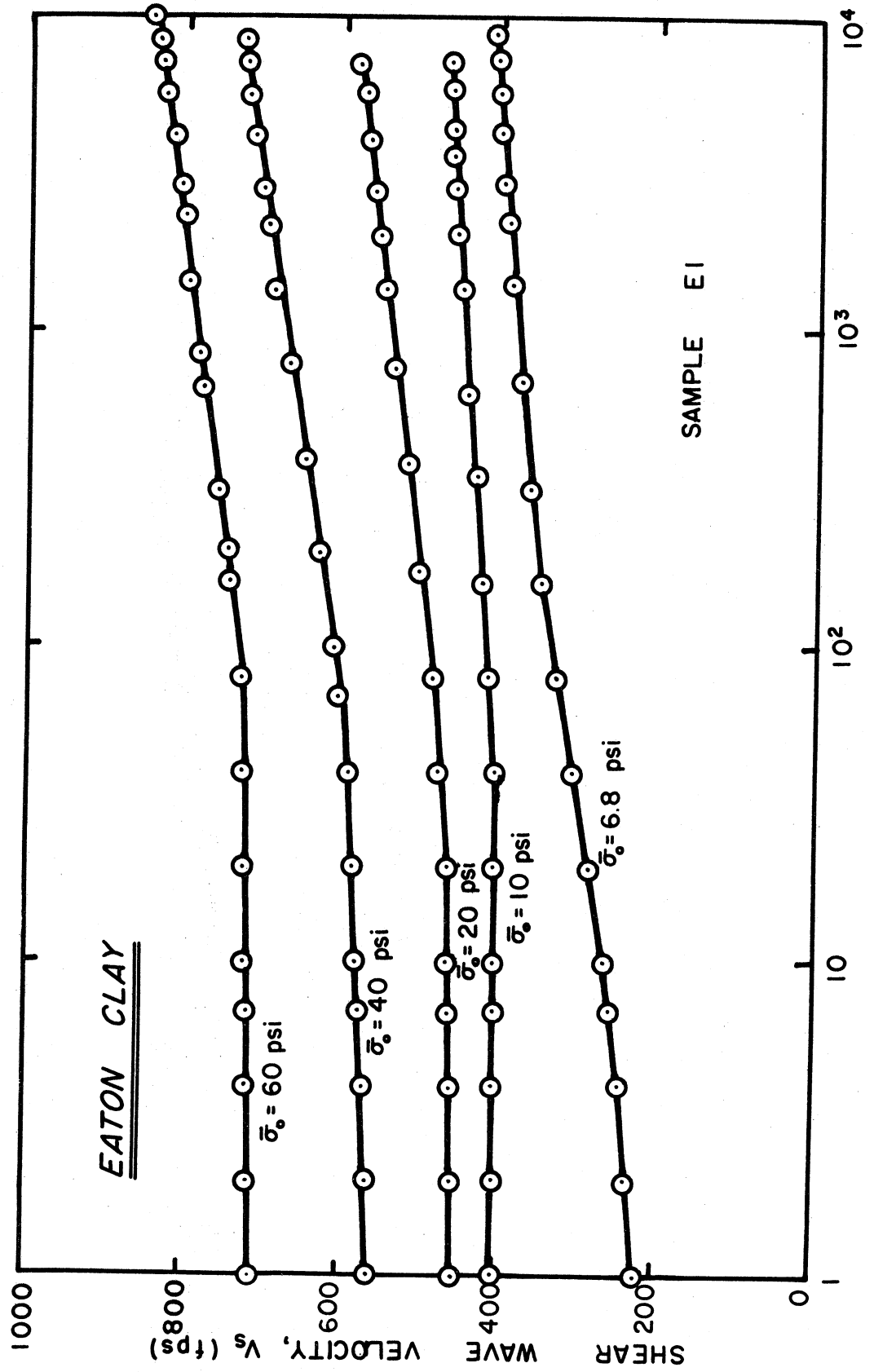

Figure E.3. Comparison of V_s with time for Eaton Clay (E1).

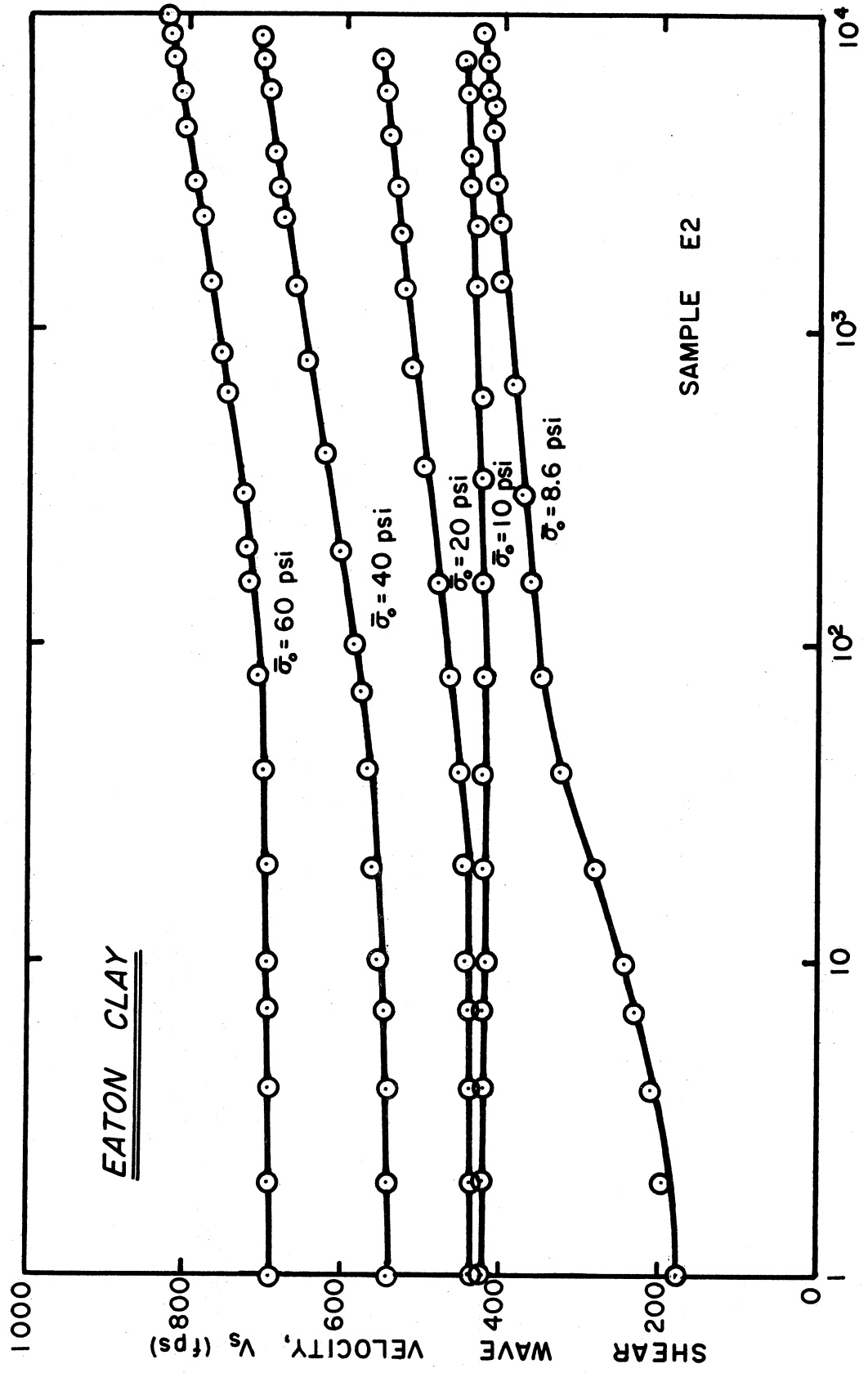

Figure E.4. Comparison of V_s with time for Eaton Clay (E2).

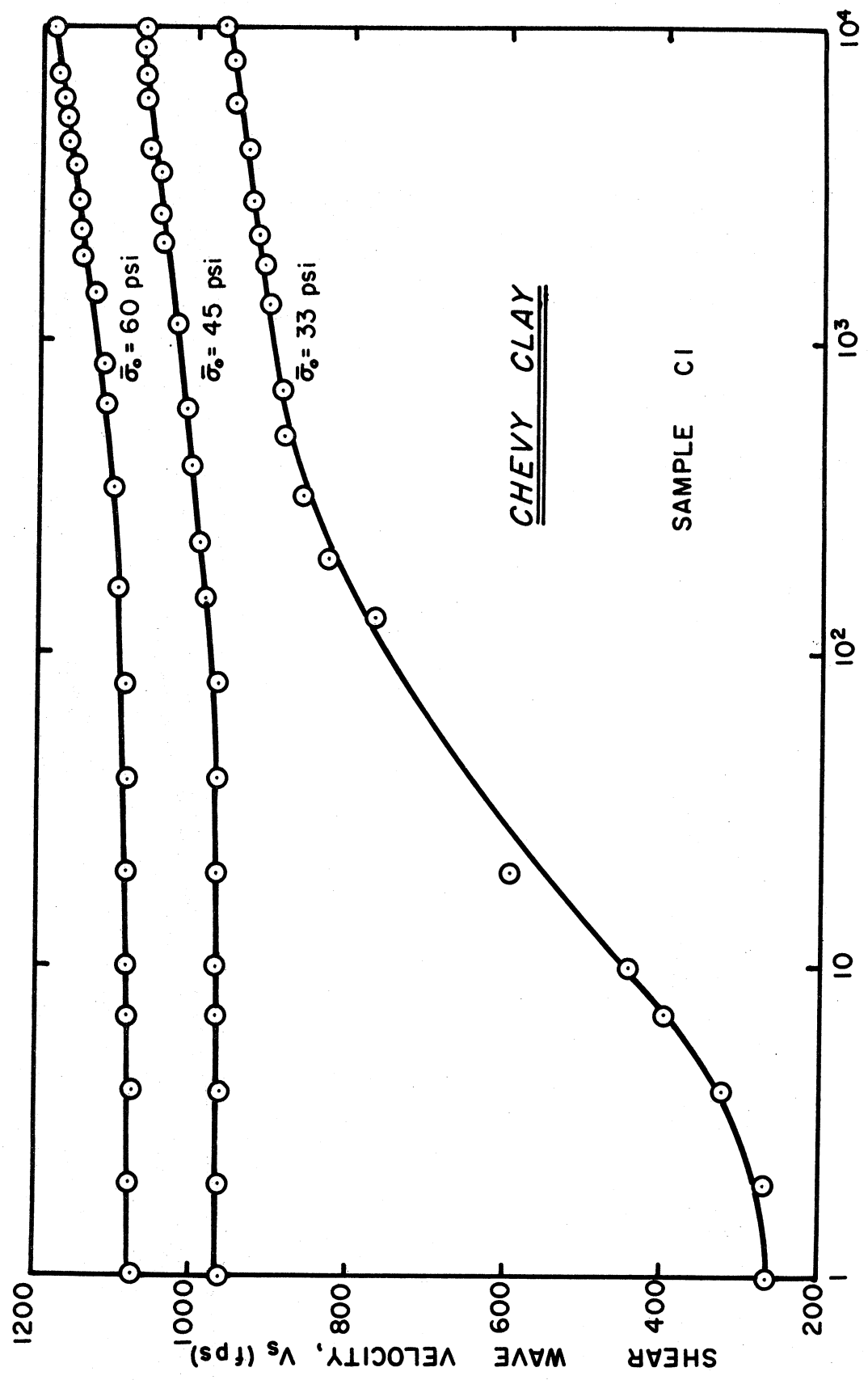

Figure E.5. Comparison of V_s with time for Chevy Clay (C1).

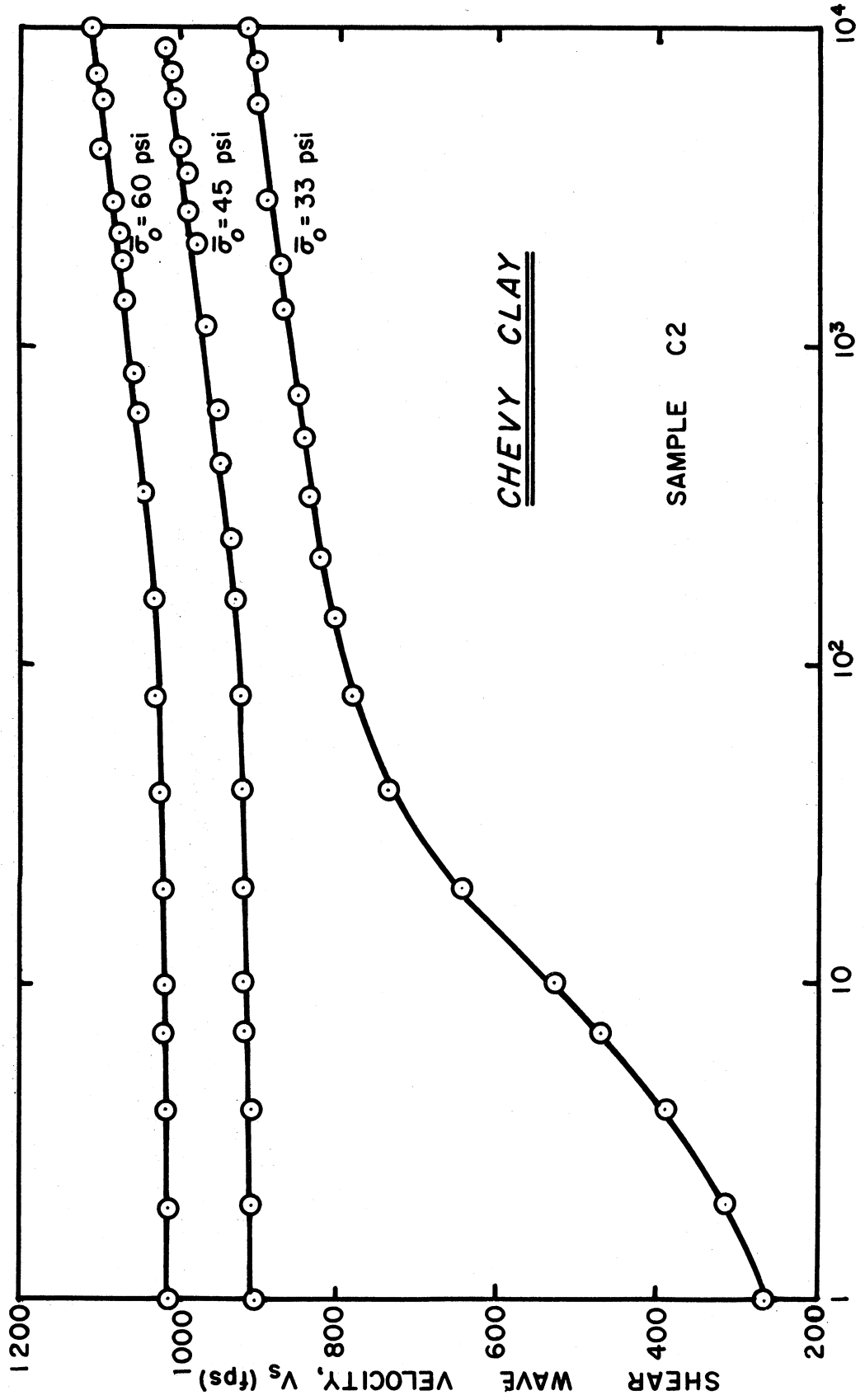

Figure E.6. Comparison of V_s with time for Chevy Clay (C2).

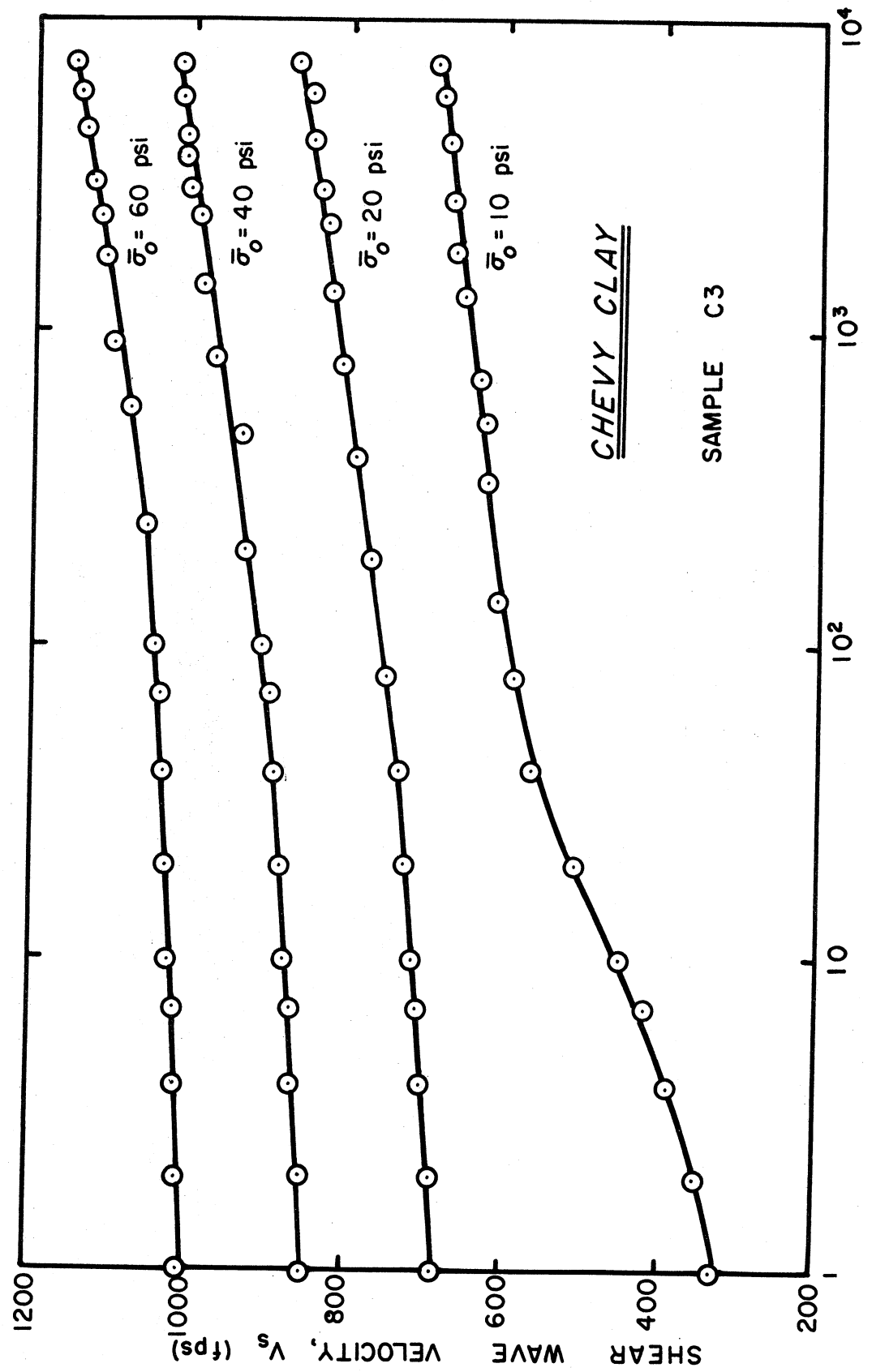

Figure E.7. Comparison of V_s with time for Chevy Clay (C3).

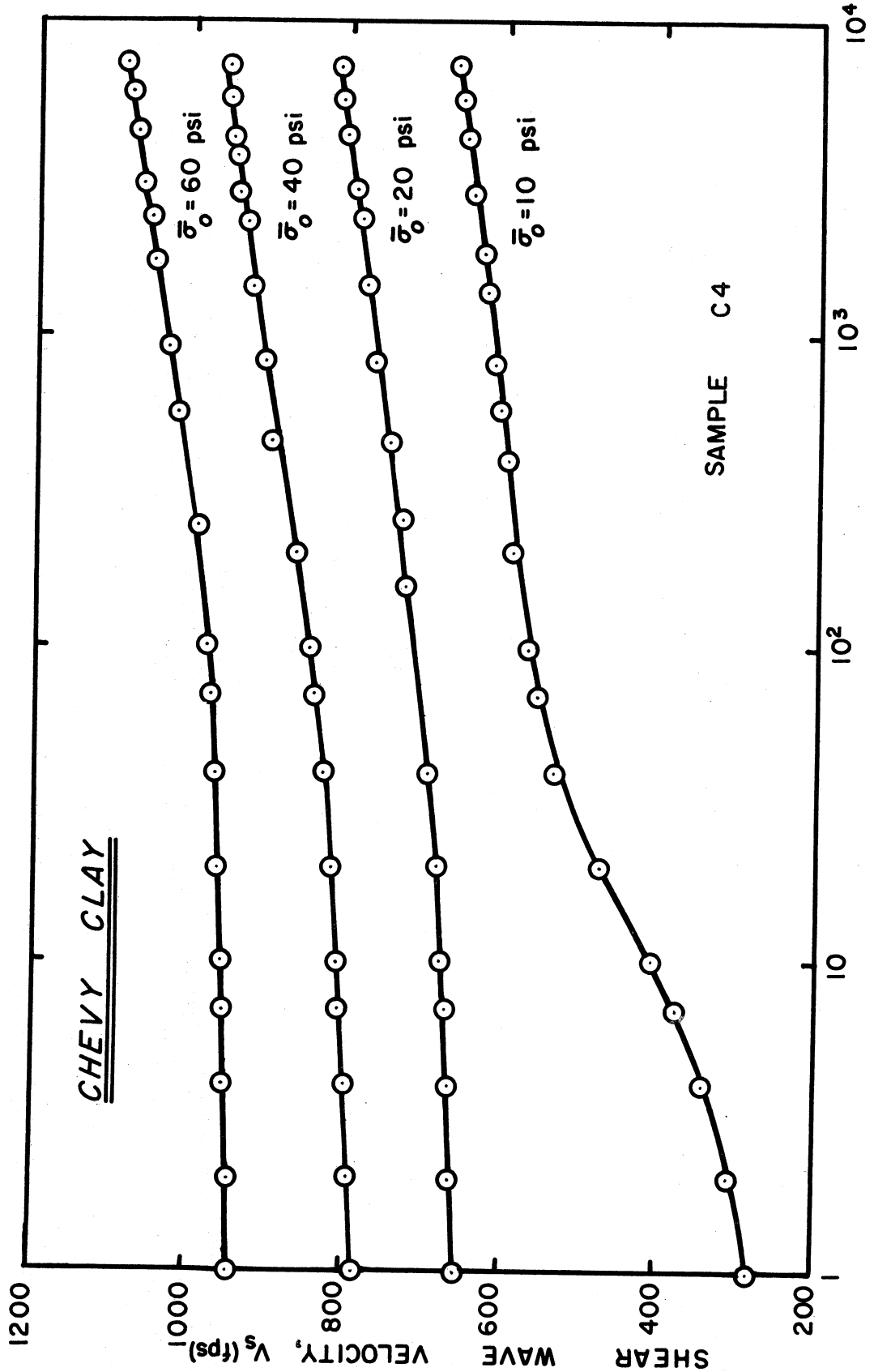

Figure E.8. Comparison of V_s with time for Chevy Clay (C4).

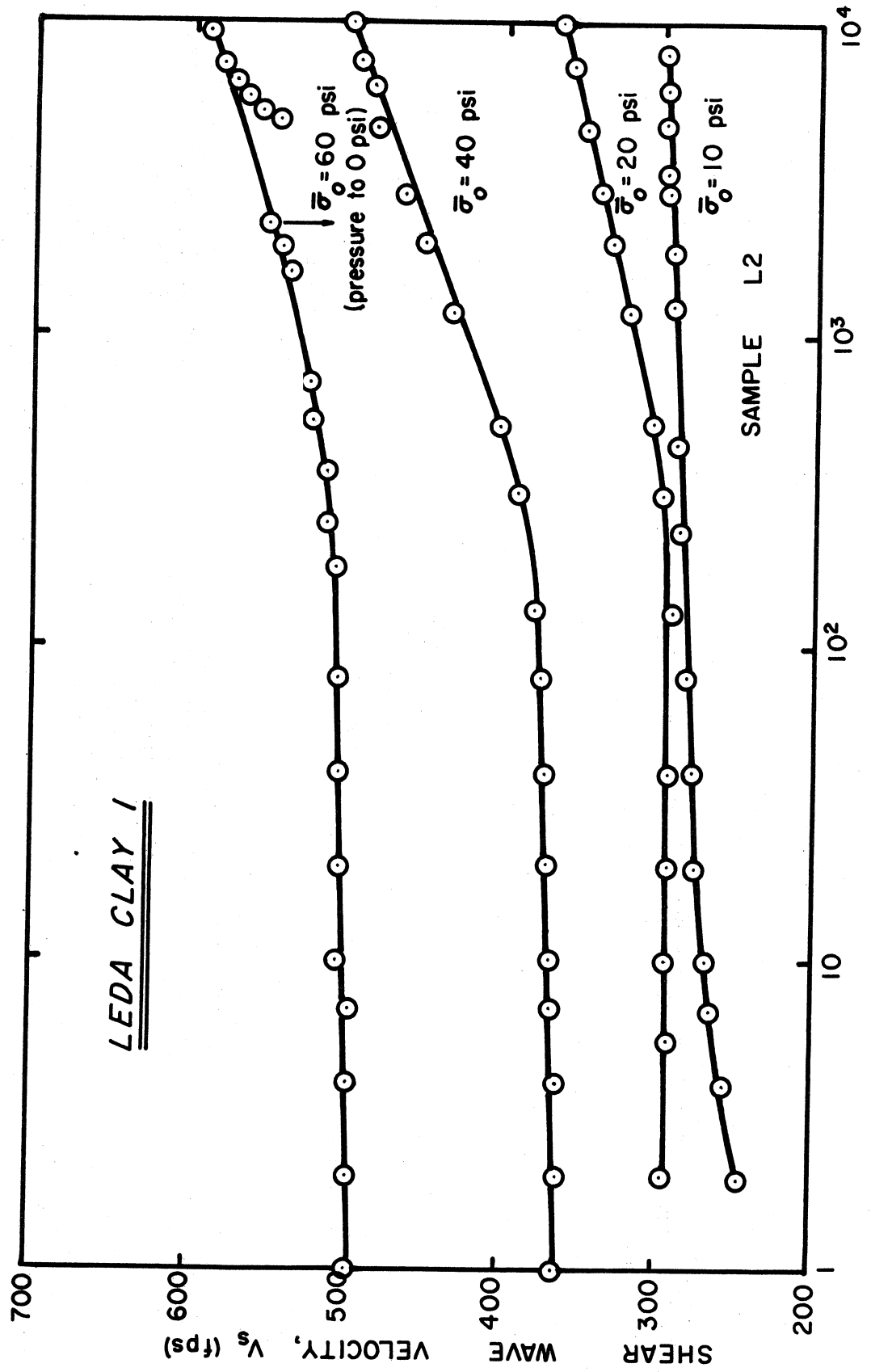

Figure E.9. Comparison of V_s with time for Leda Clay I (L2).

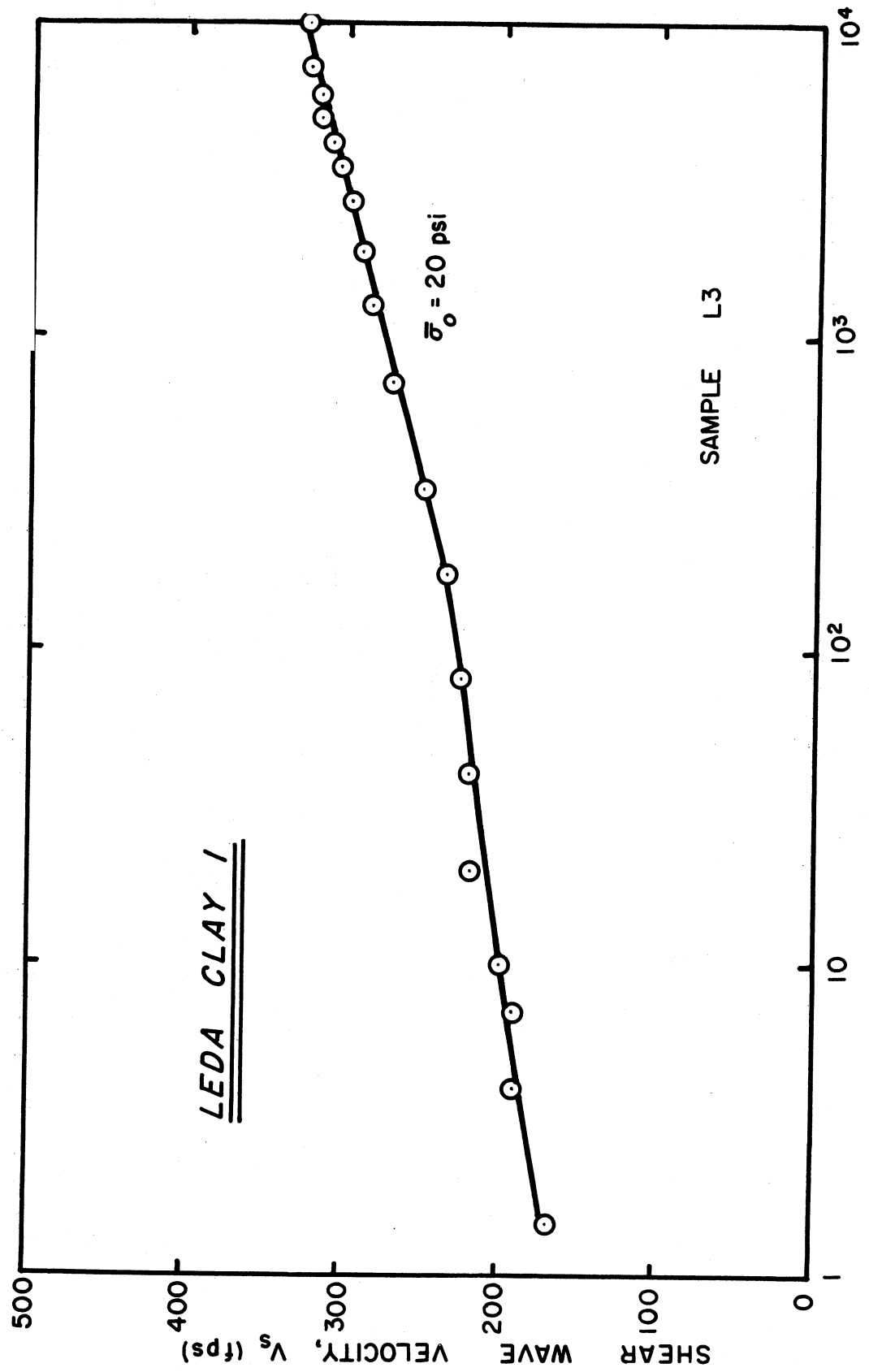

Figure E.10. Comparison of V_s with time for Leda Clay I (L3).

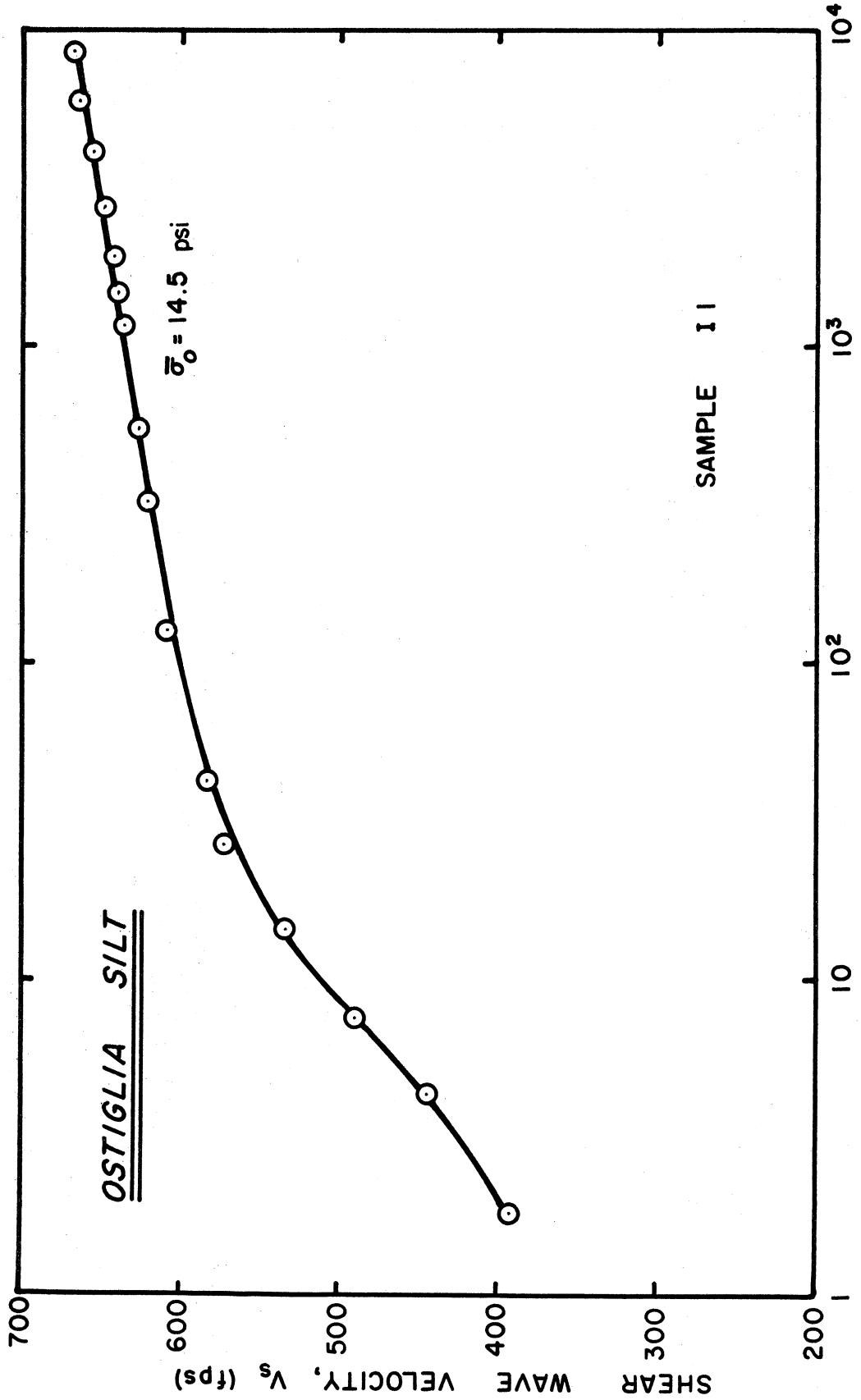

Figure E.11. Comparison of V_s with time for Ostiglia Silt (I1).

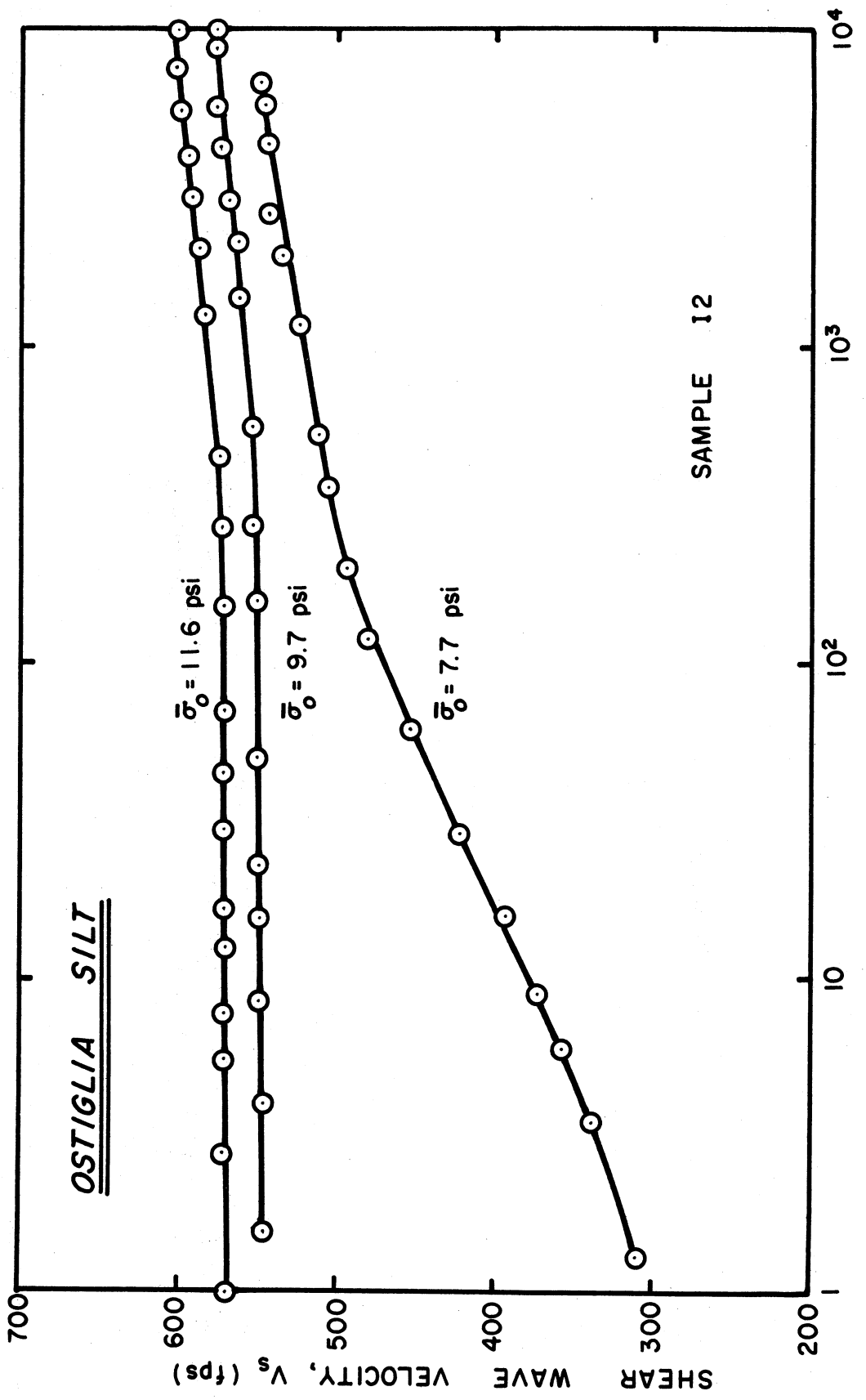

Figure E.12. Comparison of V_s with time for Ostiglia Silt (I2)

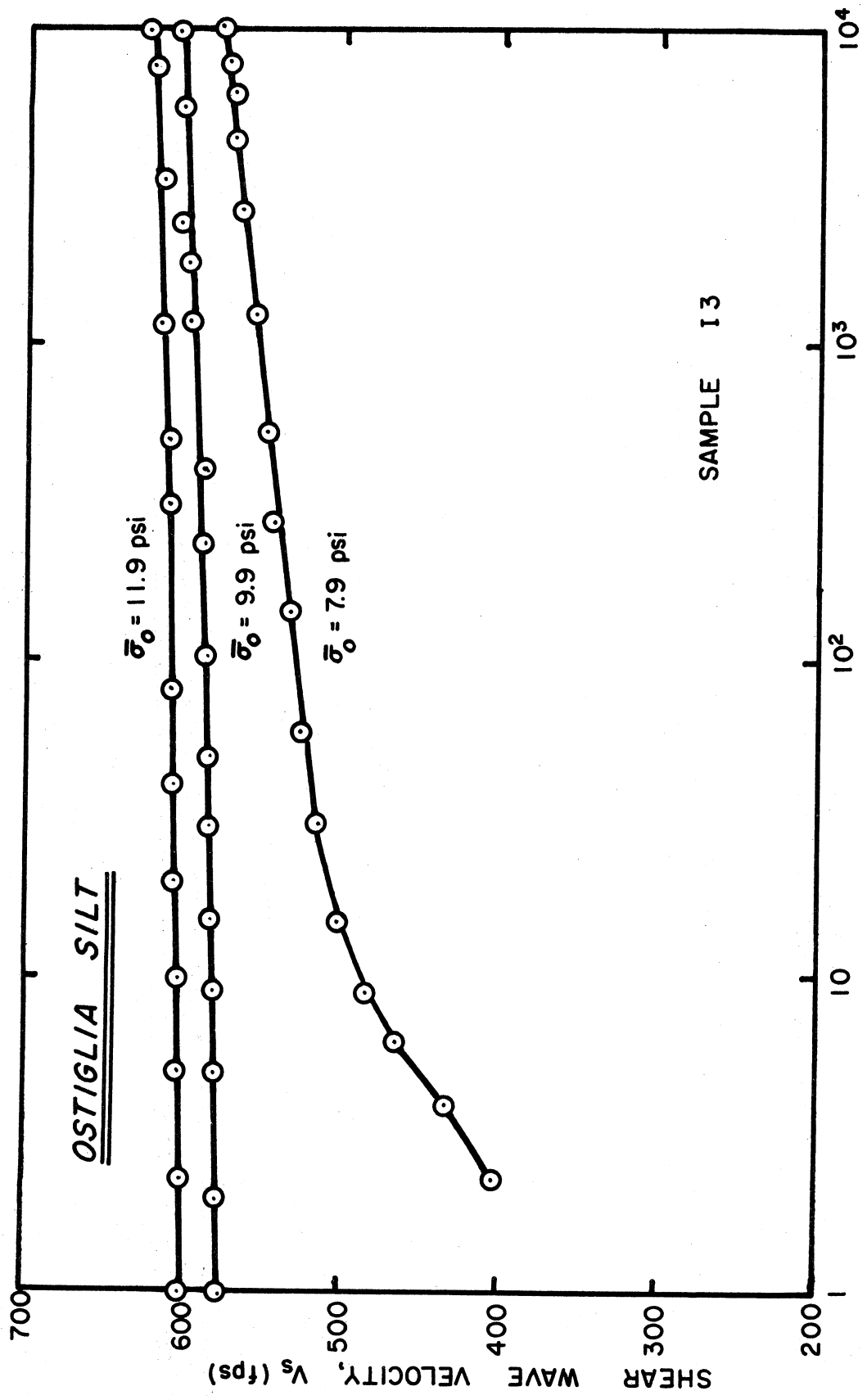

Figure E.13. Comparison of V_s with time for Ostiglia Silt (I3).

APPENDIX F

LOW AMPLITUDE TEMPERATURE PLOTS

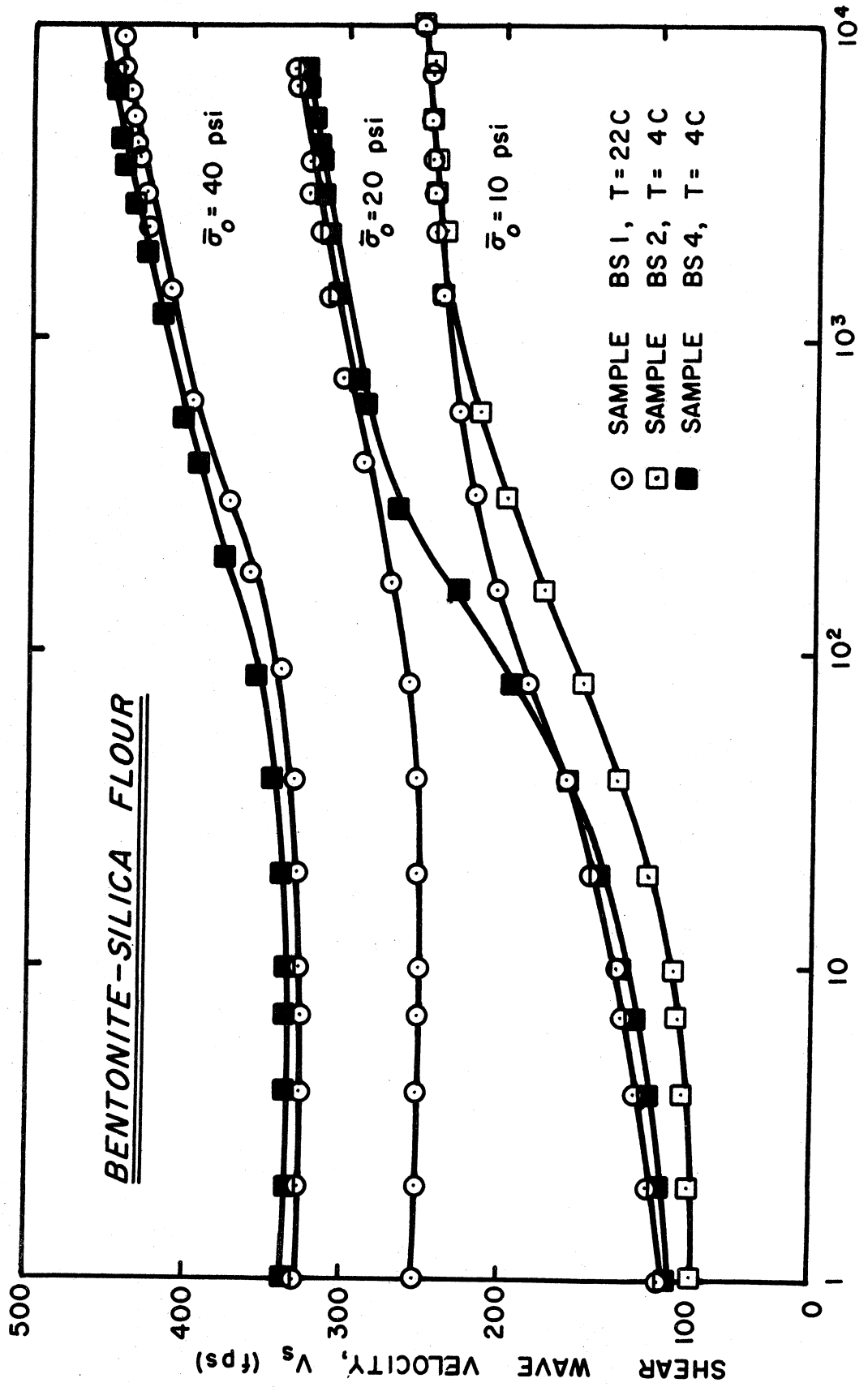

Figure F.1. Comparison of V_s with time at T = 4° and 22°C for Bentonite-Silica Flour (BS1, BS2 and BS4)

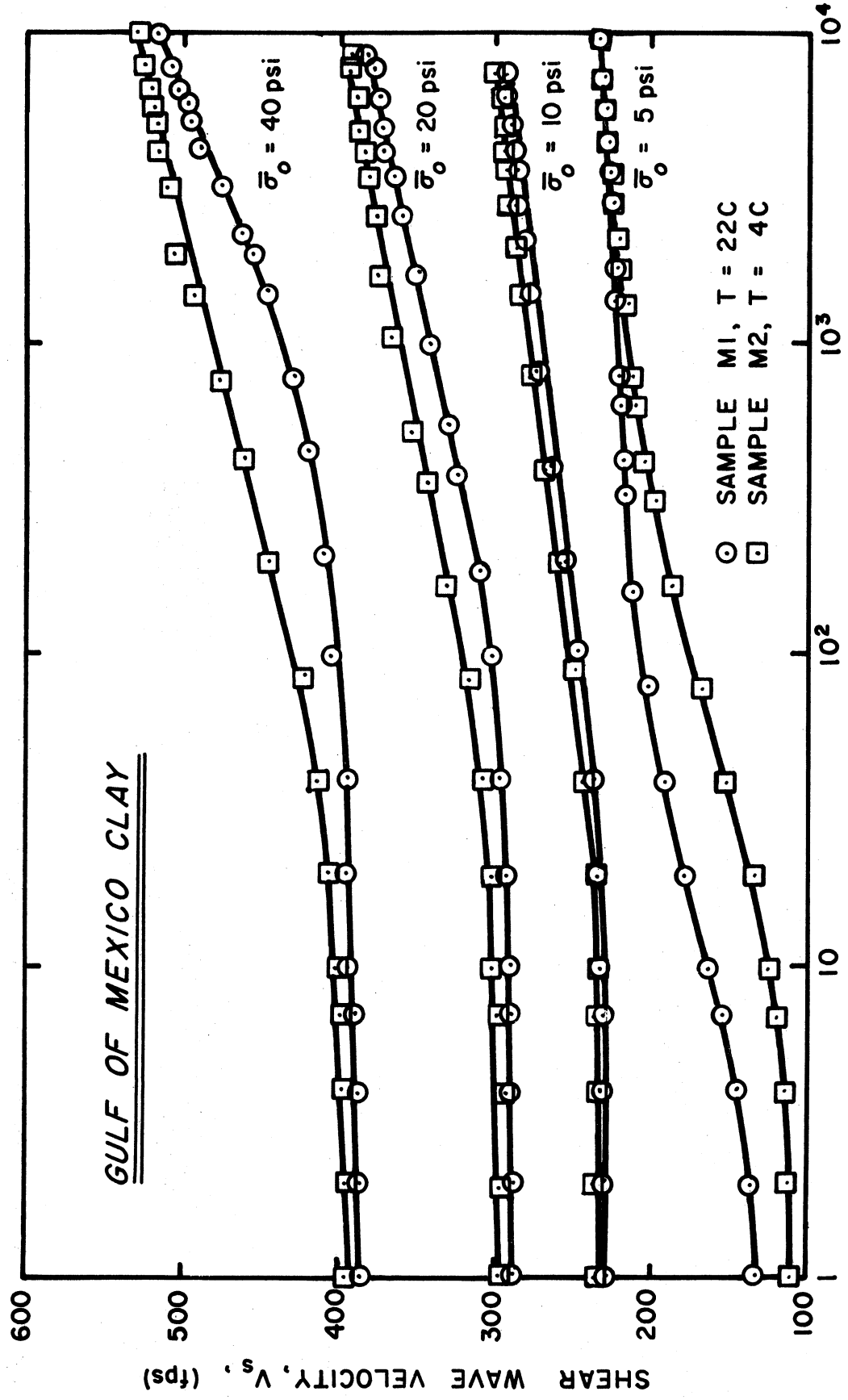

Figure F.2. Comparison of V_s with time at T = 4° and 22°C for Gulf of Mexico Clay (M1 and M2).

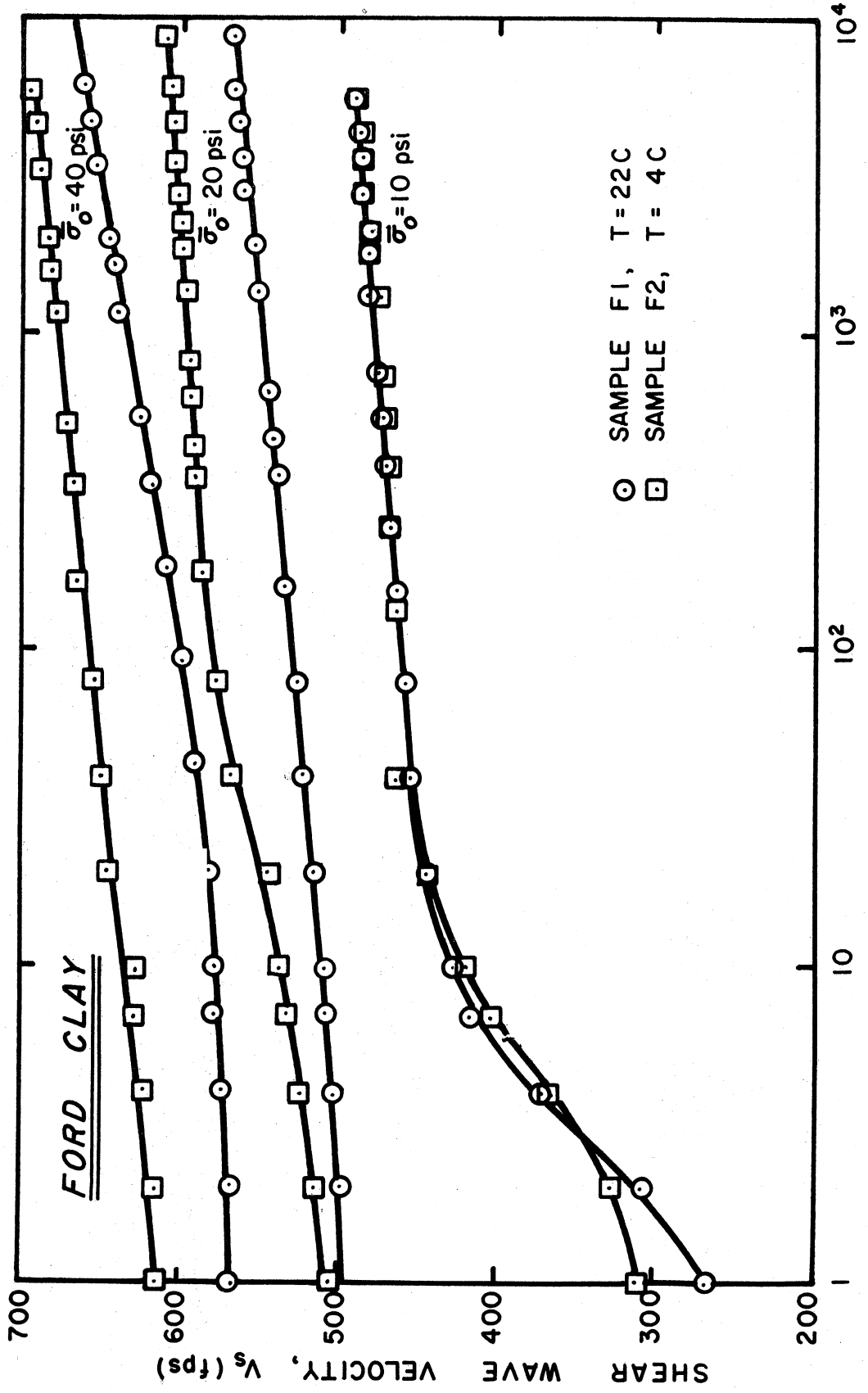

Figure F.3. Comparison of V_s with time at T = 4° and 22°C for Ford Clay (F1 and F2).

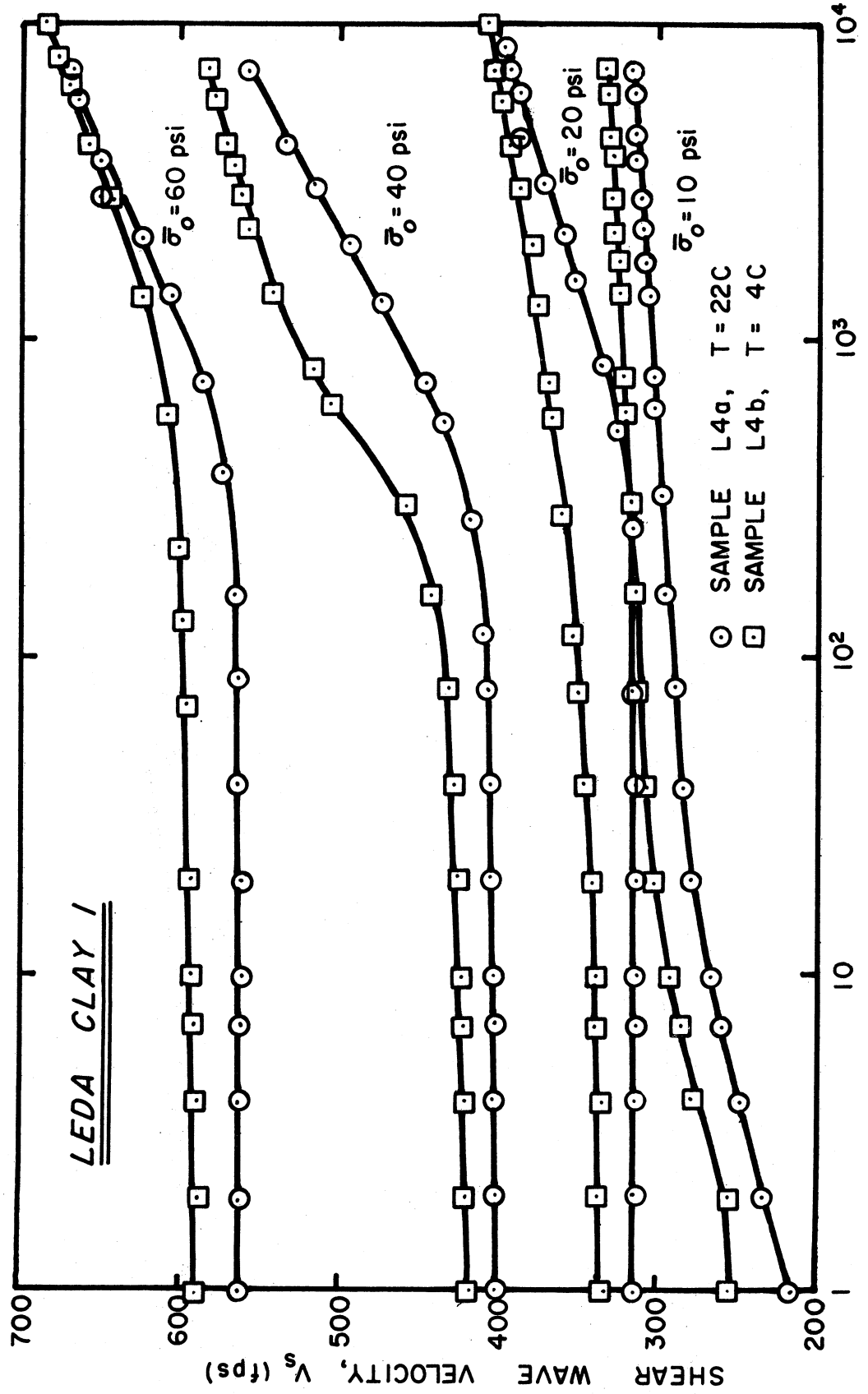

Figure F.4. Comparison of V_s with time at 4° and 22°C for Leda Clay I (L4a and L4b).

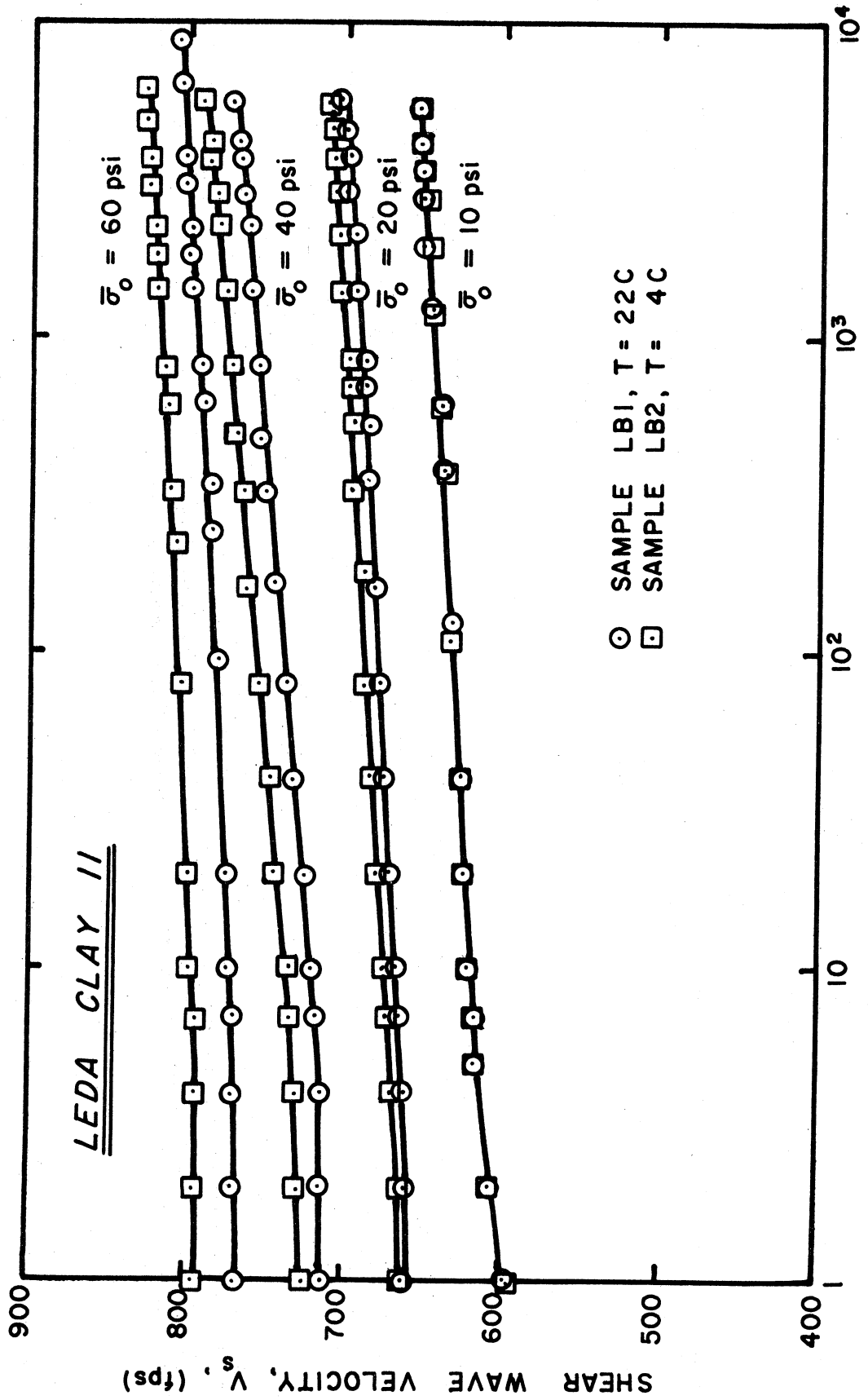

Figure F.5. Comparison of V_s with time at 4° and 22°C for Leda Clay II (LB1 and LB2).

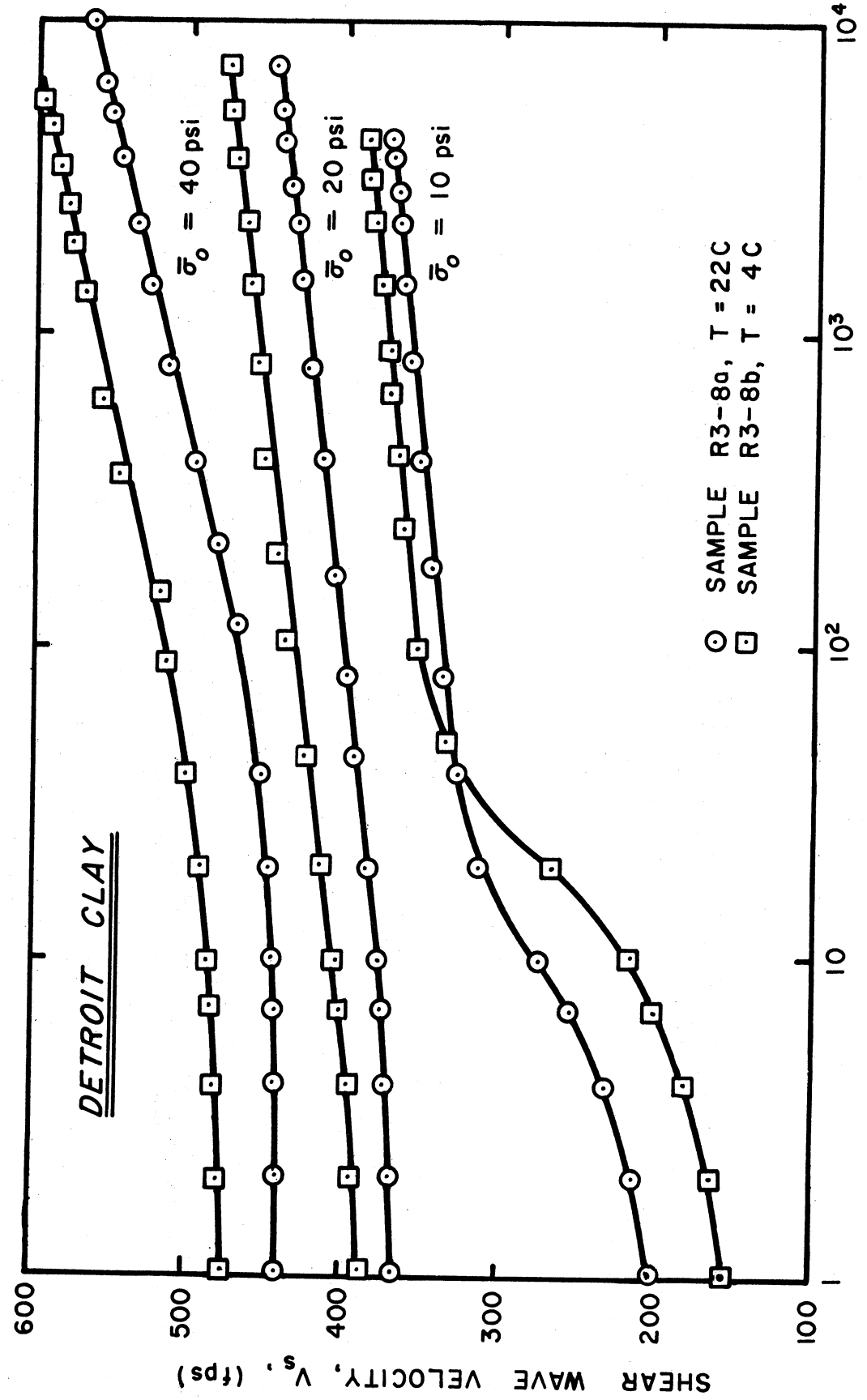

Figure F.6. Comparison of V_s with time at 4° and 22°C for Detroit Clay (R3-8a and R3-8b).

APPENDIX G

DEVELOPMENT OF V_s VERSUS LOG TIME RELATIONSHIPS

As noted in the Discussion of Results (Chapter VII), two empirical relationships were derived to define V_s in terms of void ratio, overconsolidation ratio and the confining pressure. These equations were determined by first observing the increase in V_s per change in confining pressure. A plot of this behavior is shown in Figure G.1. The average slopes of the normally consolidated portions of the plotted lines are summarized in that figure.

The average slope, as tabulated in Figure G.1, included an increase due to change in void ratio as well as change in confining pressure. When the change in void ratio was plotted against the slope of each line shown in Figure G.1, then the trend indicated in Figure G.2 resulted. The changes in void ratio were plotted for equal increments of pressure change. A linear regression analysis of this line was performed. The zero intercept, i.e., the zero void ratio change, was 0.25. It should be noted that the slope of the line shown in Figure G.2 changed as the void ratio increment changed; however, the zero intercept remained constant.

Although the results described above might be statistically weak, they did suggest that V_s increased as the 0.25 power of the confining pressure if the change in void ratio were zero, i.e.,

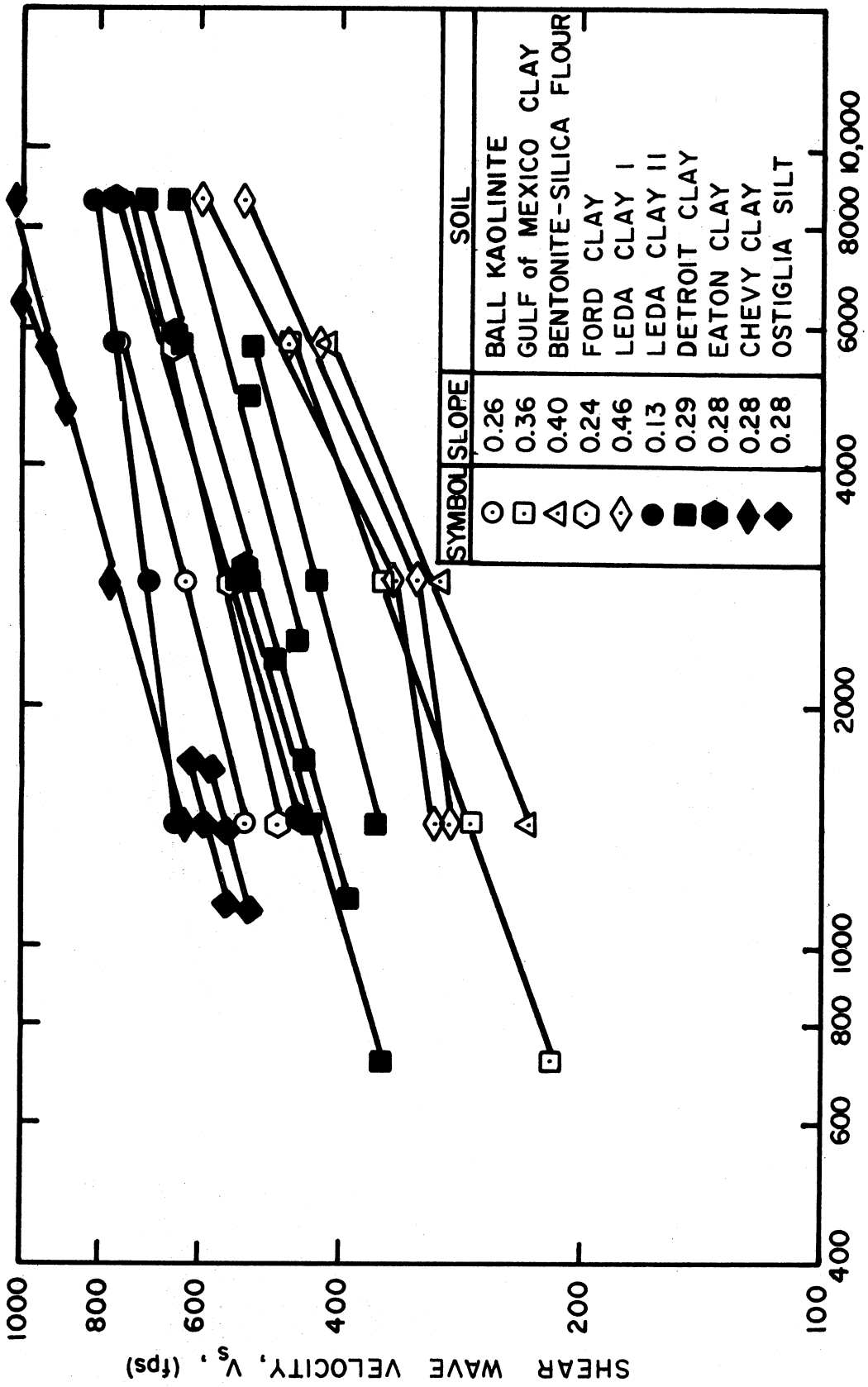

Figure G.1. Comparison of V_s to confining pressure.

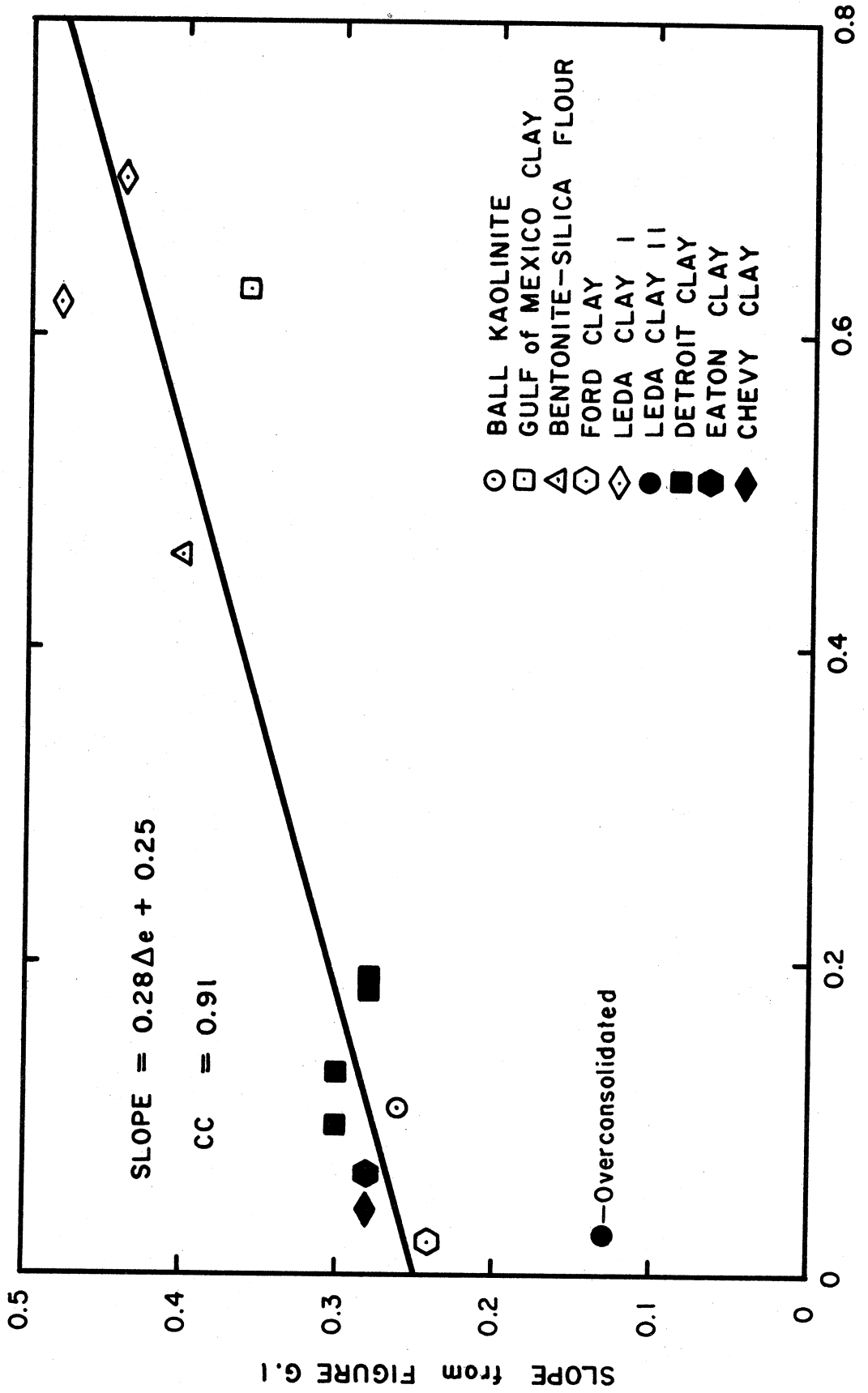

Figure G.2. Slope of $\bar{\sigma}_o$ - V_s relationship from Figure G.1 versus the change in void ratio for constant pressure increment.

$$V_s = f(e)\, g(OCR)\, \bar{\sigma}_o^{0.25} \qquad (G.1)$$

where $f(e)$ = some function of void ratio

$g(OCR)$ = some function of overconsolidation ratio

For subsequent analysis the overconsolidation function was assumed to be

$$g(OCR) = OCR^{K/2} \qquad (G.2)$$

where K was defined in Chapter II. This behavior conformed in general to that suggested by Hardin and Black (1968). Insufficient data were available to actually confirm the relationship.

After determining the relationship between velocity and confining pressure, the effect of void ratio on response was established. Figure G.3 shows a plot of V_s normalized for confinement and overconsolidation effects, $V_s/(\bar{\sigma}^{0.25} * OCR^{K/2})$, versus the void ratio at 1000 min. A linear regression analysis of the data gave the void ratio function as

$$f(e) = 134 - 63e \qquad (G.3)$$

The correlation coefficient, 0.75, indicated fair agreement; however, a visual examination of data suggested that the resulting void ratio function departed from the general trend of data at high void ratios. This zone described a region of increased surface activity, for which Hardin and Black cautioned against use of Eq. (7.1).

The data in Figure G.3 was re-analyzed in a bilinear form to account for the noticeable variation in response at higher void ratios.

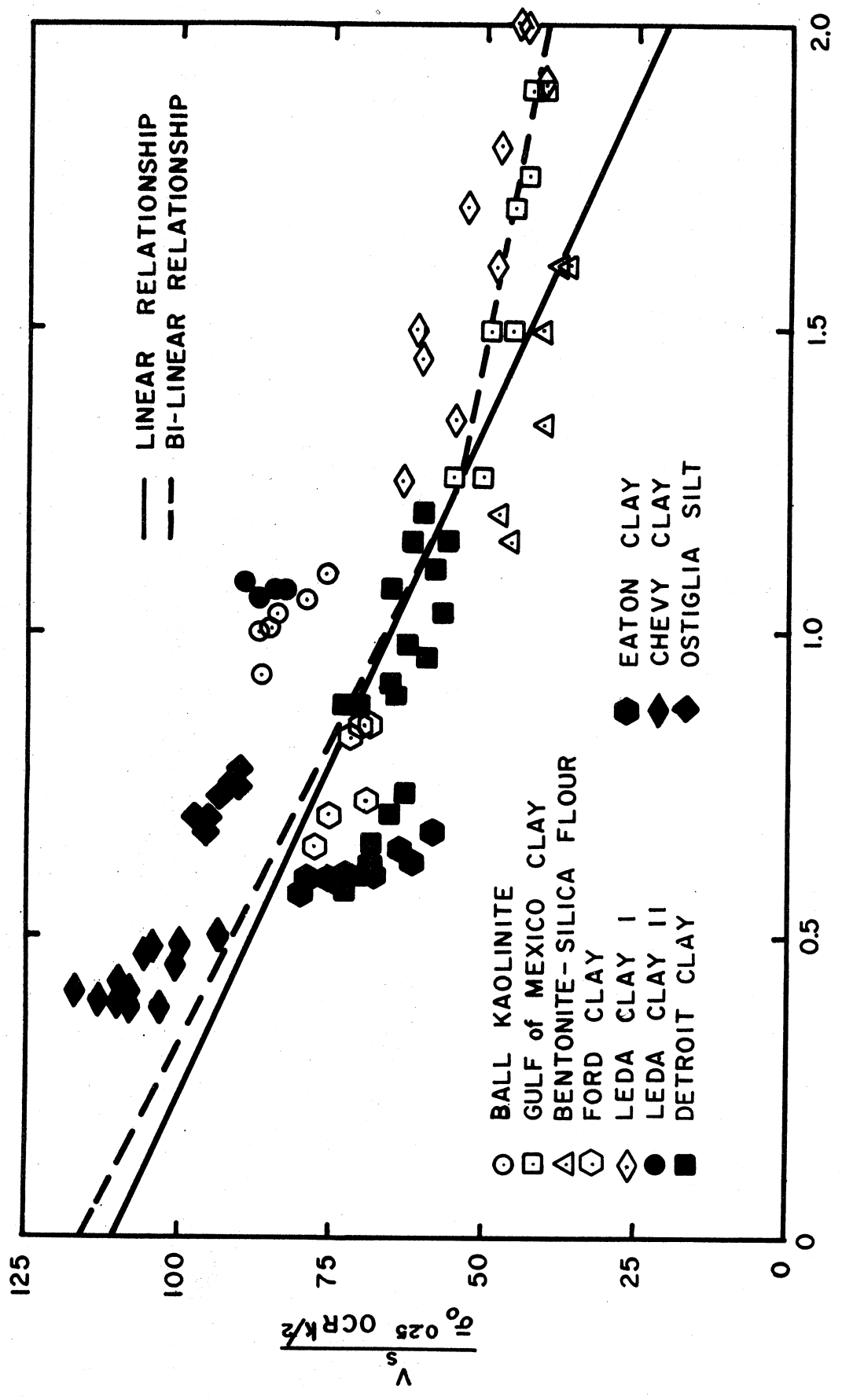

Figure G.3. Normalized V_s versus void ratio.

A linear regression analysis performed on data with void ratios greater than 1.25 gave

$$f(e) = 75 - 17e \qquad (G.4)$$

A similar analysis for data with void ratios equal to or less than 1.25 defined

$$f(e) = 117 - 48e \qquad (G.5)$$

The correlation coefficients for both equations were approximately 0.7.

The data from Figure G.3 was also replotted as a function of the logarithm of the void ratio. This plot is shown in Figure G.4. As seen in this plot, the logarithmic relationship also seems to adjust for some of the variations observed in Figure G.3. A regression analysis of the data defined the void ratio function as

$$f(e) = 66 - 123 \log e \qquad (G.6)$$

The correlation coefficient for this function was 0.86, a 10 percent improvement over the linear and bilinear relationships.

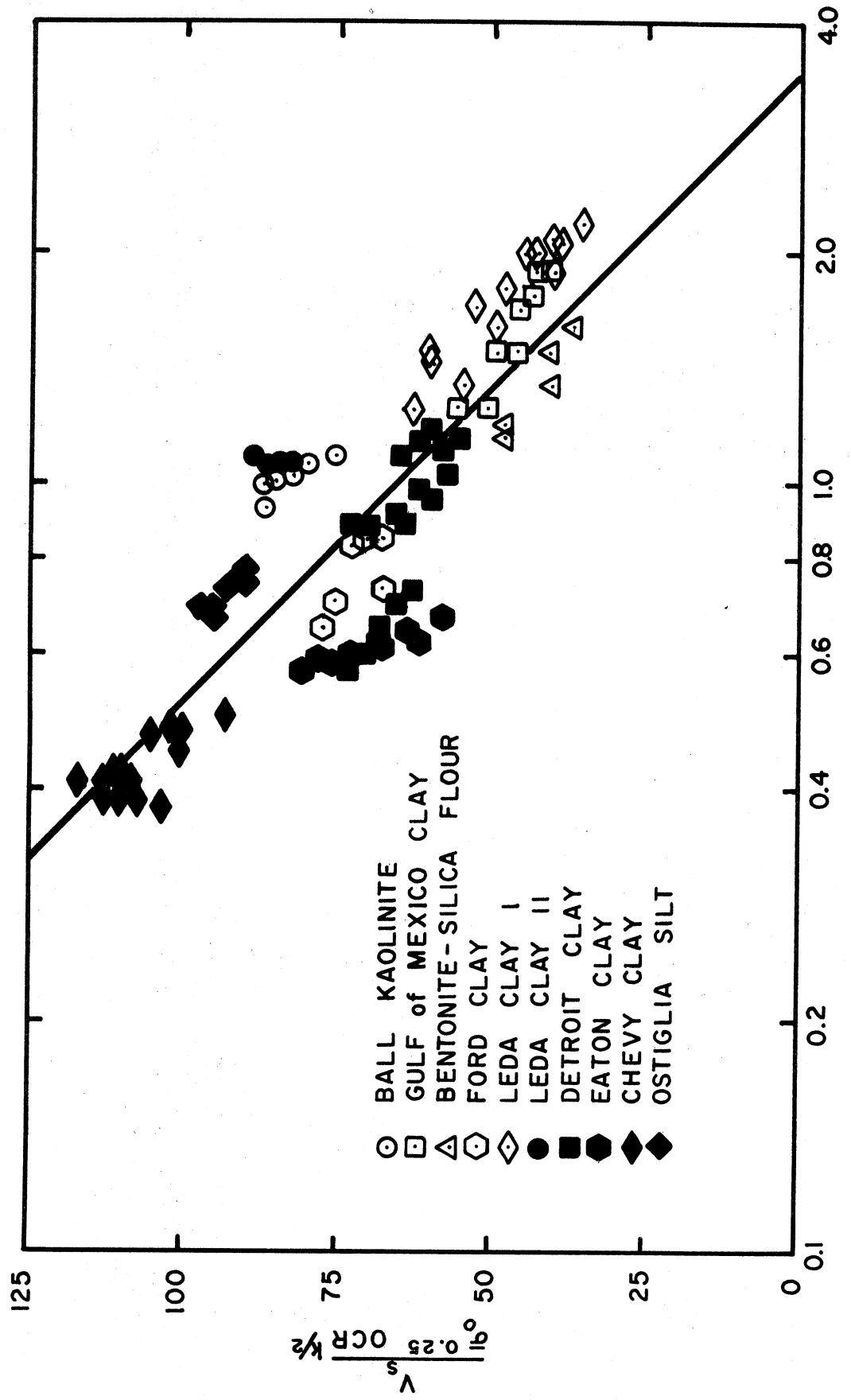

Figure G.4. Normalized V_s versus the logarithm of the void ratio.

APPENDIX H

EFFECTS OF AIR MIGRATION

The effects of air migration on dynamic properties were determined by performing three types of tests. During the first test, the effects of air migration on the water content of the various test materials were evaluated. It was expected that any change in water content distribution would represent sample drying. As a sample dried the degree of saturation and total weight would change. Both of these effects could alter test results.

Two additional tests were conducted to ascertain the influence of air migration on shear wave velocity. These tests were performed on Ball Kaolinite. As will be shown, confining conditions were varied to permit different rates of air migration prior to and during the resonant column test.

1. EFFECTS OF AIR MIGRATION ON WATER CONTENT DISTRIBUTION

The effects of air migration on water content distribution were determined by comparing the water content at the exterior of the sample to the water content in the interior of the sample. The procedure for accomplishing this comparison was given in Chapter IV. If air came out of solution and dried the sample, then the inner water content was expected to exceed the outer water content by some detectable amount. It should be noted that a small variation in water content was expected because of

the hydraulic gradient introduced during consolidation. This gradient would cause the inner water content to be slightly higher than the outer.

The results of this comparison are presented in Figure H.1. As can be observed from this figure, there is little, if any consistent difference in results. All of the 105 data points fall within plus or minus 6 percent of the equality line. The distribution of data is such, therefore, that no conclusive statement can be formulated regarding the effect of air migration on water content.

2. EFFECTS OF AIR MIGRATION ON SHEAR WAVE VELOCITY—TEST 1

The effect of air migration on V_s was evaluated by performing resonant column tests on specimens of Ball Kaolinite which had been subjected to different confining conditions. Ball Kaolinite was selected as the test material because of its uniformity, as discussed in Chapter V.

The confining conditions were varied to control the rate of air migration through the specimen. The specific types of confinement for the four specimens are defined in Table H.1. Air was used to pressurize the first three systems. The water and mercury and the foil membrane were intended to allow decreasing rates of air migration. The fourth condition utilized de-aired, distilled water as the pressurizing medium and, therefore, air migration was not expected to be a problem. The specimens were subjected to a constant confining pressure of 20 psi for six months. Drainage was permitted throughout the interval.

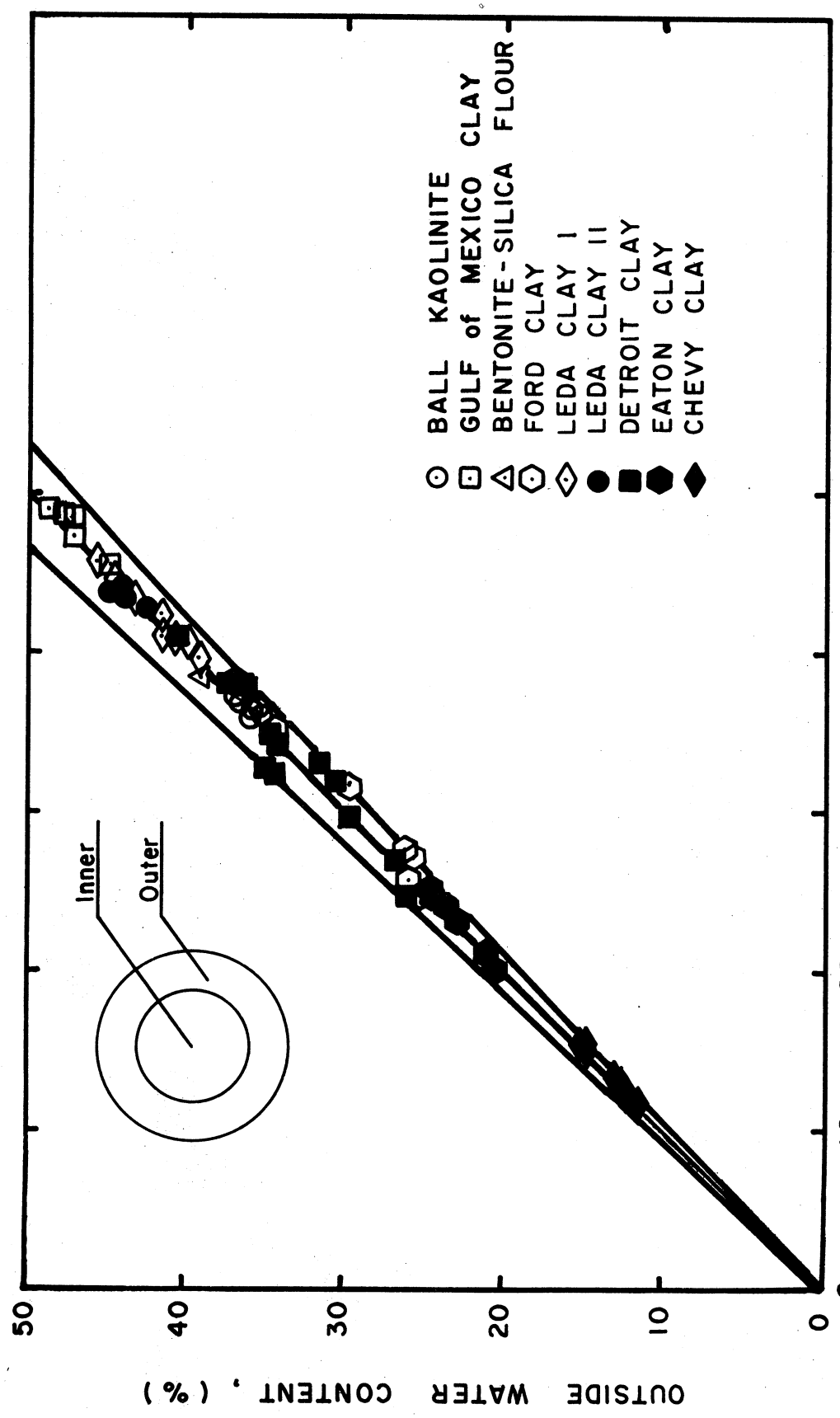

Figure H.1. Comparison of inner water contents to outer water contents.

TABLE H.1. AIR MIGRATION TEST DATA

Test No.	Pressure System	Fluid Around Sample	Type of Membrane	Rate of Air Migration*
1	air	water	rubber	1×10^{-3}
2	air	mercury	rubber	1×10^{-5}
3	air	water	al. foil	5×10^{-7}
4	water	water	rubber	none observed

*cc/min

The rate of air migration varied in the expected manner. Water permitted the highest rate, and aluminum foil allowed the lowest. No migration was noted when water was used as a confining fluid. The magnitude of these rates are tabulated in Table H.1.

At the end of the 6-month period, the confining pressure was released, and the samples were transferred to low amplitude resonant column devices. Specimens were re-weighed and re-measured during the transfer process. The foil membrane surrounding Test Specimen 3 was removed, thereby eliminating unwanted stiffness contributed by the aluminum. Once the driving and confining systems for the low amplitude devices were in place, confining pressures were reintroduced. The subsequent test procedure conformed with that described in Chapter IV for low amplitude resonant column tests. The specific confining pressure intervals were 10, 20, 40 and 60 psi.

The results of this study are shown in Figure H.2. This plot suggests that a small difference in the magnitude of V_s measured at 1000 min occurred for the four specimens. The magnitudes differed most

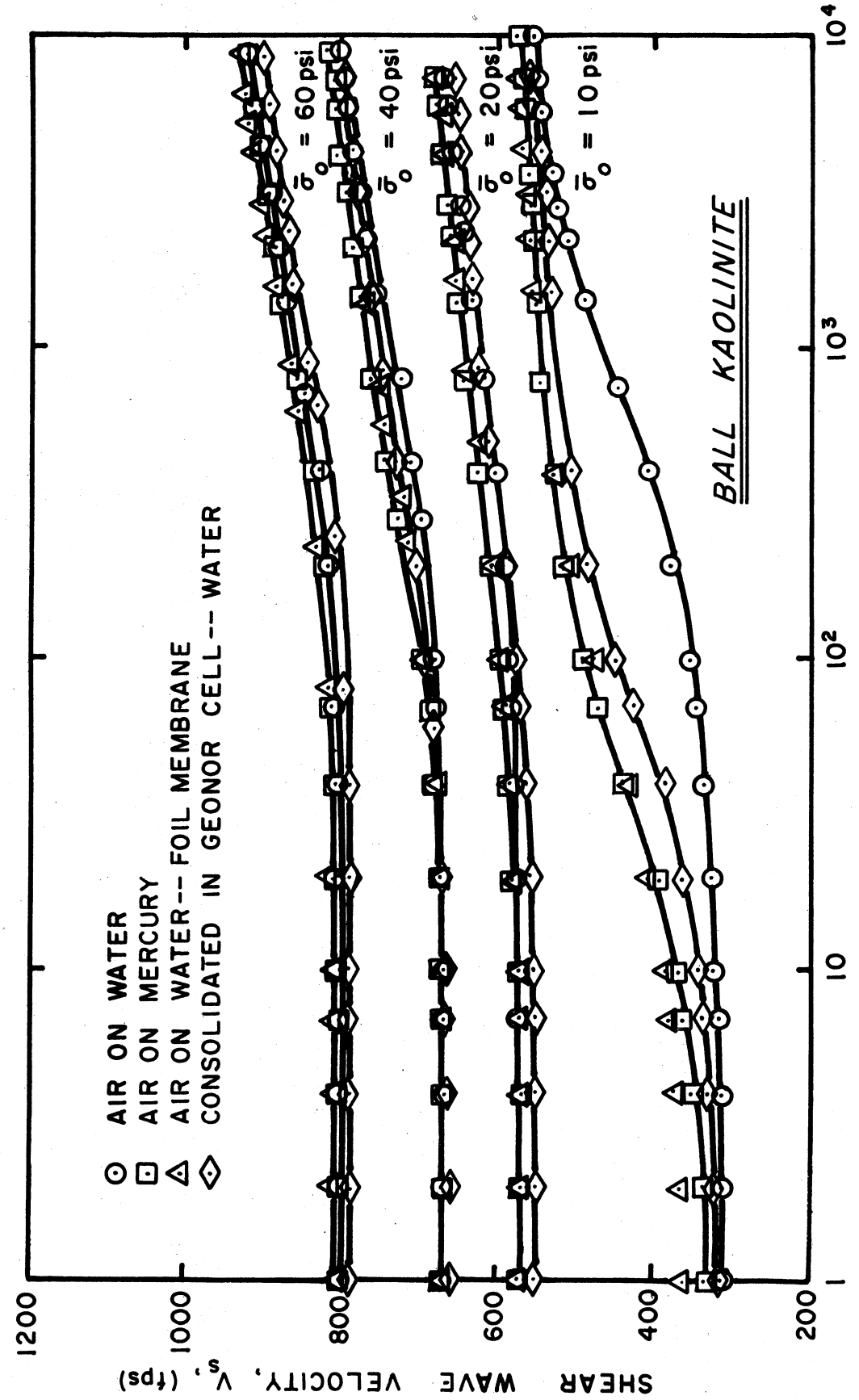

Figure H.2. Comparison of V_s versus time for different conditions of confinement before resonant column testing.

noticeably during primary behavior at the first pressure level. Subsequent to that point results converged. A variation of 4 percent or less was noted thereafter. This magnitude of variation fell within the range of expected variation in test results for samples exhibiting the same properties.

3. EFFECTS OF AIR MIGRATION ON DYNAMIC RIGIDITY—TEST 2

The effects of air migration on shear wave velocity were also evaluated by comparing the low amplitude test results for two specimens subjected to different confining conditions during testing. The first specimen, Ball Kaolinite, was tested in the normal manner, i.e., with a water bath around the specimen. The second specimen, also Ball Kaolinite, was tested without a water bath. The rate of air migration for the second case exceeded that of the first by a factor of 100 or more.

The results of this comparison are shown in Figure H.3. As can be seen, little difference occurred when the water bath was removed. Such behavior suggested that the air migrating through the filter strips did not cause any noticeable sample drying. It was expected that if the sample had dried, the stiffness would have increased. Drying appeared not to be a significant consideration as long as the pressure increment was applied for less than five days.

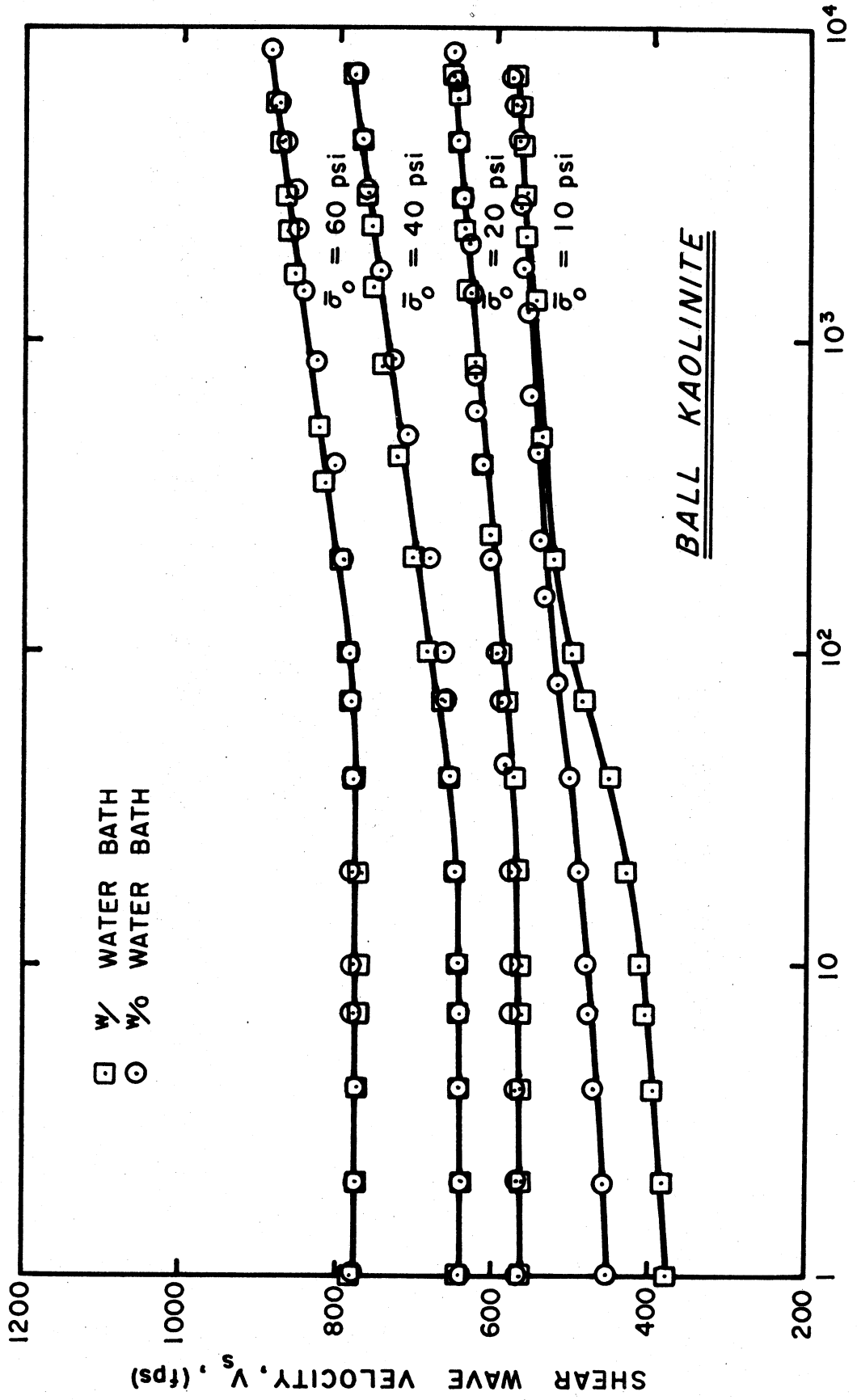

Figure H.3. Comparison of V_s versus time for different conditions of confinement during the test.